2D and 3D Geophysical Imaging of Polygonal Patterned Ground in the McMurdo Dry Valleys, Antarctica.

A project submitted in partial fulfilment of the requirements for the degree

of

Master of Science in Geology

at the

University of Canterbury

by

Myfanwy Jane Godfrey

Department of Geological Sciences,

University of Canterbury,

Christchurch, New Zealand

September 2008

Frontispiece:

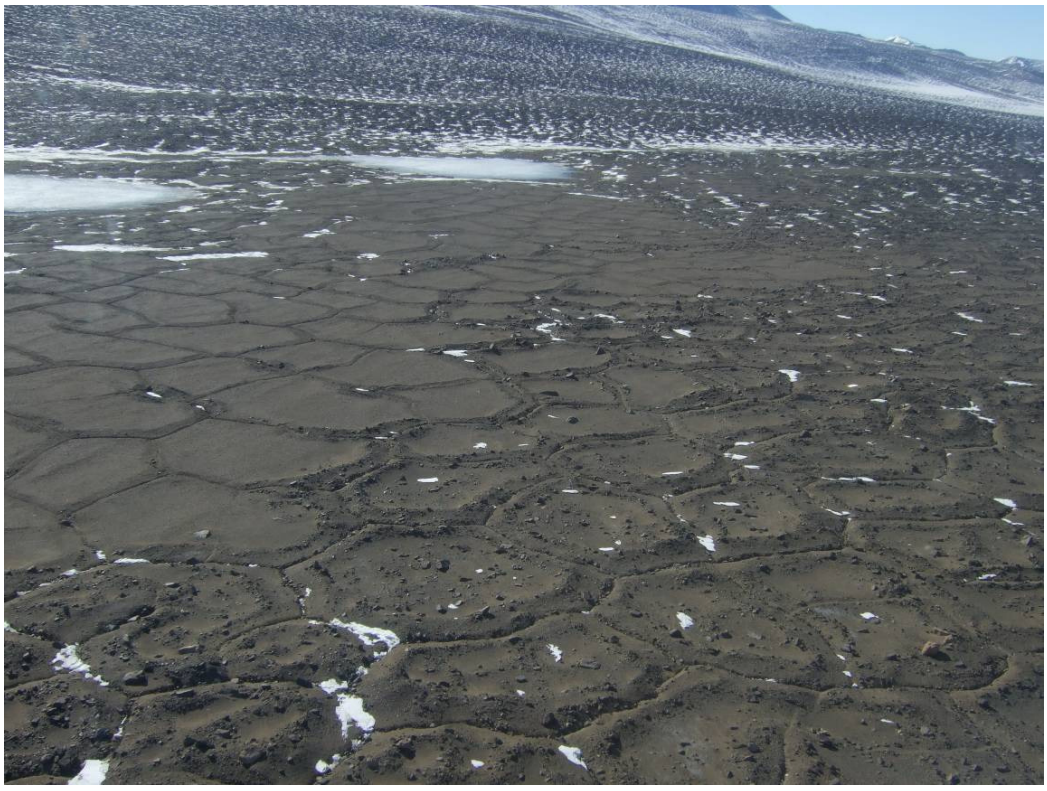

Frontispiece: Aerial photograph of Polygonal Patterned Ground in Victoria Valley

Abstract:

The PPG found in the Dry Valleys is some of the oldest on the planet with ages of up to 8 million years assigned to them. The activity of some of these Antarctic PPG areas has come into question with the proposal that they may be the result of sublimation processes rather than actively re-working freeze and thaw processes.

Near surface geophysical methods of ground penetrating radar (GPR), resistivity tomography and electromagnetism have been applied to four Antarctic Dry Valleys polygonal patterned ground (PPG) areas; two in Victoria Valley and two in Beacon Valley. The aim was to resolve subsurface structure and activity of the PPG without disturbing the delicate permafrost soils.

Multiple techniques were used so that there could be greater reliability on the interpretations of this data without the need for damaging subsurface geological calibration of the geophysics by obtaining direct subsurface data through methods such as trenching or drilling.

Subsurface structure of the PPG was resolved; active layer depth, deformation of permafrost in the vicinity of contraction cracks and zones of attenuation were identified. Significant deformation in the subsurface horizons of the permafrost and associated with thermal contraction crack wedge growth was identified over PPG suggested to be formed only by sublimation in Beacon Valley, thus calling into question this interpretation of the PPG activity.

The most reliable identification of subsurface features occurred with correlation between GPR and resistivity tomography results.

Acknowledgements:

I must thank my other (field work) half Jon Lapwood – you were my rock (thanks Tracy and Connor for letting me borrow him). Thanks also to Michele Bannister who was a pivotal member of "team extreme". Without both of these people it would have been impossible to surmount the difficulties posed during the 2006/07 K054 field season. The same sentiment must be said to Antarctica New Zealand for their remarkable professionalism and field support during my time in Antarctica. It was much appreciated at the time and still is now. In particular, Rob McPhail, the brilliant helicopter pilot who transported all our unwieldy geophysics gear between sites and provided me with some beautiful photographs of my field area.

I thank the Department of Geological Sciences at Canterbury University, my official supervisors David Nobes and James Shulmeister and my unofficial supervisor Ron Sletten. Thanks David Bell and Margaret Bradshaw for your input, and Steve Arcone for scaring the bejesus out of me and getting me in contact with James Doolittle (thanks as well). Thank you Jon Southward my computer guy, who is probably the most acknowledged man in the department. Masters students would despair without you.

Thank you to Greer Gilmer for your continual comic relief and never ending distraction from things I really didn't want to do. The same goes for the rest of the geology crew graduating year 2006 you guys were the core of my university experience.

Thank you to the Mason Trust and the Federation of Graduate Women for financial support for my field work and conference attendance.

Thank you to my Grandparents, Ray and Shirley Milne for continuous cups of tea and home baking as well as a refuge when it was time for me to "throw my toys out of the cot"

Most importantly Thank you to my parents Megan and Robert Godfrey for allowing me the freedom to keep surprising you while secure in the knowledge that you love me enough to help me with whatever outcomes came from my decisions.

Thank you to all others who had a hand in helping me with this endeavour.

Myfanwy Godfrey

Table of contents:

List of Figures

List of Plates:

List of Tables

1: Introduction to this thesis; background information and context of this research:

PPG is commonly a feature of permafrost environments. The two main forms of PPG are ice-wedge PPG and sand wedge PPG. Previous works on permafrost mechanisms have produced working models for the formation of polygonal patterned ground (PPG) (e.g. the iconic paper by Lachenbruch 1962) applicable in general to PPG. Whether ice wedge or sand wedge PPG is formed depends on the local area conditions such as water content, ground thermal regime, salt concentrations, and soil composition. In general ice wedge PPG is associated with humid permafrost conditions and is far more common (Black 1976). Most PPG areas in the Arctic are attributed to ice wedge processes. Sand wedge PPG is the product of arid permafrost conditions and Antarctica is classed as the coldest desert on Earth. Studies of PPG in the Arctic are only applicable in general terms to Antarctic examples.

The polygonal patterned ground (PPG) in Antarctica was first documented in 1904 by Robert Falcon Scott's attempt on the South Pole (Scott 1905) but has not received as much scientific attention as its Arctic equivalent in the North. This is mostly due to the relatively short period of extensive research in the Antarctic as major scientific focus has only been since the International Geophysical Year (IGY) in 1957. There is also a lack of accessibility of the frozen continent as field work seasons are limited to southern hemisphere summer months November to February.

Antarctica is 98% covered in ice and any areas exposed are under strict environmental protocols under the Antarctic treaty. Research into PPG processes in ice free areas in Antarctica must limit the disturbance to the environment as much as possible. As such; to date, superficial trenching (<1.5m) and surface monitoring have been the most common research methods for examination of PPG subsurface structure and activity in the Antarctic. However they are highly invasive in this environment.

The primary aim of this thesis is to use near surface geophysical techniques to resolve subsurface structure and seasonal activity over thermal contraction and expansion.

Specific PPG research targets associated with the chosen field areas are discussed, as well as the implications this research has for further geophysical PPG studies in the Antarctic.

Near surface geophysical techniques provide a means of interpreting changes in physical properties in the subsurface and relating them back to geological structures with no invasion and limited disturbance of delicate soils. Previous applications of near surface geophysical techniques (Arcone et al. 2000, Guigliem et al. Petterson and Nobes 2002, Davis 2002 etc) have shown that substantial subsurface data can be obtained by applying these techniques in the Antarctic environment. With the application of near surface geophysical techniques to Antarctic PPG in the McMurdo Dry Valleys it is expected that significant subsurface data on PPG structure and activity will be available.

Within the Dry Valleys two conflicting views dominate the interpretations of PPG surfaces: stable surfaces (e.g. Marchant et al. 2002) vs. active and re-working surfaces (e.g. Sletten et al. 2003). The survey areas in Victoria and Beacon Valley were chosen to expand on a theme of development progression of PPG processes. They represent the development of polygonal patterned ground from young and immature (Victoria Valley estimated age 10^4yrs) to old and mature PPG surface expression (Beacon Valley estimated age 10^6).

A secondary line of enquiry was developed for the PPG in Beacon Valley. This involved the relationship between PPG surface expression and subsurface structure; and activity of PPG over underlying buried massive ice bodies. The buried massive ice body in Beacon Valley has been well established in the literature, and questions remain as to whether the overlying PPG is active, relic, or sublimation related. The answer to these questions will have implications for the age of the valley floor surface and related interpretations of glacial history and development. This line of enquiry was expanded with the location of a previously unknown buried massive ice body within Victoria Valley and underlying one of the PPG survey areas.

1.1 Permafrost and Polygonal Patterned ground:

In this section the basic terminology for understanding PPG is defined, and PPG processes are outlined. Factors such as the common physical properties of permafrost and PPG due to the formation processes are important for interpretation of the geophysical data collected for this research.

1.1.1 Permafrost:

The subsurface of permafrost soil areas can be divided into three main zones (Figure 1): the *Active layer* (sometimes referred to as a Talik(s) or freeze thaw zone), *Permafrost*, and *Permafrost base*. These zones are based on horizons of temperature range and pore water phase. The definitions for terms relevant to permafrost and PPG are as follows:

Average annual ground temperature is required to be below zero for two consecutive years to be classed as permafrost.

Active layer occurs at the surface and represents the body of soil that has temperatures that vary from below 0°C during the freeze period to above 0°C during the thaw. The variation in soil temperature results in the freezing and thawing of pore water within this layer. This produces varied geophysical properties within the course of a season.

Permafrost is the zone below the active layer and above the permafrost base. Permafrost has soil temperatures permanently below zero. In permafrost pore water is permanently frozen and the material is often referred to as "ice-bonded".

Permafrost Base is the subsurface horizon at which the geothermal gradient of the soils creates a soil temperature of 0°C. Temperatures underneath this horizon will continue to increase above 0°C with depth. The depth of the permafrost base is dependent on the local ground surface thermal regime. As surface temperatures differ so too does the temperature vs. depth profile, colder temperatures at the surface will result in greater penetration of the permafrost before the geothermal gradient of the

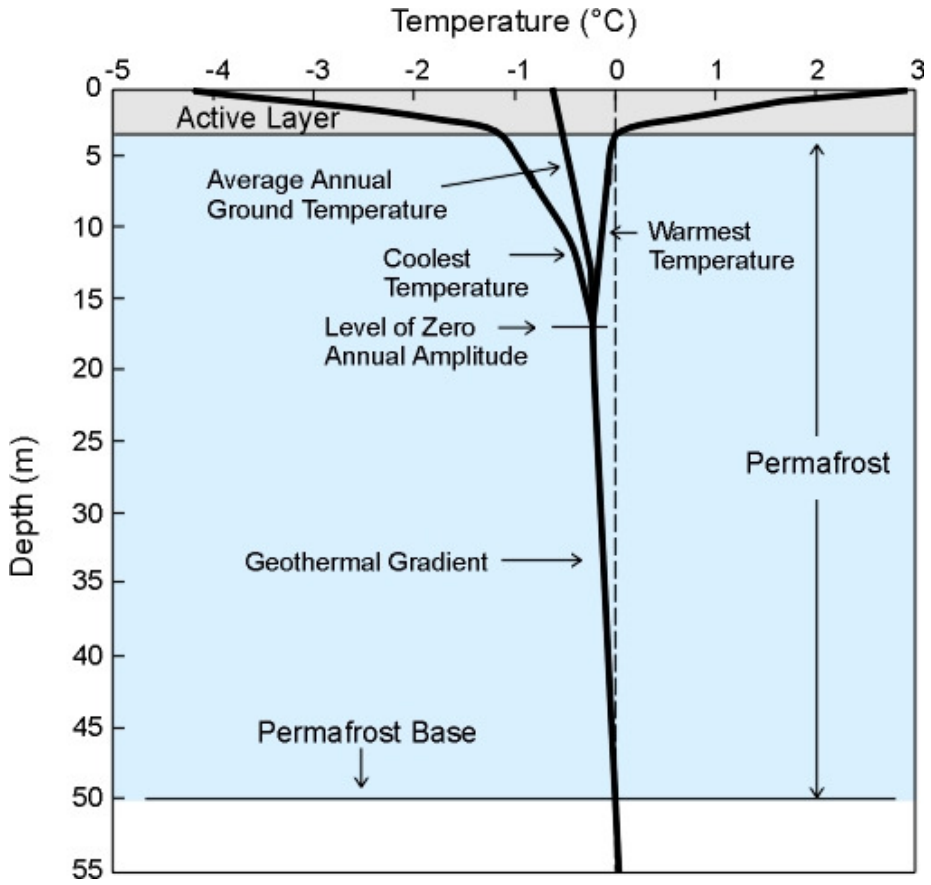

Figure 1: Generalised structure of permafrost temperature vs. depth. Depths are approximate and vary with local ground thermal conditions (Geological survey of Canada)

soil creates a soil temperature of 0˚C. Therefore as climatic conditions get colder permafrost thickness increases and vice versa. This results in increased distribution and thickness of permafrost at cold climate, high latitudes, high altitudes, and in Periglacial environments.

Level of zero annual amplitude is where ground temperatures cease to vary over the seasons. This depth represents where climatic influences on the ground thermal regime cease to have effect.

1.1.2 The development of polygonal patterned ground

The formation of PPG is conventionally associated with expansion and contraction processes found within permafrost conditions which form thermal contraction cracks at the surface. Polygonal patterned ground is classified according to the infilling material found within these contraction cracks, such as ice wedge PPG or sand wedge PPG. The infilling material is determined by the local ground and hydrological conditions specific to each zone of permafrost. In the Dry Valleys of Antarctica where

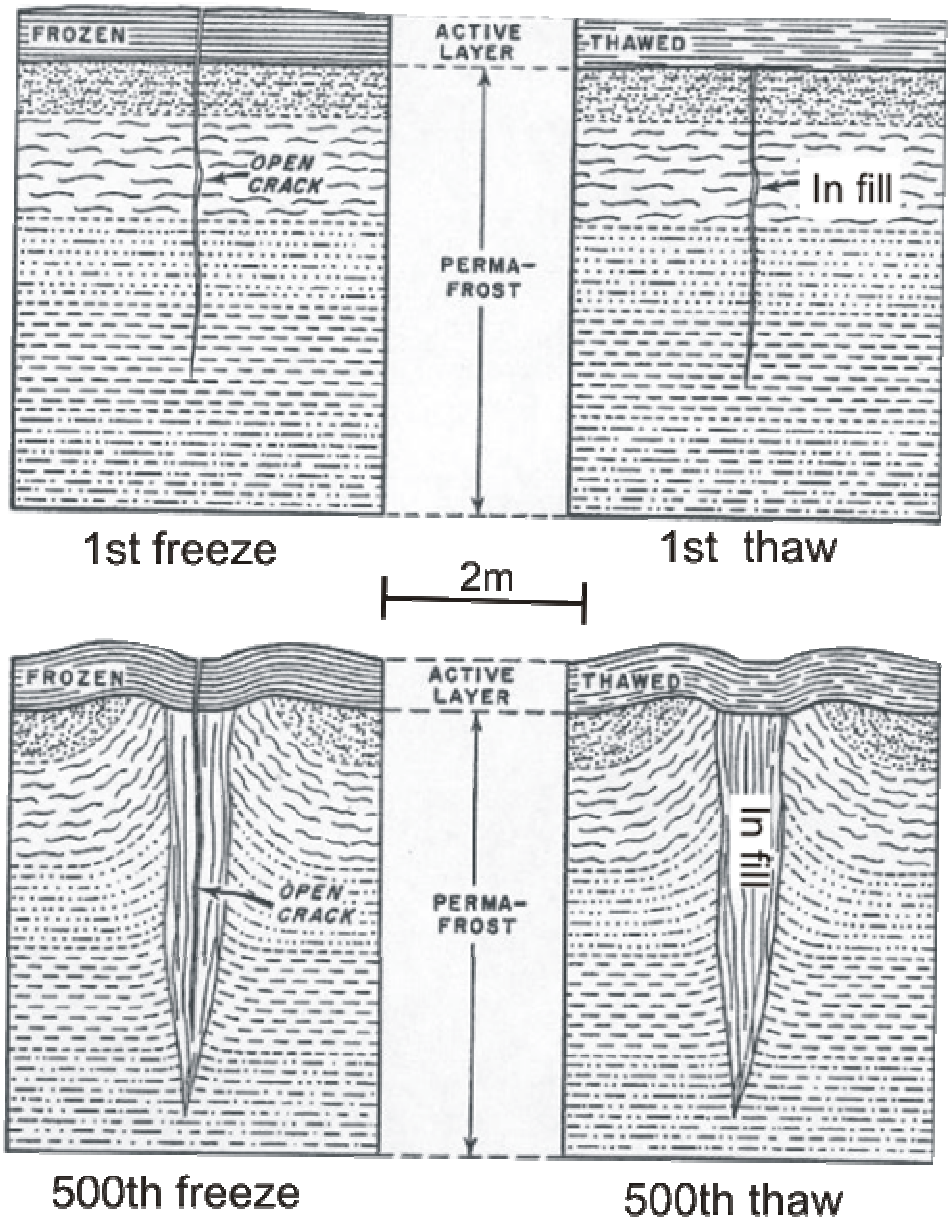

Figure 2: Simplistic diagrams showing the cross-sectional development of PPG over successive seasons. Modified from Lachenbruch (1962)

the research for this thesis was conducted, the PPG predominantly comprises sand wedge polygons. This is due to the arid nature of the Dry Valleys environment. Research on polygonal patterned ground received much attention in the 1960s and 1970s, predominantly by researchers such as Black and Berg (1963), Black (1976), Lachenbruch (1963) and Péwé (1974). The generalised mechanism for the formation of ice wedge and sand wedge PPG is similar but ice wedge formation has received far more attention in the literature. For example ice wedge PPG has been the focus of progressive studies by Mackay (1971, 1974, 1984, 1986, 1992, 1993, and 2000), whereas sand wedge PPG has no equivalent.

In general in PPG, thermal contraction and expansion of the soil volume over successive seasons forms a downward propagating crack. This contraction and expansion is within the top 5 – 10 m of permafrost and for contraction cracks to form the ground conditions must have a level of zero annual amplitude less than 5˚C and seasonal temperature changes of 8-10˚C (Black, 1976). Over a large area these cracks form a connected polygon (singular) or a network of polygonal patterned ground (plural). Figure 2 shows the theoretical development of an ice wedge in permafrost soils. When the ground is cooled horizontal tension in the soils is generated as soils attempt to contract. As soils are volumetrically constrained this tension in the soils is released as contraction cracks.

Lachenbruch (1962) relates the generation of these contraction cracks as similar to a stack of horizontal thin lubricated Plates. If a cut were to be made down through this stack of Plates the width of the cut would be proportional to the amount of horizontal tension created by the cooling temperatures. As you moved down through the Plates the amount of thermal horizontal tension would decrease (and so the width of the cut) as insulating effects and the geothermal gradient negated the surface cooling effect. With a thermal change of 10˚ C most rocks would contract about 1mm over 10m and ice would contract 5 mm over 10 m (Black, 1976). These cracks are often filled in with water and/or soil and rock material and as the soil thaws and starts to expand again, the infilling material in the cracks prevents full closure, thus causing the expansion of the soils to deform the surrounding material (Figure 2). Deformation in the soils adjacent to the crack is by flow and shear to accommodate thermal expansion (Black, 1976). This results in raised rims on either side of the crack.

In extensive and continuous permafrost, contraction cracks develop into a network of interlocking polygonal structures, usually with six to eight sides and diameters of 1 – 25 m across (depending on local conditions and maturity of the PPG). Subsequent contraction re-opens the pre-existing cracks and forces propagation to depth to accommodate the thermal contraction. Mackay (1984) suggests that in early stage PPG development the re-opening of previous seasons' cracks rather than generation of a new crack network the following season is the result of maximum stress being found at the bottom of the active layer. Therefore crack propagation is towards the

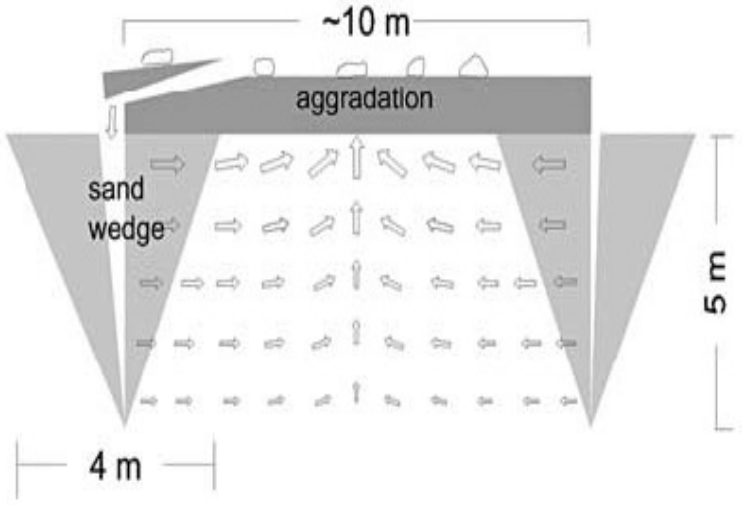

Figure 3 Soil movements and deformation associated with wedge growth and aggradations in permafrost soils Light grey is the wedge volume; dark grey represents the inflated volume of permafrost during thaw season. Arrows show soil deformation stress field. (From Sletten et al. 2003)

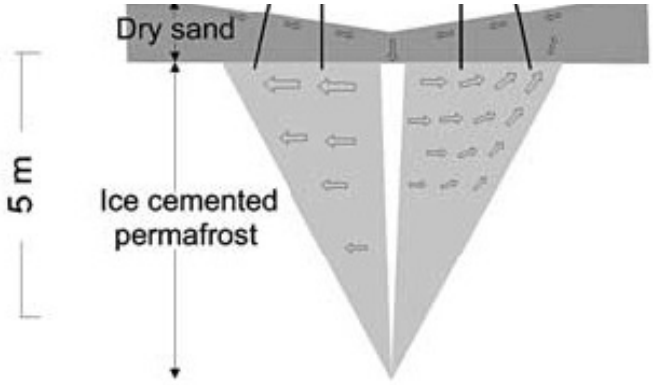

Figure 4: Deformation of soil material found within contraction cracks resulting in the formation of raised ridges in the immediate vicinity of PPG contraction cracks. The displacement field shows that circulation of the soil occurs within the crack infill material. This model has been developed by Sletten et al. (2003) based on displacement of steel rods placed into the crack shoulders at 13 sites established by Robert Black in the early 1960s.

surface generated from the weakness of the previous season's infilling material. The cracks expand further at the surface and accumulate more infilling ice and/or rock and soil material. With time and multiple seasons' ice wedges develop. The development of this wedge geometry results in the deformation of the permafrost as the additional ice wedge volume is accommodated (Figure 3).

The deformation of the soils in the proximity of the thermal contraction crack wedge is displayed at the surface as raised edges. Figure 4 shows a model for the development of raised ridges within sand wedge PPG. This model is based on displacement of steel rods fixed into crack shoulders at 13 locations in the early 1960s by Robert Black (Sletten et al. 2003). In developed polygonal patterned ground the interlocking cracks and associated deformation ridges may show a "doughnut" surface geometry of raised edges and depressed centres.

In arid cold climate conditions such as those found within the Antarctic Dry Valleys, the growth of polygonal patterned ground crack networks is associated with sand wedge growth whereby rock and soil debris are the infilling material with little or no ice wedge formation. Although ice content will develop (composite PPG), it is not the driving force behind the formation of the polygonal patterned ground networks in arid polar environments. The variations between ice wedge and sand wedge PPG is of limited importance when discussing the generation of the PPG as the formational processes are fundamentally the same. However, since the infilling material is different the tensile stresses developed over successive seasons are different and formation times and the flow-on implications of surface ages may vary. The difference between ice wedge and sand wedge PPG processes has particular importance when assessing palaeo-environmental interpretations of relic PPG as the surface expression is very similar. Ice wedge vs. sand wedge PPG cannot be determined from surface expression only (Black (1976)); Additional subsurface information is needed.

1.1.3 Primary PPG structure target identification:

As outlined previously, the development of thermal contraction cracks and propagating infill wedges are the driving force behind the formation of PPG. Thermal contraction cracks are initially developed within the fluctuating active layer where temperatures vary above 0˚C.

Figure 5 below summarises the primary targets of the PPG subsurface structure.

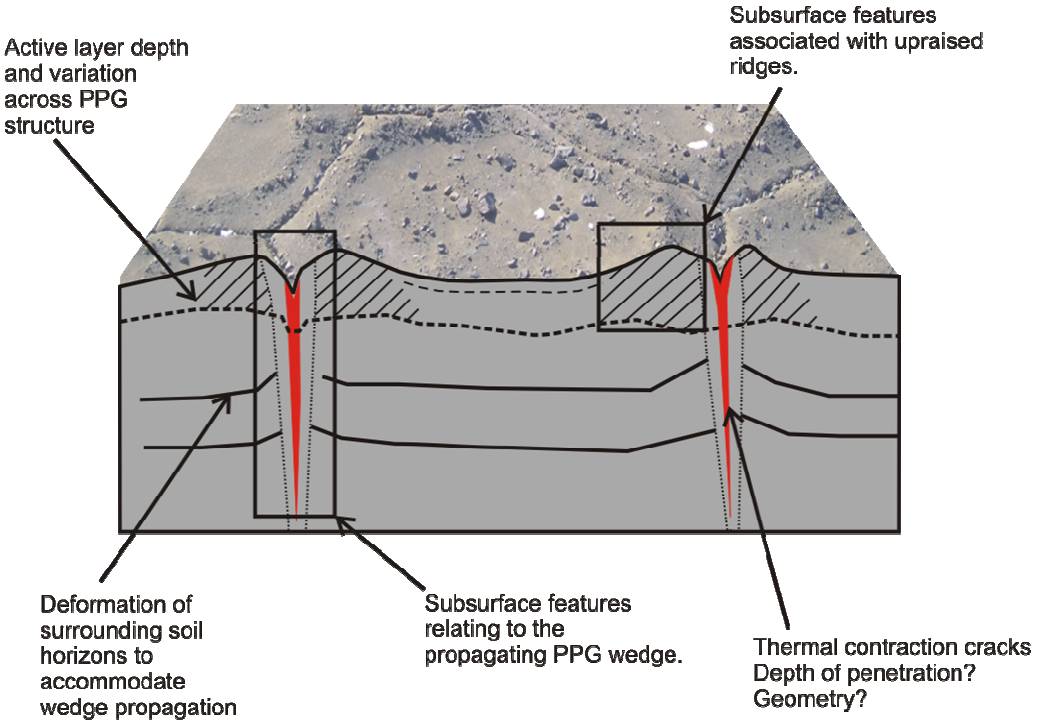

Figure 5: PPG subsurface structure block diagram marking the primary targets for the near surface geophysical methods to resolve.

Time-lapse imaging will be targeting the changes in the subsurface through the warming/expansion period of the permafrost soils. This will specifically focus on changes in the active layer and thermal contraction cracks and associated ridges and their areas of influence.

1.2 Near surface geophysics in Permafrost soils.

The success of geophysical methods in permafrost soils will depend on the individual conditions of the area. The application of near surface geophysics to permafrost soils is varied, and has been concentrated primarily in Arctic environments.

1.2.1 Physical properties of permafrost:

Permafrost does not have a specifically measured set of geophysical responses as it is found in all soils and groundwater regimes provided that the climatic conditions remain cold enough to sustain permanent freezing of the soil. For the use of near surface geophysics the dominating physical properties of a body of permafrost will come from the general geophysical relationships such as: increased resistivity with grain size, degrees below 0°C and ice content (Haeberli, 1985). These factors are the standard relationships of geophysical response from the earth surface and will vary location to location according to the specific composition of the permafrost soils, source rocks, water content, and vegetation cover. Freezing may cause these properties to be varied from what might normally be expected. Salt and mineral concentrations within the soils may decrease the freezing point of the water content and skew the temperature – depth profile of the permafrost at specific locations. Frozen soils have different physical properties from their un-frozen equivalents primarily because water is constrained differently within the frozen structure. Freezing materials often results in an increase in resistivity/decrease in conductivity. Annan and Davis (1978) conducted laboratory tests with clay soils showing that as the temperature decreases there is a reduction of the dielectric constant (k).

The dielectric constant is sometimes called the specific inductive capacity or the dielectric coefficient and is dimensionless but relates to the generation of a displacement current due to electrons being slightly displaced from their nuclei in poorly conductive mediums (Telford et al. 1990). The dielectric properties of a material are of more importance when employing high frequency geophysical techniques such as ground penetrating radar, as was used in this study of polygonal patterned ground. Apitakev (1964) showed that compression and shear wave

velocities increase with decreasing temperature in materials containing water. This is due to the increase in density as the water content freezes, thus changing the physical properties with decreasing temperature. Further work on velocities by King (1984) refined this more to show that the increase in velocity was a function of "water-filled porosity" as it was discovered that significant amounts of water may remain unfrozen down to temperatures of -5 ˚C. Despite the low levels of ground water in Antarctic permafrost soils, this is important to note due to the poorly sorted gravely composition of the soils and high salt concentrations within pore water.

Although Arctic soil examples are useful for examining the potential for geophysics in Antarctica, there are issues surrounding the relative soil conditions found in these polar environments. Primarily the effect of free water within the soils is important when evaluating Antarctic examples. Antarctica is classified as a desert; the annual precipitation, in water equivalent measurements, across the continent is just 166 mm/year, and < 100 mm/year in the Dry Valleys (Doran et al. 2002). The lack of vegetation cover means that salt and mineral concentrations in the subsurface are higher as they are not used as nutrients for growth. Katabatic winds generated on the ice sheets maintain arid conditions by evaporating surface moisture and removing snow accumulations. These conditions create a barren, armoured rock strewn landscape with arid climatic conditions with little free water to be involved in permafrost processes. In general Antarctic permafrost soils have higher resistivities than their Arctic equivalents

1.2.2 Applications of geophysics in permafrost and the Antarctic:

Much of the research surrounding the use of geophysical methods in permafrost soils has been conducted in labs or in Arctic localities (e.g. King 1984, Hauck 2001, Brandt et al. 2007). These studies have shown that geophysical methods can be used to great effect when evaluating the subsurface within permafrost and periglacial environments but that the geophysical response is highly individual according to the specific location of study and local geological and climatic conditions. The use of geophysical methods to determine permafrost features such as the thickness of the active layer has proved successful in high latitude Northern hemisphere locations (Hinkel et al. 2001, Brosten et al. 2006, and Munroe et al. 2007). Munroe et al. (2007) and Doolittle et al.

(2008) present results from 3D GPR surveys of active and relic PPG structures in Alaska and mid west USA. Applications of geophysical techniques in the Antarctic soils has garnered results in the field of sedimentary and valley structure evaluations (e.g. Bristow et al. 2008, Arcone et al. 2003), and contaminant location (e.g. Pettersson and Nobes 2003). Near surface geophysics PPG studies have previously not been conducted in the Antarctic.

The short working season and difficult accessibility of the area combined with challenging and isolated working conditions are not ideally suited for conducting geophysical surveys. However, the extremely delicate nature of the environment coupled with the importance of scientific study of the area should be a strongly positive factor when considering the use of non-invasive near surface geophysics in the Antarctic and its ice free areas.

2: Field area : The Dry Valleys

This section focuses on the location of the field work that was conducted for this thesis. The environmental factors that may contribute to PPG formation and specific characteristics found at each field location are discussed. Working conditions and survey areas are described in the context of the geophysical results for PPG subsurface structure.

2.1 Introduction to the field area: The McMurdo Dry Valleys

Antarctica's landmass is 98% covered in ice. The McMurdo Dry Valleys with an approximate area of 4800 square kilometres represents 95% percent of this 2% ice free area and the largest ice-free area of Antarctica. The McMurdo Dry Valleys is surrounded by the East Antarctic Ice Sheet (EAIS) to the West, North and South, which blocks and dams valleys, as found in Beacon Valley and Taylor Valley, and feeds into the Dry Valleys in the form of glaciers such as the Victoria and Taylor Glaciers. To the East, the McMurdo Dry Valleys are bounded by the McMurdo Ice Shelf which is part of the larger Ross Ice Shelf. McMurdo Dry Valleys are classified as a permafrost zone; subsurface soil temperatures are below zero degrees Celsius. The cold dry conditions found in the Antarctic are unique and although similar to frozen regions in the Arctic the lack of free water does result in variations within the permafrost. The Antarctic Dry Valleys have been suggested as the closest environmental analogue to the conditions found on Mars meaning that any research conducted there has implications for extraterrestrial applications.

Field work for this project was conducted in two locations in the Dry Valleys of Antarctica for 9 weeks during the 2006/2007 austral summer: one in Victoria Valley and the second in Beacon Valley. Each location had two polygonal ground areas surveyed. Refer Figure 6 below. Our field party consisted of four team members and designated K054.

Original photo images courtesy of Jacques Descloitres, MODIS land rapid response team at NASA GSFC

Figure 6: Satellite images of the Ross Dependency McMurdo Sound region in Antarctica with the inset showing a larger scale view of the McMurdo Dry Valleys where the field work was conducted. The two field sites of Victoria and Beacon Valley are labelled and outlined with an orange box.

Please note that although this thesis will refer to the American conventions of East and West Antarctica as seen in most Antarctic maps, maps will in fact be oriented for New Zealand as will any directional information such as East, West, North and South. For example the orientation of polygon surveys to the North, is North, consistent with longitude orientation and towards New Zealand.

2.1.2 Polygonal patterned ground in the McMurdo Dry Valleys, Antarctica.

The polygonal patterned ground (PPG) found within the McMurdo Dry Valleys is thought to be some of the oldest on the planet with estimated ages for some surfaces being of the order of 10^6 years (Sletten et al. 2003, Marchant et al. 2002). Black (1976) identifies the PPG in the Dry Valleys Antarctica as predominantly sand wedge and composite PPG. The established cold climate conditions and its polar position results in permafrost estimated to be between 240 – 970 m to permafrost base (Decker and Bucher 1980).

With the exception of the first identification of PPG in McMurdo Dry Valleys by Scott (1905), the literature surrounding PPG in Antarctica derives from the late 1950's onward. Much attention was paid to Antarctic PPG in the 1970's e.g. Péwé (1959), Black and Berg (1963, 1964, and 1966) Berg and Black (1966), Black (1973), and Ugolini et al. (1973). Recently literature has reflected an ongoing debate about the relative activity of PPG in the Dry Valleys. Sugden (1995) and Marchant (2002) propose that PPG surfaces in the Dry Valleys have been stable for millions of years, while Sletten et al. (2003) suggest that PPG surfaces in the Dry Valleys show evidence of growth and resurfacing.

The two field locations represent two distinct ages of PPG surfacing. Victoria Valley is considered to be "young" with underdeveloped PPG surface expressions (low topography and smaller dimensions of the polygonal networks measured from centre to centre) while Beacon Valley exhibits "old" mature and well formed polygonal networks (Sletten et al. 2003). The PPG areas were selected to evaluate the subsurface resolution of features through the progression from "young" to "old" polygonal

patterned ground. Refer Figure 7 for a comparison of polygonal cross-sectional profiles from the two field locations and field site descriptions following.

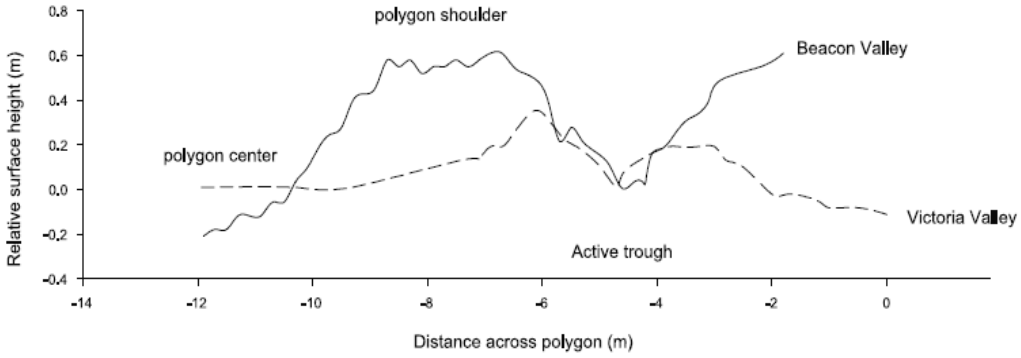

Figure 7: Surveyed topographic profiles of Victoria Valley PPG vs. Beacon Valley PPG. Note how Beacon Valley PPG shows a further developed ridge structure with more extreme topography associated with PPG processes. (Sletten et al. 2003)

Debate continues over the exact ages of the PPG surfaces in Victoria and Beacon Valley. Estimates for the ages of Victoria Valley are of the order of 10^4 years while Beacon Valley ages are on the timescale of 10^6 years.

Glacial history interpretations of the Dry Valleys use surfaces to produce ages for the advance and retreat of glacial movements through these areas. Interpretations of these surfaces are important for interpretations of glacial history.

Controversy over the age of PPG in the Dry Valleys is most evident in the interpretation of Beacon Valley PPG. Marchant et al. (2002) describes the PPG found there to be sublimation driven due to ice mass loss from an identified buried massive ice body (granite drift reference). Within the PPG of Beacon Valley is a subsurface tephra layer that has produced radiocarbon dates of circa 8 Ma. This tephra layer is recorded as being <1 m beneath the subsurface and relatively continuous across the areas studied in Beacon Valley (Marchant et al. 2002). If this tephra layer is *in situ* and not reworked it can be used to confidently date the age of the formation of the surface; if not then there is no confident age constraint on the PPG in Beacon Valley. Sletten et al. (2003) discuss the PPG processes in relation to the time required for these processes to rework the surface of a permafrost area and interpret Beacon Valley

PPG as actively reforming thus limiting the age of the surface at 1 – 2 million years. If the surface is actively re-forming then the tephra layer can not be considered to be a stratigraphic marker and any age associated with it cannot be used as a minimum age for the underlying buried massive ice body found within Beacon Valley. Hence the *activity* of the PPG is central to the question of PPG age in Beacon Valley.

2.1.2 Additional factors for geophysical surveying of polygonal patterned ground in the Dry Valleys.

2.1.2.1 Delicate environment:

The McMurdo Dry Valleys are classed as an Antarctic Specially Managed Area (ASMA) with areas within the ASMA additionally identified as Antarctica Specially Protected Areas (ASPA). As such work conducted in the Dry Valleys undergoes strict environmental screening before permission to conduct the research is granted. All work conducted in the Dry Valleys must class their environmental impact as minimal and transitory. Classification of what is transitory impact is sometimes difficult in the Dry Valleys as environmental response times appear to be significantly longer than elsewhere in the world. This is most likely due to the lack of biological activity and cold short summer period reducing seasonality effects. Wind is a predominant re-working tool in the Dry Valleys but is only superficial in its effects. Significant subsurface disturbance such as trenching and drilling must have large scientific benefits to justify permission to be conducted in the Dry Valleys. As such the potential application of near surface geophysics to the identification of subsurface structures in the Dry Valleys is an issue which may provide a means of gathering additional subsurface information while limiting the disturbance of the environment. This thesis represents one possible ongoing application of these techniques in the Dry Valleys environment as a means of gathering subsurface data.

2.1.2.2 Mars Analogue:

The arid conditions within the Dry Valleys environmental regime are consistent with what is known of the Martian surface. Satellite images of Martian surfaces show the presence of PPG. Mellon et al. (2008) discus the polygonal patterned ground

identified on Martian surfaces at the Phoenix landing site using the High Resolution Imaging Science Experiment (HiRISE) program. Images from Mars show clearly formed polygonal patterned ground suggesting the presence of ice rich permafrost beneath the surface.

2.1.2.3 Climate Change:

Antarctica's polar position makes it a hub for many global systems. For example, atmospheric circulation cells transfer heat and moisture from the equator to the poles ending in a permanent high pressure system over Antarctica, and the thermohaline conveyor belt global oceanic current is driven by the generation of Antarctic Bottom Water beneath the Antarctic sea ice and ice shelves. This combined with the relative lack of anthropogenic influences make monitoring changes in Antarctica a good way of monitoring human influences on Earth global systems. In Antarctica, the PPG is directly coupled with the atmosphere (Doran et al. 2002) due to the lack of overlying vegetation cover and isolation from anthropogenic influences on local conditions. Monitoring of PPG processes can thus be used as another tool for monitoring climate change.

2.1.2.4 Buried Massive Ice:

Buried massive ice bodies are documented in most glacial environments and are often a by-product of glacial advance and retreat. Sublimation of buried massive ice bodies can cause depressions at the surface and change the thermal regime of the subsurface in the immediate vicinity of the body. The effect on PPG in the area of buried massive ice bodies in permafrost has not been studied in detail. Marchant et al. (2002) suggest that the surface expression of PPG in areas of Beacon Valley are formed by sublimation of an underlying buried massive ice body without thermal contraction and expansion deforming subsurface horizons. The use of near surface geophysics in this area to help determine sub-surface structure of PPG overlying the buried massive ice body in question will provide additional subsurface data to help resolve this issue.
In general, greater examination of the relationships between buried massive ice bodies and the PPG surface expression may allow for identification of underlying and previously unknown buried massive ice bodies from PPG characteristics. This will

add a means of collecting additional information to glacial history interpretations and help with identifying future water sources on Mars.

2.2 Victoria Valley:

Victoria Valley is one of the three main valleys in the Dry Valleys and has the Victoria Glacier feeding into its Western extent (Figure 8 a.). The Victoria Valley is the northern-most of the Dry Valleys; valley floor elevations in our general field area ranged from 380m (ASL) near Lake Vida to 436m (ASL) at the foot of the Victoria Glacier.

2.2.1 Specific characteristics

The polygonal patterned ground found within Victoria Valley contained two distinct morphologies, one moderately developed with defined ridge and depressed centre geometries, and the other exhibited little to no ridge/crack relief. The moderately developed polygonal ground showed a larger range of clast sizes distributed at the surface with lateral sorting evident moving from coarser/larger clasts on the ridges to finer/smaller clasts within the depressed centre. The lateral sorting may be the result of freeze thaw frost heave processes or may simply be the result of katabatic wind sorting. The PPG surface did exhibit armouring where coarse clasts are concentrated at the surface as fine particles are removed by wind action thus protecting the underlying finer material. Polished sides to surface clasts that extended above the surrounding material were observed indicating the "sand-blasting" effect often associated with the formation of ventifacts in high wind environments such as the Dry Valleys during katabatic events.

2.2.2Field work location and environmental factors.

The field camp for K054 was located in the floor of Victoria Valley at approximately E 161º 37.273' S 77º 20.219 in close proximity to the eastern toe of the Victoria upper lake as a water supply. The relatively low elevations and northerly location makes Victoria Valley environmental conditions to be relatively mild with summer

a.

b.

Figure 8: Views of Victoria Valley field locations a. above shows a ground photograph looking west towards Victoria Glacier which flows down from the East Antarctic Ice Sheet. Note the low topography of the PPG with Snow settling in the PPG depressions b., below shows an aerial view of the field site with X and Y marking the locations of VVP1 and VVP2 respectively. The PPG seen from this aerial view are approximately 8 – 15m from centre to centre.

temperatures during our field season ranging from -11 to +6 degrees Celsius (field observations November/December 2006) Working conditions were mostly good with delays due to weather only occurring on one day due to low visibility (refer appendix 1 logistics report and activity log K054).

2. 3 Beacon Valley:

Beacon Valley is located at the southern end and in the inland reaches of the McMurdo Dry Valleys (Figure 5). Beacon Valley has the Mullins and Friedman debris covered glaciers feeding into the southern end of the valley while the northern end of the valley is dammed by the junction of the Turnabout and Taylor Glaciers.

2.3.1 Specific characteristics:

The Granite Drift and associated buried massive ice body found at the field site are suggested to be the result of a collision between those glaciers during the last glacial maximum when they extended down and into the main body of Beacon Valley (ref). The altitude of Beacon Valley is much higher than Victoria Valley with Beacon Valley floor occurring at an elevation of 930 m at the northern end and up to 1400 m at the southern end of the valley. The valley sides and surrounding mountain topography extends on average another 1000 m above the valley floor and reaches spot heights of > 2500 m (near Friedman Valley at the south end of Beacon Valley). From the valley floor the edges of the East Antarctic Ice sheet can be seen topping the valley sides. The proximity of the EAIS affected the weather conditions found within Beacon Valley with significantly stronger winds directed along the valley from the EAIS. The PPG observed in Beacon Valley exhibited high relief with well defined ridge/crack and depressed centre geometries.

2.3.2 Field work location and environmental factors.

The field location in Beacon Valley was placed in the centre of the valley floor on an area with a greater concentration of lighter coloured granite boulders previously identified as the “granite drift” (Sugden, 1965). The field camp was located at E 160º 35.737 S 77º 50.851. The weather conditions found in Beacon Valley were more marginal than Victoria Valley for working, with significantly colder temperatures and stronger winds. Batteries used for the surveys held less charge resulting in logistical issues surrounding the completion of the work within set timeframes. Time-lapse

surveying was not possible in Beacon Valley due to the loss of a team member to injury, but the unpredictable lengths of time required to complete one methodology survey in Beacon Valley would have made a systematic time-lapse survey difficult regardless.

Figure 9 views of Beacon Valley field sites: A. above shows a view from our campsite (refer text for specific locations) towards Taylor glacier which dams the northern end of the Valley. Note the rougher topography and coarser ground cover. B, below shows an aerial view of the PPG in Beacon Valley. The PPG is approximately 15 – 20m from centre to centre of the PPG.

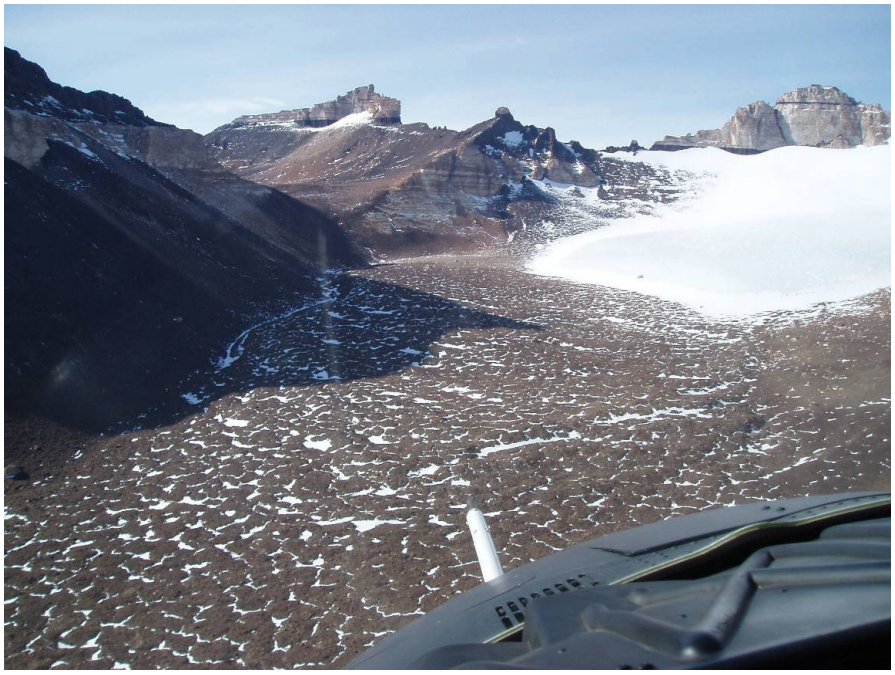

2.4 Polygonal ground survey areas: identification and specifics

In total four areas of PPG were surveyed over the course of our 8 week field season. K054 also conducted cross-valley transects in conjunction with this PPG work, which will be referred to in the discussion of the results. The four areas of PPG range from "young" and immature PPG in Victoria Valley to "old" and developed PPG in Beacon. Two PPG areas were surveyed at each valley location: VVP1 and VVP2 represent the Victoria Valley PPG areas while BVP1 and BVP2 represent the Beacon Valley PPG areas. The specifics of the PPG survey areas and reasoning behind their selection is outlined in the following sections.

2.4.1 VVP1:

VVP1 was a low relief polygon exhibiting immature and underdeveloped ridge and crack morphology. The survey area covered 20 x 24 m with the co-ordinates of the four corners being; NE corner E161º 37148 S 77º 20.225, NW corner 161º 37.087 S 77º 20.222, SE corner E 161º 37.135 S 77º 20.236, SW corner E 161º 37.076 S 77º 20.238. The relief of VVP1 was limited to 0.2 - 0.3 m topography on the crack and ridge geometries. The polygons in this PPG area have a smaller diameter than surrounding PPG; with distance between polygon centres being only 6 - 8 m. Four distinct polygons were included in this area with the crack and ridges created an intersecting cross in the centre of this PPG area. A plan of the PPG area for VVP1 is shown in Figure 9, marking the locations within the survey grid of ridges and cracks. At the surface the PPG soil composition exhibited a large range of grain sizes from fine sands to large cobbles. The soils appeared to have a vertical sorting with larger clasts being concentrated at the surface, probably as a result of secondary sorting due to removal of fine compositions from the surface by wind action. The clasts at the surface reflected the local source rocks of fine grain limestone, fine grain quartzose sandstone and basalt (Figure 10b.) These clasts were polished on the faces that were exposed to the wind. The concentrations of large clast sizes at the surface and polished clast faces give the impression of armouring of the soil surface. This feature was observed throughout the Dry Valleys.

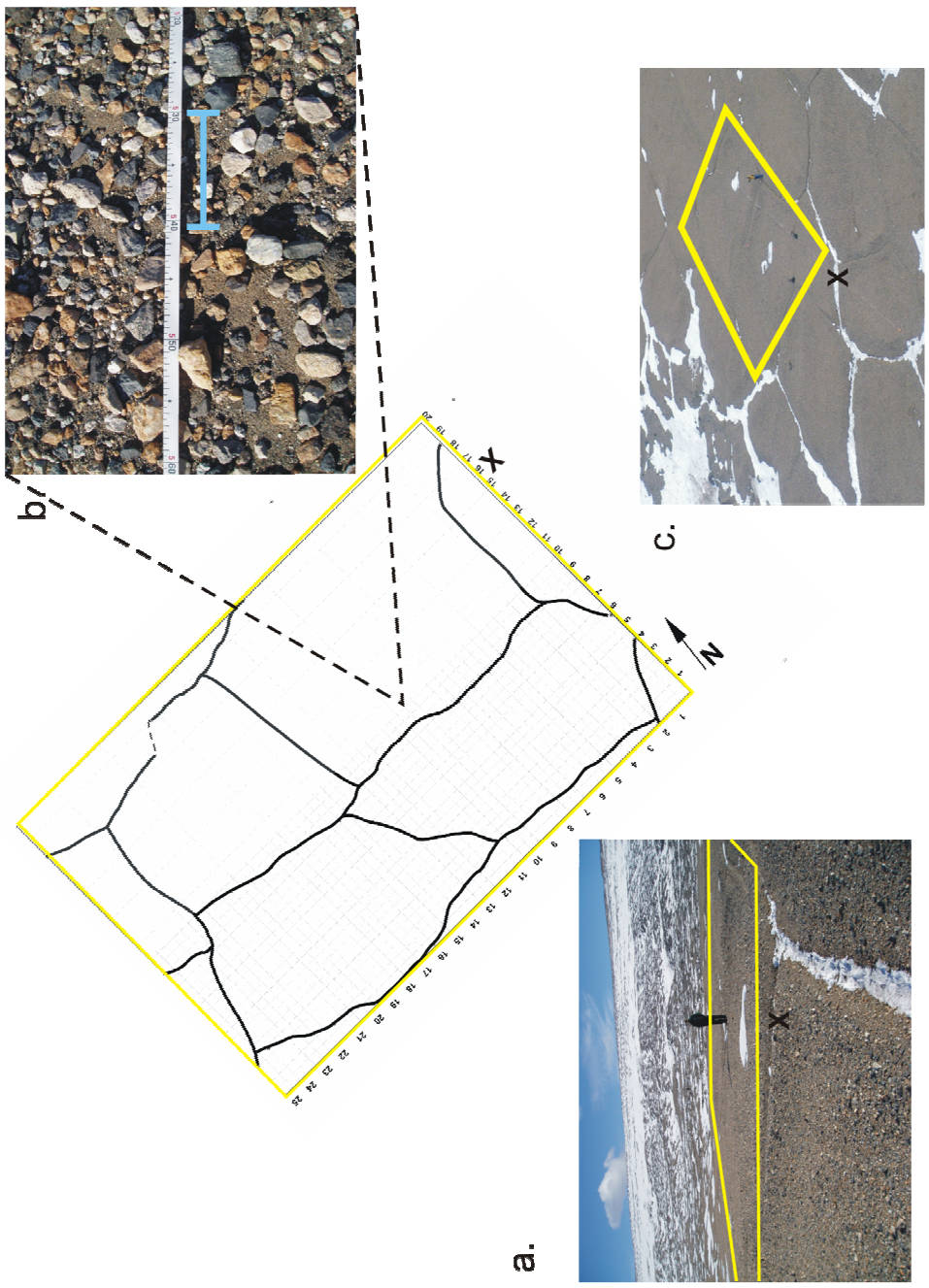

Figure 10: A plan of the crack networks found within survey area VVP1. Note the four intersecting cracks that meet in the centre of this survey area. a) Shows a ground view of the PPG area note the limited surface relief (the Figure in the picture is 1.9m tall) b) shows the composition and clast size of the surface cover from marked location. This composition was consistent over the whole of the PPG survey area c) shows an aerial view of the survey area. X marks the position of photographs.

2.4.2 VVP2:

VVP2 was located in the moderately developed PPG on the floor of Victoria Valley. It exhibited moderately defined ridge and crack morphologies with relief within the survey area being between 0.5 – 0.75 m. The surface expression of the cracks were approximately 0.2 m across and showed a concentration of large clasts (generally elongate 0.1 - 0.2 m long axis length) infilling the crack. The associated ridges were well developed and encircled the corresponding depressed centre of the PPG area. The area was 20 x 12 m with the perimeter extending between these co-ordinates: NE corner E 161º 37.281 S º 77 20.159, NW corner E 161 º 37.253 S º 77 20.157, SE corner E 161 º 37.272 S º 77 20.169, SW corner E 161 º 37.243 S º 77 20.166 Figure 11 below shows the topographic data collected for correcting the geophysical data displayed in surface form to illustrate the morphology and geometry of VVP2.

The composition of the clasts was the same as found within VVP1, but larger clast sizes with clasts up to 0.3 m rough diameter was found on the surface and the presence of a large boulder (0.75 m rough diameter) within the survey area. This indicates the same source rocks for these soils but reflects either a lower amount of primary sorting of the rocks before PPG processes, or that the advanced PPG processes have resulted in larger clasts at the surface of VVP2. The presence of the boulder on VVP2 suggests the first explanation as it is unlikely that PPG processes would be able to exert any effective motion on a rock so large. The effective differences within the grain size ranges may be a contributing factor towards the limited relief and final geometry of VVP1 vs. VVP2. The distribution of the clasts within the PPG area of VVP2 ranged from larger clast sizes concentrated on the ridges to smaller clast sizes found within the depressed centre of the polygon (Figure 11 c. and d.) probably as a result of gravity movements and secondary deposition of smaller clasts by katabatic winds during the winter months.

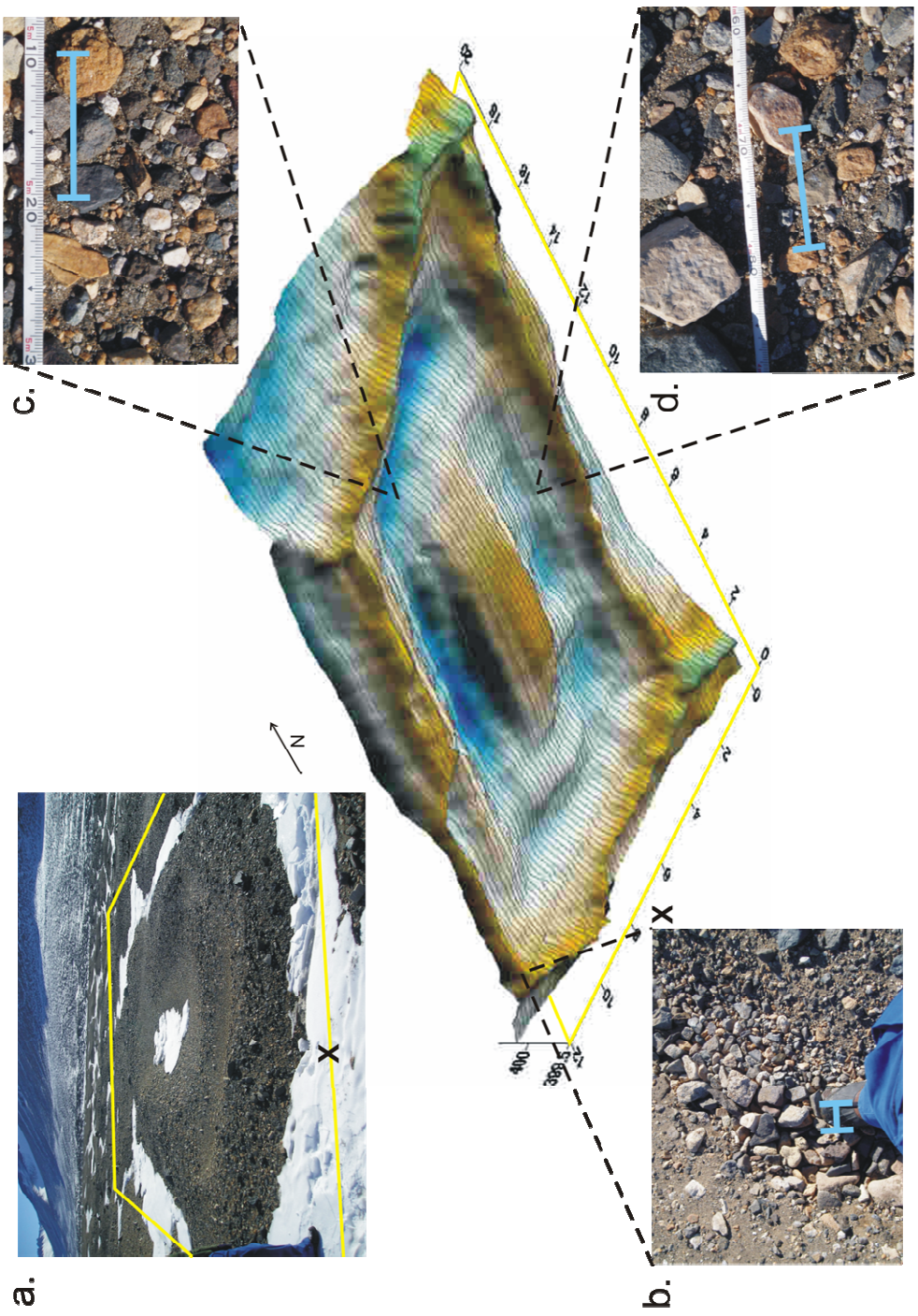

Figure 11: The topography and morphology of VVP2 survey area is shown in the surface displayed at the centre of this Figure. Topography displays raised edges and a relatively depressed centre. a.) shows the view of VVP2 survey area from position X. b.) The clast compositions found within the surface expression of the cracks note the coarse clast sizes and rudimentary sorting. The surface expression of the cracks shows high concentrations of large clast sizes. c.) clast compositions and sizes found within the depressed centre of the survey area. d.) raised ridge clast composition is much coarser and exhibits less sorting. Blue scale bars represent 10cm increments.

2.4.3 BVP1:

The co-ordinates of the survey area are: NE corner E 160º 36.435 S 77º 50.999, NW corner E 160º 36.399 S 77º 50.994, SE corner E 160º 36.420 S 77º 51.004, SW corner E 160º 36.385 S 77º 51.000. BVP1 was of moderate to high surface relief and of a slightly irregular geometry with ridges not consistent with the classic polygon described in theoretical developments of PPG (Figure12). The survey area was 18 x 12 m and was located on the rim of a large depression approximately 75 m diameter. This depression may represent sublimation of the underlying buried massive ice body. The ground surface material exhibited intense iron staining creating a red brown landscape. The staining on the rocks seen at the surface made identification of the lithological composition difficult. Granites, granodiorites and beacon sandstones were identified in the survey areas. The ground material exhibited a range of clast sizes from fine sands to large boulders with larger clast sizes being concentrated at the surface. As seen in VVP2 there was sorting of the clast sizes across the polygon structure with smaller clasts being found within the depressed centre of the polygonal structure (Figure 12 b. – e.)

2.4.4 BVP2

BVP2 was a high relief "doughnut" geometry polygon with well defined crack and ridge morphology (Figure 13). The area of the survey was 20 x 23 m extending around the perimeter described by these GPS co-ordinates: NE corner E 160º 35.714 S 77º 50.903, NW corner E 160º 35.668 S 77º 50.900, SE corner E 160º 35.693 S 77º 50.915, SW corner 160º 35.649 S 77º 50.911. The composition and sorting was similar to BVP1 with the addition of a large boulder in the south west corner. Survey lines that ran over the top of this boulder were excluded from the GPR for logistical reasons. BVP2 displayed evidence of disturbance at the surface from possible previous studies. The disturbance was noted on the eastern ridge surrounding the depressed centre of the polygonal structure and along the northern ridge face. Examination of the disturbed subsurface area can be found within the results and discussion chapters of this thesis.

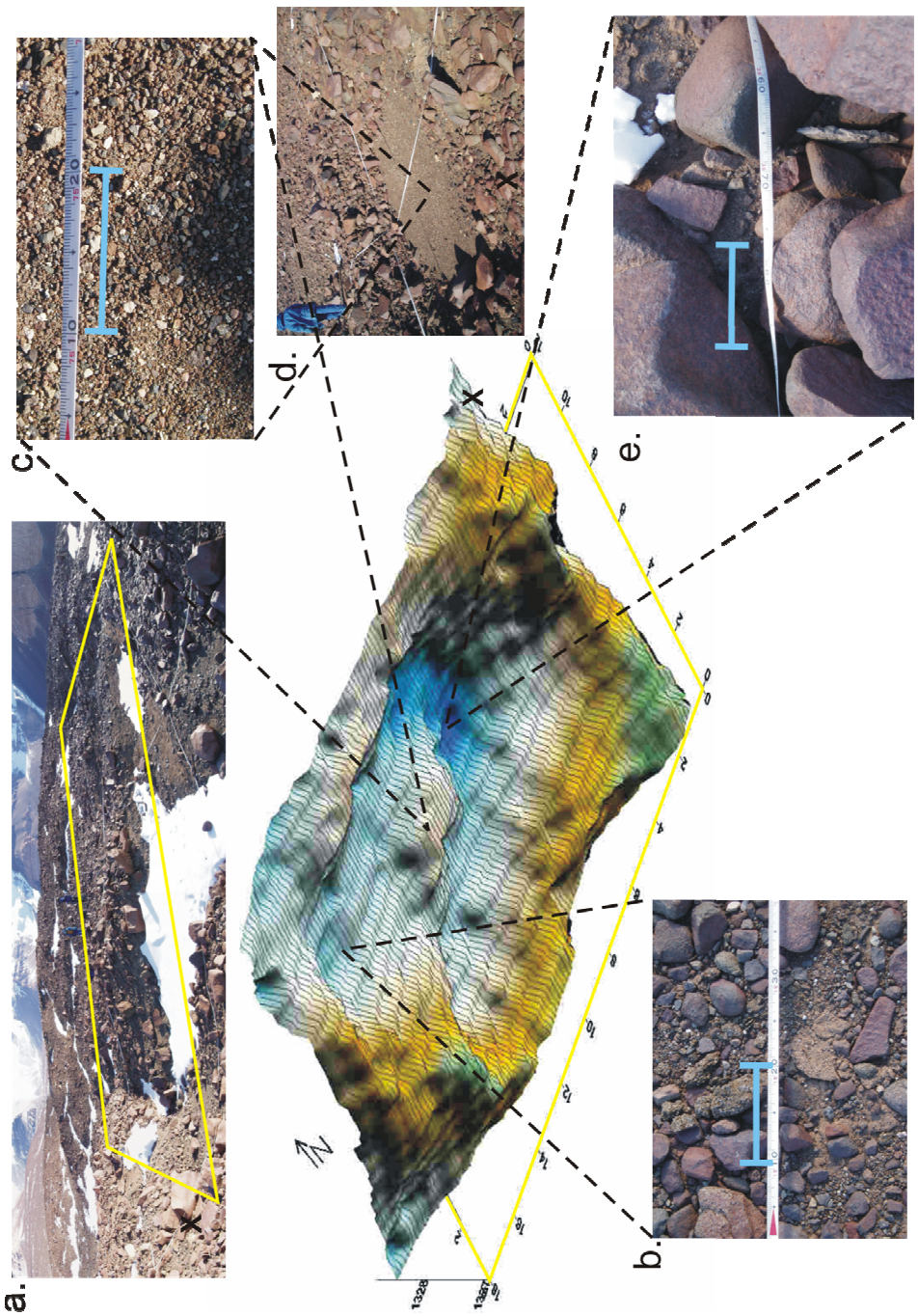

Figure 12: representation of the topography found in BVP1 survey area. a.) ground view of BVP1 survey area outlined in yellow from location X b.) Clast composition found on ridge. c.) composition of clasts found within depressed centre, moderately well sorted. d.) ground view of depressed centre in BVP1. e.) clast composition of raised ridge. Blue scale bars represent 10cm.

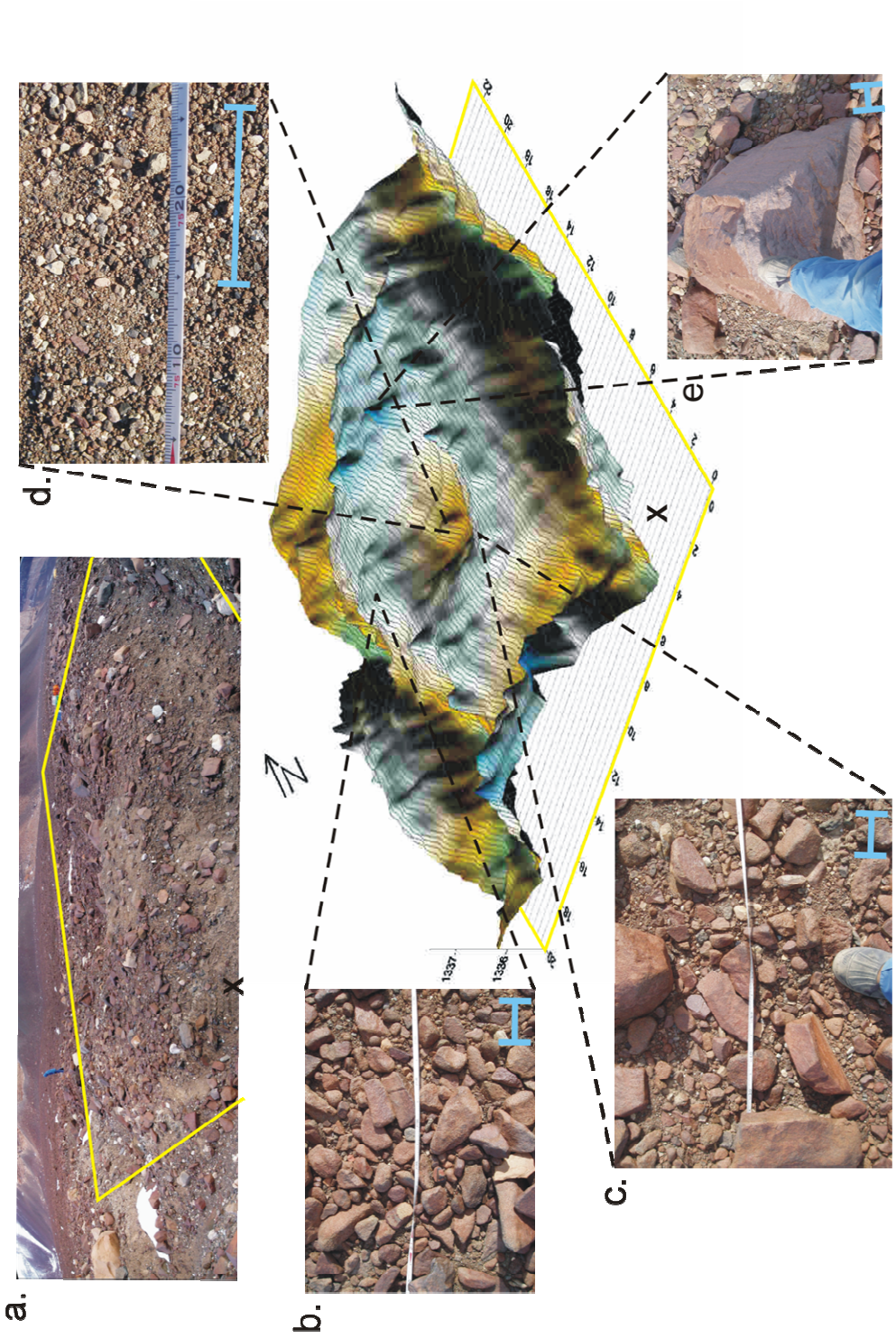

Figure 13: representation of the surface topography found in BVP2 survey area a.) Shows ground view of survey area outlined in yellow from position X b.) Clast compositions found on raised ridges showing interlocking "armoured" surface or large clasts c.) Ridge clast compositions large sizes poorly sorted d.) Depressed centre contains moderately well sorted pebble grains e.) One of several large boulders found within survey area. Blue scale bars represent 10cm.

3: Near Surface Geophysics

This chapter will cover the basics of near surface geophysical techniques, theory and practise, so that the results and discussion presented here can be considered in context. Appropriate targets and the sensitivity of each method are discussed from a theoretical standpoint in the geophysical principles subsection. For a practical evaluation of the methods used in this research please refer to the methodology chapter.

3.1 Basic Geophysical principles:

Near surface geophysics is the use of techniques that measure the changes in subsurface physical properties within the Earth's upper surface (100 m or so depending on the specifics of the method). Measuring these properties may involve putting a current into the Earth's surface to measure electrical response, or may involve the propagation of a wave through the material, or may be related to creating a secondary magnetic field. The response from the subsurface is measured and recorded and is related to the physical properties of the underlying material.

The important physical properties that need to be understood for the use of near surface geophysics are:

Dielectric permittivity: (ε) is an electrical property that is related to the propagation of electromagnetic energy through a material and relates to the dielectric charge found at the atomic level. Often the dimensionless relative dielectric permittivity (ε_r) is used. This property depends on the ability of molecules or atoms to be electrically polarised (Musset and Kahn 2000); this affects the material's ability to store charge and impede flow of a current through the material (Plewes and Hubbard 2001). The velocity of an electromagnetic wave (essentially a light wave (m/ns)) will be affected by this property. This property is most relevant to GPR methods.

Electrical conductivity: (σ) in siemens/meter (S/m) (inversely related to electrical resistivity (ρ) in ohm-meters (Ω/m)) is a measure of the ability of an electrical current to pass through a given volume of material. Electrical conductivity can be related to clay or water content within a subsurface lithology. Resistivity and electromagnetic methodologies are most relevant to this property but this is also linked to dielectric permittivity and so can effect electromagnetic wave propagation.

Magnetic susceptibility: (k) dimensionless and relates to the ability of a material to amplify an external magnetic field. The magnetic susceptibility is directly related to the concentrations of magnetic minerals, such as iron, within the subsurface. Most relevant to magnetic methodologies. The magnetic permittivity (μ) can effect the velocity of electromagnetic waves.

Density: (ρ) the mass of a material in a given volume, measured in kilograms/cubic meter (kg/m^3). Density will effect the propagation of waves through a medium and changes in density will result in reflection and refraction of wave energies. ε_r is related to ρ and so this property can effect GPR propagation.

Different physical properties determine how energy will behave when interacting with subsurface materials. Each soil, lithology and rock type will have different physical properties depending on their individual geological parameters. Knowledge of how these physical properties relate back to geological parameters such as mineral compositions and water content can be used to image geological structures to great depth without physical invasion of the subsurface.

For geophysical methods there is an inverse relationship between resolution and depth of penetration. It is the physical properties that we target and responses that they invoke that use the geophysical energy as it travels through the subsurface. As the geophysical energy moves further away from its source more of it is used up in the subsurface which in turn reduces the strength of the geophysical response at greater depth.

The loss of energy that occurs with depth is referred to as *attenuation* and it reduces the measurable responses that enable us to interpret subsurface conditions. Attenuation relationships refer to an attenuation constant (α) defined by:

$$\alpha = \omega \{\mu_a \varepsilon_a [(1 + \sigma^2/\omega^2 \varepsilon_a^{\,2})^{1/2} - 1]/2\}^{1/2}$$

Where ω = angular frequency of the signal μ_a and ε_a = the absolute values of magnetic and electrical permittivity respectively and σ = conductivity (Milsom 2000)

It is important to note that when using geophysical methods that the data recorded relates to the physical properties and changes within these physical properties and may not directly correlate to changes within geological units. Ideally a drill hole or trench would be used to correlate physical response to geological units, but multiple techniques can also allow for greater control on geological interpretations.

Geophysical methodology has developed a number of ways to measure specific physical properties. The methods used in this research were ground penetrating radar (GPR), electrical resistivity tomography, and electromagnetic surveying.

3.2 Ground Penetrating Radar:

Ground penetrating RADAR (radio wave detection and ranging) is a wave propagation geophysical method used to resolve physical property changes within the subsurface by measuring two-way travel time of the reflected radar energy.

The energy used in GPR is electromagnetic containing a co-joined oscillating electrical and magnetic field which have the following relationship:

$$V = f \lambda$$

Frequency (f) is inversely proportional to wavelength (λ) and the velocity (v) of the wave. In a vacuum the velocity of the wave is the speed of light (c), in ground materials it is less due to the electrical properties found within those materials. The

velocity of the wave through the ground is directly linked to the relative dielectric permittivity such that:

$$V = \frac{c}{\sqrt{(\varepsilon_r \mu_r)}}.$$

Since GPR waves are electromagnetic this relationship between electrical properties and velocity can affect the motion of the wave as it travels through the given material. This is commonly seen in increased attenuation of the signal through mediums with high conductivities. Table 1 shows the dielectric permittivity and conductivity in relation to the resulting electromagnetic wave velocity.

Material	ε_r	σ (mS/m)	v (m/ns) electromagnetic wave
Air	1	0	0.3
Fresh water	80	0.01	0.033
Dry sand	3 – 5	0.01	0.15
Saturated sand	20 – 30	0.01 – 1.0	0.06
Limestone	4 – 8	0.5 – 2	0.12
Silts	5 – 30	1 – 100	0.07
Clays	5 – 40	2 – 1000	0.06
Granite	4 – 6	0.01 – 1.0	0.13
Ice	3 – 4	0.01	0.16

Table 1 Modified from Annan and Cosway 1992, and Milsom 2000, showing typical physical property values for some common materials relevant to applied geophysical methodologies.

GPR electromagnetic waves are commonly between 25 MHz to 1 or 2 GHz in frequency. The frequency values describe the central frequency (f_c), as electromagnetic energy for GPR may be +/- 50% of the central frequency i.e. a 100 MHz signal will include electromagnetic energy down to 50 MHz and up to 150 MHz.

Electromagnetic waves are subject to reflection (where signal is "bounced" back towards the surface) and refraction (where signal is "pushed" deeper into the

subsurface) when travelling through a boundary where the physical properties of the two media are different (Halliday et al. 2002). It is reflection from buried boundaries that allows GPR to be used to create a subsurface profile of the physical properties which may be interpreted for geological information. Figure 14 shows how wave reflection and refraction as utilised in GPR.

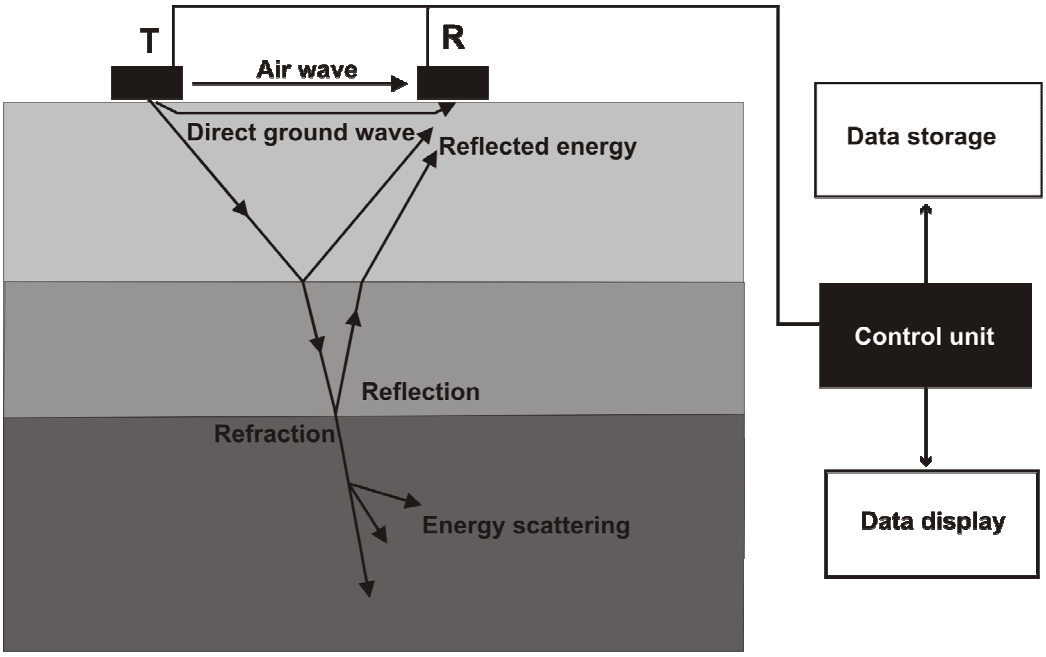

Figure 14: GPR technique summarized: The transmitter (T) generates a pulse of electromagnetic energy that propagates to depth. Where boundaries between differing physical properties occur the energy is reflected to the surface and refracted to greater depth. Air wave, direct wave and reflected wave responses are detected by the receiver (R). The general survey parameters such as, stacking and time windows are controlled by a central unit which will also amplify and digitise the reflected signal to be saved and stored, or displayed. Modified Davis and Annan (1989), Reynolds (1997) Milsom (2000).

Reflection and refraction is generated at a boundary representing a change in properties. Signal reflected back towards the receiver is amplified digitised and stored (Davis and Annan 1989).

The travel time of the reflected wave can be used as a proxy for depth of the reflector and the nature of the reflected wave can be used to determine relative physical properties of the boundary. The relative physical properties on either side of the boundary will determine if the reflected wave will undergo a phase change whereby

the reflected wave is rotated to a different orientation from the transmitted wave (Halliday et al. 2002).

Deeper reflections take more time to travel the wave path back to the receiver at the surface. The time taken to travel the reflected wave path is called the two-way-travel time. GPR traces plot the two-way-travel time and wave form of the reflected electromagnetic wave. The subsurface velocity can be used to convert two-way-travel time to accurate depth placements for a reflective boundary. Multiple GPR traces along a line can be used to create a profile cross-section of the subsurface.

The step increments at which the antennas are moved along a line must not exceed the nyquist sampling interval to avoid under-sampling and allow proper resolution of the subsurface feature targeted.

$$Nx = c / (4f \sqrt{\varepsilon_r}) = 75 / (f \sqrt{\varepsilon_r}) \qquad \text{(in m)}$$

where c is the speed of light, f is the antenna centre frequency in MHz and ε_r is the relative permittivity of the host material.

As multiple traces from different step positions are collected, linear or planar reflectors within the subsurface display as lines, and point source reflectors plot as diffraction curves (Figure 15). The true dip of angled reflectors may need to be corrected for and diffraction curves may be collapsed to represent the original source geometry by using migration and a known velocity for the subsurface.

Velocity can be measured in the laboratory or common mid point (CMP) surveys can be completed and analysed in the field. CMP surveys involve the transmitter and receiver being moved apart at a constant step size (Figure 16a). Theoretically, to determine velocity CMP surveys assume a regularly increasing two-way-travel time from a single reflective source in the subsurface. Velocity is determined from the gradient of the line formed by the increasing two-way-travel time as wave path is increased.

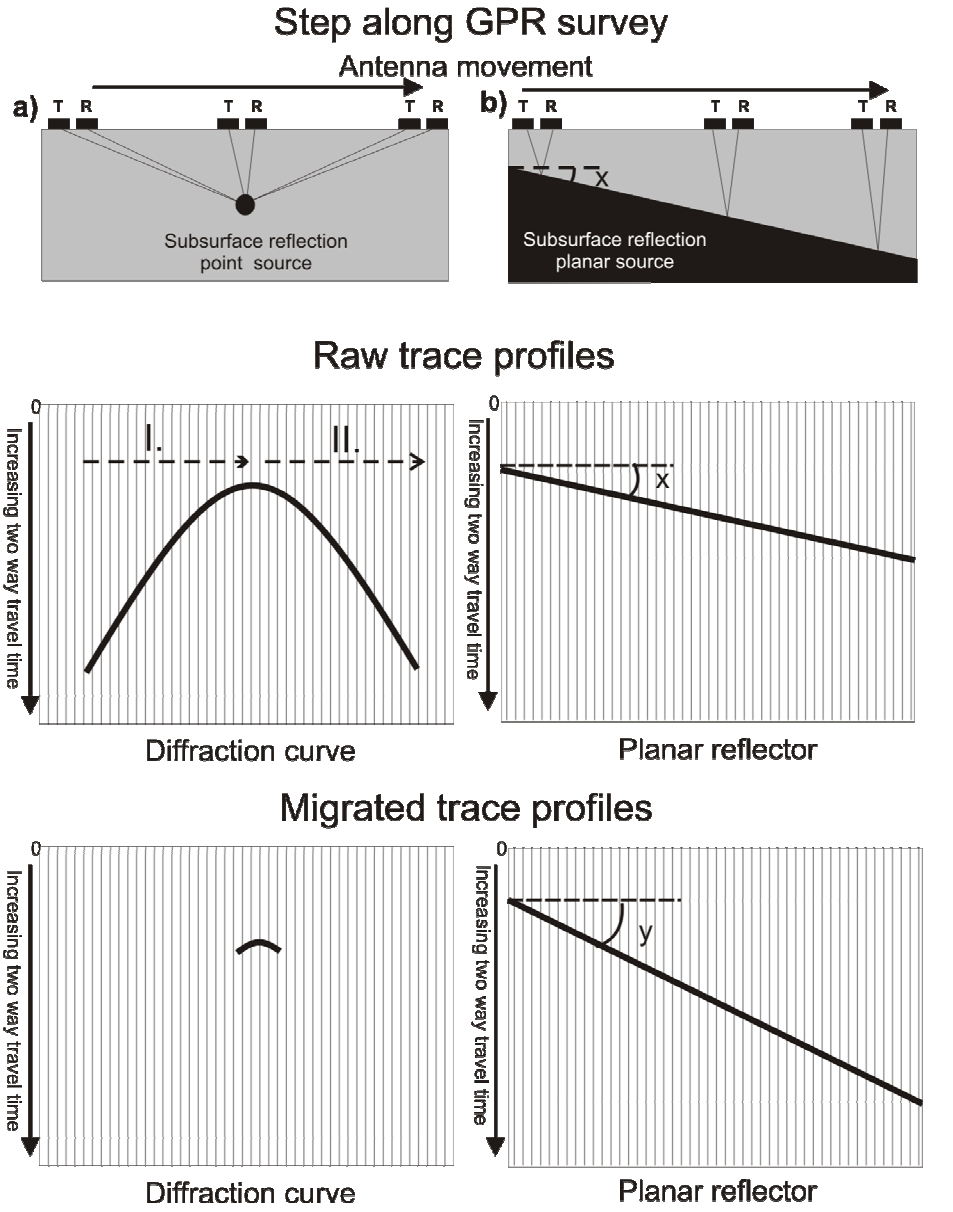

Figure 15: The generation of reflection profiles with diffraction curves and linear features from the transmitter (T) and receiver (R) being moved across the subsurface feature. a) The decreasing (I.) then increasing (II.) travel time of the reflected wave as the antennas move over a point source creates a curve called a diffraction curve. If the correct velocity is known this curve can be collapsed to represent the original point source through the use of migration. b) dipping reflectors can plot with incorrect dip angles before migration with the correct subsurface velocity.

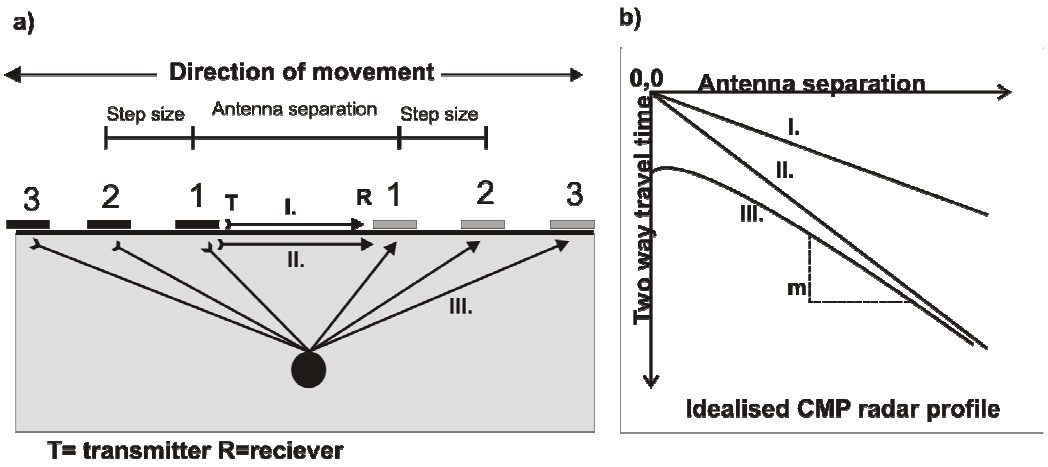

Figure 16: CMP step out geometry for collection of subsurface velocity data in the field. a) Antennas are stepped away from each other at a constant rate so that the increased distance the wave has to travel to reflect off appoint source is increased systematically b. shows an idealised resulting reflection profile where the relationship between antenna separation (and path length) is plotted against travel time between the antennas. CMP profiles show the arrival of the air wave (I.), the direct ground wave (II.) and the reflected wave (III.) Velocity of the events is determined by the gradient (m) of the wave path plots where antenna separation is divided by travel two-way-travel time (distance/time in m/s or m/ns).

3.3 Resistivity:

At its simplest, resistivity uses an array of electrodes to create a current (I) within a volume of ground and measure the resulting voltage (V).

Using Ohms law, resistance (R in ohms Ω) is:

$$R = V/I.$$

Resistivity (ρ) of a given volume is the resistance over the cross-sectional area (A) divided by the distance the current must travel (x) through the volume so that

$$\rho = AR/x \text{ in } \Omega.m$$

Due to the contact resistances of ground materials the application of these principles are not as simple as passing a current through electrodes planted in the ground and measuring the resulting voltage (Milsom 2000). To bypass the problem of contact resistances, multiple electrodes are arranged in an array which allows voltage to be measured separate from the induced current. This methodology does not measure resistivity directly but rather gives a value of the apparent resistivity (ρ_r). Apparent

resistivity is related to the average of all the resistivities down to a depth and the electrode spacing of the array so that:

$$\rho_r = K \Delta V/I$$

where ΔV is the voltage required to pass a current between two electrodes through a given medium, and K is a coefficient based on the geometry of the electrode arrangement used during the survey. The data collected in this thesis was collected using a Wenner array where electrodes are spaced evenly apart so that:

$$K= 2 \pi a$$

where "a" is the spacing between electrodes at the surface. As "a" increases so to does K which represents the relationship of ρ_r to depth.

Figure 17 shows the way a multiple electrode array using Wenner geometry would be used to measure the resistivity of the top layer of the ground surface. If the array contains sufficient electrodes, the electrical properties at greater depths may be surveyed by using non-adjacent electrodes, which is equivalent to increasing the electrode spacing.

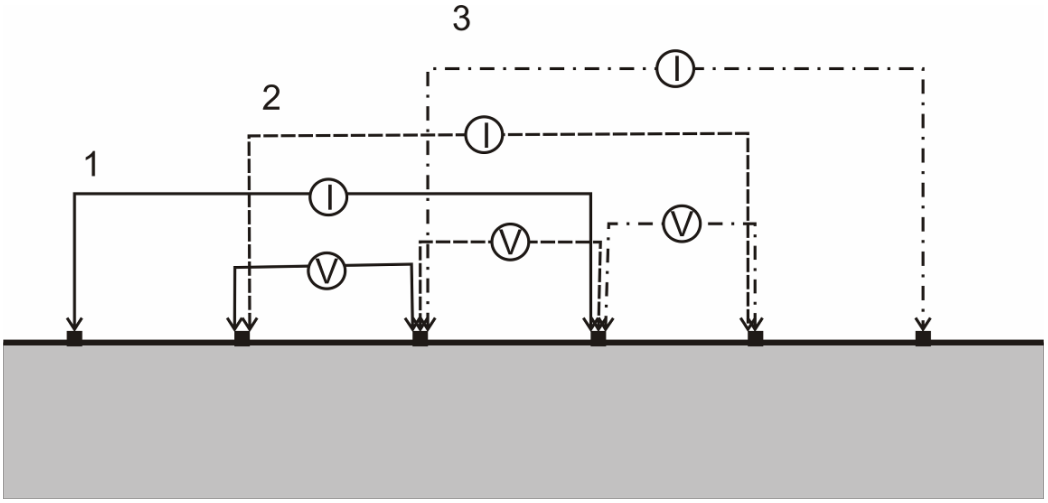

Figure 17: A single layer multi electrode Wenner array geometry showing the use of electrode arrays to take multiple resistivity readings. I represents current input and V; voltage measurements. Adjacent electrodes are used to the shallowest measurements and non-adjacent electrodes (where "a" is kept constant between the electrodes being used) are used to gather resistivity values for greater depth.

The overlapping measurements of multiple electrode arrays increase reliability of results. Reliability of the resistivities is least at the edges where resistivity values may rely on one measured value; subsequent analysis may produce edge effects in the resulting cross-sectional profile. Similarly, the reliability and resolution of resistivities is highest at the surface as deeper levels of resistivity will not have as many "overlapping" readings.

The apparent resistivity data can be converted into resistivity values using a mathematical inversion. The subsurface is divided into a number of rectangular blocks related to the electrode array configuration. A value of resistivity is assigned to each block to create a model of the subsurface that could result in the apparent resistivity values obtained during data collection and a profile of modelled resistivity is built up to create a "psuedosection". The profile of the modelled resistivity is called a psuedosection as it represents a theoretical model of the possible true resistivity values which would create the apparent resistivity measured at the surface. The mathematical inversion does not have a unique solution (Geotomo software, 2004).

With the exception of metallic bodies most ground materials have low conductivities (and therefore high resistivities) meaning that they impede the flow of electrons within their structure. Table 2 shows a comparison of resistive and conductive common subsurface materials.

In addition to the intrinsic resistivity values of the material are the influences of secondary resistivity/conductivity parameters. Archie's law states that resistivity is inversely proportional to fractional porosity raised to the power of a "shape factor", between 0.2 – 1.8. Real world resistivity measurements are mostly determined due to pore water concentrations as water is a relatively good conductor compared to most ground materials. As such, resistivity methods are sensitive to water content.

Table 2 Table of common resistivity values (from Milsom 2002)

Material	Resistivity (Ω.m)
Ore minerals:	
Pyrite	0.01 - 100
Magnetite	0.01 - 1000
Galena	0.001 – 100
Common ground materials:	
Gravels	100 - 600
Loose sand	500 – 5000
Granite/basalt	100 – 100,000
Quartzite	500 – 800,000
cf. Copper	0.0000000168

3.4 Electromagnetism (EM):

Electromagnetic fields are magnetic fields that are generated in response to a moving charge (electrical current) and vice versa. Figure 18 shows an example of how the secondary electromagnetic response is generated by a horizontal loop-loop electromagnetic technique as used in this research. Electromagnetic methods generate a primary magnetic field over the targeted subsurface by inducing current in the transmitter loop. This current in a loop produces a magnetic field which in turn creates currents within conductive bodies within the subsurface. For simplicity, the currents generated within a subsurface geological conductor will be referred to as eddy currents rather than examining the response in depth. These secondary eddies

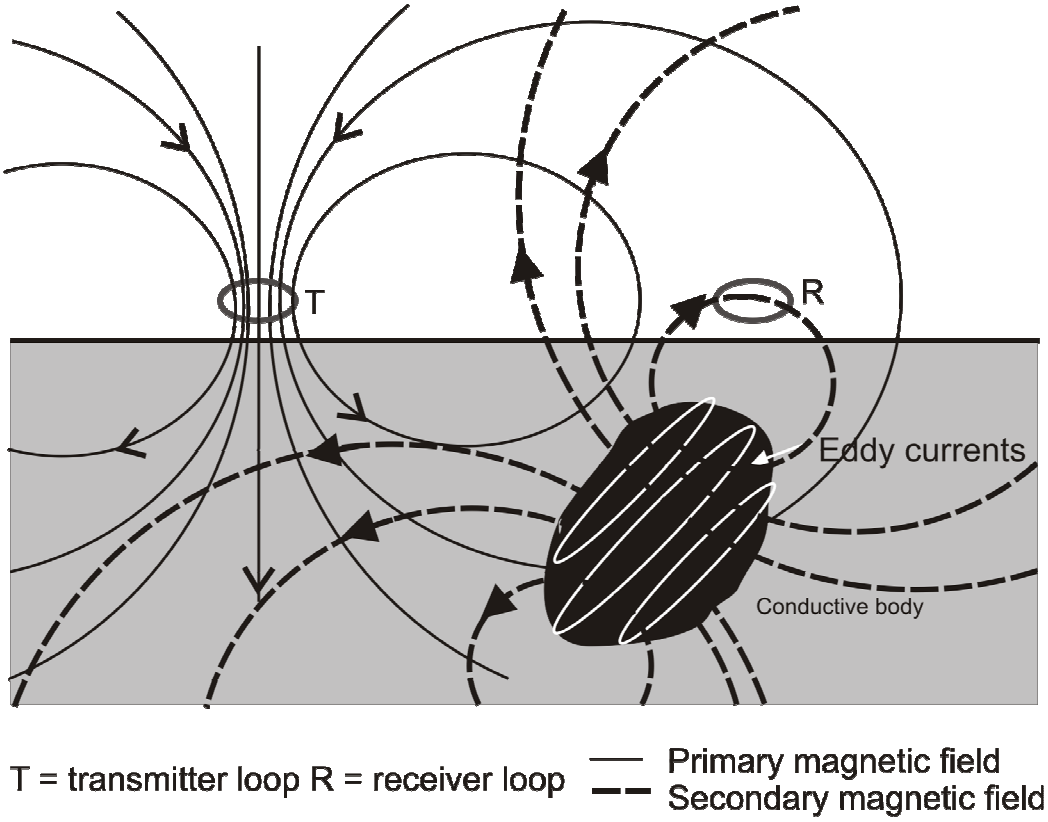

Figure 18: Electromagnetic generation of a secondary magnetic field using a primary magnetic field generated from current travelling through a conductive loop. The secondary magnetic field then generates a measurable current in the receiver loop which is recorded.

currents in turn generate a secondary magnetic field that induces a current in the receiver loop at the surface.

The induced response will differ in phase from the primary EM fields and measured EM data can be divided into in-phase (often referred to as real) and out of phase (often referred to as quadrature or imaginary). This is illustrated in Figure 19. Conductive bodies will exhibit a large in-phase response as phase is rotated towards 180˚ and as such, the real response is often used as a metal detector. Quadrature response has a linear relationship to conductivity (McNeill, 1983) and are more frequently used in geological interpretations as it is roughly proportional to conductivity when conductivities are generally low (Gibson and George 2003).

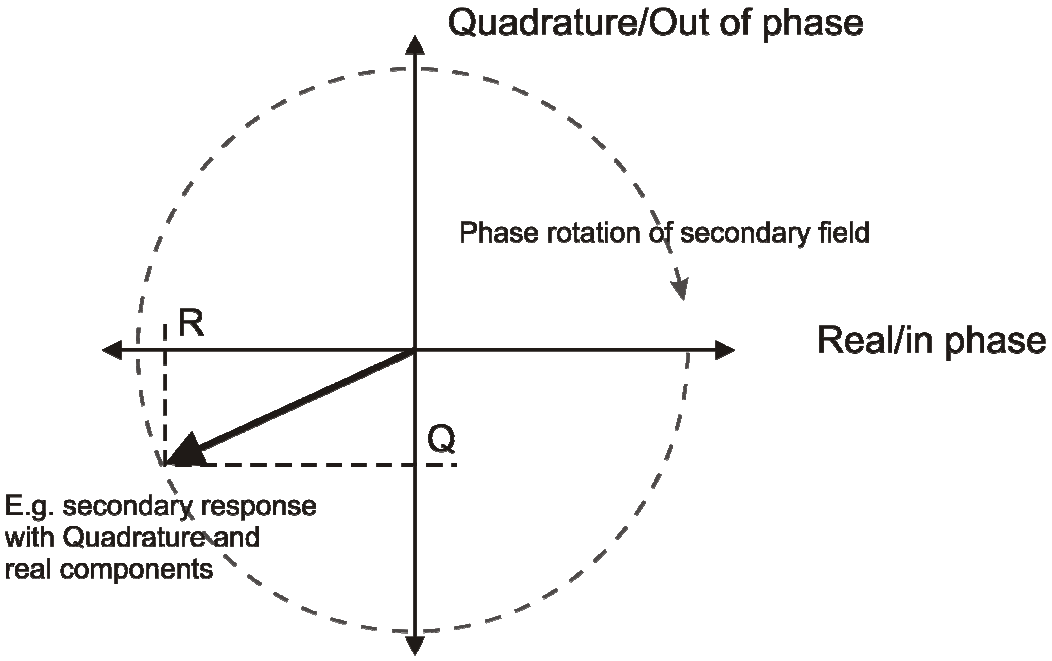

Figure 19: A possible secondary EM response showing a rotation in Phase with Quadrature and real components.

Maxwell's equations describe how the electromagnetic response is generated and the relationships between the strength of the magnetic field and magnitude of the induced current (conductivity) within the subsurface (Haliday et al. 2002). In general the more conductive a body is, the stronger the secondary magnetic field, as stronger electric currents are generated.

For high conductivities; penetration of signal using EM methods is often related to a "skin depth" which is the reciprocal of the attenuation constant (α refer previous) so that:

$$\text{Skin depth} = 1/\alpha$$

In most EM surveys conductivity values will limit the effect other parameters have on α calculation, simplifying the skin depth to:

$$\text{Skin depth} = 1/(\mu_a \sigma \omega)^{1/2}$$

In areas of low conductivities the depth of penetration of EM methods is roughly proportional to the loop separation so that:

$$\text{Depth of penetration} \approx 1.5 \times \text{loop separation}$$

4: Methodology:

4.1 General survey set up:

After identification of the target ice wedge polygon, four corners for the survey area were chosen and fixed using an optical square. Survey areas were oriented so that surveys requiring sequential lines would run roughly north-south. Line spacing refers to the common offset of these north-south lines along the east-west baseline.
GPS measurements of the location of each corner were taken at least twice over the course of a day to reduce error associated with low satellite coverage of a location. The satellite coverage in Antarctica is not optimal for GPS accuracy as it needs both numerous satellites and for them to be spread out across the sky. This inaccuracy was seen best in the elevation data which could vary by up to as much as 20m for one location.

Electromagnetism and GPR surveys were conducted over the entire polygon area, while electrical resistivity surveys were conducted as cross-sectional lines through the polygon and over features of interest.

4.1.1 Factors involved in working in the Dry Valleys:

The cold weather and rough terrain found within the Dry Valleys effects the efficiency of collecting geophysical data. Batteries used to power resistivity and GPR antennas and consoles as well as the EM31 laptop, held less capacity than they would have in temperate conditions. For the best use of our time in the field additional planning was needed so that battery shortages would not cause a delay in the work schedule.

Laptop chargers were adjusted so that laptops could be run off large capacity high voltage batteries. For EM31 the nearness of this battery for powering the recording laptop should be taken into account when evaluating the relative electrical properties from this data set.

The cold conditions affected the fibre optic cables used in GPR by making them brittle and prone to breakages. In particular the casing surrounding the fibre-optic cables was very sensitive to breakages in the cold and had to be monitored carefully. For resistivity, the relative battery power and time required to run resistivity surveys was such that 3D geometries were not practical in the Dry Valleys during our field season.

Due to the delicate nature of the Dry Valleys environment and the relative difficulty of trenching or drilling in glacial diamict material no ground truth measurements were obtained to correlate this data.

Appendix 1 is a modified logistics report collated for K054's field season in the Dry Valleys. The timeline for the data collection is outlined and the number of days required to complete each survey can be used as a guide for further research. Bad weather delays were minimal but injury to a party member caused re-assessment of the work achievable. Logistics issues surrounding the use of geophysical equipment are also noted there.

4.2 Topographic correction data:

One of the causes of error within geophysical methods is a lack of topographic correction which allows for the geophysical response to be corrected for variations in mass due to topography or displacement of reflected responses. The most detailed geophysical survey that was conducted as part of this project was the GPR with a line spacing of 0.5 m with the 200 MHz and 100 MHz surveys being offset by 0.25 m. For topographic measurements to run along each GPR line a 0.25 m grid was needed. This grid density was used for VVP2 but soon proved to be too labour intensive to be applied in Beacon Valley. As a result Beacon Valley topographic data was collected at 0.5 m x 0.5 m data density which corresponded to the 100 MHz and EM31 survey grid.

Please note that although the measurements for topography had to follow these lines they were not required to be the same as the GPR 0.1 m step size values along the line

as the program for processing this information is capable of inferring the missing values and the benefits of such high data density had to be weighed against the time constraints.

Resistivity surveys extended past the limitations of the GPR grid and additional topographic measurements were taken at each electrode along the North-South and East-West strings.

4.2.1 Data collection:

Using an optical level and staff, measurements were taken from a standard datum level above the polygon surface (Figure 20). The tripod for the optical level was set up outside the survey area and used to measure the points along the survey grid.

GPS elevation measurements were taken at the base of the optical level tri-pod (X on Figure 20) and used to correct staff measurements to topography in m ASL (above sea level)

As the topography on VVP1 was limited to relief of less than 0.3m it was decided that the topographic corrections were of minor importance due to minimal effect on the placement of reflectors within the profiles

4.2.2 Data processing:

Topographic information was manually entered into digital spreadsheets using Microsoft Excel, see Appendix II. The raw data was an inverted measurement from the staff height along a datum level set height above the ground surface (Figure 20).

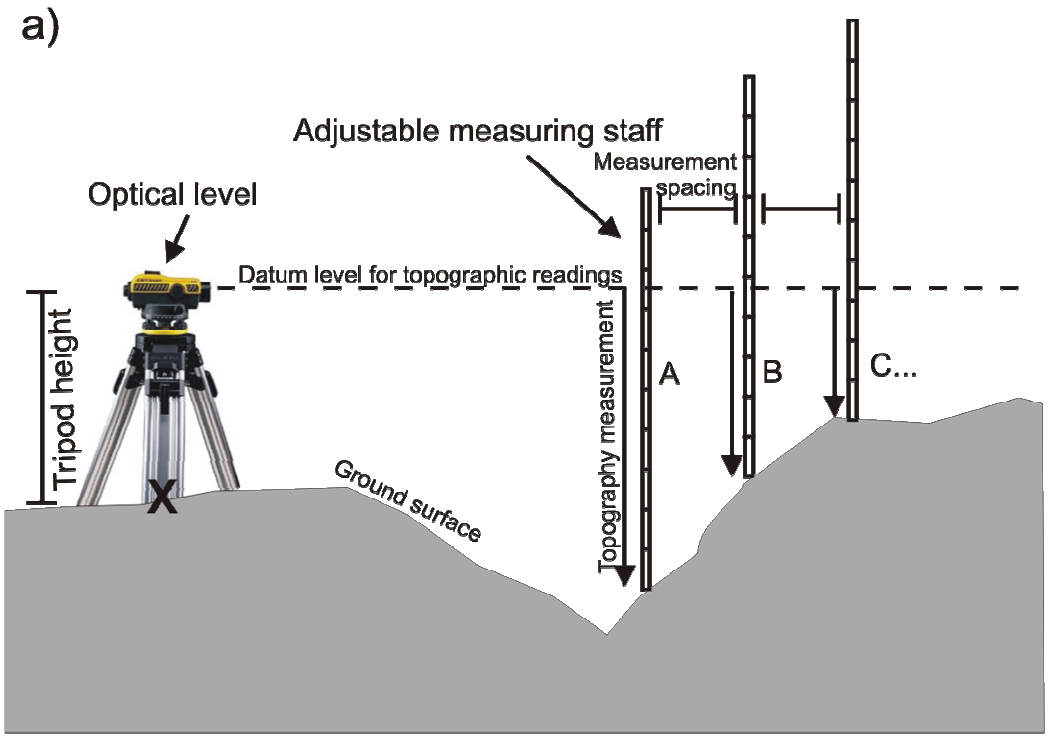

b)

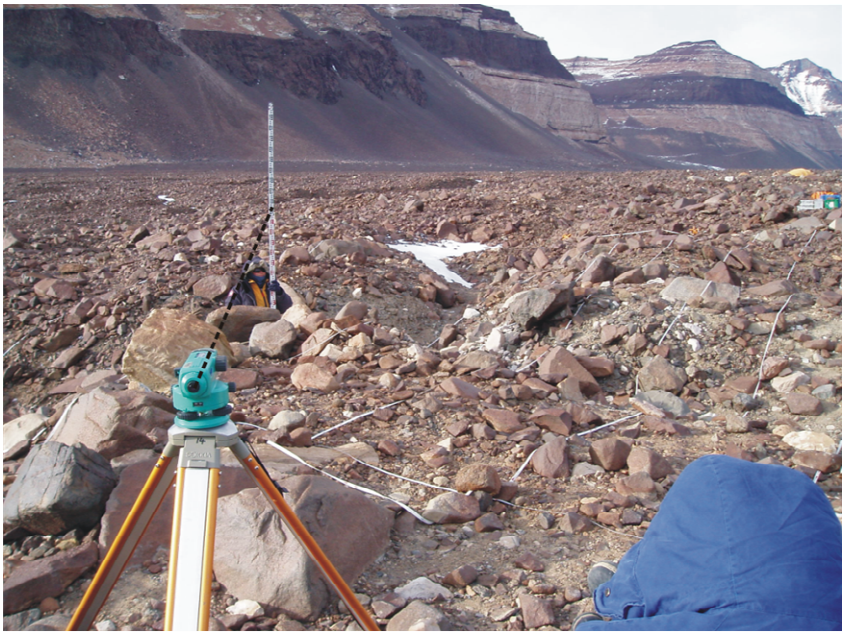

Figure 20: a) the geometry of collecting topography data using an optical level and measuring staff. Raw topography measurements represent the distance from the ground to the optical level sight line (datum level). Raw topography measurements were then corrected to absolute topography using GPS data from location "X" and tripod height. A B C… is successive readings along a line. b) taking topography measurements in Beacon Valley (BVP2)

To correct the topographic staff measurements to elevation ASL the GPS elevation measurement from the base of the optical level (X on Figure 17) was added to the measured tripod height. Staff measurements were subtracted from the corrected elevation value using the equation line tool in Microsoft Excel. 200 MHz GPR lines were offset 0.25 m from the 0.5 m topographic grid. The averages of the topographic data from the lines of either side were taken to give approximate values. Data was sorted into the correct format for graphical gridding program (Surfer8) and used to

create topographic surfaces to record morphology and geometry. Individual line topographic data sets were saved in the form of a tab delimited ASCII file of ".TOP" file extension for topographically correcting GPR. Resistivity topography measurements were plotted as X-Y graphs showing topography features along the line and used to topographically correct modelled profiles.

4.3 Ground Penetrating Radar:

GPR data was collected using the pulseEKKO sensors and software 100A system using 50, 100 and 200 MHz antennas. The 50 MHz antennas were used for cross-sections through the surveyed polygon area, while the 100 and 200 MHz antennas were used for lines within the survey areas on 0.5m line spacing across the area to be merged for three dimensional analyses.

4.3.1 Data collection:

A CMP was conducted in Victoria Valley over VVP1 and along a cross valley transect line (Bannister, unpublished 2007). The CMP analysis was used to determine a subsurface velocity used in migrating the GPR data, discussed in data processing. All of the GPR PPG survey areas were covered using a reflection survey in step mode where each antenna is moved and placed a set distance from the last measurement. Step surveying was used because of the rough terrain where the placement of antennas would provide greater accuracy.

Lines were run from east to west with the (0,0) corner being in the southeast of the surveyed polygons. GPR lines had a spacing of 0.5 m. To avoid excessive tape

movements and increase the efficiency of the GPR, the survey lines for the 100 and 200 MHz antennas were run with a 0.25 m offset between them (refer Figure 21 for the resulting geometry). This methodology was applied to all of the polygonal areas surveyed in Victoria and Beacon Valley.

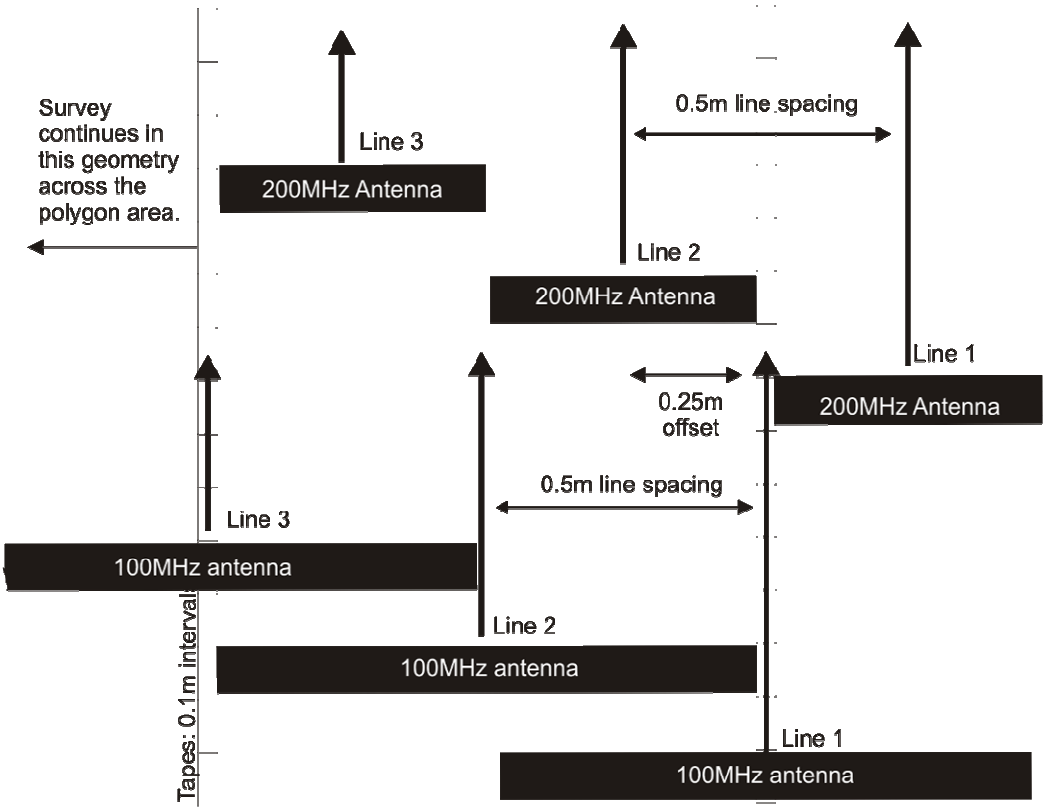

Figure 21: GPR survey geometry and methodology relating to line positions of the collected data. 100 and 200 MHz surveys were offset by 0.25m. The orientation of the 0, 0 corners in the bottom right is consistent with the requirements for processing 3D data in EKKO 3D software (discussed in data processing)

Figure 22 shows the components of the GPR system and images of the GPR data collection from Victoria and Beacon Valley.

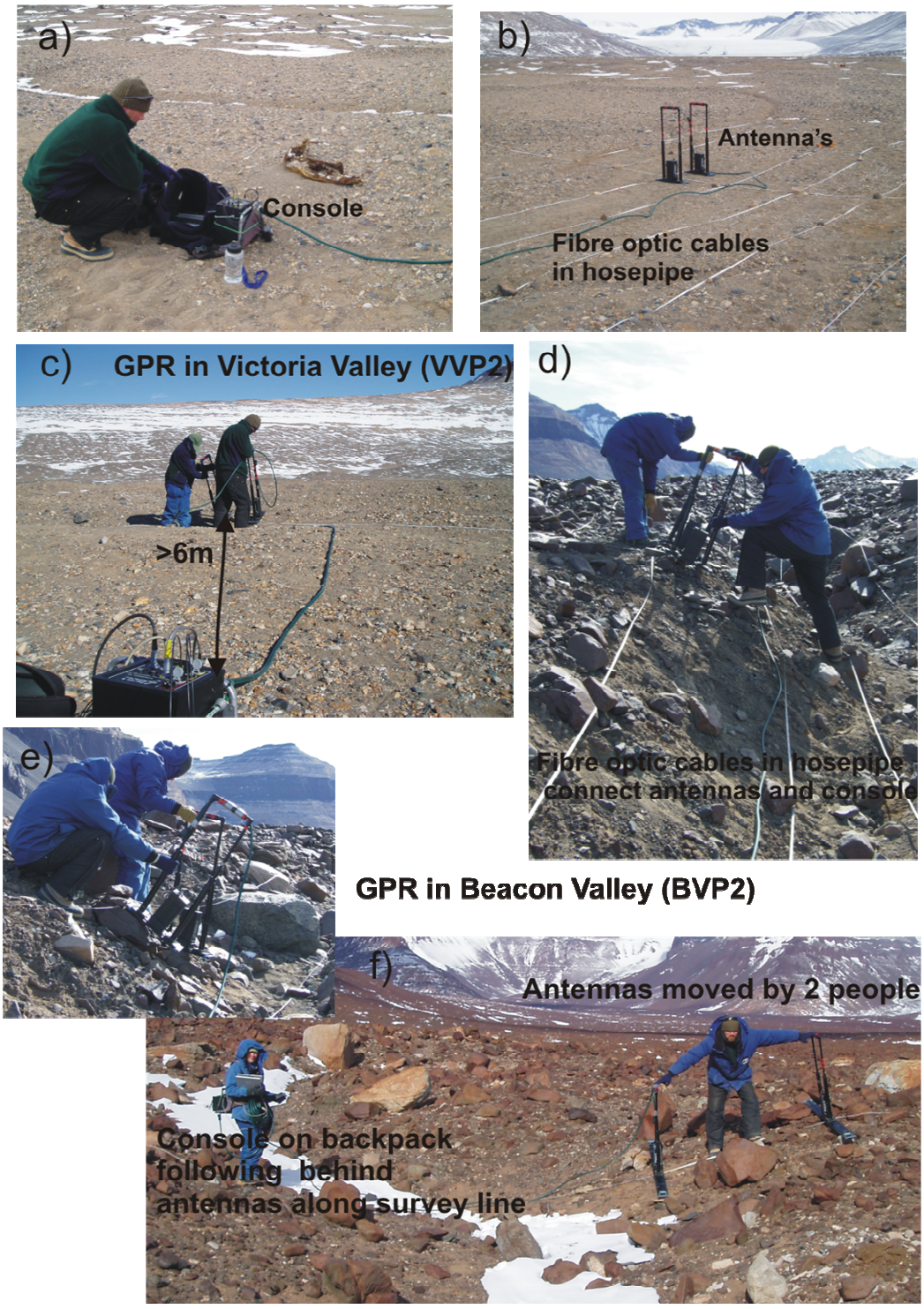

Figure 22: GPR surveying in the Dry Valleys. a) pulseEKKO data acquisition control console and laptop. b) Antennas and console connected by Fibre optic cables protected by hosepipe. c) Conducting GPR in Victoria Valley required minimum of 2 people as the console could be positioned on the ground a set distance away from the antennas as they were moved along a line d) and e) The rougher topography in Beacon Valley posed problems when attempting to move antennas along a line. f) GPR in Beacon Valley required a minimum of 3 people as the rougher topography and boulder strewn surface meant that the console had to be moved along behind the antennas along a line to prevent damage to the cables and allow free movement of the antennas.

3D GPR data is collected in multiple lines covering the entire area. Grasmuek et al. (2005) examines the data density required to fully resolve subsurface features with GPR and concludes that full GPR resolution can only be achieved with line spacing being equal to 2 times the step size. For working in 3D in the Dry Valleys this would have resulted in a line spacing of 0.2 m for the 200 MHz which was not practical for completion of the surveys in the given time. However, the line spacing of 0.5 m for 100 MHz is close to the 0.4 m requirement and so can be classified as full resolution 3D GPR. Data density is still greater in the south – north orientation than in the west – east orientation.

Antennas were separated by 2m for 50 MHz antenna GPR lines, 1 m for 100 MHz and 0.6 m for 200 MHz, as recommended by sensors and software pulseEKKO guidelines (Annan and Cosway, 1992) To avoid sampling errors, we applied a 0.5 m step size for the 50 MHz, 0.2 m step size for the 100 MHz and a 0.1 m step size for the 200 MHz antennas. Trace positions along the line are the position of the midpoint between the two antennas.

4.3.2 Data Processing

GPR data was processed using Sensors & Software pulseEKKO 4.2 for filtering migration and topographic corrections. EKKO3D and T3D were used for 3D merger and examination of the 3D data set. For consistency and to work within time constraints batch file processing was used for the 3D GPR data sets. Appendix 3 shows the GPR trace lines at raw, topographically corrected, and fully migrated stages of processing and the resulting 3D volumes.

CMP analysis:

The first data set to be processed was the CMP data so that the derived velocity could be used in the subsequent migration of the GPR profiles. CMP analysis was completed using pulse EKKO 4.2 software. Figure 23 shows a semblance analysis of the CMP response where the concentration of velocity response can be seen between 0.12 – 0.14 ns.

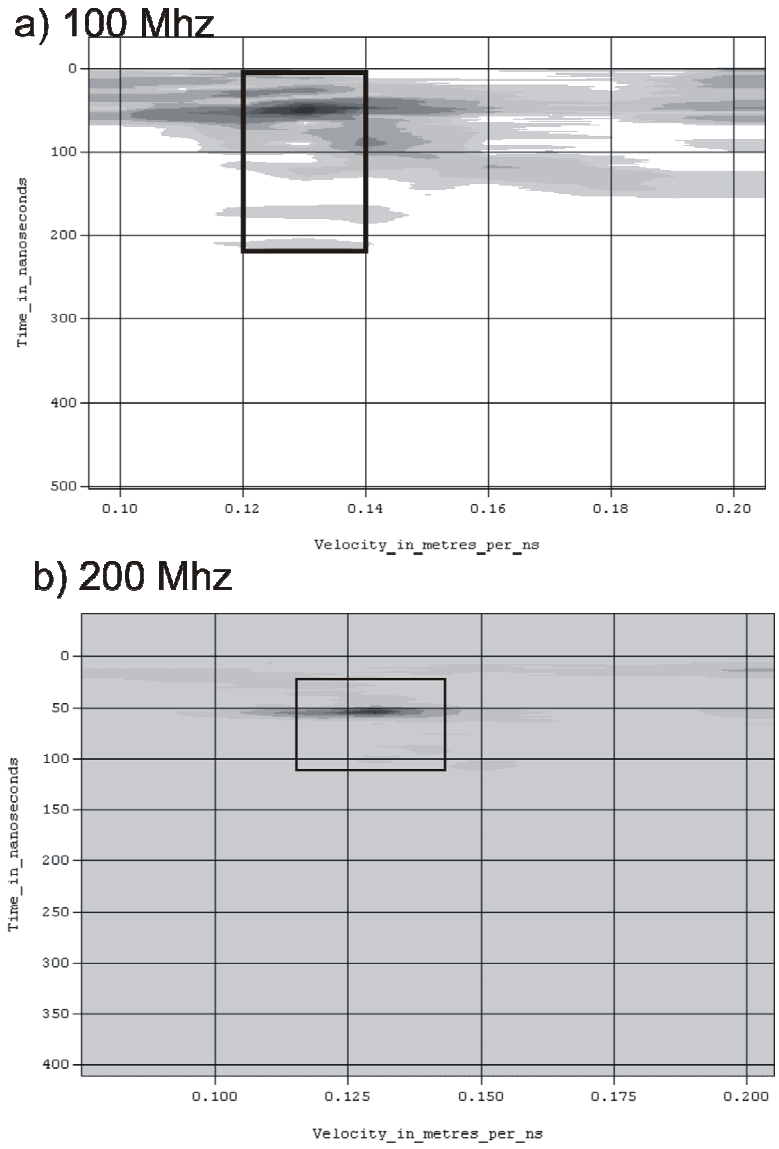

Figure 23: CMP semblance analysis showing a plot of velocity measurements from within the subsurface of VVP1. In both a) and b) the highest concentration of velocities interpreted from the subsurface response is outlined by the box and is seen between 0.12 – 0.14 m/ns.

A mean velocity of 0.13 m/ns was used for the purposes of processing.

Topographic corrections:

The topography in these surveys effected the placement of the reflectors within the GPR line profiles. To correct the placement of reflectors to correct relative locations the topographic data collected (appendix 2) was applied to the GPR data using topographic addition where the trace profile is distorted to show the topographic effects, and topographically shifted where the reflector positions are repositioned using the topographic information and the subsurface velocity (determined by CMP).

Migration:

To collapse diffraction curves and position reflectors correctly within the profile. Two types of migration were used; mathematical Fourier transform migration in the frequency wave number domain (F-K) (refer to Stolt 1978 for details of this methodology), and synthetic aperture migration where a width of window has a conical filter applied to collapse diffraction curves. F-K migration was applied in batch file form while synthetic aperture migration was applied during merger into 3D cubes.

Filters:

To reduce the "wow" of the signal where ---- is amplified and distorts the response a "dewow" filter was applied whereby the low frequencies were removed from the traces.

Gain functions:

To correct for the loss of signal with depth due to signal attenuation; two types of gain functions were applied to these data sets; AGC and SEC gains.

- AGC (Automatic Gain Control) is an exponential gain function that applies a gain inversely related to the original signal strength (Annan 1993). Therefore with AGC gain weak responses will receive a larger applied gain than strong responses thus creating a levelled signal response throughout the profile. This corrects for the loss of signal with depth by boosting late response signals, but will not maintain the recorded signal strengths of the data which may indicate physical property relationships important to an advance data interpretation. AGC gains are useful for evaluating the signal response to depth and assessing the continuity of

reflectors across a profile but are less useful when evaluating signal response type and quality.

- SEC (Spreading and Exponential Compensation) is a limited exponential function where a limited gain inversely related to signal strength is applied (Annan 1993). The limited function allows weaker signals to be boosted but not to the point where relative signal strength relationships are filtered out. Late responses associated with greater depth are boosted but not to the level seen with an AGC gain, and weaker signals within the main body of the signal response maintain their correct *relative* signal strength.

4.3 3 Data display:

The GPR data in this thesis is displayed in Variable Area Display (VAD) greyscale with phase of GPR signal being represented by black for positive amplitude and white for negative amplitude. Large amplitude of signal from strong reflectors will produce strong signal patterns of black and white. Figure 30.

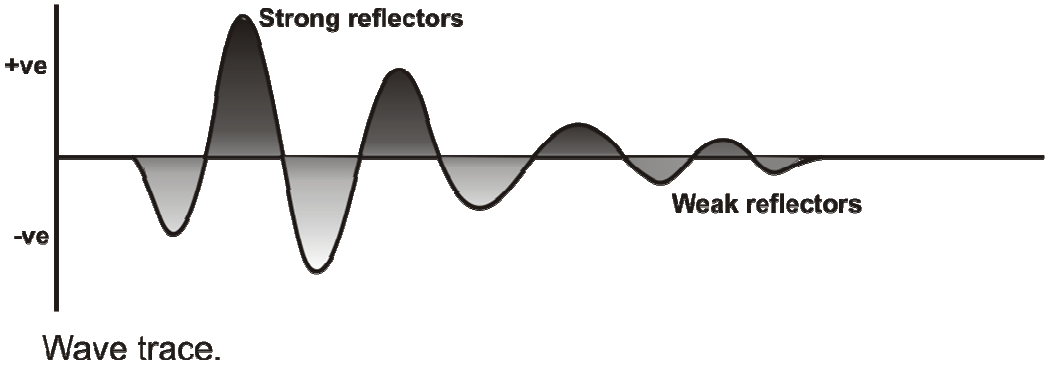

Figure 24: A wave trace showing the positive and negative amplitude variations for strong and weak reflectors. Each GPR reading has a wave trace, when multiple wave traces are put together a profile as seen in the GPR results Plates is made. Where many strong positive or negative amplitudes are aligned (i.e. from a similar two way travel time) they form a line representing the position of the strong reflector.

The relative phase of a reflector can indicate specific changes in the physical properties. The Airwave and groundwave have a - + - amplitude phase (refer profile lines Appendix IV). A strong reflector with a change in phase can indicate that the reflector represents a change into a medium of higher dielectric conductivity.

GPR data is presented in individual profile format (Refer to Appendix IV for full record of all profile lines collected for this thesis) and merged into 3D cubes using EKKO 3D

4.3 Resistivity:

Electrical imaging in the form of resistivity surveys were conducted in cross-sectional positions across the four surveyed polygonal ground sets and was the only method used that required any subsurface disturbance due to the penetration of electrodes to maintain electrical contact with the ground. The positions of the cross-sectional lines of resistivity were roughly central but varied according to the specific geometry of the polygonal areas and according to features to be targeted.

4.3.1 Data collection

Resistivity data were collected using a Geotomo resistivity system and ImagerPro software. All surveys were conducted using the Wenner array configuration using 32/64 electrodes with 0.5 or 1 m electrode spacing. Figure 24 shows images of the resistivity data collection during our field season.

The Geotomo resistivity tomography system passes current through multi channel electrode cables connected to a central control unit. (Figure 24a). The multi channel electrode cables allow initial current and electrical response to be isolated and recorded separate from each other. The electrode cables make contact with the ground through metal spikes planted into the ground and clipped onto the cable (Figure 24b). To avoid induction of a secondary current within the subsurface (refer EM theory section for the physical principles of this phenomena) the electrode cables are positioned so that no loops of cable are created (Figure 24c, d, and e.). The electrode cables are also shielded to further reduce risk of an unwanted secondary response.

In general electrode contact was good for the surveys conducted, with minor problems occurring when the spacing for the electrode arrays placed an electrode directly within a contraction crack. The gravel framework found within these contraction cracks often

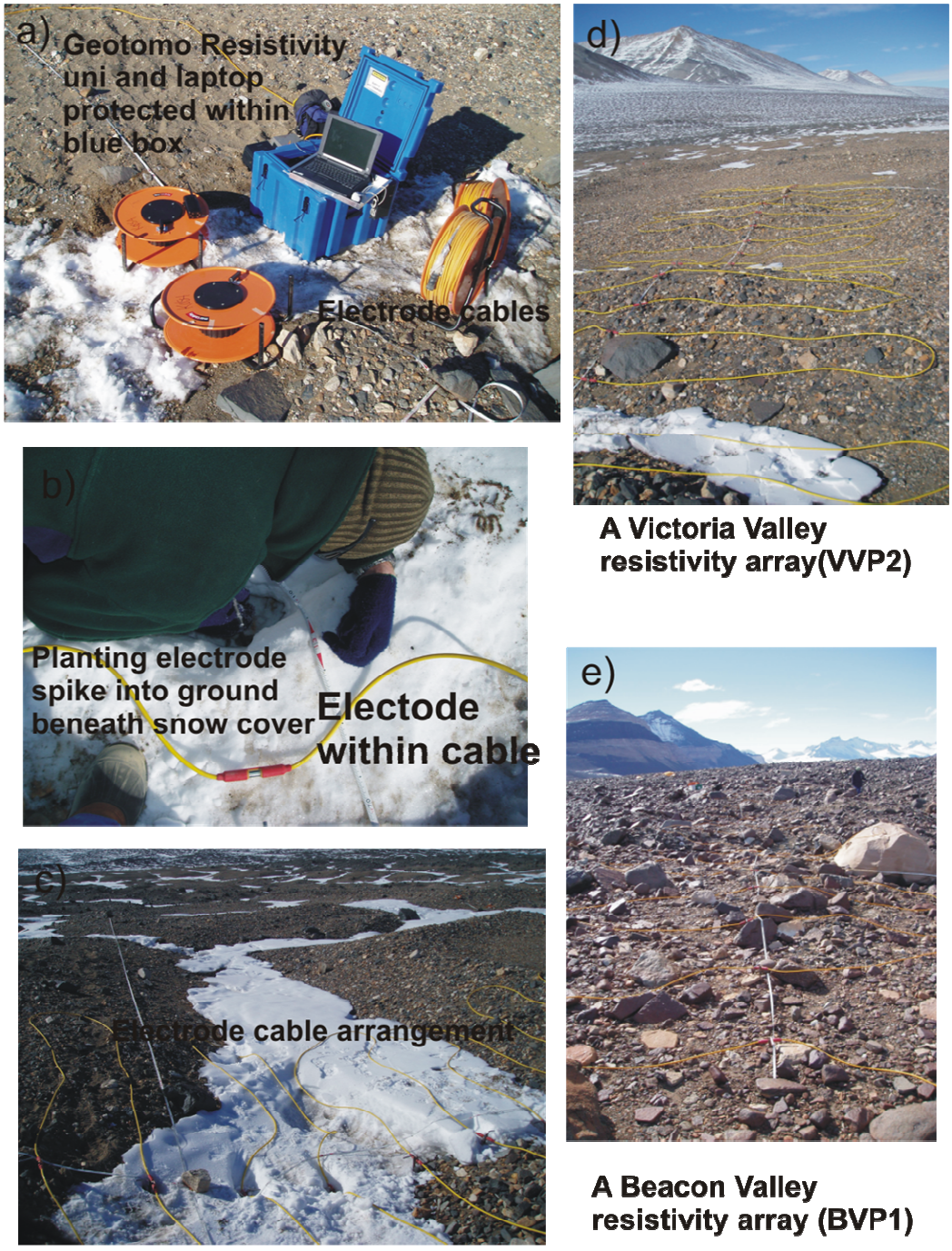

Figure 24: Resistivity surveying in the Dry Valleys a) Geotomo data collection system with laptop running data acquisition software and multi channel electrode cables b) electrode within the multi channel cable and planting an electrode spike for ground contact beneath snow c) arrangement of electrode cable to avoid induction loops d) Victoria Valley resistivity survey e) Beacon Valley resistivity survey

made establishing and maintaining electrical contact with the ground surface difficult. Resistivity surveys were not run unless contact resistance tests came back without errors.

Figures 25 – 28 illustrate the positioning of the resistivity lines over PPG topography. Topography maps made from topography data with low elevation to high elevation being represented by dark to light shading. Lines slicing through topography profile plots of resistivity lines represent the GPR and EM survey area extent.

4.3.1.1 VVP1:

Once set up, the resistivity surveys were conducted as time lapse over VVP1. VVP1 was chosen for the intersecting contraction crack at its centre. Four resistivity lines were set up crossing through the central crack intersection (Figure 25) at right angles to each other running North – South and West – East respectively. The surveys were conducted using 32 electrodes at 1 m electrode spacing.
Electrodes were left in their positions in the ground for the duration of the time-lapse survey and resistivity lines were run every 4 days.

4.3.1.2 VVP2:

Three cross-sectional lines were conducted on VVP2; one Sorth – Nouth bisecting the long axis of the polygon and two running West – East offset from each other each centred on opposing contraction cracks (refer Figure 26). The surveys were set up using 32 electrodes and 0.5m electrode spacing for the West – East lines and 1 m spacing for the South – North line

4.3.1.3 BVP1:

Two cross-sectional lines were run over BVP1 at right angles to each other. They bisected the polygonal area in the centre running North – south and west - east, using 32 and 64 electrodes at 1 and 0.5m line spacing (Figure 27)

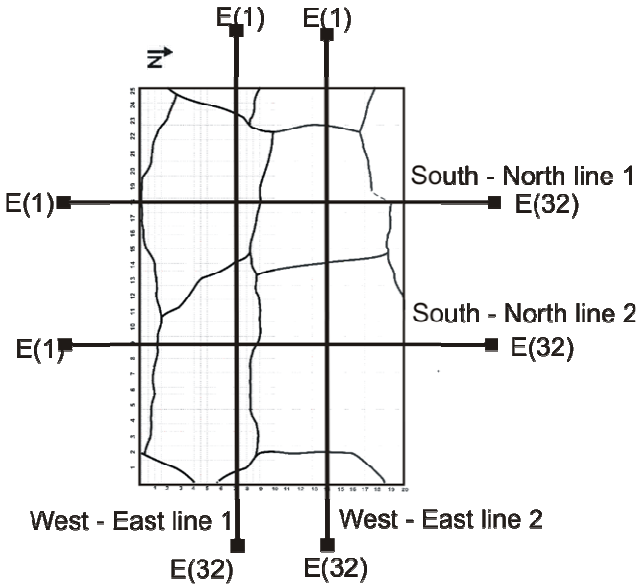

Figure 25: VVP1 survey area geometry and relative positioning of Resistivity lines within the survey area. Electrode 1 (E (1)) represents the start of the resistivity line which runs to electrode 64 (E64))

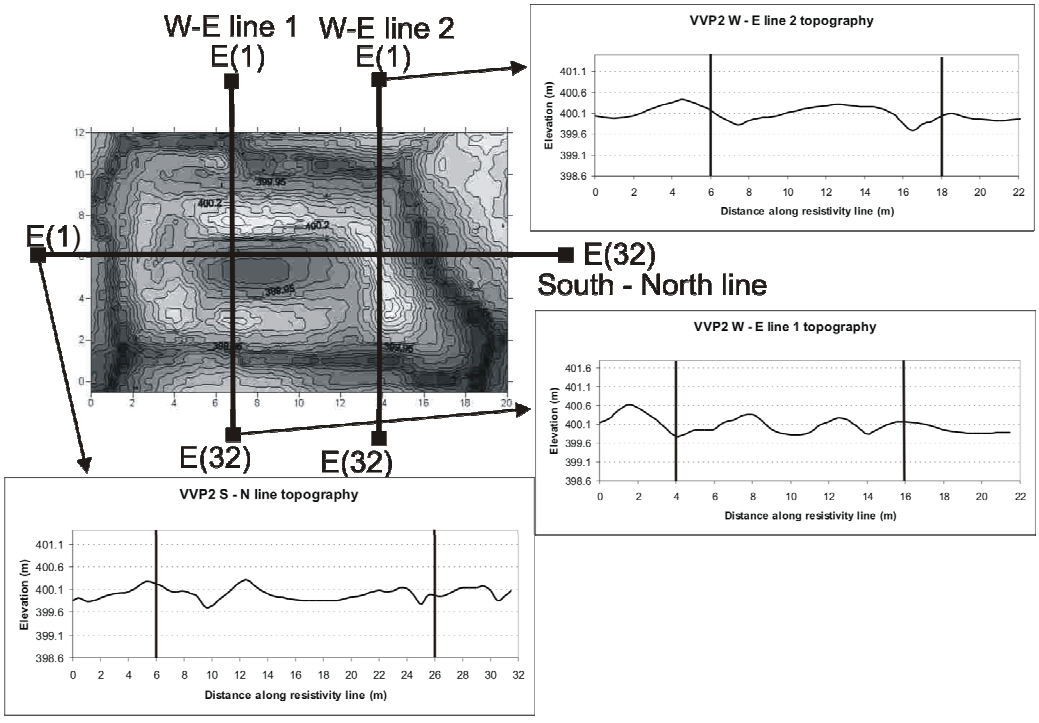

Figure 26: VVP2 resistivity positions relative to survey area rectangle. Topographic data collected at 0.25m grid

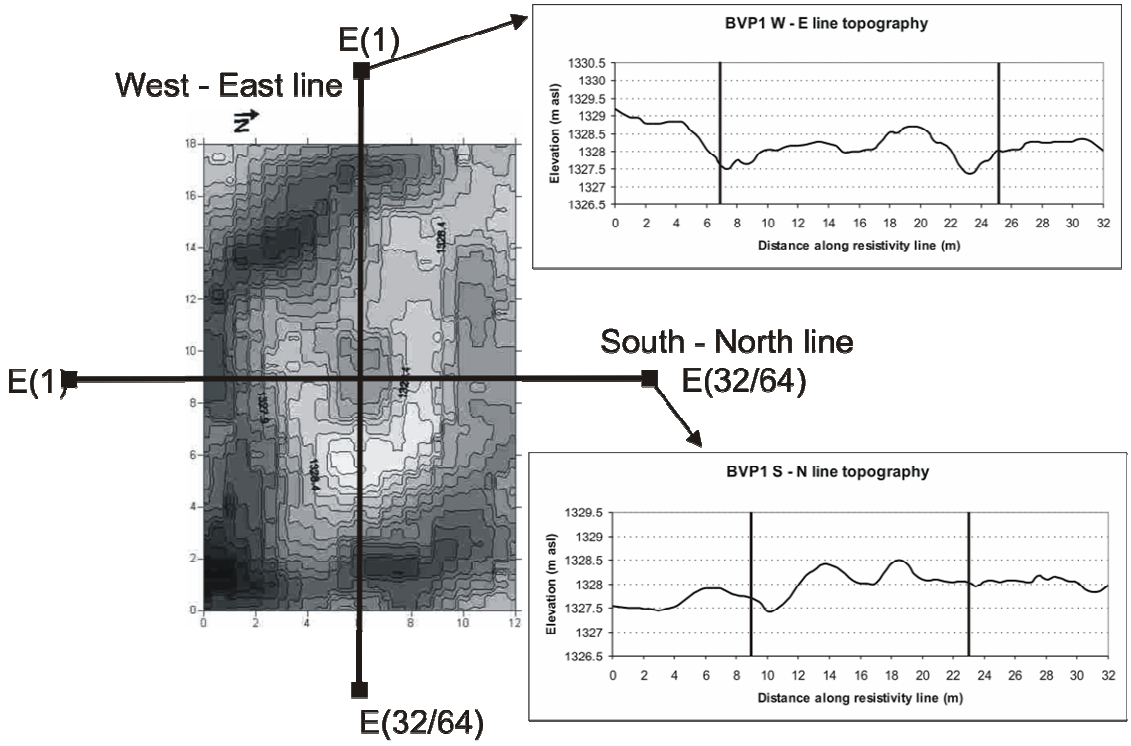

Figure 27 BVP1 resistivity line positions relative to survey area. Map plan of survey area created using Surfer8 topographic map. Topography collected at 0.5m grid

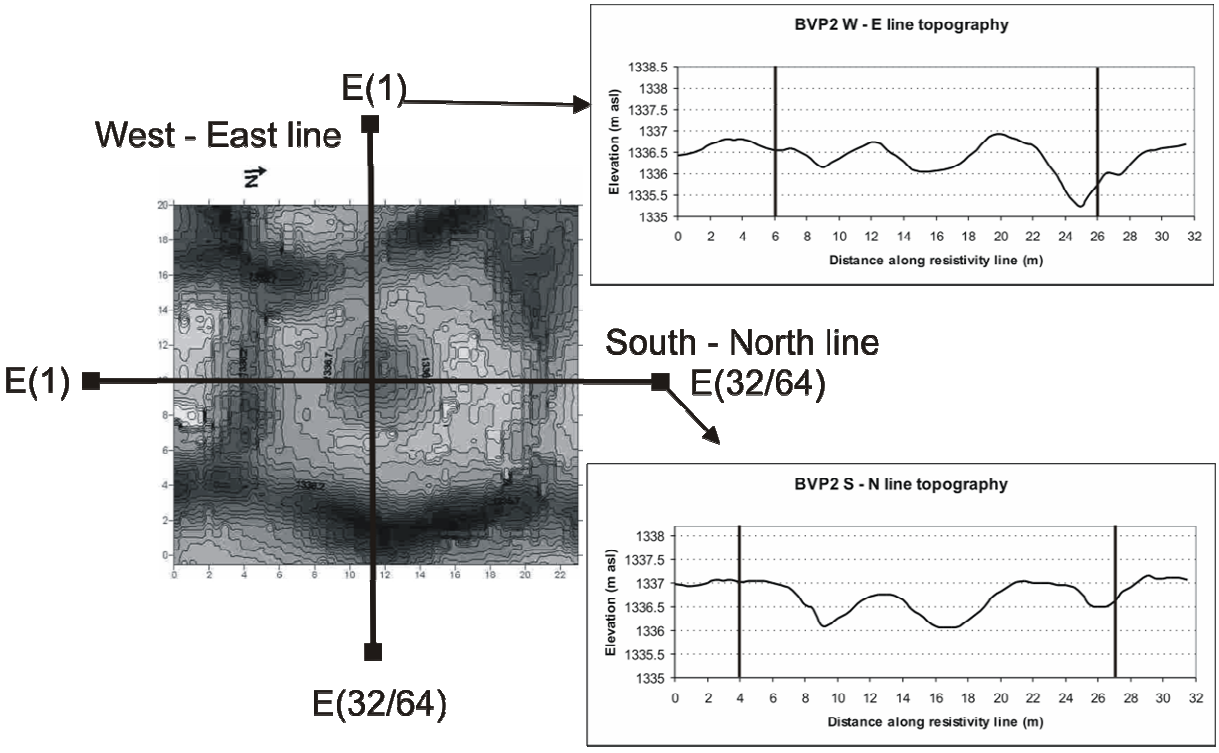

Figure 28 BVP2 resistivity line positions relative to survey area and PPG geometry. Survey area map created from topographic data. Topography collected at 0.5m grid.

4.3.1.4 BVP2:

BVP2 cross-sectional lines were run through the middle and used a combination of 32 and 64 electrodes at 1 and 0.5 m electrode spacing (Figure 28) running North – south and west – east.
The 32 electrode 1 m spacing lines fro BVP1 and BVP2 were collected as back up but illustrate the change in resolution from using a larger electrode spacing over the same line. Refer appendix V.

4.3.2 Data processing:

Data was collected in the field directly onto a laptop using ImagerPro in a ".res" file format. For editing in windows Notepad software and processing in Res2D inversion software the ".res" file was converted to ".dat" so it could be viewed and edited as an ASCII file (Appendix V).

In Notepad, topographic data in ASCII file format was appended to the resistivity file for inclusion into data display in Res2D. The topography was applied using a distorted finite element grid with a dampening factor of 0.75, which distorts the resistivity model blocks to accommodate topography effects but limits this effect at depth.

The inversion routine used in Res2Dinv is based on smoothness-constrained least squares algorithm (Loke and Barker 1995) where various filters and dampening factors are applied to a matrix of partial derivatives (refer Appendix V for inversion equation and parameters).

For each model an RMS (root mean square) value is assigned to represent the difference between the raw (apparent resistivity) data model and the processed inversion model (true resistivity).

For the purposed of continuity the same processing parameters were applied to the data sets for each PPG survey area. The modelling programme Res2D many settings

for processing resistivity data. Full inversion parameter files for the data can be found in Appendix V.

The resistivity model was refined by applying an inversion cell block width that was half the electrode spacing. This was to compensate for the high resistivities found within the Dry Valleys data sets.

The inversion method was adapted to "robust" inversion which allows for sharp boundaries to be created in the resulting resistivity psuedosection.
Edge effects were limited, but the resulting resistivity values were not.

An RMS convergence limit was used to stop continuing iterations (repetitions) of the inversion process once the RMS change was at 3%. A maximum of 10 iterations was applied to the data sets.

Model data was plotted in Res2Dinv software and model sensitivity, uncertainty, and maximum and minimum models produced so that the quality of the inversion could be analysed.

The log of the model resistivities was exported from Res2Dinv program to Surfer8 where plots of the data could be manipulated with greater ease. The large range of model resistivities is best displayed as a logarithmic function so that rapid changes in the resisitivity are more easily identifiable.

Time-lapse resistivity data was formatted into a single file with time-lapse readings for each measurement. Inversion was applied to the single file to allow for time-lapse analysis through sequential inversion where the resistivity response is dampened by the previous time-lapse inversion routine. This reduces instability within the inversion process between iterations (Geotomo Software, 2004)

The log of the model resistivity for each time-lapse sequence was exported to Surfer8 so that the difference between adjacent time-lapse sequences could be calculated by subtracting one grid from the other before plotting. This function was not available in

the Res2Dinv package where differences in resistivity between time-lapse sequences could only be calculated from the first time-lapse data set.

4.4 Electromagnetism:

Electromagnetic surveying was conducted over the whole of the survey area on a 1m x 1m station grid. This data creates a map of the electrical properties of the survey area.

4.4.1 Data collection:

Electromagnetism was conducted on a 1m x 0.5 m station grid along the lines laid out for the GPR 3D surveys. Data was collected using the Geonics EM31 using normal/vertical dipole-dipole arrangement (horizontal loop – loop (HLEM) configuration as illustrated in Figure 18, Chapter 3) and manual trigger control. Figure 29 displays selected images of electromagnetic data collection using the EM31 system.

The Geonics EM31 operates at 9.8 kHz (low frequency) and has a boom length/loop separation of 3.7 m giving a maximum depth of penetration at approximately 6 m (Milsom 2000). However, most estimations of the depth of penetration for EM31 use the approximation of 1.5 times the coil separation to attempt to take into account target size and conductivity factors (Gibson and George, 2003). Thus the EM31 data collected here will most likely reflect electromagnetic properties down to 5.55 m.

EM31 pro software was run in DOS for data collection saving data in ".R31" file format. Survey lines were run twice with differing boom orientations, first parallel to surveys lines and secondly perpendicular to survey lines. Perpendicular boom orientation data was recorded as being 0.5m offset from the correct line position to speed data collection as the DOS collection program gave no option for changing orientation of the boom without restarting the data collection.

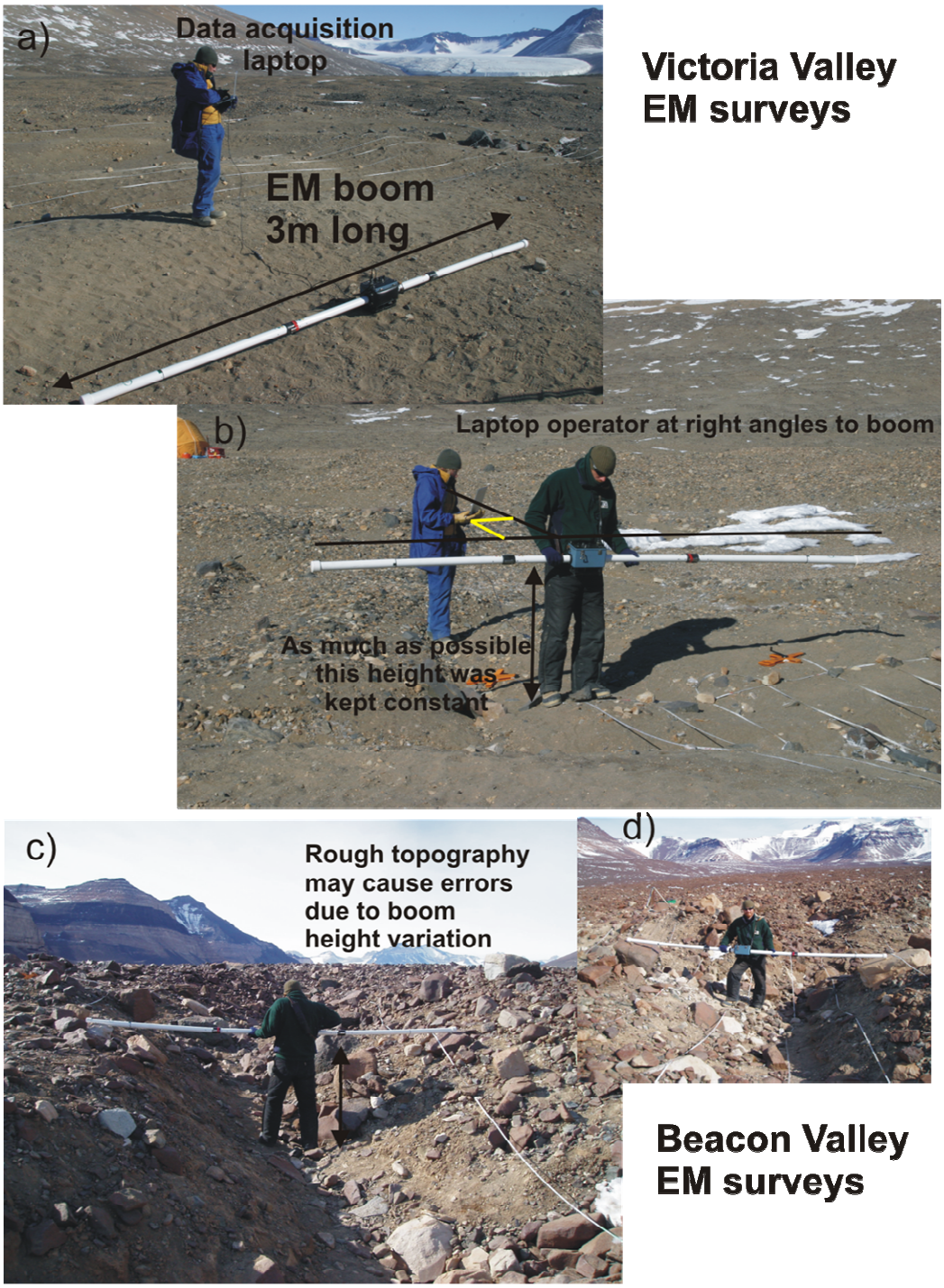

Figure 29: Conducting electromagnetic surveys in the Dry Valleys using the Geonics EM31 system a) EM31 boom set up, the data acquisition laptop was connected to the EM31 controls through a 2 m long cable b) running the EM31 survey over VVP2, the data acquisition laptop was kept at right angles to the boom to keep it as far away from the electromagnetic current loops at either end of the boom c) and d) conducting EM31 in Beacon Valley posed difficulties with maintaining constant conditions such as boom height. The width and depth of the contraction cracks were such that contact between the boom and topography could not be avoided. Additionally the boom was not able to be oriented parallel to topography at the point where the measurement was taken which may also cause error within the data.

Both in-phase (real) and out of phase (quadrature) components of the secondary response were recorded. EM31 instrumentation records quadrature response in milliohms/m (mΩ/m) and in phase as parts per thousand (ppt) of the input signal strength (Lapwood unpublished 2006)

4.4.2 Data processing:

".R31" format files were converted to ".G31" file format in Dat31 software so that data could be displayed as XYZ coordinates with line and station position and electromagnetism reading. XYZ data was then imported and edited in spreadsheet form in Microsoft Excel before gridding and plotting in Surfer8.

Editing the data consisted of deleting multiple readings from the beginning of each line, and renumbering the line positions of the data collected with perpendicular boom alignment.

Data was processed by applying averages and taking the difference of parallel and perpendicular data sets.

Strong along-line trends were seen in the data. These trends reflected the difference in conditions between different line data collection and were swamping the signal from PPG structure. To alleviate this, the median of each line was determined and subtracted from the set of line data. This was done for the already determined averages and differences as well as raw data which was subsequently re- averaged, differenced, and gridded and plotted.

Plotting of raw data showed areas of anomalous response interpreted as being associated with error rather than targeted structure. These values were deleted and subsequent equations that involved these data points were modified.

Appendix V contains the images of these data transforms for the collected electromagnetism data.

5: Results and Interpretation:

This section will present the results from this research. The two "umbrella" sections evaluate the resolution of subsurface structure, and resolution of seasonality within the subsurface. The analysis of the quality and limitations of the data collected is also included in this section.

5.1 Resolution of subsurface structure of PPG:

This section presents the results from the three different geophysical methods used to resolve subsurface structure within PPG in the Dry Valleys. For temporal continuity the GPR and resistivity results for VVP1 and VVP2 are from the first survey in the time lapse sequences. For time lapse analysis refer to the following section of this chapter.

5.1.1 GPR:

5.1.1.1 General comments:

Please refer to Plates 1 to 4 for selected examples of GPR results. To view the full record of GPR profile lines please refer to Appendix IV which contains raw, topographically corrected, and migrated and topographically corrected profile lines for each GPR survey.

Depth of resolution:

The greatest depth of resolution is attained when an AGC gain is applied to boost the amplitude of late responses within the GPR profile. Using the measured subsurface velocity (0.13 m/ns) from the CMP, the depth of resolution reached maxima of ~ 22 – 25 m (345 – 385 ns two way travel time) with 50 MHz antennas, ~ 12 – 15 m (195 –

230 ns two way travel time) with 100 MHz antennas, and ~ 10 – 13 m (155 – 195 ns two way travel time) with 200 MHz antennas.

Evaluating signal and data quality:

In general the signal quality for the data presented here was very good. With topographic correction and migration, selected reflectors can be traced along profile lines and through 3D cubes to resolve subsurface structures. The clearest signals are received in Victoria Valley where significantly less scattering is seen compared to the data collected in Beacon Valley. This is most likely due to the rougher topography and higher concentrations of large boulders at the Beacon Valley surface. The surface compositions of the soils of Beacon Valley contained large boulders compared to Victoria Valley (refer Chapter 2 Field area and survey characteristics). If this composition is inferred to continue into the subsurface, boulders of 0.5 – 1.5 m diameter may be causing increased scatter of the signal at depth. The most scattering of signal can be seen in BVP2 profiles.

The 50 MHz profiles were conducted near the end of our field season when temperatures were considerably warmer (refer appendix 1 for logistics report). The significant signal ringing and thus lower signal quality within these profiles are attributed to increased salt mobilization with the release of free water in the subsurface after the thaw.

Two main methods of migration were used in the processing of this data with differing effects on the quality of the data. Batch file migration involved a mathematical Fourier transform function in the frequency wave number domain (F-K) migration technique (Stolt, 1978) and is applied before merger into a 3D cube. The other method used is synthetic aperture migration where diffused/diffracted energy is "refocused" and is applied to the profiles during merger into a 3D cube. F-K transform migration reduces the number of points in a trace to 256 which reduces the detail of resolution seen within resulting data cubes. However, with synthetic aperture migration artefacts are created. These artefacts resemble the "smiles" seen when an incorrect subsurface velocity is applied during F-K migration. These artefacts are more obvious towards the bottom of the 3D cubes seen in Plates 1- 4.

F-K migration with an AGC gain proved to be the most effective in creating usable reflector traces to depth while the synthetic aperture migration with SEC gain showed the relative signal strengths to greater effect than simply applying a SEC gain to F-K migrated profiles. The contrast between areas of weak and strong GPR response is seen with SEC gain and shows deeper responses of strong physical property contrast to greater effect than with an AGC gain boosting signal to depth. Resolution of deep structures may sometimes be clearer with SEC gain due to the lack of weaker boosted signals adding unwanted signal.

5.1.1.2 Subsurface features:

This section will expand on identification of the subsurface structure seen within the GPR profiles. The numbers and letters relate to notations on Plates 1 – 4. Numbers [1] – [3] refer to GPR response features that are prevalent throughout the GPR survey areas and represent PPG related structure. [A] – [D] are anomalous responses that may represent features outside of PPG structure. These GPR responses are discussed with reference to subsurface interpretation of the possible structure causing them

[1] Deformation in the vicinity of thermal contraction crack locations: The contiguous horizons within the subsurface identified in yellow on Plates 1 – 4 often exhibit irregularities in the subsurface near the vicinity of the thermal contraction crack surface expression. These irregularities show deformation such as upturning and doming. The models for the formation of PPG surface expression require the surrounding permafrost soils to accommodate a propagating thermal contraction wedge over successive seasons. The up-turning of subsurface reflectors as seen in the GPR profiles is consistent with these models. The “doming” geometry of this deformation can be attributed to two possibilities: buckling of the surrounding permafrost rather than horizon upturning; or complete overturning of the deforming beds to accommodate wedge propagation (Sletten pers. comm., 2006). There is not sufficient resolution within the GPR profiles to determine which is prevalent. The upturning of soil horizons in the vicinity of thermal contraction cracks has been documented by Black (1976), Black and Berg (1963), and Pewe (1974). It is interesting to note that the sightings of these features are almost exclusively limited to the very near surface of PPG (< 1.5 m) and not at depths seen in the GPR profiles.

The 50 MHz profiles show larger scale deformation of the reflectors which can be seen to be undulating in geometry on a scale of 10 – 20 m consistent with PPG surface expression scale.

[2] Zones of attenuation are commonly found in the subsurface profiles spatially related to the surface expression of the thermal contraction cracks. Greater attenuation of a GPR signal is associated with changes in the physical properties in that area. In this case the energy is essentially used up within the subsurface without generating significant GPR reflections. The attenuation of the signal is more likely the result of secondary factors rather than direct PPG structure such as the propagating wedge. At the surface the thermal contraction cracks exhibited a clast supported framework for the infilling material (Chapter 2 Field area) which would provide a preferential pathway for any free water content movement. The Dry Valleys' soils contain high concentrations of salts. Free water movement concentrated over successive seasons would most likely result in higher concentrations of salts found in the vicinity of the thermal contraction crack.

Additionally, the thermal contraction cracks were surrounded by raised ridges providing wind shelter and contributing to snow accumulation within the crack areas. Snow content was at its highest at the beginning of each time period for each valley and may contribute to attenuation of GPR signal. Refer to the time lapse analysis for greater discussion of this effect.

[3] Wedge geometry and on lap structures radiating from raised contraction crack ridges. Best seen in individual profile lines of 200 MHz profiles which have the highest resolution near the surface of the three frequencies used. (Figure 30 and Plates 1 – 4 or appendix IV). The deformation of the permafrost soils surrounding thermal contraction cracks results in raised ridges. These wedge geometries may be the result of soil material shedding from the upraising ridges or from the complete overturning (Sletten pers. comm., 2006).

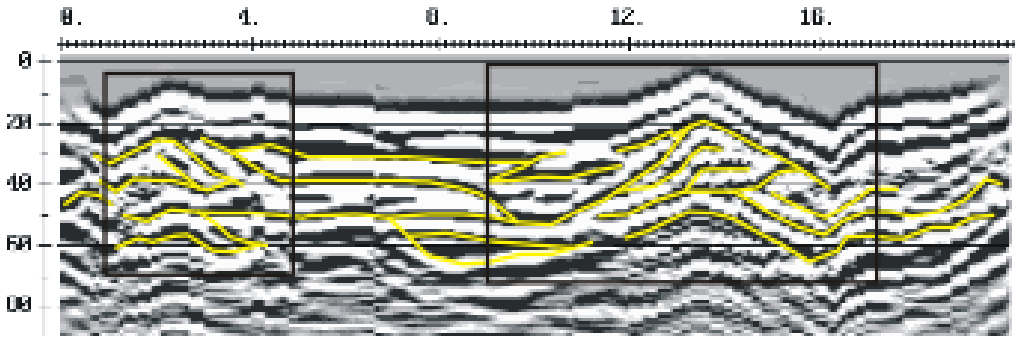

Figure 30: Cropped section of line 14, VVP2 200 MHz profile with trace position vs. two way travel time. Debris wedge and on lap geometries outlined in by the black boxes.

Features of note:

[A] Sub horizontal surface reflector which can be seen at approximately 1.3 – 3.3 m depth (20 – 50 ns two way travel time). This reflector can be seen resolved into a single planar surface in volumes x and y on Plate 1. [A] dips towards the North. The GPR data for VVP1 did not have topographic correction applied as the time constraints were too limiting for a topographic survey to be completed. The surface relief was not more than 0.3 m but the surface did slope towards the South. Had the correction for this slope been included [A] would most likely be situated horizontally. When examining the surface created in x and y volumes, slight variations in the surface can be detected. These variations correlate well with the plot of the PPG surface expression found over survey area VVP1.

[A'] Plate 2: This reflector does not resolve into as continuous a planar surface as [A]. It is located at approximately 2.6 – 3.3 m (40 – 50 ns) depth. The higher scattering of the signal in VVP2 may be reflective of the larger clast sizes found in the VVP2 survey area. When examined closely, the general geometry of this surface reflects the overlying topography of VVP2.

Guglielmin (2006) measured Active layer depths in Northern Victoria land, Antarctica and found that the active layer was within 0 – 0.93 m by calculation of the 0˚C isotherm. The depths of [A] and [A'] are more than this with minimum depths of > 1.3 – 2.6 m. However, Gulglielmin (2006) also notes that due to the high salinity found in Dry Valleys soils (0.2 – 7.4 % for the active layer and up to 68 % for

underlying permafrost) the depth at which the soils actually freeze would be deeper than the 0˚ C isotherm (-0.4˚C for active layer and -4˚C for permafrost). These [A] and [A'] reflectors may thus represent the base of the active layer.

[B] Horizontal reflector at depths of approximately 5.2 – 6.5 m (80 – 100 ns) on VVP1 (Plate 1): this signal has a - + - phase and is best seen in the synthetic aperture SEC gain cubes and within them can be seen throughout the data cube. This signal is lost within the AGC gain F-K migration cubes but can be seen in the individual profile lines. Responses from below this reflector are seen to be stronger than the signal directly above it. Continuous reflectors can be traced through profile lines and slice lines indicating that they likely represent continuous surfaces.

VVP1 was located within a zone of low relief "young" PPG surrounded by moderately more developed PPG (refer Chapter 2, Field area and survey characteristics). The contrast in development seen in this zone of low relief PPG could be explained by a delay in the start of active PPG processes working on this area of the valley floor. In the environmental context of the VVP1 survey area, this could be achieved in two simple ways; a concentration of water requiring evaporation before the surface is exposed to the atmosphere or a debris fan from the side of the valley. Many lake deposits have been found in the Dry Valleys, both modern and ancient (e.g. Péwé 1961, Stuiver et al. 1981, Denton et al. 1989, and Clayton-Greene et al. 1988) Victoria Valley currently has a lake fed from glacial melt of Victoria Glacier. Expansion of the lake past its current extent can be traced in well formed lake deposits on the floor or Victoria Valley. Large glacial lakes have been suggested in Victoria Valley by Hall (2002) which would support the possibility of a water body as an explanation for the lower level of maturity of this PPG area. The break in slope indicating the change from valley floor to valley side was difficult to determine without plotting the topography but is estimated to be approximately 150 – 200 m away from VVP1 survey area. At this distance defined debris fan geometry would be expected rather than the zoning seen on Victoria Valley floor. The development of these zones of young PPG requires further investigation.

Another possible interpretation of [B] relates to VVP1 survey areas' close proximity to a cross valley near surface geophysical transect. This was conducted in conjunction

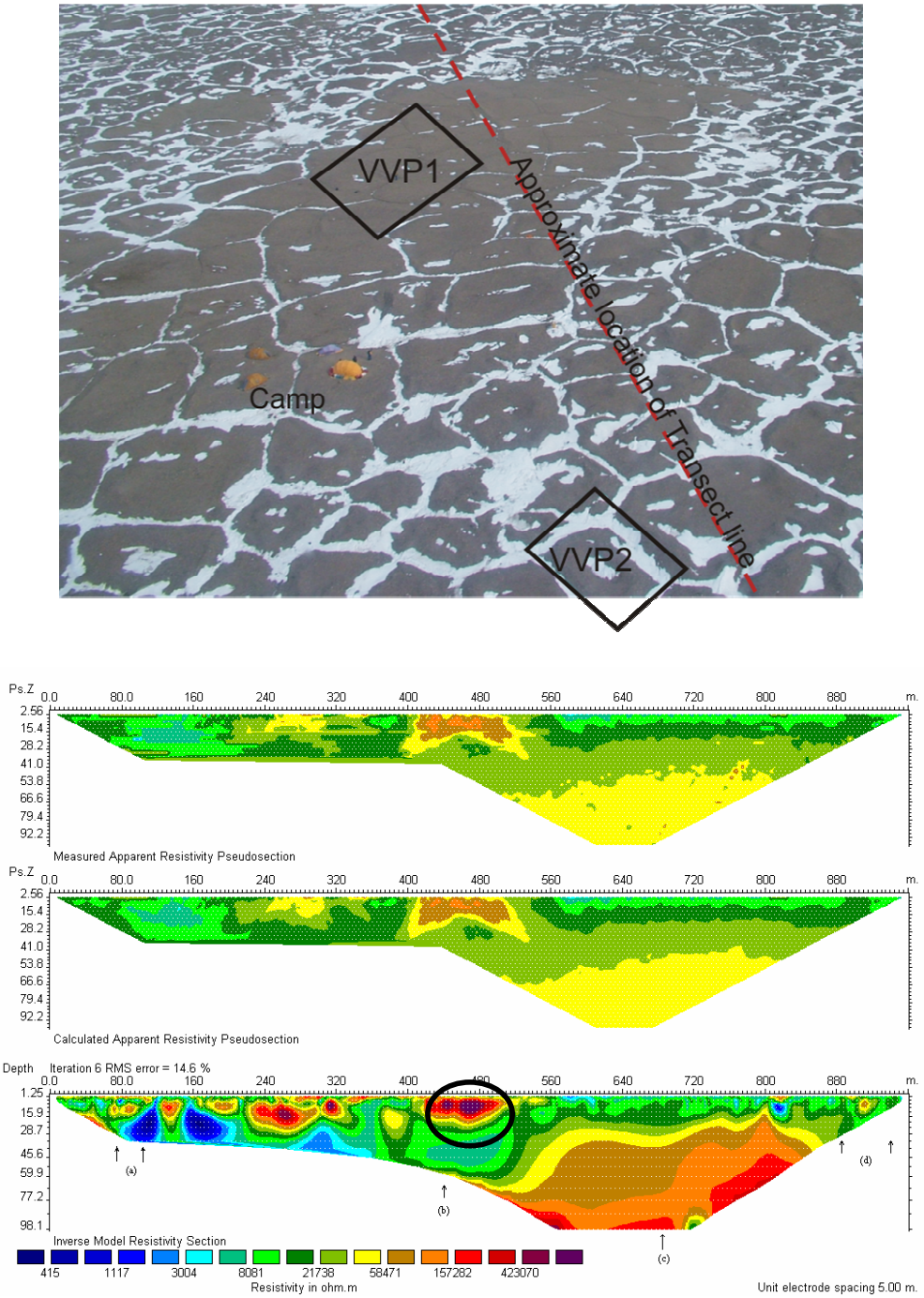

Figure 31: Resistivity cross valley transect conducted by K054, processed by Bannister (unpublished 2007) resolving anomalous feature at (b circled) in close proximity to VVP2.

with this project during the same field season and an anomalous body was identified in the subsurface (Figure 31, Bannister, unpublished 2007). The anomalous feature has been provisionally identified as a previously unknown buried massive ice body by Bannister (unpublished 2007) and [B] may be related to this. However, a reflector

from this feature would be expected to be from a greater two-way-travel time (140 ns or similar), and the delineation of the low relief area is more indicative of a newer surface rather than an underlying buried massive ice body.

[C] Strong SEC reflector seen at approximately 5.2 m (80 ns two way travel time). In the AGC gain profiles this reflector is not defined as seen in SEC. The weaker boosted signal has overwhelmed the strong contrast seen in

VVP2 survey area was located in close proximity to a cross valley transect conducted in conjunction with this field work and mentioned previously in relation to [B]. In the transect in the vicinity of VVP2 survey area an anomalous geophysical response is identified and interpreted as a previously un-known buried massive ice body, Figure 31. [C] could be associated with the transition into a massive ice body but is inconclusive without further correlation.

[D] Deep reflector at approximately 9.1 (140 ns two way travel time seen in individual profiles) in VVP2 survey area (Plate 2). The resolution of these reflectors is best seen in the synthetic aperture migration cubes with SEC gain but can also be traced through the individual profiles for the VVP2 survey area. There is a partial surface reflected in the limited range volumes x' and y' but in general the reflector is not strong enough to form a continuous surface in these volumes.

With reference to the anomalous body seen in Figure 31, this reflector is at a depth appropriate for the base of the interpreted buried massive ice body.

[E] Limited resolution of reflector seen near base of GPR resolution across multiple lines, at approximately 13 m depth (200 ns two way travel time): this is best seen in 100 MHz data displayed as successive individual profile lines or in the synthetic aperture migrated SEC gain cube. This reflector is near the base of resolvable signal in Beacon Valley GPR surveys. BVP2 was located near the edge of a large depression on the valley floor (approximately 100 m diameter and 20 m depth). The buried massive ice body associated with the Granite drift found in Beacon Valley (refer Chapter 2, Field area) has been speculated to be approximately 20 – 30 m thick due to the depth of these depressions interpreted as sublimation related

(Sletten, pers comm., 2006). If [D] is interpreted as being associated with the base of the buried massive ice this would indicate significant thinning of this ice body in the BVP2 survey area. This is not an unreasonable conclusion considering the proximity of BVP2 to a sublimation related depression.

5.1.2 Resistivity tomography:

5.1.2.1 General comments:

Please refer to Plates 5 – 8 for selected resistivity survey results for each PPG survey area. Appendix V has full records of this data if more detail is required.

Presented here are the psuedosections from the Res2Dinv inversion process as well as log plots of the model data. Three log plots are presented for each resistivity psuedosection: 1 showing normal scale log plot of the model resistivity; 2 showing the log plot of the model resistivity with the scale skewed towards greater definition within the high resistive response, and 3 showing a log plot of the model resistivity with the scale skewed towards greater definition of the low resistivity response.

Depth and resolution:

The depth of the response of the resistivity models relates to the length of the electrode array, which in turn relates to the number of electrodes and their spacing. For an array of 32 m length, a maximum depth of ~ 6 m was achieved. This depth is the same with 32 electrodes at 1 m spacing or 64 electrodes at 0.5 m spacing, but the 0.5 m spacing will produce better *lateral* and *veritcal* resolution within the profile. In Victoria Valley 32 electrodes at 0.5 m spacing was used with a maximum depth of response being ~ 3 m.

Evaluating response and data quality:

The psuedosections presented in Plates 5 – 8 show the models for the transition from measured apparent resistivity data to inverted resistivity models. Appendix V contains full sets of resistivity analysis with model uncertainties, sensitivities and differences

from the measured apparent resistivity to the modelled apparent resistivity. In general the quality of the data was good with few errors from bad electrode contact. VVP1's Southernmost West – East line required editing of bad data points before inversion.

The majority of the model uncertainties range from 3 – 9 % indicating that the models presented here are a good fit for the data collected in the field. When model uncertainties are higher than 15 – 20 % they are considered borderline for reliability. Sensitivity of the data is highest at the surface where there is greater data density.

The change into a highly resistive medium occurs near the surface in most of the psuedosections. This interface has a very high contrast in resistivity and as a result the scale used to encompass the entire range of resistivities is often too large to view details within these two units. By adjusting the scale the plots of the resistivity models, the variations within the higher or lower resistivity zones can be analysed with greater detail.

RMS and model quality:

RMS values have all converged to less than 3 % change between iterations of the inversion process. The accuracy of the resistivity model is limited by the non-unique nature of resistivity modelling. That is, many models of resistivity may produce the apparent resistivities recorded at the surface. The modelling constraints have been maintained through this thesis so that data sets can be compared directly, but this may also reduce the accuracy of the resistivity model by not tailoring the parameters for each individual data set. All of the model RMS misfit values are less than 15 % which is considered good. However, low RMS values do not necessarily correlate to geologically accurate or appropriate models.

5.1.2.2 Subsurface features:

General subsurface features seen throughout the results for all the PPG survey areas are denoted [1], [2], [3]… and specific subsurface features are denoted [A], [B], [C]... etc. Note that the resistivity values presented here are all high and the use of the

terms “resistive” and “conductive” are relative to the data here and do not represent absolute values.

[1] Strong interface with a high resistivity contrast in evidence 0.75 – 1.5 m beneath the surface. At this interface the resistivity effectively doubles from measurements typically around 4 kΩ.m to measurements in excess of 10 kΩ.m. Haerberli (1985) concludes that resistivity differences for frozen and unfrozen material can be up to two orders of magnitude. Given that high contrasts in resistivity between frozen and unfrozen material is more likely to be the result of water content, it is unlikely that the Dry Valleys soils would produce a frozen/unfrozen resistivity contrast of more than one magnitude and so this is interpreted as the base of the active layer. This interface has relief through the psuedosection and is generally depressed in the vicinity of contraction cracks. This depth is consistent with Guglielmin’s (2006) measurements of active layer depths in northern Victoria land, discussed previously.

[2] Decreased resistivity associated with thermal contraction crack expression, and associated increased resistivity in the vicinity of the upraised ridges: the decrease in resistivity over contraction cracks must be the result of a secondary factor involved in the electrical properties of the PPG subsurface as the thermal contraction cracks exhibited an open framework clast-supported composition at the surface. Gravels have extremely high resistivities (refer Table 2 Chapter 3, Near surface geophysics) due to the large amounts of air-filled spaces within an open framework. Even with infilling material such as sands, the unconsolidated material should maintain high resistivities. For the PPG resistivity profiles to show a relative decrease in resistivity compared to the surrounding soils there must be an additional electrical component within these structures. Although the Dry Valleys have little free groundwater within the permafrost soils (e.g. Denton et al., 1993, Sugden, 1995, and Summerfield et al., 1999), the open framework of the thermal contraction cracks would provide preferential pathways for groundwater movement and secondary concentration of salts within the cracks. The flow of groundwater and secondary salts could be a possible explanation for the decreased resistivity found within PPG thermal contraction cracks. Dickenson and Rosen (2003) examine development of concentrations of salts within Dry Valleys soils and propose that diffusing water

vapour and concentrated brines travel along moisture and chemical gradients and micro-channels which corresponds with the evidence seen here.

VVP1 displays an increase in resistivity within thermal contraction crack areas. If the decrease in resistivity is interpreted to be the result of preferential groundwater flow, then the lack of decreased resistivity in VVP1 could be attributed to the relative youth of the PPG survey area. If the groundwater paths have not been established along VVP1's contraction cracks the development of relatively conductive conditions within the cracks may not have happened yet.

[A] VVP1 zone of increased conductivity to the north dissipating to the south: the resistivity varies from ~ 20 kΩ.m immediately beneath the active layer to the North, to between 80 and 95 kΩ.m to the South. The surface expression of the survey area did not suggest an anomaly of any sort in the vicinity of VVP1.

[B] VVP2 zone of anomalous conductivity cutting through the location of an upraised contraction crack ridge: this feature lowers the resistivity and overprints the contrast of the active layer base [1].

Figure 32 shows F-K migrated profile lines from VVP2 that cut through a trough structure between 9 and 16 m along the line. The position of the Northern, West – East resistivity line was at right angles to these profiles cutting through at 14 m along the line. The depth of the trough in Figure 32 corresponds to approximately 2 m (30 ns two way travel time) consistent with the depths seen in the resistivity psuedosections.

The increased conductivity of the zone is explained by the same reasoning as the increased conductivity of the contraction cracks where concentrations of salts and metals in ground water have occurred due to preferential pathways. The geometry of the GPR reflector supports this as an area along which groundwater may pool.

[B] is not part of the conventional PPG structure, but field observations show that the standard model of a hexagonal roughly circular PPG structure was rare within the Dry Valleys surface. Inhomogeneity at the surface of the soil compositions may be a

contributing factor to the irregular propagation of PPG crack networks. This requires further research but is outside the scope of this project. [B] is speculated to be a relatively young feature formed by propagation of the thermal contraction crack to the east, propagating from the south to the north. The contraction crack to the east was seen to be shallower than either cracks to the north or south and may be actively dissecting the VVP2 and adjacent PPG area. The contraction crack to the East is thus interpreted to be young; as a result of the young age the previous soil deformation has not yet been overridden by new ridge formation.

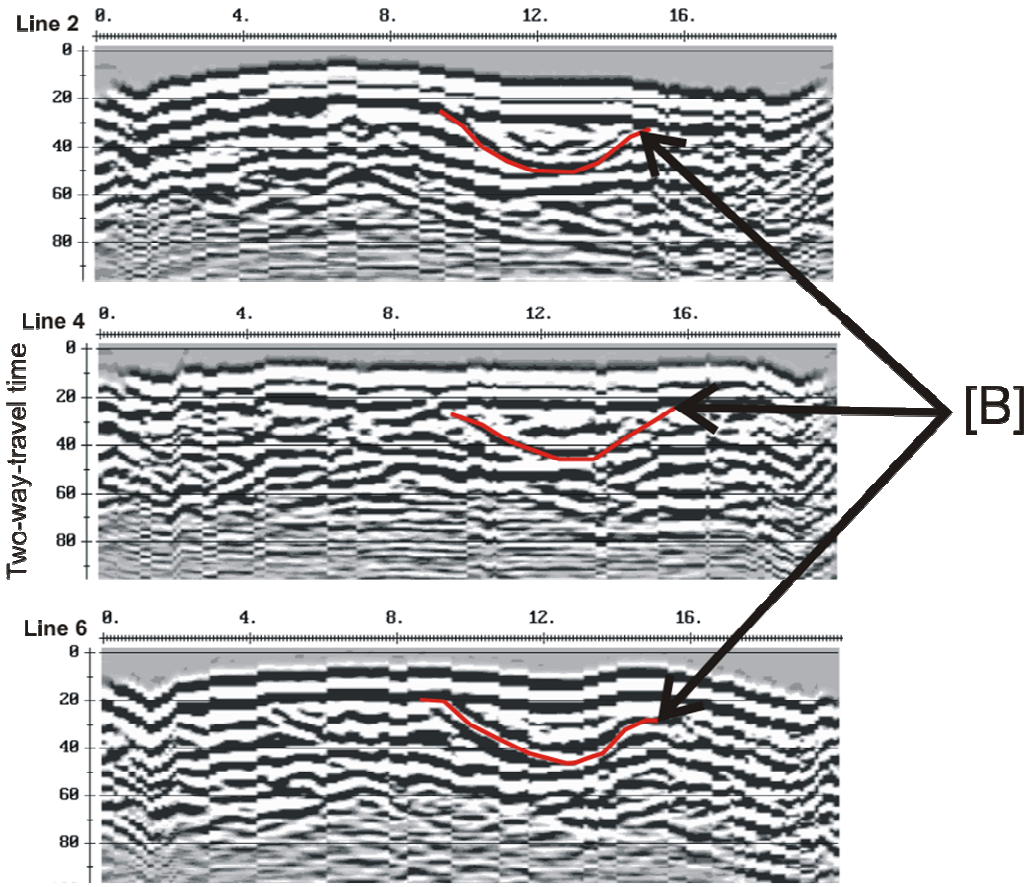

Figure 32: Cropped VVP2 200 MHz lines showing the reflector from the same location as [B].

[C] A second significant increase in resistivity found within BVP1 and BVP2 at ~ 1 m below the surface beneath upraised ridges and deeper in the contraction crack zones: the increase in resistivity is significant, typically changing from ~ 1200 ohms to > ~ 20000 ohms. In BVP2 [C] is found closer to the surface than in BVP1. The

buried massive ice body found in Beacon Valley has not yet had its spatial extent fully determined, but BVP1 and BVP2 were located in areas where surface features such as the granite drift and sublimation depressions have been associated with the presence of the buried massive ice body (Sugden, 1995, Marchant et al 2002). This interface is interpreted as the top of this buried massive ice body. The deeper positioning of [C] under BVP1 is also consistent with the proximity of a sublimation related depression (refer [D] GPR subsurface features).

The geometry of the interface of the buried massive ice body with the surrounding permafrost soils is linked to the surface expression of the overlying PPG. Depressions in the top of the buried massive ice body correlate with the surface position of thermal contraction cracks. This indicates that sublimation/mass loss of the buried massive ice body is linked to PPG structure. Marchant (2002) suggests that the PPG surface expression is driven by the sublimation of the underlying buried massive ice body. But a far more likely scenario is that preferential sublimation of the underlying buried massive ice body has been generated by propagating thermal contraction cracks. The gravel framework of the contraction crack infill would provide a less-insulating cover for the buried massive ice body than the permafrost soils covering the remainder of the PPG structure. Certainly, sublimation of the Beacon Valley buried massive ice body is connected to the PPG found overlying it. The question is, is it the driving force of, or a by-product of PPG formation and activity? Further research into this issue is required.

Banister (2007) relates anomalous buried massive ice relief to the centre of PPG structure. This data suggests that the relief seen on the buried massive ice body is directly related to the thermal contraction cracks. The depth of the buried massive ice body was not able to be resolved in this cross valley transect and the data suggested that the top of the massive ice body was at a greater distance beneath the surface than what has been seen here. The proximity of the interpreted interface between the Beacon Valley permafrost and buried massive ice body to the base of the active layer would not be likely to be resolved with the 5 m electrode spacing applied for the data presented by Bannister.

5.1.3 Electromagnetism

5.1.3.1 General comments:

Please refer to Plates 9 – 12 for selected results from the PPG surveys. For full electromagnetism results refer to Appendix VI. The response from the PPG structure is seen more clearly in the real component of the electromagnetism response as opposed to the quadrature component.

Depth of response:

The electromagnetic results represent bulk measurements of a volume of ground surface. The maximum depth of investigation for this method is estimated to be approximately 5.5 m (i.e. 1.5 times the loop separation/boom length). For the data collected in HLEM (Figure 18, Chapter 3) the sensitivity is at its maximum at approximately 1 m beneath the ground surface. However, the concentrations of salts and metals in the near surface of Dry Valleys PPG may result in the sensitivity being "skewed" slightly towards the surface.

Evaluating response and data Quality:

For geological surveys the targeted response is more commonly found within the quadrature component of the electromagnetic response. However, the response from the PPG structure underlying the survey areas is strongest in the real domain. The real component of electromagnetic response is more commonly considered to be the "metal-detector" function of electromagnetic surveys and usually reflects high conductivities (e.g. Telford et al., 1989, Milsom 2000 Gibson and George 2003). It should be noted that the real component recorded in this data is still low but does record the response of PPG, whereas the quadrature lacks any definable PPG relationship.

Previous use of EM31 over hydrocarbon contaminated PPG ground at Lake Vida (Petterson and Nobes 2002) showed a response predominantly in the quadrature

domain and it was anticipated that PPG structure in non-contaminated areas would still be predominantly in the quadrature component. It appears that the contaminant plume may have had a "dampening effect" and that the dominant electromagnetic factor in the Dry Valleys' permafrost soils may be the high concentrations of salts and secondary metals concentrated by dry conditions and wind blown deposition. The metallic content (particularly iron within the soils (Gibson et al., 1983) and secondarily deposited from EAIS concentrations via katabatic winds) has amplified the PPG response and has overprinted a phase rotation which has resulted in PPG response being found in the real component. High iron content has had similar effects elsewhere, as observed by Beeching (1999) in the Taharoa iron sands.

That said, the real response does display a stronger relationship to PPG structure that can be evaluated. The EM31 instrument used in this study has recorded the real response in parts per thousand (ppt) of the original input signal. Negative values of this relate to phase rotation over 90˚ and approaching 180˚ (refer Chapter 3, Near surface geophysics, Electromagnetism principles). The values over 0 represent a possible zeroing problem often found in real component data (Nobes, pers. comm 2008) but do still represent correct *relative* real component within the data.

The quadrature response is expressed in milliSiemens/m (mS/m) as a measurement of conductivity. The conductivity ranges for each survey areas are low, all within and less than a range of 2 mS/m, with VVP2 having the smallest range and BVP2 the largest.

Discussion of "high" or "low" conductivities/resistivities/responses refers to high or low values within the limitations of the data set unless otherwise stated.
In EM31 surveys the instrument will exhibit a sensitivity to structures oriented roughly perpendicular to the boom orientation. As such the parallel boom orientation will be more sensitive to East – West trending features, and the perpendicular boom orientation will respond more to North – South trending features. The difference of the parallel and perpendicular responses will identify areas of variation. Averages of parallel and perpendicular boom orientation data represent the subsurface conductivity of the volume beneath the instrument (Gibson and George 2003).

The electromagnetic data collected showed very strong along-line trends that overwhelmed ground response (refer to Appendix VI raw results). As much as possible the orientation and distance of the laptop and operator to the EM31 boom was kept constant. However, variations in the orientation and distance between lines could be the cause of the strong along-line trends. The subtraction of the median of each line lessened the effect of these along-line variations such that the resulting PPG response could be isolated. Care still must be taken when interpreting North-South running features.

5.1.3.2 Subsurface features:

As in previous sections, features that are prevalent through all of the data sets and represent generalised PPG structure resolution will be numbered [1], [2], [3]… , and discussed in the following text and labelled on Plates 9 – 12. Anomalous responses outside of PPG interpretable structure will be labelled and discussed under [A], [B], [C]... etc.

[1] Altered response can be found over contraction cracks and correspondingly increased resistivity over associated ridge geometries: this is consistent with the electrical properties of the PPG structure seen in the resistivity tomography results previous. This response is best seen in VVP2 and BVP1 where it is clearly defined and is also exhibited in BVP2. This response is most likely the result of increased volume of dry material in the upraised ridges compared to the water and salt pathway created in the contraction cracks. However, VVP1 displays a different response style over the contraction cracks. The topography is limited on VVP1 and upraised ridges are not a dominant feature which may explain the lack of increased resistivity if there is no significant extra volume found there.

[A] Trend of increasing resistivity from the Northeast to the South – south west in VVP1 (Plate 9). This is correlated with [A] seen in 5.1.2.2 [A] resistivity results. [A] may be related to 5.1.1.2 [B] GPR results. No conclusions can be made without further data on this anomaly.

[B] A zone of higher real response cutting through the spatial distribution of the contraction crack ridges in VVP2: the topography survey for VVP2 shows a minor depression in the ridge geometry in the vicinity of this anomaly but is not defined as part of the contraction crack network of VVP2 as exhibited at the surface. This feature is correlated with [B] from section 5.1.2.2 resistivity results. The relative conductivity of this feature appears to be due to ground moisture pooling and the associated concentrations of salts.

5.1.4 Synthesis:

The previous sections have identified features seen in individual methods and results. The correlation across methodologies allows for positive identification of features such as the active layer and buried massive ice bodies, and more complete integrated interpretation.

The use of multiple techniques has allowed for further resolution of the physical properties of the PPG subsurface. For example, the velocity determined through GPR using a CMP survey was found to be between 0.12 – 0.14 m/ns; an average of 0.13 m/ns being used for processing of the results. This value is low for velocities found in equivalent non-Dry Valleys examples (e.g. Munroe et al. 2007). When examining the electromagnetism results we see that the PPG response has been shifted from the quadrature component of the secondary field (where most geological targets are resolved) to the real component of the secondary field (where highly conductive targets are normally resolved). This is attributed to the high levels of iron found in the Dry Valleys (Gibson et al. 1983), as observed at the surface as iron staining, creating the “red” landscape seen there (Marchant et al., 2002, Maurice et al., 2002). The velocity of electromagnetic signal has a component of magnetic susceptibility [eq. --] (Chapter 3 Near surface Geophysics) which is normally disregarded as the effect on the velocity is minimal in the majority of geological surveys. However, Beeching (1999), found the effects of iron concentrations was to reduce the velocity of electromagnetic waves in the Taharoa iron sands, which supports the lower velocity found within the Dry Valleys.

The iron staining was stronger in Beacon Valley, possibly due to its closer proximity to the East Antarctica Ice Sheet, compared to our field location in Victoria Valley.

Velocity analysis was not able to be completed at our field location in Beacon Valley. Further research should attempt to gather CMP data for the Beacon Valley subsurface for comparison with the Victoria Valley CMP data presented here.

5.1.4.1 Active layer resolution:

The active layer is best resolvable with resistivity methods as the difference between the electrical properties above and below the base of the active layer are roughly an increase of an order of magnitude of the resistivity response, creating a large contrast in the resulting psuedosections. The clarity of the resolution of the active layer within the resistivity data allows for correlation to GPR reflectors, when the strength of the GPR reflectors indicates a change in dielectric properties across the boundary.

5.1.4.2 Contraction crack resolution:

The geometry of the contraction cracks at depth has not been determined using these techniques due to the inability to resolve the contraction crack directly. GPR energy did not reflect from the boundary between the permafrost and contraction crack, indicating that the contraction crack maintains a vertical or near vertical position, or that the dielectric difference between the two medium is too low to be resolved. The gravel infill material seen in the contraction cracks is also likely to cause significant scattering of the GPR wave.

Although the mechanics of thermal crack generation and continued propagation has been developed in the literature (refer Chapter 1, Polygonal patterned ground processes), there has been no evaluation of whether contraction crack geometries are expected to remain vertical with depth. Given the highly irregular geological composition of most periglacial soils, with grainsizes ranging from fine sands to large boulders, the concept of deflection of the contraction crack with depth may warrant further investigation. However, without being able to trace the geometry from the surface, a reflector from a dipping contraction crack would be unidentifiable as being generated from the contraction crack.

Resistivity tomography identifies areas of higher conductivity that are spatially related to the thermal contraction crack surface expression but does not define the wedge as it propagates to depth. This is most likely the result of the diffusive nature of the salts causing the increase in conductivity of the thermal contraction crack rather than a lack of wedge definition at depth.

Electromagnetism and resistivity tomography can locate areas of increased conductivity associated with the location of thermal contraction cracks. However, these methods area essentially a bulk measurement technique and do not have the required resolutions for tracing a thermal contraction crack to depth. The electromagnetic results present a 2D plan of the electrical properties of the survey area, with the measurements representing down to approximately 5 m depth with maximum sensitivity at approximately 1 m. The resulting map of the electrical properties is useful for identifying areas of anomalous response which may interfere with interpretation of PPG structure in the other methods, but does not provide additional information on the PPG subsurface structure than what can be deduced from the surface expression. Resistivity tomography produces psuedosections of the resistive properties of the subsurface but lacks the resolution to define thermal contraction cracks. With a minimum of 0.5 m spacing (as used in this research on VVP2, BVP1 and BVP2) more detail cannot be obtained using the system that was available.

Despite not being able to delineate the thermal contraction crack geometry to depth these methods yielded information regarding the interactions between thermal contraction cracks and the surrounding permafrost. The increase in attenuation of the GPR signal and conductivity in proximity to thermal contraction cracks indicates that secondary enrichment of the contraction cracks with salts has likely occurred. The concentrations of salts within these zones indicates that despite low water content within Dry Valleys' soils some mobilisation of free water does occur.

The indirect identification of the contraction cracks limits interpretation of the development of this feature at depth from young PPG (VVP1) to mature PPG (BVP2). However, there is a general increase in the depth of the associated features that have been used to indicate the presence of the thermal contraction cracks. In particular, the

deformation of the surrounding permafrost soils is seen to be of a larger magnitude and propagating to greater depth as PPG maturity increases; consistent with PPG theory. Similarly there is a general increase in the zones of attenuation of GPR signal (this is best seen in the SEC gain profiles) that could be attributed to greater salt concentrations built up over a longer time period for mature PPG.

5.1.4.3 Buried massive ice bodies and relic surfaces:

Buried massive ice bodies are identified in 3 of the four PPG survey areas. This was unintentional but has highlighted the ability of near surface geophysics to evaluate the subsurface and find previously un-identified features such as buried massive ice bodies.

The clearest resolution of buried massive ice bodies was within the resistivity data where high contrasts between the resistive properties of the Dry Valleys' permafrost and underlying buried massive ice bodies could be identified with ease as they were of an order of magnitude between the buried massive ice body and the permafrost, and two orders of magnitude between the buried massive ice and the unfrozen Dry Valleys soils. The depth of the resistivity profiles was not great enough to correlate the GPR reflector reflector (GPR 5.1.1.2 [D]) with the base of the buried massive ice. I propose that future work on the Beacon Valley buried massive ice body should involve a small electrode spacing (0.5 – 1 m), long line survey (128 electrode string) over this area to attempt to delineate the extent of the buried massive ice body. The cross-valley transect conducted in conjunction with this field work and presented by Bannister (2007) indicated that the minimum depth to the base of the buried massive ice would be at least 110 m. The large (5 m) electrode spacing may have affected the resolution of the interface between the buried massive ice and underlying soils.

The provisional identification of a buried massive ice body beneath VVP2 is due to cross-valley transect work processed by Bannister (2007), (Figure 31). This resistive body is correlated to a reflector near the base of resolution for the GPR surveys conducted over VVP2. Unfortunately the other methods used did not achieve a comparable depth to enable correlation of this feature with other physical property

data. As such the association of this feature with the buried massive ice body is provisional and not able to be confirmed using these results

5.2 Resolution of seasonality in the subsurface (time lapse):

This section presents the results from the time-lapse GPR and resistivity tomography imaging conducting for this research. Subsurface structure that has been resolved by these methods has been discussed in section 5.1 and will only be discussed here in terms of the *changes* across the time-lapse period. The time-lapse analysis will follow the format of general trends and then identification of specific aspects of these results.

5.2.1 VVP2 time-lapse GPR:

5.2.1.1 General comments:

Please refer to Plates 13 and 14 and Appendix IV for GPR results. GPR resolution of PPG subsurface features has been discussed in section 5.1.1.2.

Depth of penetration:

As with the subsurface structure GPR results the depth of penetration for the 100 MHz was ~ 13 m and ~ 10 m for the 200 MHz

Evaluating signal and data quality:

Unlike with previous interpretation of GPR data the signal quality itself is not as important as the way it changes through the time-lapse period. As such, the synthetic aperture migration with SEC gain proved to be more effective at evaluating the change in signal through the season.
Attenuation, signal ringing and reflector resolution contrast are the dominant features of the time-lapse trends. These are best seen in synthetic aperture migrated SEC gain cubes. F-K migrated data with AGC gain is not useful for evaluation of changes within signal through this time-lapse sequence and is not presented here.

5.2.1.2 Time-lapse trends:

There is a loss of signal through the season with weaker reflectors being lost as the season progresses. This indicates a change in the attenuation factors found within the PPG subsurface. This loss of signal affects the amount of signal being received back from the subsurface resulting in boundaries with large contrasts in the dielectric constant being resolved with greater clarity. This can be seen particularly well with the resolution of the previously discussed [A'] from section 5.1.1.2. Figure 33 from Godfrey et al (2008) shows the resolution of [A'] into a defined continuous layer near the end of the season.

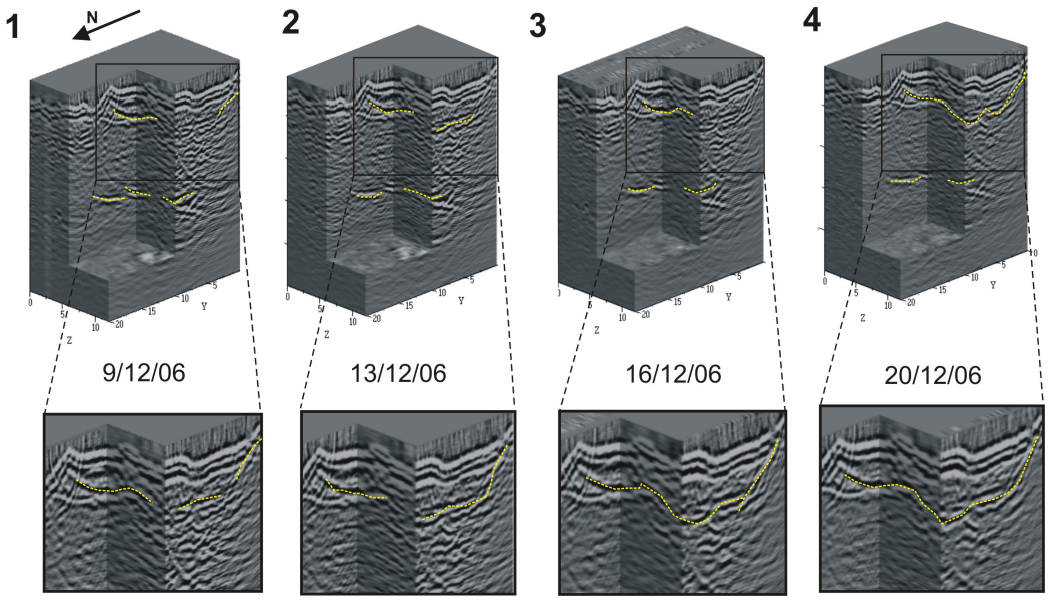

Figure 33: resolution of a single continuous layer (yellow line) of high dielectric contrast seen in synthetic aperture migrated SEC gain cubes. VVP2 200 MHz. (Godfrey et al., 2008).

[A'] was previously interpreted as the base of the active layer, with correlation from the resistivity profiling. This increased resolution as the season progresses means that for clearer resolution of the active layer, GPR surveys should be conducted later in the season.

The zone of attenuation that has been associated with the location of thermal contraction cracks expands as the season progresses. The increased loss of signal concentrated in the area of the thermal contraction cracks can best be seen in Plate 14.

The loss of signal through the warming/thaw season is attributed to the release of salts and increased levels of water in liquid and vapour form within the soils (Dickenson and Rosen 2006).

5.2.2 VVP1 time-lapse Resistivity tomography:

5.2.2.1 General comments:

Please refer to Plates 15 to 18 and Appendix V for resistivity tomography results. Resolution of subsurface PPG features has been discussed in section 5.1.1.

The psuedosections created by resistivity inversion program Res2D were too coarse to determine the changes in resistivity within VVP1 surveys. The plots of the log of the model resistivity had the advantage of being able to adjust the scales to focus on high or low resistivity response. The difference of the log resistivity models show relative changes between time-lapse runs.

The resistive properties found within the subsurface have remained largely neutral over the time lapse period with plots of the difference between time-lapse surveys being close to 0.

There were more subsurface features identified in resistivity data conducted over PPG areas with greater maturity. In general the subsurface features were more defined within the older PPG survey areas. Future time-lapse resistivity surveying should take be conducted over moderately developed PPG to determine if variations in the subsurface can be quantified better than what has been achieved here.

5.1.2.2 Time-lapse trends:

The differences between time-lapse 1 (TL1) and time-lapse 4 (TL4) show that the majority of change in the resistive properties of the subsurface are concentrated at the active layer base. An increase in resistivity can be seen to occur there between TL1 and TL4. This increase is best defined on Plate 15. The majority of this change occurs between TL1 and TL2 (time-lapse 2) where the horizon can be seen to be forming on all TL1 – TL2 profiles. West – East line 1 (Plate 14) exhibits this feature as having a greater depth of influence than seen in West – East line 2 (Plate 15)

Dickenson and Rosen (2003) propose that highly saline water concentrations form within the PPG subsurface and that during the summer months are diluted. High levels of dissolved salts within water will lower the freezing point below 0˚C and it is proposed by Dickenson and Rosen, that brine layers of sufficient salt concentrations to stay liquid, are formed in the winter months. During summer months an increase in water vapour diffusing through the cold subsurface dilutes these brine layers resulting in the freeze of the layer at the ground ice interface (i.e. active layer base where temperatures drop below 0˚C). The presence of an increasingly resistive layer being concentrated at the base of the active layer is supportive of this proposal for ground ice generation during the summer months. The increased depth of influence of this feature as seen in West – East line 1 is attributed to that lines proximity to a thermal contraction crack which has been suggested as a preferential pathway for groundwater and vapour (refer 5.1 Resolution of subsurface structure).
This formation of ice at the active layer base is proposed as a mars analogue for ground ice formation.

Above the active layer base there is a general trend for minor increases in conductivity in the across the four time-lapse lines. This increase in conductivity through the warming period is consistent with increased diffusing of water vapour and free water movement above the freeze level represented by the base of the active layer.

The anomalous feature [A] discussed in 5.1.2.2 has increased conductivity to the north in South – North line 1 but increases in conductivity in South – North line 2.

The log of the resistivity plots for South – North line 1 (Plate 20) shows the development of a downward propagating plume of increased conductivity from TL1 to TL4. Magnetic susceptibility

5.2.3 Synthesis:

Resistivity lines and GPR surveys were repeated over VVP1 and VVP2 respectively, to gather time-lapse data so that changes in the physical properties of the PPG subsurface could be monitored over the thaw period.
The progressive loss of signal over the warming/thaw period of the PPG cycle is consistent with the increased conductivity seen above the active layer in the resistivity data.

5.2.3.1 Resolution of the active layer:

The active layer and the changes associated with the thaw/thermal expansion part of the PPG activity cycle can be seen in both methods.

The resistivity method showed a localised increase in resistivity at the base of the active layer that has been associated with freeze of diluted brine horizons as water vapour is diffused through the subsurface through the warmer months (Dickenson and Rosen 2003).

The resolution of the active layer within GPR data increases as the warming period of the PPG cycle progresses. The identified active layer seen within the time lapse over VVP2 is easier to resolve into a single continuous surface later in the season as the warming/thaw progresses. The increase in conductivity seen over the active layer base would result in an increase in attenuation of GPR signal within this zone. This increased attenuation of signal from above the active layer is a contributing factor to the increased resolution of the active layer within GPR time-lapse surveys.

5.2.3.2 Resolution of PPG structure:

Contraction cracks were not directly identified (as discussed previously) within the subsurface data and changes within the resistivity results were not attributed to

thermal contraction crack processes. However, the size of the attenuation zones seen in the GPR profiles increased as the season progressed. This has been attributed to the increase of free water and salt mobilisation with the thaw/warming period but cannot be related directly to the development of PPG structure.

Changes in the subsurface properties were detected but due to the variations in the exact state of the climate year to year, further research in this area should conduct surveys over the entire summer season for comparison. The resolution of the active layer was of a high quality within the resistivity results. Changes in the active layer could be monitored over a PPG area using 3D and time –lapse resistivity to build up a picture of how the active layer changes over the freeze thaw period. This has implications not just for evaluation of the PPG structure but for climate change monitoring within the Dry Valleys (refer to discussion for further examination of this).

5.3 Summary:

The PPG near surface geophysical response is summarised in Figure 34 where the determined relative physical properties of the Dry Valleys' PPG structure is displayed and the best target method recommended.

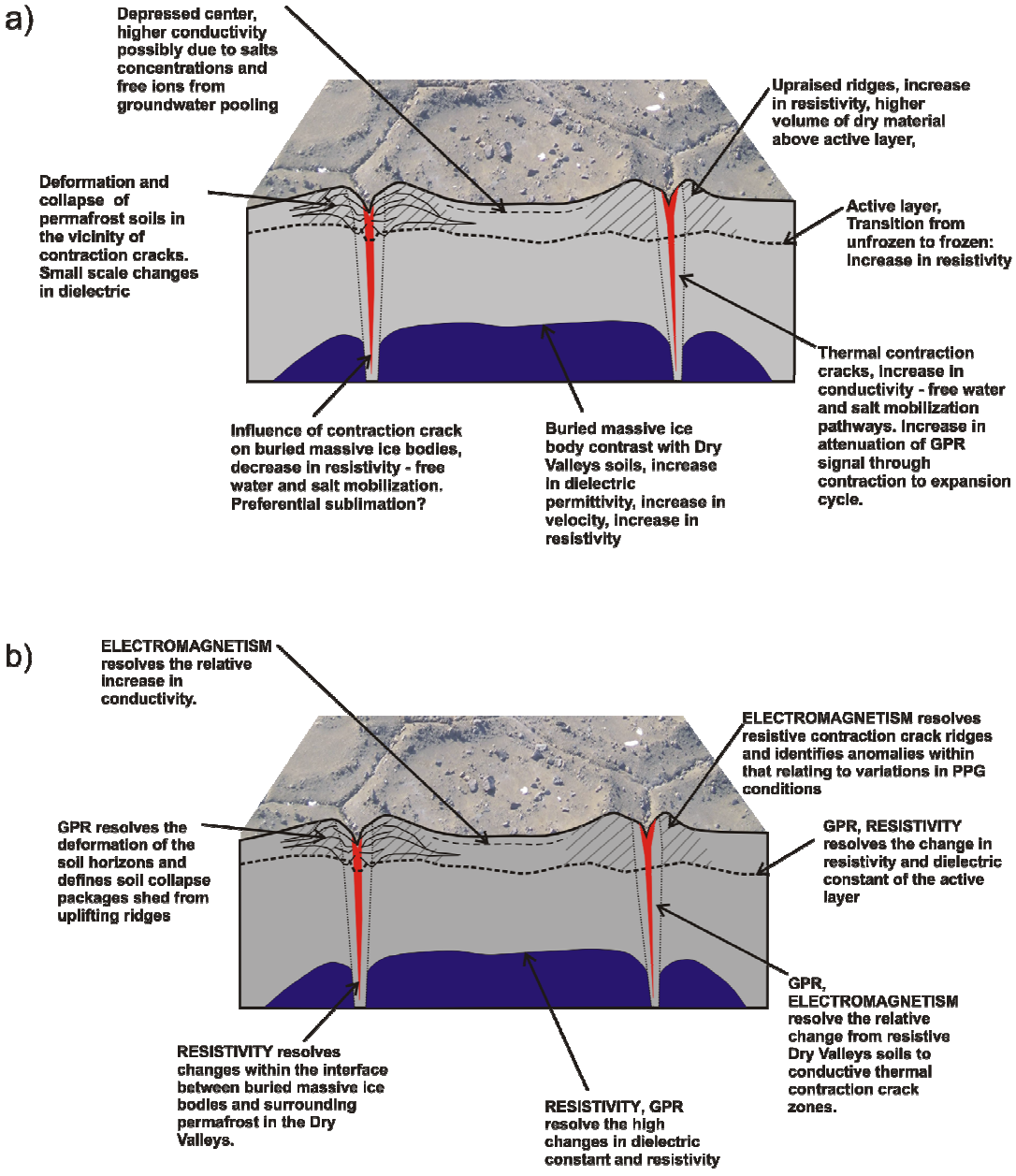

Figure 34: PPG structure and near surface geophysical response and surveying a) summarises the relative physical properties of Dry Valleys' PPG b) identifies the methods best able to resolve each of the PPG structure targets for future applications of this research.

5.4 Data limitations:

The primary limitation for interpretation of this data set is the lack of subsurface data for correlation with these results. In applications of near surface geophysics outside of ASMA's (Antarctic specially managed areas) it is common practise to calibrate the geophysical data with data from a borehole or trench. The reasons for not disturbing the Dry Valleys soils to obtain similar calibration data for this research are as follows:

- This research was primarily driven by the need to find a non-invasive method to evaluate PPG subsurface structure and activity in the delicate Dry Valleys soils

- Obtaining permission to disturb Dry Valley's soils is a difficult process and would have required planning outside the time frame allowed for completion of this thesis.

- Drilling or trenching in the Dry Valleys is difficult due to the gravely and glacially derived sediments that are the predominant soil composition in our field areas.

- Disturbance of the subsurface within the PPG survey areas would have reduced the value of these PPG survey area sites for future re-surveying or continuation of time lapse imaging.

To minimise the error associated with the lack of subsurface calibration, multiple methods were used. This allows for cross-checking of responses across different methodologies to isolate the cause of the response, for example, defining an identified GPR reflector as being from a change in electrical properties rather than a change in density, by correlating with resistivity results.

6: Discussion:

6.1 Resolution of the PPG structure and activity:

The resolution of PPG subsurface structure was limited by only being able to achieve indirect identification of thermal contraction crack lateral positions. Resolution of the depth of thermal contraction cracks could not be achieved in this research. As a result, the variation in the contraction cracks was not able to be evaluated in the time-lapse methodologies. Active layer identification and resolution across the PPG survey area was achieved in both resistivity and GPR and changes could be tracked over the time-lapse methodologies. In addition to PPG structure, buried massive ice bodies and relic surfaces were resolved, and additional anomalous features requiring more research were identified.

GPR and resistivity tomography were the most effective in identifying aspects of PPG structure in the subsurface. GPR was the most detailed of the surveys with individual reflectors being able to resolve deformation of soils horizons in the vicinity of the contraction cracks. However, positive identification of active layer base and buried massive ice bodies within the GPR data was not possible without correlation with resistivity tomography results. The electrical contrast seen in the transition from unfrozen to frozen sediments is clearly identifiable in resistivity profiles but resolution of other PPG structure was limited by the lack of fine resolution of this method. Thus the combination of the two methods yielded more information than either separately.

Electromagnetism methods resolved anomalous zones affecting the resolution of PPG structure. The rotation of the PPG electromagnetism response into the real component highlighted the increased magnetic susceptibility of the Dry Valleys' soils due to the high iron and salts concentrations found within them. This affected not just the electromagnetic response but the attenuation of the GPR signals.

In general the most reliable interpretation of the subsurface was achieved by correlating resistivity and GPR results.

6.2 Applications of Geophysics in Antarctic Dry Valleys:

Future applications of near surface geophysics in areas of PPG in the McMurdo Dry Valleys will need to be allow of the effects of seasonality on the collection of data. In addition to resolving subsurface structure the time lapse GPR surveying revealed a progressive loss of signal to depth over the thaw period. This has been attributed to the release of salts as the soil temperatures increase over the course of the summer. Future applications of GPR in the McMurdo Dry Valleys will not only need to identify targets but also appropriate timing of data collection relative to the progress of summer.

For targets at depth such as valley structure or buried massive ice bodies an early field season is more appropriate to avoid attenuation of the signal within the top of the penetration depth. However, for full resolution of the depth to freeze for the active layer or similar shallow targets a later field season is more appropriate. Seasonal variation did not seem to affect the resolution of subsurface features within the resistivity data. The relative timing of the thaws progress will not need to be factored into planning future resistivity surveys in the Dry Valleys.

The use of resistivity tomography over PPG in Beacon Valley has shown that it can be applied with success to evaluation of PPG structure and underlying buried massive ice bodies. The resistivity contrast between the PPG and the buried massive ice body was high enough to resolve the buried massive ice body interface as being separate to the active layer base despite their similar depths. The work conducted by Bannister (2007) used resistivity tomography at a much larger scale to that which has been presented here. The surveys over BVP1 and BVP2 were along the cross-valley transect that suggests that the minimum thickness of the buried massive ice is 110 m. The resolution of the top of the buried massive ice body appears to be at close to 20 m depth where the transition from ~ 15 kΩ.m to ~100 kΩ.m occurs (Figure 35)

In the resistivity tomography over BVP1 and BVP2 this transition is seen to occur at

between 1 – 3 m depth which is consistent with field observations by Sugden et al. (1995) and Marchant et al. (2002). This indicates that there may be issues surrounding interpretation of the buried massive ice interface when using large scale resistivity tomography surveying.

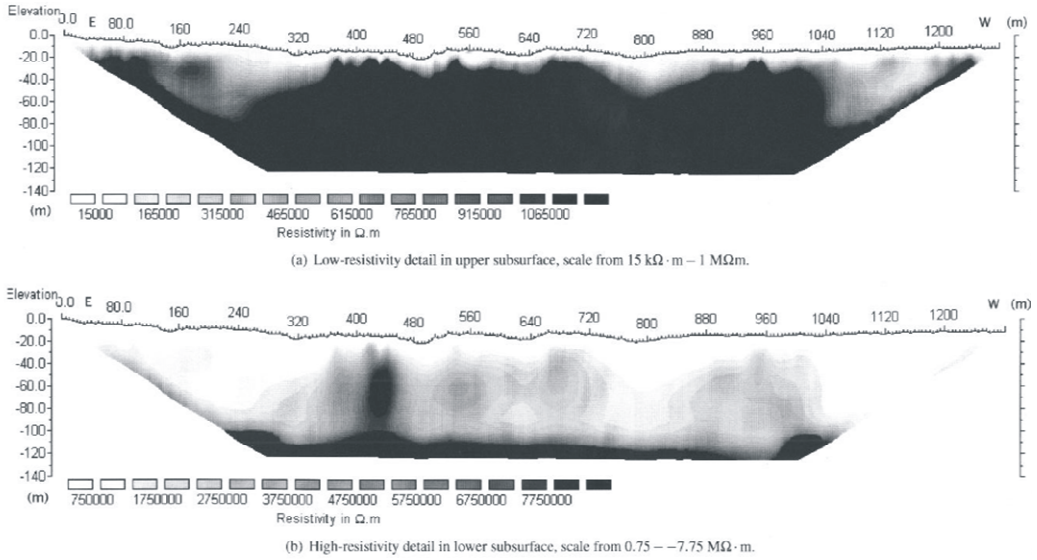

Figure 35: High and low resistivity features of the cross-valley transect conducted by K054 and processed by Bannister (unpublished 2007)

6.3 Buried Massive Ice Bodies and PPG

The relationship between PPG surface expression and buried massive ice bodies has been contested in Beacon Valley. Marchant et al. (2002) suggests that the PPG found overlying the Beacon Valley buried massive ice body, are sublimation polygons rather than the product of thermal contraction and expansion driving wedge growth supported by Sletten et al. (2003). The solution to this issue may be the key to dating the age of the Beacon Valley buried massive ice body, as the permafrost soils contain a layer of tephra dated at 8 Ma. If sublimation is the driver for the PPG surface in Beacon Valley then this age may be taken to represent the minimum age for the buried massive ice body. However, if active thermal expansion and contraction is driving wedge growth and PPG development, then the tephra layer cannot be interpreted as being in-situ within the permafrost soil horizons; due to re-working.

The resistivity data have resolved the interface between overlying permafrost and the underlying buried massive ice. The interface was also apparent in the field (Figure 36)

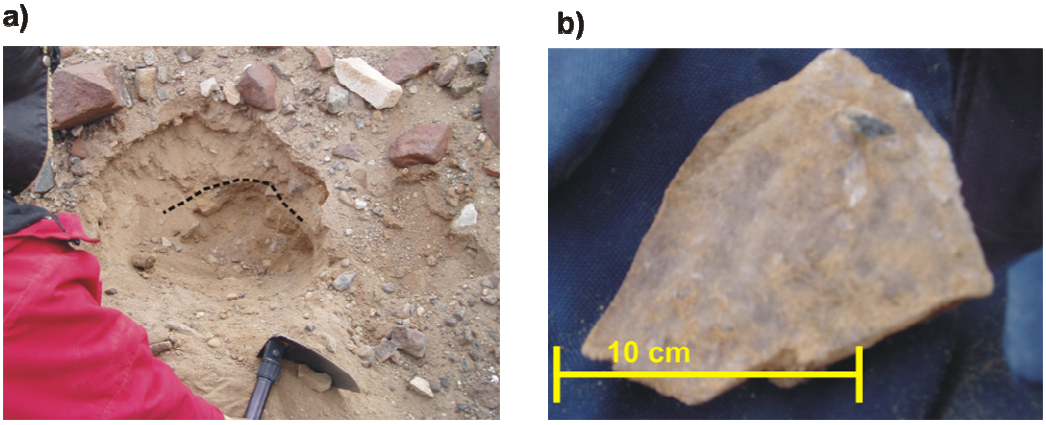

Figure 36: Beacon Valley buried massive ice body a) dashed line marks the location of the top of the buried massive ice body beneath a contraction crack ridge at approximately 0.4 m depth beneath the surface b) is a piece of the buried massive ice body from Beacon Valley. The ice is dark in shade because of high sediment content (Sugden et al., 1995).

at shallow depths beneath upraised contraction crack ridges.

The resistivity showed variations in the relative depth to the buried massive ice body beneath contraction cracks and associated upraised ridges. The buried massive ice body interface was seen to be deeper underneath the contraction cracks and shallower under upraised ridges. The relief on this surface is indicative of sublimation processes being present within the buried massive ice body in the vicinity of the contraction cracks. However, it should be noted that the propagation of a thermal contraction wedge into the subsurface is a process that will change the thermal regime found therein and some preferential sublimation under contraction cracks should be expected (Berg and Black, 1966)

So is sublimation the only processes operating within the subsurface of Beacon Valley?

According to Marchant et al. (2002) the sublimation polygons will exhibit the same surface expression as standard thermal contraction crack polygons but have none of the associated internal structure. Most importantly, there will not be evidence of deformation of the surrounding permafrost soils as no propagating wedge needs to be accommodated within the subsurface. These deformation features were resolved with the use of GPR and can be seen in BVP1 and BVP2. This would indicate that thermal contraction crack propagation has occurred within the Beacon Valley PPG surface

and that the Tephra layer cannot be reliably interpreted as not re-worked.

Sletten et al. (2003) discusses alternative estimations of the age of the Beacon Valley surface based on reworking approximations for mature PPG from the ratio of PPG size to wedge growth rates. This methodology suggests that the floor of Beacon Valley is on the order of 10^5 years old which is considerably younger than the c. 8 Ma interpreted from the tephra layer. This is because the PPG is considered to resurface the valley floor over this time period essentially "resetting" the clock on the age of the surface.

Buried massive ice bodies and their relationship to PPG are difficult to study without prior knowledge of the location of buried massive ice bodies. Victoria Valley transect work conducted in association with this research (Bannister, 2007) identifies an area of high resistivity and GPR signal anomaly which has been provisionally identified as a previously unknown buried massive ice body. The location of the Valley transect was in close proximity to the VVP2 survey area (Figure 31 previous) where a strong reflector was seen at the base of the GPR resolution. Unfortunately the resistivity surveys did not reach deep enough to correlate the deep reflector back to the resistivity anomaly resolved by Bannister (2007).

The use of near surface geophysical methods to resolve buried massive ice bodies has been shown to be effective in the Dry Valleys and provides another tool for the evaluation of PPG development and underlying buried massive ice. With application of time-lapse imaging of PPG in areas of buried massive ice the effects of the buried massive ice on seasonality within PPG subsurface could be evaluated.

6.4 Climate change monitoring and PPG

The Antarctic Dry Valleys are increasingly being recognised as an important place to monitor changes in climate (e.g. Guglielmin, 2001, Doran et al., 2002, Guglielmin, 2006).

Environmental conditions on earth are maintained by large scale global systems that attempt to attain equilibrium of conditions across the globe. A relevant example of this is the movement of heat through atmospheric and oceanic circulation cells (Figure 37). Antarctica has the unique condition of being an intricate link in global system science while being far removed from anthropogenic influences. As such, Antarctica is an ideal location for monitoring changes within these systems that might be a result of human activity. The reasoning behind is that if human activity has effected change within these global systems this change will be able to be detected in Antarctica, through these global linkages. Measuring change in these systems in Antarctica can

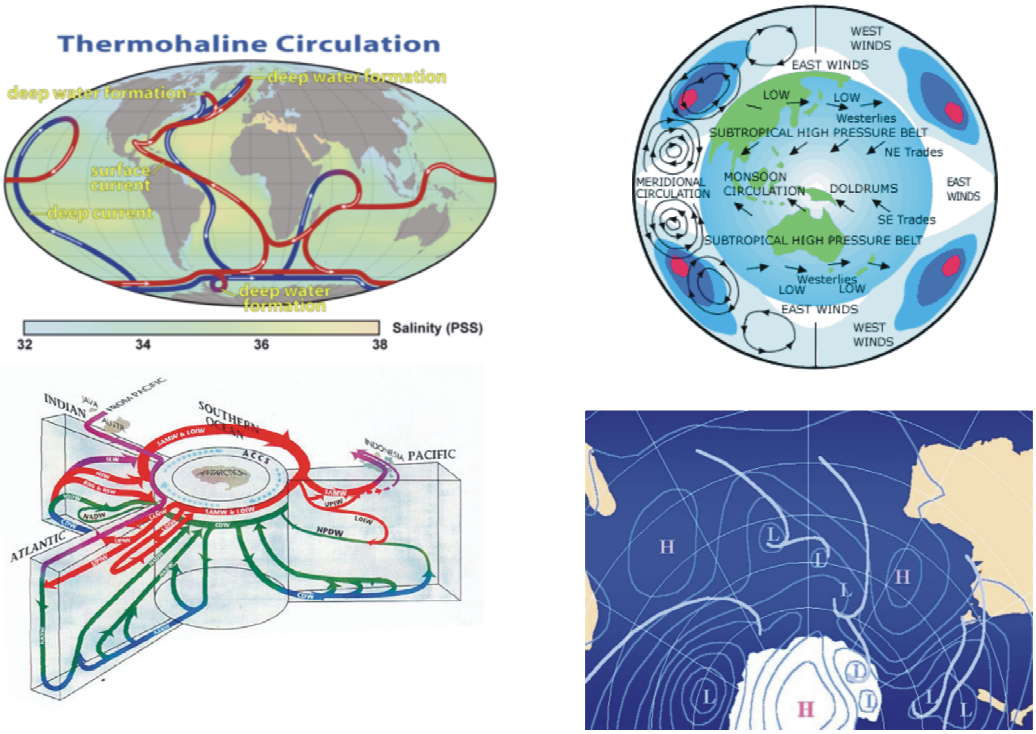

Figure 37: models of global systems; thermohaline conveyer belt driven by Antarctic bottom water generation which links the three ocean basins of this giant circulation cell, and atmospheric circulation cells which redistributes heat and generates dominant pressure systems such as the permanent high pressure over Antarctica which contributes to its continued frozen state by maintaining the supply of cold dry air washing over the East Antarctic Ice Sheet.

evaluate change within the global system without the local and small scale human influences contaminating the measurements as found elsewhere in the world.

Research on ground surface and subsurface temperatures show that the PPG in the Dry Valleys are directly coupled with the atmospheric temperatures. This coupling of temperatures is reflected in the active layer depth and level of zero annual amplitude (Doran et al. 2002). Active layer depth has been resolved in this thesis using GPR and resistivity over PPG. The use of GPR and resistivity in the Dry Valleys is relatively non-invasive and provides another tool for monitoring the active layer through the seasons for changes in response to climate change.

Resistivity tomography proved to be the most successful for positive identification of the base of the active layer. Only 2D resistivity data was collected for this research but 3D arrays and modelling are available (Geotomo software, 2004 ?). 3D resistivity would provide an image of the morphology of the active layer over a given area. Time-lapse imaging over the course of the austral summer would produce a model for the changes of the active layer through over the thaw period. Subsequent seasons could re-produce the time-lapse imaging to evaluate changes in the active layer depth over a given area over successive seasons. This would provide a tool for monitoring climate change within the Dry Valleys with minimal disturbance of the subsurface and high data quality. The identification of the active layer within resistivity data is shown to be clear and concise due to the increase in resistivity of an order of magnitude. Common alternative methodologies involve probing of the subsurface to identify the change from unfrozen to frozen sediments (i.e. the density increase and higher ice content of the frozen sediment will resist probing more than overlying unfrozen sediment) or temperature gradient analysis. For time-lapse analysis the collection of this data over an area would be labour intensive. In contrast, once the electrodes are in place repeat collection of resistivity data over a time-lapse period requires minimal labour.

However, Guglielmin (2000) suggests that relevant PPG monitoring for climate change should use the depth to the $0^{\circ}C$ isotherm as the high salinity of the Dry Valleys soils can effect the temperature at which they freeze. Although there is a gradual change in physical properties with a reduction in temperature a dielectric

interface is required for reflection of GPR energy and modelling of electrical properties is not accurate enough to resolve the gradual change to a degree where temperature could be isolated. A change in state is required to determine temperature variations in the subsurface otherwise the physical properties of the cooling soils are too similar to be resolved by near surface geophysical methods. In general resistivity will increase with degrees below zero and increasing ice content. This relationship is somewhat complicated by the addition of salts to the subsurface regime of the McMurdo Dry Valleys.

Thus, while the zero degree isotherm may not be resolvable, the active layer is.

6.5 Martian PPG

The Dry Valleys' have been suggested as an analogue for the Martian surface since the 1970's (Morris et al. 1972) and is considered the testing ground for Mars research methods. Recently Mars analogues have been receiving more attention due to the publicity surrounding the Phoenix Lander that touched down on Mars in 2007. The Phoenix Lander has been positioned on the Martian surface in an area interpreted as being permafrost - and ice-rich due to the identification of polygonal networks at the surface (Figure 38).

Greater understanding of the processes that operate and form PPG and ground ice within the Dry Valleys can be applied to evaluating Martian equivalent processes. This has implications for evaluation of buried massive ice beneath the Martian surface and subsequent interpretations of water resources and potential for life. Since investigation of Martian permafrost conditions is largely limited to satellite coverage and photographs, the relationships between surface expression and underlying structure are of particular importance.

The future Mars expedition, Exo Mars, will incorporate both low and high frequency GPR to evaluate subsurface structure (Hamran et al. 2008, Corbel et al. 2008).

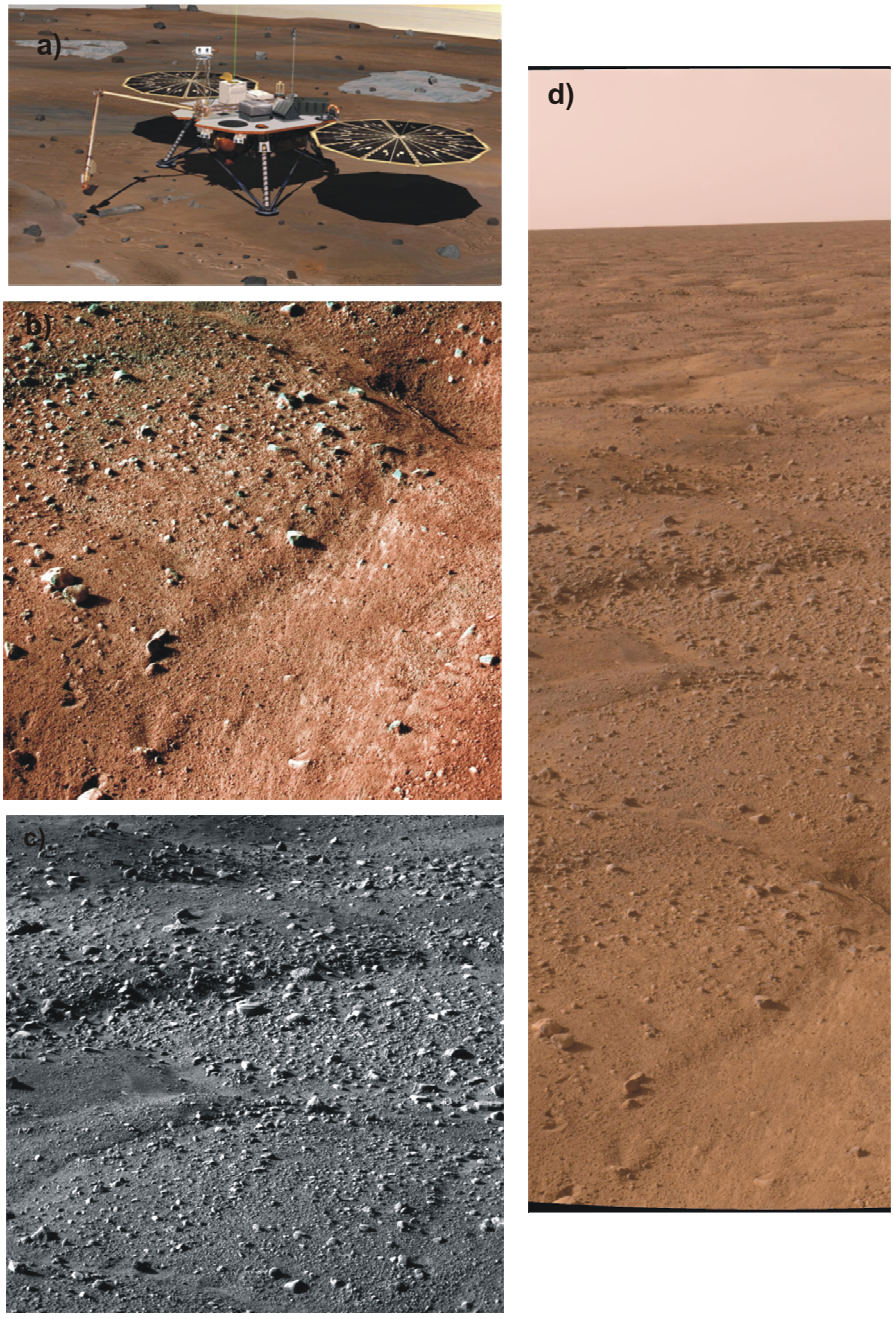

Figure 38: Polygonal patterned ground images from the phoenix Lander Mars mission that landed on the Martian surface in 2007 a) a graphic of the mars Lander b) midrange colour composite image of PPG on Mars c) black and white mid range image of PPG on Mars d) long range image of PPG networks extending over the permafrost interpreted area of the Martian surface

7 Conclusions and Recommendations

This research presents the first application of 3D and time-lapse near surface geophysical methods on PPG in the McMurdo Dry Valleys.

It has been shown that near surface geophysics can be used effectively in the McMurdo Dry Valleys to evaluate the subsurface structure of PPG and variations in the subsurface can be seen over the warming/thaw period.

The methodologies that were particularly successful were: the use of resistivity for resolution of the active layer and underlying buried massive ice bodies; GPR for imaging deformation structures within the upraised ridges relating to contraction wedge propagation; and electromagnetism for identification of anomalous zones that may interfere with response from PPG or may cause misinterpretation of PPG-related structures.

Although direct identification of thermal contraction crack depths and morphology could not be achieved with these methods, the identification of zones of influence relating to thermal contraction cracks, such as areas of attenuation of GPR signals, and zones of increased conductivity (in resistivity tomography and electromagnetic results) can be used as a proxy for evaluation of the effects of these structures in the subsurface. There is significant scope for continuation of this research in the future.

The identification of deformation features within the PPG of Beacon Valley is indicative of thermal contraction crack processed operating there and calls into question Marchant et al. (2002) interpretation of the PPG as sublimation related.

The previous discussion of this research has more implications for the broader application of these techniques within the Dry Valleys and my recommendations for further research are as follows:

- 3D resistivity over PPG to evaluate the relationship of active layer morphology with PPG structure.

- The time-lapse surveys should be completed over a larger length of time and in close proximity to soil and climate monitoring station for an in-depth analysis of the relationship between resolvable variations within the physical property variations in the subsurface and measured conditions such as soil temperatures and salt concentrations. 3D resistivity time-lapse should be used to evaluate the active layer morphology interactions with PPG over the active warming/expansion period of development. It is expected that this would show the insulating effects of the upraised ridges and the accelerated warming/increase in thaw depth locally over the contraction cracks. Data relating to the effect of thermal contraction cracks to the underlying thermal regime would be useful for evaluating the relative importance of preferential sublimation of buried massive ice bodies to the formation of PPG surface expression.

- Multi method, time-lapse analysis over Beacon Valley PPG would help to determine subsurface activity of the PPG over the buried massive ice body. Is this different from seasonal activity of PPG not located over buried massive ice bodies? Can this be resolved?

- Establishment of long-term time-lapse/repeat surveying of PPG areas to monitor changes on larger time frames than a single season. This would allow the evaluation of climate trends due to the direct coupling of the atmosphere and Dry Valleys' soils discussed previously.

The Team, K054 2006/2007

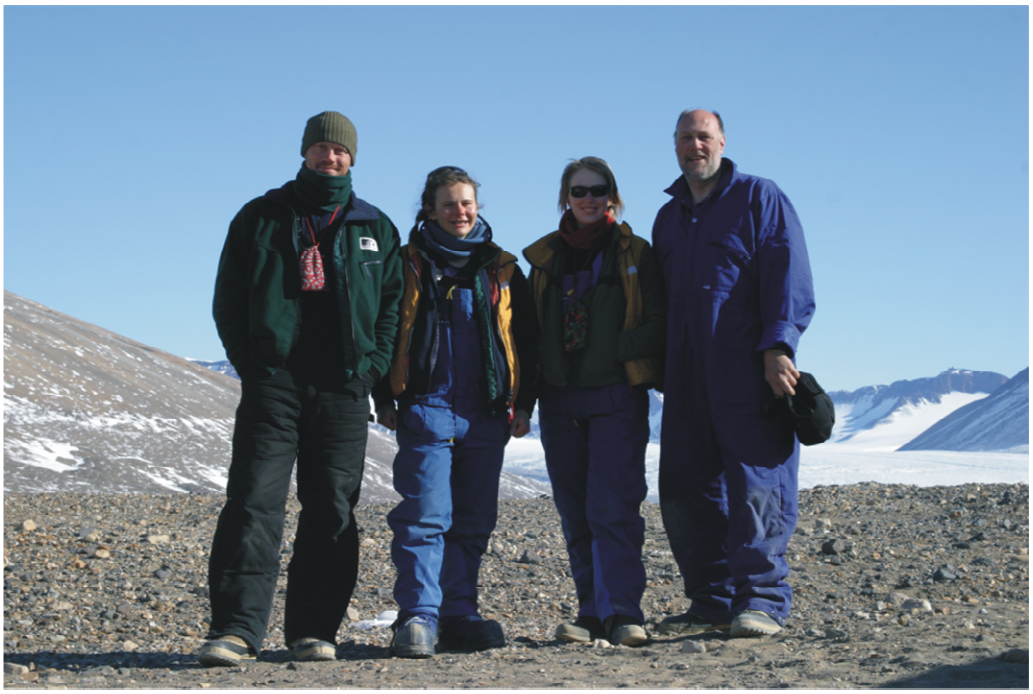

Victoria Valley. From left, Jonathon Lapwood, Michele Bannister, Myfanwy Godfrey, and David Nobes

Beacon Valley. From left, Michele Bannister, Jonathon Lapwood, and Myfanwy Godfrey.

References:

Annan, A P, 1993: Practical processing of GPR data, Proceedings of the second government workshop on ground penetrating radar, Columbus, Ohio

Annan A P and Cosway S W, 1992: Ground Penetrating Radar survey design, for Annual meeting of SAGEEP, Chicago USA.

Arcone S A, Delaney A J, and Prentice, M E, 2000: Stratigraphic profiling in the Dry Valleys, In Proceedings of GPR2000: the eighth international conference on ground penetrating radar, Sydney Australia 771 – 777p

Bannister, M T, 2007: Polygonal patterned ground and ancient buried ice on Mars and in Antarctica., Unpublished B.Sc. (Honours) project in Astronomy and Geology, Department of Geological Sciences and Department of Physics and Astronomy, University of Canterbury

Beeching A J, 1999; The potential of ground penetrating radar and other geophysical methods for delineating subsurface clay layers at the Taharoa ironsand mine, Unpublished B.Sc (Honours) project, Department of Geological Sciences, University of Canterbury.

Berg T E, and Black R F, 1966; Preliminary measurements of growth of non-sorted polygons, Victoria Land, Antarctica, In, Tedrow J F C ed, Antarctic Soils and Soil Forming Processes, Washington D.C., AGU.

Black R F, 1976: Periglacial features indicative of permafrost: Ice and soil wedges, Journal of Quaternary Research, vol 6, pg 3 – 26

Black R F and Berg T E, 1963: Patterned ground in Antarctica, In Proceeding: Permafrost International Conference, National academy of science and natural resources, Washington D.C. pg 121 - 128

Brandt O, Langley K, Kohler J, and Hamran S E, 2007: Detection of buried ice and sediment layers in permafrost using multi-frequency Ground Penetrating Radar: A case examination of Svalbard, Remote Sensing of Environment, vol 111, 212 – 227

Berkman D A, 2001; Field Geologists Manual 4th edition, Victoria, The Australian institute of mining and metallurgy, 395 p

Bockheim J G, 1997; Properties and classification of cold desert soils from Antarctica, Soil Science Society of America Journal, vol 61 pgs 224 – 231

Brosten T R Bradford J H McNamara J P Zarnetske J P Gooseff M N and Bowden W B, 2006: Profiles of temporal thaw depths beneath two Arctic stream types using ground penetrating radar, Permafrost and Periglacial processes, vol 17 pg 341 – 355

Clayton-Greene J M, Hendy C H, and Hogg A G, 1988; The chronology of a Wisconsin age proglacial lake in the Miers Valley, Antarctica, New Zealand Journal of Geology and Geophysics , vol 31, pg 353 – 361

Conyers L B, 2004. Ground-Penetrating Radar for Archaeology. USA, Alta Mira press, 203p.

Corbel C, Ciarletti V, Dolon F, le Gall A, Berthelier J J, Hamran S E, Plettemeier D, and the EISS team, 2008; The EISS Monostatic and Bistatic GPR on ExoMars Mission, in Proc. 12th International conference on Ground Penetrating Radar, Birmingham, UK.

Davis E F, 2003. Geophysical investigation of the Pram Point folds, McMurdo Ice Shelf, Antarctica. Unpublished MSc thesis, University of Canterbury, Christchurch, New Zealand.

Davis J L and Annan AP, 1989: Ground Penetrating Radar for high resolution of soil and rock stratigraphy, Geophysical Prospecting, vol 37, 531 – 551

Decker E R and Buchner G J, 1980: Geothermal studies in Antarctica, Antarctic Journal of the United States, vol 12 pgs 102 – 104

Delaney A J, Peapples P R, and Arcone S, 2001: Electrical resistivity of frozen and petroleum-contaminated fine-grain soil, Cold Regions Science and Technology, vol 32, pg 107 – 119

Denton G H, Bockheim J G, Wilson S C, and Stuiver M, 1989; Late Wisconsin and early Holocene glacial history, inner Ross Embayment, Antarctica, Journal of Quaternary research, vol 31, 151 – 182

Denton G H, Sugden D E, Marchant D R, Hall B L, and Wilch T L, 1993; East Antarctic ice sheet sensitivity to Pliocene climatic change from a Dry Valleys perspective, Geografiska Annaler vol 75 A pgs 155 – 204

Dickenson W W, Rosen M R, 2003; Antarctic permafrost: an analogue for water and diagenetic minerals on Mars, Geology, vol. 31, pgs 199 – 202

a. Doran P T, McKay C P, Clow G D, Dana G L, Fountain A G, Nylen T and Lyons W B, 2002: Valley floor climate observations from the McMurdo Dry Valleys, Antarctica, 1986 – 2000, J. Geophysical research, vol. 107, NO. D24, 4772

b. Doran P T, Priscu J C, Lyons W B, Walsh J E, Fountain A G, McKnight D M. Moorhead D L, Virginia R A, Wall D H, Clow G D, Fritsen C H, McKay C P, and Parsons A N, 2002: Antarctic climate cooling and terrestrial ecosystem response, Nature, vol 415, 517-520

Doolittle J A and Nelson F E, 2008: Using GPR to characterise cryogenic macrostructures in former periglacial areas of the USA., Proc. 12th international conference on Ground Penetrating Radar, Birmingham, UK

French H M, 1996: The periglacial environment 2nd ed, Singapore, Longman ltd, 341 pgs

French H M and Guglielmin M, 2000: Frozen ground phenomena in the vicinity of Terra Nova Bay, Northern Victoria Land, Antarctica: a preliminary report, Geografsika Annaler, series A, Physical Geography, vol 82 no 4, pg 513 – 526

Gibson P J, and George D M, 2003; Environmental Applications of Geophysical Surveying Techniques, New York, Nova Science Publishers Inc, 317 p

Gibson E K, Wentworth S J, and Mackay D S, 1983; Chemical weathering and diagenesis of a cold desert soil from Wright Valley, Antarctica: an analogue of Martian weathering processes. Journal of geophysical research, vol 88, pgs 912 – 928.
Grasmuek M, Werger R, and Horstmeyer H, 2005: Full resolution 3D GPR imaging, Geophysics, vol 70 no 1, k12 – k19

Godfrey M J, Bannister M T, Nobes D C, and Sletten R S, 2008; 3D Time-Lapse imaging of polygonal patterned ground in the McMurdo Dry Valleys of Antarctica, Proc. 12th International conference on Ground Penetrating Radar, Birmingham, UK.
Goldthwait R P, 1976: Frost sorted patterned ground: A review, Quaternary research, vol 6, pg 27 – 35

Guglielmin M Biasini A and Smiraglia C, 1997: The contribution of geoelectrical investigations in the analysis of periglacial and glacial landforms in ice free areas of the northern foothills (northern Victoria Land, Antarctica), Geografiska Annaler, Series A Physical geography, Vol 79 pg 17 – 24

Guglielmin M, 2006: Ground surface temperature (GST), active layer and permafrost monitoring in continental Antarctica, Permafrost and Periglacial Processes, vol 17, pg 133 – 143

Haeberli W, 1985; Creep of mountain permafrost: internal structure and flow of alpine rock glaciers, Mitteilungen der Versuchsanstalt für Wasserbau, Hydrologie und Glaziologie an der Eidgenossischen Technischen Hochschule, Zurich.

Hall B L, Denton G H, Overturf B and Hendy C H, 2002: Glacial lake Victoria, a high level Antarctic lake inferred from laucustrine deposits in Victoria Valley, Journal of Quaternary Science, vol 17 pg 697 – 706

Hall B L, Hendy C H, and Denton G H, 2006; Lake ice conveyor deposits: Geomorphology, sedimentology and importance in reconstructing the glacial history of the Dry Valleys, Geomorphology, vol 75 pgs 143 – 156

Halliday D, Resnick R, and Walker J, 2001. Fundamentals of Physics, 6th Ed. New York USA, John Wiley and sons pp 1144

Hamran S E, Ciarletti V, Corbel C, Plettemeier D, Øyan M J, Bergen T, and Hanssen L, 2008; The WISDOM Shallow Sounding GPR in the ExoMars Mission, in Proc. 12th International conference on Ground Penetrating Radar, Birmingham, UK.

Harris C, Morton J B and Davies M C R, 2005, An analysis of mechanisms of ice-wedge casting based on geotechnical centrifuge simulation, Geomorphology, vol 71 pg 328 – 343

Hauck C, Isaksen K, Voder Muhll D, and Sollid J L, 2001: Geophysical surveys designed to delineate the altitudinal limit of mountain Permafrost: an example from Jotunheimen, Norway, Permafrost and Periglacial Processes, vol 12, 179 – 190

Hauck C, Vieira G, Gruber S, Blanco, J, and Ramos M, 2007; Geophysical identification of permafrost in Livingston Island, maritime Antarctica, Journal of Geophysical research, vol 112 (F2), pgs

Hauck C, Vonder Muhll, D, and Maurer H, 2003; Using DC resistivity tomography to detect and characterize mountain permafrost, Geophysical prospecting, vol 51, pgs 273 – 284

Hendy C H, 2000; Late Quaternary Lakes in the McMurdo Sound region of Antarctica, Geografiska Annaler Series A Physical Geography, vol 82 no 2/3, pgs 411 - 432

Hinkel K M, Doolittle J A, Bockheim J G, Nelson F E, Paetzold R, Kimble J M, and Travis R, 2001: Detection of subsurface permafrost features with ground penetrating radar, Barrow, Alaska, Permafrost and Periglacial processes, vol 12, 179 – 190

Jorgensen A S and Andreasen F, 2007: Mapping of Permafrost surface using ground penetrating radar at Kangerlussuaq Airport, western Greenland, Cold Regions Science and Technology, vol 48, pg 64 – 72

Kearey P, Brooks M, and Hill I; 2002; An Introduction to Geophysical Exploration, Malden, Blackwater Publishing, 262 p

Lachenbruch A H, 1962: Mechanics of Thermal Contraction Cracks and Ice-Wedge Polygons in Permafrost, Special Geological Survey of America paper, No 70, New York

Lewkowicz A G and Harris C, 2005: Morphology and geotechnique of active layer detachment failures in discontinuous and continuous permafrost, Northern Canada, Geomorphology, vol 69 pg 275 – 297

Mackay J R, 1971: The origin of massive icy beds in permafrost, western Arctic coast, Canada, Canadian journal of earth sciences, vol 8 pg 397 – 422

Mackay J R, 1974: Ice wedge cracks, Garry Island, Northwest Territories, Canadian journal of earth sciences, vol 11 pg 1366 – 1383

Mackay J R, 1984: The direction of ice wedge cracking in permafrost: downward or upward?, Canadian journal of earth sciences, vol 21 pg 516 – 524

Mackay J R, 1986: The first 7 years (1978 – 1985) of ice wedge growth, Illisarvik experimental drained lake site, western Arctic coast, Canadian journal of earth sciences, vol 23 pg 1782 – 1795

Mackay J R, 1992: The frequency of ice wedge cracking (1967 – 1987) at Garry Island, western Arctic coast, Canada , Canadian journal of earth sciences, vol 29 pg 236 – 248

Mackay J R, 1993: The sound and speed of ice wedge cracking, Arctic Canada, Canadian journal of earth sciences, vol 30 pg 509 – 518

Mackay J R, 2000: Thermally induced movements in ice-wedge polygons, western arctic coast: a long term study, Geographie Physique et Quaternaire, vol 54 pg 41 – 68

Marchant D R, Lewis A R, Phillips W M, Moore E J, Souchez R A, Denton G H, Sugden D E, Potter Jr N and Landis G P, 2002: Formation of patterned ground and sublimation till over Miocene glacier ice in Beacon Valley, Southern Victoria land, Antarctica, GSA Bulletin, vol 114 no. 6, 718-730

Maurice P A, McKnight D M, Leff L, Fulghum J E, and Gooseff M, 2002; Direct observations of aluminosilicate weathering in the hyporheic zone of an Antarctic Dry Valley stream, Geochemica et Cosmochimica Acta, vol 66, no * pgs 1335 – 1347.

McNeil J D, 1983; Technical note TN-11, Use of EM31 inphase information, Missauga Ontario, Geonics Ltd, pp 2.

Milsom J, 2000. Field geophysics, 2nd ed. Chichester UK, John Wiley and sons. 187p

Moorman B J, Robinson S D, and Burgess M M, 2003: Imaging Periglacial Conditions with Ground-penetrating Radar, Permafrost and Periglacial Processes, vol 14, 319 – 329

Morris E, Mutch T, and Holt H, 1972; Atlas of geologic features in the Dry Valleys of South Victoria Land, Antarctica: possible analogs of Martian surface features. Intragency report: Astrogeology 52, United states Department of the Interior Geological Survey, for the National Aeronautics and Space Administration.

Munroe J S, Doolittle J A, Hinkle K M, Nelson F E, Kimble J M, Jones B M and Kanevisky M Z, 2007: Application of Ground penetrating radar imagery for three-

dimensional visualization of near surface structures in ice rich permafrost, Barrow, Alaska., Permafrost and Periglacial Processes, Vol 18 no. 4, 309 – 321

Musset A E and Khan A, 2000: Looking into the earth: an introduction to geological geophysics. Cambridge University press.

Vonder Mühll D Hauck C Gubler H McDonald R Russil N, 2001: New geophysical methods of investigation the nature and distribution of mountain permafrost with special reference to radiometry techniques, Permafrost and Periglacial processes, vol 12 pg 27 - 38

Nobes DC, Ferguson RJ and Brierly G J, 2001: Ground penetrating radar and sedimentological analysis of Holocene floodplains: insight from the Tuross valley, New South Wales, Australian Journal of Earth Sciences, vol 48, 347 – 355

Nobes D C, and Annan P A, 2000: “Broadside” vs. “End-fire” radar response: some simple illustrative examples, In Proceedings of GPR2000: the eighth international conference on ground penetrating radar, 696-701

Osterkamp T E, 2003: Establishing long term permafrost observatories for active layer and permafrost investigations in Alaska, Permafrost and Periglacial Processes, vol 14, 331- 342

Petterssen J K and Nobes D C, 2003: Environmental geophysics at Scott Base: ground penetrating radar and electromagnetic induction as tools for mapping contaminated ground at Antarctic research bases, Cold Regions Science and Technology, vol 37, 187 – 195

Péwé T, 1961; Multiple glaciations in McMurdo Sound region, Antarctica – a progress report, Geology, vol 68, pg 498 – 514

Péwé T L, 1974: Geomorphic processes in polar deserts, In: Smiley T L and Zumberge J H, Polar deserts and modern man, University of Arizona Press Tuscon,

Plewes LA and Hubbard B, 2001: A review of the use of radio-echo sounding in glaciology. Progress in Physical geography, vol 25, 203-236

Scott R F, 1905: The Voyage of the Discovery, New York C Scribner's sons,

Scott W J, Sellmann P V and Hunter J A, 1990: "Geophysics in the study of permafrost", in Geotechnical and Environmental Geophysics, 355 - 384 ed. Ward, S. H., Society of Exploration Geophysics, Tulsa

Sensors and Software Inc., 1999: EKKO_3D User's guide version 2.0, Technical manual 27, 41 pgs

Sletten R S, Hallet B and Fletcher R C, 2003: Resurfacing time of terrestrial surfaces by formation and maturation of polygonal patterned ground, Journal of Geophysical research, vol 108, no. E4,

Stolt R H, 1978: Migration by Fourier transform, Geophysics. 43, pg 23 – 48

Stuiver M, Denton G H, Hughes T J, and Fastook J L, 1981; History of the marine ice sheet in West Antarctica during the last glaciation, a working hypothesis, In, Denton G H, and Hughes T J (ed.), The Last Great Ice sheets, Wiley interscience, New York, pg 319 – 436.

Sugden D E, Marchant D R, Potter N J, Souchez R A, Denton G H, Swisher C C I, and Tison J L, 1995; Preservation of Miocene glacier ice in East Antarctica, Nature vol 376 pgs 412 – 414

Summerfield M A, Stuart F M, Cockburn H A P, Sugden D E, Denton D H, Dunai T, and Marchnt D R, 1999; Long term rates of denudation in the Dry Valleys, Transantarctic mountains, southern Victoria land, Antarctica, based on in-situ produced cosmogenic ^{21}Ne, Geomorphology, vol 27 pgs 133 – 129.

Telford W M, Geldart, L P, and Sheriff, R E, 1990. Applied geophysics, 2nd ed. Cambridge UK, Cambridge University Press, 770

Todd B J and Dallimore S R, 1998, Electromagnetic and geological transect across permafrost terrain, Mackenzie River delta, Canada, Geophysics, vol 63 pg 1914 – 1924 (EM)

Ugolini F C, and Anderson D M, 1973; Ionic migration and weathering in frozen Antarctic soils, Soil Science vol 115 pgs 461 – 470

Vaikmae R, Bose M, Michel F A and Moormann B J, 1995: Changes in permafrost conditions, Quaternary International, vol 28 113 – 118,

Wilson A T, 1979; Geochemical problems of the Antarctic dry areas, Nature vol 280 pgs 205 – 208

The physics hyper text book, edited by Glenn Elert. (Resistivity of copper)
http://hypertextbook.com/facts/

Killer in our midst evaluating earth systems and natural hazards for image of Antarctica as generation of thermohaline conveyor belt oceanic circulation cell.
http://www.killerinourmidst.com/THC.html

Thermohaline circulation wikipedia entry for images….
http://en.wikipedia.org/wiki/Thermohaline_circulation

Council of managers of National Antarctic Programs, atmospheric page for Antarctic pressure system image.
http://pdf.comnap.aq/comnap/comnap.nsf/P/Pages/Operations.Meteorology/

NASA images from Phoenix probe for images of Martian PPG
http://www.nasa.gov/mission_pages/phoenix/images/index.html

Appendices

Appendix I: Logistics report K054 2006/2007

Modified Logistics report from data collection field season detailing field experiences, dates and progress of research and local weather conditions.

Appendix II: Topographic data

Topography data in spread sheet form showing raw collected data measurements and the subsequent calculations to correct to absolute topography and interpolate values between grid points.

Appendix III: Batch files processing scripts

Batch file commands for the GPR processing conducted in batch file mode.

Appendix IV: GPR data.

Due to the large volume of data this appendix is in digital format. A CD containing PDF's of formatted GPR profile lines is included

Appendix V: Resistivity data.

The inversion model results for the resisitivity data.

Appendix VI: EM data.

The plotted real and quadrature electromagnetic results with averages and differences between parallel and perpendicular boom orientation data.

Appendix VII: Data disk.

Appendix I:

Antarctica New Zealand Logistics Report for K054 field season

LOGISTICS REPORT

K054: Non-invasive Imaging of Polygonal Patterned Ground in Antarctic Permafrost Soils
ANTARCTICA NEW ZEALAND 2006/07

Event Personnel:

Dr D. C. Nobes	University of Canterbury
Ms M. Godfrey	University of Canterbury
Ms M. Bannister	University of Canterbury
Mr J. Lapwood	University of Canterbury

Name of compiler: M. J. Godfrey Signature of compiler: _____

AIMS

Our aims for this field season were to use non-invasive, non-destructive geophysical methods to obtain three-dimensional images of the permafrost and polygonal patterned ground (PPG) in the cold hyper arid McMurdo Dry Valleys of Antarctica. We worked specifically at two sites, one in Victoria Valley, and the other in Beacon Valley, to try to address some fundamental questions, including: What is the depth to and thickness of ice cement? What is the subsurface structure of PPG in the Dry Valleys? Can seasonal activity be resolved using time lapse geophysical methods? How prevalent and thick are buried massive ice bodies? What is the depth to bedrock? At each location, there were two types of targets for geophysical imaging:

1. deep features, such as bedrock and the thickness of buried massive ice; and
2. small near-surface features, in particular the PPG subsurface structure, and resolving seasonal changes within the subsurface.

Deep Imaging

To detect and resolve the base of any massive ice and the top of bedrock, we used the complementary two-dimensional electrical resistivity imaging and time-domain EM (TEM) are two of the more common techniques for such surveys, and resistivity and EM complement each other. Low-frequency, deep ground penetrating radar (GPR) was also used to obtain the deeper stratigraphy which could be correlated with the TEM and resistivity images. The detection of deep structures was limited to resolving lateral extent by applying the mentioned techniques along two cross-valleys transects; one in Victoria Valley and one in Beacon Valley.

PPG Imaging

The other objective was the "4D" imaging of PPG, i.e. three-dimensional (3D) changes in physical properties over time. At each location, two sets of PPG were selected and surveyed using an optical level. Initial surveys using 2 sets of 2 perpendicular electrical tomography profiles and pseudo 3D GPR were completed on one polygon or polygon set, and then the electrical and GPR surveys were swapped to the second polygon set for the time lapse imaging. The tomographic imaging was repeated at regular intervals, i.e. every few days.

PERSONNEL

Name	Designation	Organisation	Departed Chch	Returned Chch
David C. NOBES	Principal Investigator	University of Canterbury	21/11/2006	30/12/2006
Myfanwy GODFREY	MSc student	University of Canterbury	21/11/2006	27/1/2007
Michele BANNISTER	BSc (Hons) student	University of Canterbury	21/11/2006	27/1/2007
Jon LAPWOOD	Field Assistant	University of Canterbury	21/11/2006	27/1/2007

EVENT DIARY

Date	Main Activities and Location	Other Comments
23/11/06	**Flight to Antarctica**. Arrive at Scott Base.	
24/11/06 – 26/11/06	**At Scott Base** preparing for the field. - checking equipment - completing AFT	• Full AFT required by David Nobes, Michele Bannister, Jonathon Lapwood. • Only an AFT refresher was required

	- completing sign out procedures.	for Myfanwy Godfrey allowing enough time to complete the necessary paperwork for departure from Scott Base.
27/11/06	Clear weather, light winds. **Put in** flights in early afternoon. All team involved in **camp set up**.	• NB: additional personnel for camp put in – Ian Whitely AFT.
28/11/06	Mostly clear skies, light wind. **Reconnaissance:** Initial locations of polygon set one and transect line. **Transect line**: begin resistivity put in. **Polygon 1** – establish perimeter 20m x 27m NE corner E161º 37148 S 77º 20.225 NW corner 161º 37.087 S 77º 20.222 SE corner E 161º 37.135 S 77º 20.236 SW corner E 161º 37.076 S 77º 20.238	• K054 divides into two teams to target different aspects of the event aims. **David Nobes (DCN) and Michele Bannister (MB)** target deeper structures by running **cross valley transects**, while **Myfanwy Godfrey (MG) and Jonathon Lapwood (JL)** work on resolving Polygon features by 3D surveying **two polygon locations**
29/11/06	Light winds, clear sky, warm approx 3º **Polygon 1** – CMP surveys to determine subsurface velocities. **Transect line** – Continue Resistivity.	• Antarctica New Zealand environmental audit. • Ian Whitely returned to Scott base with this flight. • NB: American Film crew arrived on this flight making footage for Dry Valleys AFT video.
30/11/06	Overcast, cold wind from the Glacier up valley. **Polygon 1** – start 200 MHz GPR survey **Transect line** – Continue Resistivity. – problems with electrical contact resulting in watering of the electrodes.	
1/12/06	High patchy cloud, light winds. **Polygon 1** – Continue 200 MHz GPR survey **Transect line** - continue resistivity.	
2/12/06	Clear skies, no wind, warm temperatures approx. 5º **Polygon 1** – finish 200 MHz GPR survey. **Transect line** – Continue resistivity. Start roll on one.	• Visit from Ron Sletten and his PHD student. • NB: Ron Sletten is a collaborator on event K054 and associate supervisor to the thesis work to be completed by Myfanwy Godfrey.
3/12/06	High cloud, light winds from down valley. **Transect line** – continue resistivity. **Polygon 2**. Location of polygon two. 12m x 20m Lay perimeter. NE corner E 161º 37.281 S º 77 20.159 NW corner E 161 º 37.253 S º 77 20.157 SE corner E 161 º 37.272 S º 77 20.169 SW corner E 161 º 37.243 S º 77 20.166	
4/12/06	Mostly clear skies, moderate wind from down valley. **Transect line** – finish resistivity. Start TEM **Polygon 2** – place resistivity cross lines. Run initial lines.	
5/12/06	Overcast, light winds. **Transect line** – continue TEM	

	Polygon 2 – continue resistivity.	
6/12/06	Clear skies, light wind from the glacier up valley. **Transect line** – continue TEM **Polygon 2** – continue resistivity.	• Visit from Veronica Meduna, National Radio science reporter. (interview broadcast on February 2nd)
7/12/06	Low cloud, light wind. **Transect line** – finish TEM **Polygon 1 –** lay electrodes and cables for resistivity. First run of time lapse resistivity.	
8/12/06	Low cloud depositing snow on the peaks surrounding the valley. Cold wind from the Glacier. **Polygon 2** – first run of time lapse GPR. Begin 200 MHz survey MB assist.	
9/12/06	Still low cloud and cold wind. **Polygon 2** – finish first run of 200 MHz. Start and finish first run of 100 MHz GPR. MB Assit.	
10/12/06	Lowering cloud throughout the day. Light wind. **Transect line** – CMP along transect line to determine sub-surface velocities. MG and JL assist.	• On request from K015, Charlie Bristow and Harry Jol visit camp to borrow 50 MHz antennas for greater resolution of deep structure in the Sand dunes approximately 8 km down valley from our site.
11/12/06	Clear skies, light wind **Transect line** – scouting out outcrop of bedrock to target the Magnetic survey on. Proposed end of transect line is 1.4 km from camp. **Polygon 1** – second run of time-lapse resistivity.	• There were problems with the variability of the magnetic field. The magnetic survey is very sensitive to solar activity. Our field season lasted over a period of unusually high solar activity with high solar flare concentrations. • 50 MHz antennas returned to camp by Harry Jol and Paul Augustinus.
12/12/06	Overcast high cloud. No wind. **Valley Transect** – magnetic conditions not suitable for survey. **Polygon 2** – start second run of 200 MHz GPR survey.	
13/12/06	High cloud, light winds from glacier. **Valley Transect** – magnetic conditions not suitable for survey. **Polygon 2** – finish second run of 200 MHz GPR. Start and finish second run of 100 MHz GPR.	• Receive optical level from K015. This allows K054 to topographically survey the lines for our geophysics and add topographic corrections.
14/12/06	Snowing, light winds. Visibility lessening throughout day but still able to see valley sides. **Valley Transect** – start GPR 50 MHz. JL assist. **Polygon 2** – set up topographic survey.	• Transect GPR requires 3 people to run it. Polygon work stalled until transect GPR finished.
15/12/06	Low clouds, light to no wind cold temperatures. **Valley Transect** – finish 50 MHz GPR. **polygon 1** – complete third run of resistivity	

16/12/06	High clouds, no wind. **Valley Transect** – magnetic conditions not suitable for survey. **Polygon 2** – start and complete time lapse 200 MHz GPR	
17/12/06	Medium winds with overcast sky. **Valley Transect**– magnetic conditions too variable for survey. **Polygon 2** – continue topographic surveying. Start and complete time lapse 100 MHz GPR. MB assist.	
18/12/06	**Rest day:**	
19/12/06	Overcast skies, no wind. **Valley transect** – magnetic conditions too variable **Polygon 1** – complete fourth run of resistivity **Polygon 2** – continue topographic survey.	
20/12/06	Clear skies, light wind from up valley. **Valley transect:** GPS survey stations. Magnetic conditions too variable. **Polygon 2** – complete fourth run of 200 MHz GPR	• DCN knee injury starts to reduce ability to help in the field.
21/12/06	Clear skies, no wind. **Polygon 2** – complete 100 MHz GPR survey. Continue topographic surveying.	
22/12/06	Clear skies, moderate wind from up valley. **Valley Transect:** SW section of Magnetometer survey completed. MG assists. **Polygon 2** – finish topographic survey Begin EM31.	
23/12/06	Beacon Valley – low cloud and moderate winds. Visibility lessening as the day progressed. **Reconnaissance:** Helicopter flight to Beacon Valley.	• Arranged by Ron Sletten for location of work sites and background field work.
24/12/06	Clear skies, cold light wind from up valley. **Valley Transect**: North east section of transect completed with Magnetometer. MG assists. Far South west section completed. JL. assist. **Polygon 2** – finish EM31. **Polygon 1** – start EM31	
25/12/06	Christmas day; Rest Day. Weather poor with high winds and poor visibility due to dense snow flurries.	
26/12/06	Overcast, cool winds from up valley. **Valley Transect**: Complete topographic survey. MG and JL assist **Polygon 1** – finish EM31.	
27/12/06	**Camp relocation** to Beacon Valley site mid afternoon. Initial camp set up. Initiation of magnetometer survey in Beacon Valley location.	• David Nobes returns to McMurdo for medical assessment. • As a team of three, for safety reasons K054 now works as a single unit rather

		than splitting into groups.
28/12/06	Low cloud and moderate winds. Approx 20km/hr Full **camp set up** and rest day.	• David Nobes diagnosed with Water on the knee. A decision not to return to the field is made
29/12/06	Overcast, cold wind from Muir glacier and East Antarctic Ice Sheet (EAIS) **Reconnaissance**. Location of polygon one in Beacon Valley, and transect line.	
30/12/06	Overcast, moderately high winds approx 25 km/hr. wind chill at approx -15 **Perimeter of polygon 1** laid. 20m x 23m NE corner E 160º 35.714 S 77º 50.903 NW corner E 160º 35.668 S 77º 50.900 SE corner E 160º 35.693 S 77º 50.915 SW corner 160º 35.649 S 77º 50.911 North-south resistivity line set up and run - 64 electrodes at 0.5 meter spacing. And 32 electrode array at 1 meter spacing. 3 hours run time each Katabatic's at 20 km/hr consistent blowing.	• David Nobes returns to New Zealand.
31/12/06	Overcast, moderately high winds approx 25 km/hr. wind chill at approx -15 **Polygon 1** - Additional run of North-south resistivity line with varied settings attempting to target greater depth. Katabatic's at approximately 25km/hr gusting to over 30km/hr.	
1/1/07	**Dangerous weather conditions**: dense snow flurries erratically restricting visibility to 100 – 20m from camp. Strong Katabatic's averaging 25 – 30 km/hr with gusting above 35 km/hr. Team decision not to work today unless conditions improve. Wind chill at approx – 25.	
2/1/07	Clear weather in middle of valley. Clouds hanging at edges of the valley. Moderate winds. **Polygon 1** - Topographic surveying of resistivity lines using optical level start on surveying GPR lines before running east – west resistivity. Both 64 and 32 electrode arrays completed.	
3/1/07	Clear weather, medium winds. **Polygon 1** - Continue topographic surveying. Start on GPR with 200 MHz antennas, 10cm step size with half meter spacing.	
4/1/07	Clear weather, light to moderate winds with snow clouds being blown towards camp in the evening. **Polygon 1** - Continue 200 MHz GPR. Continue topographic Survey.	• Repair magnetometer.
5/1/07	High winds and light snow flurries coming from approaching snow clouds.	

	Polygon 1 - Primary Processing and data back up. Start EM31. (electromagnetic survey)	
6/1/07	High winds approx 25-30km/hr, snow flurries in valley and low cloud. Clears slightly in afternoon to continue work **Polygon 1** - Continue topographic surveying in the afternoon when weather has cleared. Work into evening to make up lost time.	
7/1/07	High cloud but mostly clear in the morning. Snow flurries in afternoon. **Polygon 1** - Continue GPR. Continue EM31	
8/1/07	Snow during the night. Clear day light winds **Polygon 1** - Start 100 MHz GPR	
9/1/07	Clear skies, light winds warm temperatures approx -2ºC **Polygon 1** - Finish both 100 and 200 MHz GPR	
10/1/07	Clear skies, no wind, warm temperatures. **Cross Valley Transect line** - Start resistivity along transect line. Lay 128 electrode array from E 160 37.112 S 77 51.094 to E160 35.786 S 77 50.920	
11/1/07	Clear skies, light winds, warm temperatures. **Transect line** - Run Resistivity - run time approximately 7 hours. **polygon 1**. Finish EM31 survey and topographic survey on	
12/1/07	Clear skies, moderate winds, warm temperatures. **Transect line** - Begin Topographic survey along transect line as moving electrodes for roll on 1. Resistivity "roll on" 1: lay and run 128 electrode array along transect from E160 36.446 S 77 51.012 to E160 35.092 S 77 50.831	
13/1/07	Clear skies and no wind. The wind picked up quickly in the afternoon changing from no wind to gust over 40 km/hr. temperature -1.8. **Transect line** - Continue topographic survey as moving electrodes for roll on 2. Resistivity roll on 2 - complete laying and running 128 electrode array from E160 35.786 S 77 50.920 to E 160 34.428 S 77 50.746	
14/1/07	High overcast cloud with light cold winds. **Transect line -** Continuing Topographic surveying along transect. Begin pulling out Resistivity. **Reconnaissance** for polygon 2.	• Optical level focus broke while surveying arrange with Scott Base to provide another one.
15/1/07	Clear warm weather. Moderate light winds from EAIS. **Transect line** – Half of the valley transect	• Arrange to have one of the assigned pull out flights used to get the replacement level to Beacon Valley

	completed with 50 MHz GPR. **Polygon 2** – perimeter set up 12m x 18m. Cross lines of 50 MHz completed NE corner E 160º 36.435 S 77º 50.999 NW corner E 160º 36.399 S 77º 50.994 SE corner E 160º 36.420 S 77º 51.004 SW corner E 160º 36.385 S 77º 51.000	without additional use of resources.
16/1/07	Mostly clear skies with patchy high cloud, light winds in the morning with strong katabatic in the afternoon blowing snow onto the valley sides. **Transect line** – Pull out last part of resistivity **Polygon 2** – North south resistivity line laid and run with both 64 and 32 electrode arrays. East – West resistivity line laid and run with 32 and 64 electrode array on the same day to avoid approaching bad weather.	
17/1/07	The strong Katabatic and snow flurries seen to be approaching the previous night reach camp in the morning. Visibility clears in the afternoon allowing work. **Polygon 2** – Pull out resistivity and move back to camp site for transport out. Snow interference limits ability to start on GPR. Pack camp and make up pull out flight one to go back to Scott Base.	
18/1/07	Moderate winds and overcast weather. **Transect line** – Finish GPR along transect line. **Polygon 1** – complete cross lines of GPR at 50 MHz **Polygon 2** – start 100 MHz GPR survey.	
19/1/07	High dense cloud. Light winds. **Polygon 2** – finish 100 MHz GPR survey and start on 200 MHz	• 1st pull out flight - removal of half the camp and the gear for the completed geophysics. • Replacement of optical level with Theodolite from McMurdo. • Arrange to pull out 1 day early to fit in with Helicopter usage.
20/1/07	Light winds, high cloud, cool temperatures. **Polygon 2** – Finish 200 MHz GPR. Start and finish EM31 survey. **Transect line** – Finish topographic survey.	
21/1/07	High cloud and light winds. **Polygon 2** – Start and finish topographic survey. Start packing up camp.	• Visit from VIP's in late afternoon.
22/1/07	Clear skies, light winds. **Camp pull out** – K054 team return to Scott Base.	
22/1/07 – 27/1/07	**At Scott Base**. - Checking and cleaning equipment.	

	- Completing sign out procedures for Scott Base.	
27/1/07	**Flight to Christchurch**	Flight delayed 24 hours due to bad weather.

WEATHER

Victoria Valley:
At our location in Victoria Valley we had mostly mild weather and were located far enough up the Valley to avoid the effects of strong winds. We had isolated days where visibility was reduced enough to warrant delaying far transect work for deep imaging (refer event diary), but this weather was not bad enough to require all work be stopped. Field work was merely limited to close to camp sites.

Beacon Valley:
The Work conducted in Beacon Valley was delayed for a whole day due to bad weather on 2 occasions. In these instances it was the combination of strong katabatic winds, poor visibility due to blown snow (approximately 100m and less) and the location of field sites further from camp than in Victoria Valley. The sometimes sedentary nature of geophysical surveying made us more cautious when evaluating weather conditions in Beacon Valley as the average temperatures were colder than we were used to. In the time that we were in Beacon Valley the weather did seem to follow a pattern. Bad weather was dominated by strong katabatic and poor visibility occurred on a week long cycle with at least a day of work being lost; this would then be followed by a week to 10 days of good weather which would be again followed by a period of poor weather. We attributed this to the proximity of the east Antarctic ice sheet and the build up and release into our valley, of cold air masses.

*ACCIDENTS, INCIDENTS OR HAZARDS

K054 had one major incident with regards to the physical capability of the PI David. C. Nobes (DCN).
In Victoria Valley it was found that DCN's Arthritis was flaring up and additional pain medication beyond his personal supplies was required. The arthritis continued to be a problem with the addition of the development of "water on the knee" (diagnosed at McMurdo). To manage the reduced physical capability of DCN as a result of the pain of these conditions DCN was required to take responsibility of the field camp and his involvement in the field work was as limited as possible to reduce the risk of further aggravating his knee. Additional field work responsibilities involved in completing both aspects of the event were divided between the remaining event personnel.

This incident resulted in the removal of David Nobes to Scott Base for a medical assessment on December 27th 2006. He did not return to the field having decided not to risk further injury in the rougher terrain of Beacon Valley where the second part of our project was conducted.

As a result of the loss of a field worker the targets in Beacon Valley were re-evaluated. Simple 3D profiling of two polygons and a transect locating the lateral extent of a buried massive ice body was prioritised. This was due to the event personnel no longer being able to split into two working parties for safety reasons.

ENVIRONMENTAL IMPACT

Site name	Victoria Valley
Site location (coordinates/description including whether it is in the Dry Valleys ASMA or an ASPA)	ASMA E 161º 37.216 S 77º 20.191 The camp was located on a large area of flat lying PPG approximately 500m from the lower part of the upper Victoria lake. The camp was central to the polygon surveys with both polygon sites being within 100m of camp. The camp was also located immediately adjacent to the halfway point of the cross-valley transect.
Dates occupied	27/11/2006 – 27/12/2006
Total days (or hours) at site	30 days
Maximum number of people at site (your event)	4
Total person-days (or person-hours) at site	120 person-days.
Main activity undertaken	Geophysical surveys Namely; ground penetrating radar, resistivity, electromagnetics, time-domain electromagnetics, and magnetometer surveys. Applied at two polygon sites and a cross valley transect.
Cumulative impacts observed	
Helo landing site if not established AND marked	
Site name	Beacon Valley
Site location (coordinates/description including whether it is in the Dry Valleys ASMA or an ASPA)	ASMA E 160º 35.737 S 77º 50.851 The camp was located in a small depression with a flat area of approximately 20m² just large enough for our two dome tents and the endura. This camp site is in the middle of the valley and immediately adjacent to the helicopter landing area. The work sites were not central to this area with one polygon being approximately 100m away and the other approximately 300m away. The cross-valley transect ran through both of these polygons and extended 700m to either side of the camp.
Dates occupied	27/12/2006 – 22/1/2007
Total days (or hours) at site	27
Maximum number of people at site (your event)	3
Total person-days (or person-hours) at site	81 person-days
Main activity undertaken	Geophysical surveys Namely; ground penetrating radar, resistivity, electromagnetics, time-domain electromagnetics, and magnetometer surveys. Applied at two polygon sites and a cross valley transect.
Cumulative impacts observed	
Helo landing site if not established AND marked	Immediately adjacent to camp site. This Helo landing site has been marked by a row of white rocks.

Disturbance to ice-free areas

Location (coordinates if available)	*Nature of disturbance*	*Approximate area of disturbance (m^2)*	*Evidence of previous site use*
Victoria Valley - The exposed ground in Victoria Valley was unconsolidated sands with small gravel boulders armouring the surface. These were very easy to disturb.	Superficial disturbance, heavy surface trampling. 1) Camp site. - 2x dome tents - 1x endura tent - 1x Olympus tent. 2)polygon surveys 3) valley transect	1) 15 x15 = 225m² with a path to the toilet. 2) polygon 1 = 27 x 20m = 540m Polygon 2 = 12 x 20m = 240 m² 3) 1200 km x 1.5m = 1800m²	Semi-circle low stone wall. E 161º 37.873' S 77º 20.107' Weir with stream level monitors at outlet of Upper Lake Victoria.
Beacon Valley - The exposed ground in Beacon Valley was more protected by armouring of the surface with large boulder rocks which were difficult to disturb.	Superficial disturbance. Minor scuffing and superficial trampling. 1) camp site 2) polygon surveys 3) Valley transects.	1) 12m x 6m = 72m² 2) polygon 1 Polygon 2 3) 1300m x 0.75 = 975m²	

Appendix II:

Topographic measurements (raw) and calculations (processed)

VVP2 Topographic data

Appendix II

Pos	-0.5	-0.25	0	0.25	0.5	0.75	1	1.25	1.5	1.75	2	2.25	2.5	2.75	3	3.25	3.5	3.75	4	4.25	4.5	4.75	5	5.25	5.5	5.75	6	6.25	6.5	6.75
0	399.69	399.73	399.8	399.8	399.78	399.77	399.765	399.81	399.87	399.885	399.925	399.95	399.99	399.99	399.99	399.99	399.98	399.975	399.97	399.96	399.975	399.96	399.96	399.97	399.975	399.965	399.97	399.975	399.975
0.25	399.7	399.735	399.8	399.82	399.79	399.76	399.755	399.77	399.83	399.85	399.89	399.9	399.93	399.93	399.95	399.935	399.96	399.97	399.96	399.965	399.98	399.975	399.97	399.975	399.99	399.99	399.985	399.98	399.97	399.97
0.5	399.69	399.71	399.76	399.76	399.765	399.75	399.76	399.755	399.8	399.835	399.875	399.865	399.885	399.88	399.85	399.87	399.915	399.92	399.9	399.89	399.93	399.925	399.91	399.94	399.93	399.95	399.965	399.945	399.93	399.93
0.75	399.595	399.64	399.72	399.695	399.74	399.725	399.74	399.74	399.79	399.8	399.81	399.815	399.825	399.815	399.815	399.8	399.845	399.855	399.82	399.81	399.83	399.835	399.81	399.835	399.81	399.825	399.9	399.86	399.85	399.85
1	399.64	399.57	399.5525	399.625	399.665	399.68	399.71	399.715	399.755	399.755	399.74	399.745	399.74	399.735	399.73	399.71	399.75	399.785	399.745	399.775	399.735	399.78	399.775	399.765	399.8	399.82	399.79	399.815	399.825	399.825
1.25	399.71	399.71	399.66	399.605	399.565	399.555	399.665	399.68	399.78	399.69	399.65	399.645	399.65	399.68	399.73	399.775	399.725	399.765	399.835	399.855	399.82	399.815	399.865	399.87	399.935	399.935	399.91	399.93	399.92	399.92
1.5	399.76	399.76	399.74	399.72	399.67	399.65	399.575	399.61	399.58	399.56	399.73	399.72	399.715	399.755	399.83	399.835	399.86	399.87	399.915	399.955	399.95	399.94	399.98	399.98	399.99	400.01	399.98	400.01	399.975	399.975
1.75	399.795	399.81	399.84	399.775	399.74	399.705	399.655	399.635	399.65	399.7	399.75	399.8	399.815	399.82	399.875	399.88	399.89	399.93	399.965	399.995	400.005	399.995	400.04	400.05	400.07	400.06	400.055	400.05	400.055	400.055
2	399.84	399.85	399.845	399.865	399.785	399.765	399.71	399.65	399.68	399.71	399.78	399.91	399.88	399.885	399.935	399.945	399.95	399.97	400.03	400.04	400.025	400.07	400.09	400.12	400.13	400.125	400.12	400.12	400.11	400.11
2.25	399.88	399.845	399.88	399.875	399.835	399.81	399.76	399.785	399.695	399.78	399.965	400	399.94	399.955	399.975	400.005	400.01	400.03	400.075	400.11	400.14	400.13	400.145	400.135	400.145	400.15	400.155	400.155	400.17	400.17
2.5	399.93	399.925	399.93	399.895	399.885	399.86	399.8	399.83	399.725	399.81	399.91	399.975	400	400.03	400.025	400.055	400.07	400.07	400.115	400.15	400.145	400.145	400.14	400.145	400.13	400.125	400.145	400.15	400.185	400.185
2.75	399.965	399.93	399.9525	399.93	399.92	399.9	399.81	399.755	399.78	399.86	399.945	399.99	400.05	400.06	400.105	400.13	400.11	400.115	400.165	400.17	400.145	400.135	400.11	400.11	400.08	400.085	400.11	400.12	400.15	400.15
3	399.99	399.975	399.975	399.965	399.95	399.92	399.805	399.75	399.815	399.87	399.97	400.025	400.06	400.095	400.135	400.16	400.17	400.175	400.2	400.175	400.135	400.11	400.08	400.065	400.05	400.04	400.06	400.07	400.115	400.115
3.25	400.025	400.015	400	399.98	399.965	399.93	399.87	399.76	399.84	399.88	399.99	400.045	400.095	400.115	400.195	400.205	400.195	400.21	400.215	400.175	400.12	400.1	400.08	400.07	400.065	400.05	400.04	400.035	400.06	400.06
3.5	400.035	400.045	400.0175	399.99	399.97	399.945	399.86	399.8	399.85	399.905	399.995	400.05	400.12	400.135	400.205	400.235	400.235	400.235	400.215	400.18	400.135	400.115	400.115	400.095	400.1	400.07	400.05	400.04	400.035	400.035
3.75	400.1	400.08	400.04	400.005	399.99	399.955	399.88	399.82	399.82	399.915	400.01	400.045	400.165	400.18	400.24	400.255	400.25	400.245	400.235	400.2	400.17	400.16	400.14	400.13	400.125	400.1	400.07	400.055	400.045	400.045
4	400.12	400.1	400.065	400.025	399.995	399.97	399.91	399.84	399.84	399.895	400	400.03	400.205	400.23	400.27	400.26	400.25	400.24	400.21	400.22	400.19	400.175	400.155	400.14	400.13	400.105	400.09	400.08	400.06	400.06
4.25	400.14	400.1275	400.0775	400.045	400.005	399.985	399.94	399.895	399.845	399.89	399.99	400.08	400.205	400.215	400.255	400.255	400.25	400.22	400.22	400.22	400.215	400.195	400.155	400.135	400.1	400.08	400.085	400.08	400.075	400.075
4.5	400.1775	400.1475	400.09	400.055	400.025	400.01	399.95	399.93	399.86	399.87	400.01	400.11	400.17	400.2	400.24	400.24	400.235	400.2	400.21	400.22	400.19	400.15	400.115	400.085	400.06	400.04	400.045	400.05	400.075	400.075
4.75	400.19	400.16	400.115	400.075	400.03	400.01	399.98	399.95	399.88	399.89	399.995	400.09	400.14	400.17	400.21	400.205	400.2	400.185	400.18	400.19	400.155	400.1	400.07	400.05	400.015	399.995	400.01	400.02	400.055	400.055
5	400.1975	400.18	400.13	400.09	400.06	400.025	399.995	399.955	399.88	399.9	400.025	400.07	400.13	400.155	400.18	400.145	400.145	400.155	400.14	400.14	400.1	400.075	400.03	400.01	399.985	399.97	399.99	400	400.045	400.045
5.25	400.1975	400.18	400.1325	400.11	400.08	400.05	399.99	399.965	399.87	399.92	400.04	400.09	400.12	400.13	400.155	400.115	400.105	400.1	400.095	400.08	400.06	400.025	399.99	399.97	399.945	399.945	399.97	399.985	400.03	400.03
5.5	400.19	400.175	400.1475	400.11	400.075	400.04	400.01	399.96	399.875	399.93	400.05	400.105	400.13	400.135	400.145	400.11	400.095	400.09	400.08	400.055	400.015	399.98	399.945	399.93	399.915	399.93	399.955	399.97	400.02	400.02
5.75	400.18	400.17	400.145	400.11	400.07	400.04	400.005	399.96	399.895	399.94	400.075	400.1	400.125	400.15	400.17	400.135	400.09	400.075	400.07	400.03	399.98	399.95	399.9	399.895	399.895	399.905	399.95	399.955	400	400
6	400.175	400.165	400.1375	400.115	400.09	400.06	399.995	399.94	399.86	399.93	400.07	400.11	400.16	400.165	400.215	400.17	400.11	400.09	400.07	400	399.955	399.925	399.88	399.88	399.87	399.89	399.935	399.95	399.985	399.985
6.25	400.17	400.165	400.1475	400.12	400.085	400.06	399.97	399.91	399.865	399.91	400.05	400.125	400.185	400.19	400.25	400.22	400.15	400.105	400.075	400	399.94	399.9	399.86	399.855	399.855	399.85	399.915	399.935	399.98	399.98
6.5	400.1775	400.165	400.1625	400.135	400.09	400.04	399.95	399.875	399.835	399.925	400.055	400.12	400.185	400.21	400.26	400.245	400.135	400.115	400.085	399.995	399.925	399.88	399.84	399.835	399.83	399.83	399.9	399.92	399.995	399.995
6.75	400.175	400.18	400.175	400.14	400.09	400.045	399.99	399.905	399.825	399.915	400.05	400.135	400.19	400.24	400.26	400.245	400.145	400.115	400.075	399.99	399.905	399.86	399.835	399.82	399.81	399.815	399.88	399.895	399.98	399.98
7	400.1775	400.1725	400.16	400.125	400.07	400.03	399.955	399.86	399.84	399.94	400.04	400.14	400.215	400.235	400.27	400.24	400.17	400.13	400.08	399.975	399.895	399.85	399.825	399.81	399.81	399.81	399.86	399.9	399.98	399.98
7.25	400.175	400.17	400.1325	400.1	400.055	399.995	399.845	399.825	399.88	399.94	400.07	400.15	400.205	400.25	400.275	400.235	400.18	400.125	400.075	399.965	399.9	399.855	399.825	399.81	399.805	399.8	399.855	399.89	399.965	399.965
7.5	400.18	400.17	400.125	400.085	400.045	399.97	399.835	399.8	399.93	400	400.095	400.145	400.2	400.235	400.25	400.22	400.165	400.12	400.09	399.95	399.895	399.845	399.825	399.81	399.81	399.8	399.855	399.89	399.96	399.96
7.75	400.19	400.1575	400.135	400.075	400.025	399.96	399.855	399.83	399.96	400.01	400.08	400.115	400.185	400.215	400.23	400.195	400.155	400.11	400.085	399.94	399.895	399.85	399.815	399.805	399.81	399.805	399.85	399.885	399.95	399.95
8	400.1925	400.16	400.115	400.08	400.015	399.955	399.855	399.82	399.975	400.005	400.075	400.095	400.175	400.19	400.22	400.195	400.165	400.125	400.105	399.94	399.885	399.85	399.82	399.81	399.81	399.815	399.86	399.88	399.97	399.97
8.25	400.195	400.155	400.12	400.08	400.02	399.955	399.86	399.82	399.965	400.02	400.095	400.115	400.165	400.175	400.185	400.19	400.165	400.12	400.08	399.95	399.885	399.84	399.825	399.815	399.815	399.82	399.85	399.88	399.96	399.96
8.5	400.195	400.1625	400.11	400.07	400.025	399.95	399.83	399.82	399.945	400.035	400.095	400.125	400.16	400.17	400.18	400.17	400.155	400.115	400.085	399.96	399.89	399.85	399.82	399.815	399.815	399.82	399.855	399.88	399.955	399.955
8.75	400.195	400.16	400.11	400.07	400.035	399.94	399.835	399.83	399.97	400.015	400.07	400.13	400.155	400.18	400.18	400.16	400.14	400.105	400.055	399.975	399.89	399.85	399.83	399.825	399.82	399.83	399.855	399.885	399.95	399.95
9	400.1875	400.155	400.1075	400.04	400.005	399.95	399.835	399.82	399.96	400.005	400.07	400.12	400.175	400.195	400.18	400.155	400.125	400.1	400.05	399.98	399.885	399.86	399.835	399.835	399.835	399.84	399.85	399.88	399.94	399.94
9.25	400.165	400.13	400.08	400.035	399.98	399.94	399.825	399.83	399.96	400	400.065	400.125	400.165	400.195	400.19	400.16	400.125	400.09	400.055	399.985	399.905	399.87	399.845	399.84	399.84	399.845	399.86	399.87	399.93	399.93
9.5	400.135	400.11	400.0875	400.015	399.97	399.935	399.82	399.85	399.95	399.98	400.09	400.105	400.175	400.195	400.2	400.16	400.13	400.095	400.07	399.995	399.915	399.885	399.855	399.85	399.85	399.855	399.865	399.875	399.92	399.92
9.75	400.13	400.09	400.04	399.985	399.96	399.91	399.8	399.85	399.965	399.99	400.06	400.11	400.17	400.2	400.195	400.16	400.125	400.1	400.075	400.005	399.925	399.9	399.875	399.86	399.86	399.87	399.865	399.87	399.915	399.915
10	400.095	400.065	400.0125	399.97	399.93	399.89	399.78	399.87	399.97	399.98	400.055	400.095	400.165	400.19	400.17	400.14	400.115	400.105	400.07	399.995	399.945	399.91	399.89	399.875	399.88	399.87	399.875	399.88	399.91	399.97
10.25	400.0825	400.045	399.975	399.96	399.92	399.89	399.76	399.87	399.96	399.975	400.055	400.095	400.135	400.145	400.145	400.125	400.105	400.09	400.075	400.005	399.955	399.935	399.9	399.89	399.89	399.89	399.89	399.895	399.915	399.96
10.5	400.06	400.025	399.97	399.945	399.9	399.87	399.755	399.86	399.95	399.96	400.04	400.075	400.115	400.135	400.13	400.11	400.095	400.08	400.055	400.015	399.97	399.94	399.915	399.905	399.905	399.9	399.9	399.91	399.925	399.96
10.75	400.03	399.9875	399.9475	399.93	399.885	399.84	399.74	399.865	399.94	399.96	400.035	400.055	400.11	400.13	400.14	400.115	400.095	400.075	400.055	400.01	399.98	399.955	399.925	399.92	399.915	399.915	399.92	399.915	399.94	399.95
11	400	399.97	399.9275	399.905	399.87	399.84	399.75	399.85	399.93	399.95	400.015	400.05	400.1	400.125	400.12	400.115	400.1	400.085	400.06	400.025	399.98	399.96	399.935	399.93	399.925	399.92	399.925	399.935	399.95	399.975
11.25	399.965	399.95	399.915	399.905	399.88	399.835	399.74	399.84	399.91	399.95	400.005	400.04	400.095	400.115	400.115	400.1	400.1	400.09	400.08	400.03	399.985	399.975	399.94	399.945	399.94	399.935	399.94	399.95	399.975	399.995
11.5	399.965	399.935	399.895	399.9	399.87	399.835	399.745	399.84	399.8975	399.92	399.99	400.01	400.07	400.09	400.09	400.09	400.1	400.085	400.075	400.035	399.995	399.98	399.955	399.965	399.945	399.95	399.96	399.985	400	400.03
11.75	399.9725	399.94	399.8925	399.89	399.865	399.82	399.74	399.82	399.885	399.9	399.955	399.995	400.035	400.065	400.08	400.08	400.08	400.085	400.055	400.035	399.995	399.98	399.97	399.965	399.965	399.97	399.99	400.005	400.02	400.055
12	399.97	399.935	399.885	399.885	399.86	399.82	399.735	399.81	399.87	399.895	399.95	399.975	400.015	400.035	400.055	400.06	400.07	400.06	400.05	400.025	400	399.99	399.98	399.97	399.975	400	400.015	400.035	400.06	400.1
12.25	399.97	399.9425	399.8725	399.87	399.85	399.815	399.73	399.805	399.86	399.89	399.94	399.965	399.99	400.02	400.025	400.04	400.055	400.05	400.035	400.02	400.005	399.995	399.985	400.005	400.03	400.045	400.07	400.115	400.14
12.5	399.975	399.95	399.875	399.87	399.845	399.825	399.74	399.8	399.85	399.875	399.94	399.96	399.99	400.01	400.015	400.025	400.035	400.03	400.035	400.025	400.015	400.02	400.015	400.025	400.03	400.06	400.085	400.12	400.16	400.18
12.75	399.9775	399.95	399.865	399.875	399.85	399.815	399.72	399.78	399.85	399.875	399.935	399.965	399.985	400.015	400.02	400.035	400.035	400.035	400.035	400.035	400.03	400.035	400.045	400.05	400.08	400.11	400.13	400.17	400.2	400.24
13	399.99	399.9675	399.88	399.875	399.85	399.805	399.715	399.775	399.86	399.885	399.97	400	400.02	400.04	400.07	400.065	400.05	400.06	400.07	400.065	400.05	400.06	400.085	400.1	400.115	400.175	400.205	400.235	400.275	400.28
13.25	400.01	399.985	399.885	399.87	399.855	399.78	399.7	399.775	399.855	399.88	400.01	400.035	400.06	400.09	400.105	400.115	400.095	400.105	400.115	400.12	400.095	400.1	400.13	400.16	400.19	400.235	400.27	400.29	400.31	400.315
13.5	400.02	399.99	399.89	399.88	399.86	399.795	399.695	399.755	399.865	399.885	400.035	400.065	400.105	400.13	400.155	400.17	400.145	400.155	400.165	400.18	400.155	400.175	400.2	400.235	400.27	400.295	400.315	400.32	400.32	400.3
13.75	400.0375	400.005	399.8975	399.885	399.855	399.775	399.69	399.755	399.855	399.905	400.07	400.1	400.15	400.175	400.21	400.225	400.2	400.195	400.235	400.245	400.23	400.255	400.28	400.29	400.31	400.315	400.31	400.285	400.26	400.245
14	400.0375	400	399.91	399.88	399.85	399.74	399.69	399.775	399.855	399.94	400.085	400.115	400.19	400.22	400.255	400.285	400.25	400.26	400.28	400.295	400.3	400.305	400.315	400.295	400.275	400.25	400.25	400.22	400.215	400.19
14.25	400.025	399.985	399.8975	399.88	399.86	399.72	399.68	399.81	399.865	399.96	400.095	400.15	400.215	400.255	400.31	400.36	400.315	400.31	400.35	400.345	400.33	400.315	400.27	400.245	400.215	400.19	400.18	400.155	400.14	400.13
14.5	400	399.97	399.885	399.855	399.83	399.73	399.675	399.8	399.875	399.955	400.13	400.14	400.21	400.26	400.295	400.365	400.37	400.37	400.36	400.33	400.3	400.265	400.22	400.2	400.16	400.115	400.115	400.09	400.085	400.08
14.75	399.985	399.95	399.875	399.85	399.81	399.72	399.695	399.835	399.915	399.955	400.135	400.14	400.21	400.25	400.27	400.33	400.37	400.35	400.32	400.27	400.26	400.22	400.18	400.125	400.115	400.065	400.055	400.03	400.045	400.01
15	399.965	399.93	399.84	399.82	399.78	399.69	399.735	399.85	399.945	399.955	400.11	400.15	400.195	400.225	400.265	400.28	400.32	400.29	400.28	400.23	400.205	400.175	400.13	400.08	400.045	400.01	399.99	399.97	399.98	399.96
15.25	399.92	399.89	399.7925	399.76	399.74	399.715	399.79	399.87	399.94	399.98	400.09	400.125	400.17	400.18	400.24	400.235	400.26	400.26	400.23	400.19	400.175	400.14	400.09	400.02	399.985	399.94	399.935	399.9	399.91	399.91
15.5	399.895	399.85	399.725	399.68	399.75	399.78	399.81	399.89	399.94	399.97	400.07	400.09	400.13	400.135	400.16	400.18	400.215	400.2	400.18	400.135	400.115	400.075	400.02	399.98	399.925	399.87	399.87	399.835	399.84	399.83
15.75	399.8775	399.82	399.67	399.72	399.76	399.805	399.83	399.9	399.96	399.96	400.04	400.07	400.105	400.11	400.13	400.125	400.16	400.16	400.105	400.075	400.03	399.995	399.95	399.93	399.835	399.805	399.81	399.785	399.78	399.77
16	399.86	399.805	399.665	399.67	399.775	399.81	399.85	399.91	399.96	399.975	400.03	400.045	400.075	400.075	400.09	400.07	400.09	400.085	400.04	400	399.975	399.92	399.885	399.795	399.775	399.74	399.735	399.725	399.7	399.69
16.25	399.84	399.78	399.67	399.68	399.795	399.815	399.86	399.91	399.965	399.98	400.015	400.015	400.04	400.04	400.045	400.02	400.05	400.015	399.99	399.935	399.885	399.855	399.805	399.745	399.685	399.635	399.66	399.665	399.67	399.71
16.5	399.815	399.765	399.665	399.66	399.79	399.82	399.86	399.92	399.96	399.99	400.01	400.01	399.995	399.995	399.995	399.98	399.995	399.98	399.93	399.86	399.845	399.79	399.71	399.665	399.7	399.7	399.73	399.775	399.81	399.815
16.75	399.795	399.765	399.635	399.635	399.765	399.81	399.85	399.905	399.95	399.96	399.97	399.965	399.97	399.95	399.935	399.915	399.935	399.885	399.85	399.8	399.785	399.67	399.68	399.73	399.79	399.815	399.835	399.875	399.86	399.875
17	399.79	399.74	399.63	399.63	399.77	399.81	399.855	399.89	399.935	399.935	399.945	399.94	399.945	399.91	399.895	399.875	399.895	399.83	399.805	399.74	399.665	399.64	399.735	399.81	399.88	399.91	399.925	399.93	399.93	399.93
17.25	399.7725	399.74	399.64	399.66	399.75	399.81	399.845	399.875	399.895	399.9	399.92	399.88	399.875	399.86	399.85	399.82	399.825	399.79	399.735	399.65	399.67	399.77	399.835	399.885	399.965	399.975	399.98	399.97	399.96	399.96
17.5	399.7575	399.74	399.655	399.615	399.705	399.78	399.83	399.87	399.875	399.88	399.875	399.84	399.84	399.8	399.795	399.78	399.79	399.72	399.635	399.71	399.77	399.84	399.875	399.93	400.005	400.02	400.01	400	399.99	399.99
17.75	399.735	399.745	399.7	399.665	399.67	399.76	399.815	399.855	399.84	399.835	399.825	399.795	399.795	399.765	399.755	399.715	399.72	399.64	399.715	399.8	399.84	399.9	399.955	399.98	400.04	400.055	400.045	400.03	400.015	400.02
18	399.7	399.7275	399.725	399.64	399.67	399.72	399.78	399.89	399.8	399.8	399.76	399.755	399.75	399.73	399.675	399.635	399.625	399.64	399.765	399.85	399.91	399.96	400.02	400.04	400.065	400.07	400.06	400.05	400.045	400.05
18.25	399.635	399.655	399.6925	399.555	399.65	399.7	399.73	399.735	399.77	399.745	399.72	399.715	399.715	399.69	399.595	399.575	399.595	399.675	399.82	399.86	399.97	399.915	400.065	400.085	400.06	400.05	400.055	400.04	400.06	400.085
18.5	399.59	399.54	399.555	399.535	399.59	399.65	399.69	399.68	399.695	399.68	399.69	399.68	399.67	399.64	399.58	399.56	399.63	399.715	399.88	399.9	400.08	400.05	400.085	400.06	400.045	400.015	400.04	400.04	400.085	400.105
18.75	399.6	399.6	399.555	399.56	399.5	399.565	399.63	399.64	399.66	399.65	399.67	399.65	399.63	399.605	399.575	399.57	399.88	399.84	399.915	399.945	399.99	400.02	400.045	400.04	400.04	400.03	400.06	400.08	400.12	400.135
19	399.68	399.6675	399.65	399.605	399.61	399.6	399.49	399.555	399.6	399.585	399.66	399.615	399.59	399.585	399.58	399.645	399.93	399.92	399.96	399.97	399.995	400	400.015	400.015	400.02	400.04	400.07	400.12	400.14	400.18
19.25	399.75	399.72	399.705	399.675	399.69	399.685	399.63	399.615	399.52	399.535	399.56	399.585	399.61	399.64	399.65	399.845	399.92	399.93	399.97	399.975	399.985	399.995	400.015	400.035	400.055	400.07	400.12	400.15	400.16	400.21
19.5	399.79	399.77	399.7425	399.735	399.745	399.73	399.7	399.68	399.65	399.6	399.61	399.68	399.7	399.705	399.82	399.87	399.95	399.95	399.975	399.985	399.985	400.015	400.07	400.075	400.11	400.13	400.155	400.18	400.2	400.25
19.75	399.84	399.815	399.795	399.775	399.78	399.765	399.75	399.73	399.7	399.675	399.59	399.72	399.75	399.765	399.805	399.89	399.96	399.955	400.005	400.025	400.04	400.07	400.095	400.11	400.135	400.155	400.18	400.21	400.24	400.27
20	399.875	399.8575	399.875	399.83	399.82	399.805	399.8	399.78	399.77	399.74	399.635	399.65	399.765	399.8	399.86	399.905	399.97	399.97	400.035	400.075	400.095	400.1	400.14	400.16	400.185	400.2	400.225	400.245	400.26	400.285

7	7.25	7.5	7.75	8	8.25	8.5	8.75	9	9.25	9.5	9.75	10	10.25	10.5	10.75	11	11.25	11.5	11.75	12
399.945	399.915	399.88	399.845	399.74	399.815	399.775	399.885	399.92	399.945	399.975	399.975	400.01	400.015	400.05	400.075	400.1	400.12	400.12	400.13	400.15
399.905	399.875	399.79	399.75	399.84	399.835	399.76	399.735	399.8	399.84	399.885	399.895	399.955	399.97	400.02	400.06	400.08	400.085	400.1	400.12	400.125
399.81	399.775	399.79	399.85	399.925	399.88	399.86	399.815	399.76	399.75	399.7575	399.79	399.895	399.92	399.975	399.99	400.025	400.04	400.06	400.07	400.09
399.78	399.85	399.875	399.915	399.92	399.915	399.96	399.91	399.89	399.865	399.805	399.74	399.79	399.805	399.88	399.935	399.96	399.995	400.02	400.035	400.03
399.895	399.915	399.92	399.92	399.95	399.9325	399.945	399.94	399.925	399.92	399.9	399.865	399.8	399.725	399.77	399.855	399.875	399.91	399.96	399.99	399.935
399.96	399.96	399.96	399.96	399.975	399.9575	399.96	399.95	399.9575	399.95	399.935	400.005	399.89	399.83	399.76	399.725	399.77	399.835	399.89	399.86	399.85
399.995	400.01	399.995	399.995	400.0125	399.995	399.99	399.99	399.985	399.975	399.96	399.95	399.93	399.905	399.88	399.88	399.81	399.76	399.775	399.795	399.89
400.075	400.04	400.035	400.03	400.045	400.055	400.015	400.01	400.01	399.995	399.98	399.975	399.955	399.935	399.93	399.915	399.9	399.815	399.755	399.9	399.96
400.12	400.1	400.09	400.08	400.0975	400.055	400.06	400.04	400.03	400.02	400.02	399.99	399.98	399.96	399.96	399.93	399.94	399.9	399.795	399.885	399.985
400.17	400.155	400.15	400.14	400.155	400.11	400.095	400.035	400.09	400.0625	400.05	400.02	399.99	399.96	399.945	399.95	399.965	399.91	399.8	399.835	399.94
400.19	400.185	400.19	400.185	400.19	400.16	400.145	400.145	400.11	400.11	400.07	400.045	400.01	399.99	399.975	399.97	399.96	399.93	399.82	399.8	399.915
400.17	400.175	400.195	400.2	400.1925	400.175	400.155	400.125	400.115	400.08	400.06	400.035	400.015	400.005	400.01	399.985	399.965	399.94	399.84	399.775	399.91
400.12	400.125	400.16	400.17	400.165	400.18	400.15	400.13	400.09	400.06	400.05	400.025	400.015	400.01	400.02	400.02	399.96	399.935	399.86	399.79	399.91
400.07	400.085	400.135	400.135	400.15	400.16	400.155	400.12	400.085	400.055	400.03	400.015	400.005	400.01	400.03	400.035	399.995	399.94	399.855	399.8	399.93
400.04	400.055	400.075	400.1	400.115	400.135	400.135	400.1	400.06	400.04	400.02	399.995	399.99	400	400.045	400.04	399.99	399.94	399.82	399.835	399.93
400.04	400.045	400.05	400.06	400.0875	400.12	400.12	400.095	400.08	400.0325	400.015	399.995	400.005	400.005	400.035	400.04	399.995	399.935	399.83	399.805	399.95
400.06	400.055	400.05	400.04	400.095	400.105	400.12	400.11	400.055	400.03	400.005	399.985	399.99	399.995	400.035	400.03	399.995	399.93	399.81	399.8	399.93
400.075	400.07	400.06	400.055	400.115	400.12	400.14	400.12	400.055	400.02	400.01	399.98	399.98	399.99	400.015	400.02	399.98	399.93	399.795	399.815	399.93
400.09	400.095	400.075	400.085	400.1525	400.15	400.16	400.14	400.1	400.04	400.01	399.97	399.965	399.975	400	400.01	399.995	399.915	399.77	399.8	399.93
400.105	400.11	400.1	400.13	400.2	400.185	400.185	400.155	400.1	400.05	400.01	399.965	399.965	399.965	400	400.025	399.96	399.89	399.755	399.82	399.925
400.11	400.13	400.14	400.185	400.2175	400.21	400.205	400.17	400.105	400.055	400	399.975	399.95	399.95	400.005	400.03	399.96	399.895	399.79	399.8	399.895
400.13	400.16	400.195	400.25	400.26	400.24	400.195	400.16	400.115	400.06	400	399.975	399.93	399.935	400.02	400.06	400.01	399.92	399.79	399.74	399.9
400.13	400.165	400.255	400.27	400.28	400.24	400.2	400.155	400.09	400.055	399.995	399.96	399.92	399.945	400.05	400.075	399.975	399.91	399.785	399.745	399.885
400.145	400.215	400.285	400.305	400.3	400.245	400.21	400.155	400.1	400.075	399.995	399.99	399.945	400.02	400.06	400.115	400.04	399.95	399.77	399.77	399.87
400.145	400.25	400.305	400.325	400.3225	400.245	400.21	400.155	400.11	400.05	399.99	399.95	399.995	400.035	400.105	400.14	400.03	399.95	399.82	399.765	399.86
400.15	400.255	400.33	400.355	400.3325	400.28	400.22	400.17	400.095	400.03	400	399.935	399.975	400.03	400.12	400.085	400.025	399.91	399.82	399.71	399.86
400.175	400.275	400.35	400.37	400.35	400.3	400.22	400.155	400.07	400.035	399.9825	399.94	399.99	400.03	400.08	400.03	399.99	399.87	399.79	399.745	399.905
400.195	400.27	400.355	400.375	400.345	400.305	400.21	400.175	400.185	400.03	399.98	399.9375	399.985	400.01	400.03	399.96	399.92	399.82	399.75	399.805	399.945
400.19	400.29	400.37	400.355	400.35	400.275	400.22	400.19	400.145	400.035	399.98	399.93	399.96	399.96	399.945	399.88	399.85	399.765	399.77	399.865	399.99
400.185	400.315	400.355	400.355	400.32	400.275	400.215	400.155	400.075	400.055	399.975	399.9325	399.91	399.91	399.89	399.84	399.73	399.795	399.83	399.93	400.065
400.175	400.3	400.35	400.33	400.3	400.255	400.235	400.155	400.095	400.05	399.995	399.9	399.875	399.865	399.845	399.765	399.78	399.82	399.88	400.01	400.12
400.185	400.315	400.35	400.33	400.295	400.25	400.205	400.16	400.095	400.03	399.985	399.975	399.845	399.84	399.82	399.785	399.765	399.855	399.92	400.03	400.185
400.185	400.275	400.34	400.34	400.295	400.235	400.195	400.15	400.09	400.03	399.955	399.895	399.91	399.82	399.83	399.785	399.79	399.9	399.95	400.065	400.19
400.175	400.26	400.335	400.33	400.31	400.26	400.22	400.17	400.08	400.04	399.95	399.9	399.865	399.795	399.82	399.78	399.84	399.935	399.98	400.09	400.2
400.13	400.255	400.3	400.31	400.2975	400.27	400.22	400.1875	400.05	400.04	399.97	399.9	399.85	399.825	399.865	399.84	399.855	399.925	400.005	400.1	400.24
400.13	400.25	400.31	400.31	400.2875	400.235	400.2	400.155	400.09	400.035	399.965	399.905	399.85	399.81	399.825	399.86	399.83	399.93	400.02	400.11	400.26
400.125	400.215	400.285	400.3	400.3	400.24	400.2	400.16	400.1	400.02	399.96	399.91	399.835	399.885	399.85	399.805	399.84	399.925	400	400.12	400.28
400.1	400.19	400.305	400.315	400.305	400.23	400.19	400.15	400.095	400.0125	399.97	399.91	399.82	399.87	399.92	399.845	399.85	399.92	400.005	400.105	400.255
400.095	400.155	400.295	400.32	400.305	400.24	400.18	400.15	400.075	400.01	399.965	399.91	399.83	399.895	399.925	399.86	399.85	399.92	400.01	400.105	400.25
400.075	400.155	400.295	400.325	400.285	400.23	400.195	400.13	400.095	400.015	399.97	399.93	399.84	399.87	399.94	399.825	399.86	399.91	400.03	400.1	400.24
400.06	400.14	400.26	400.31	400.2475	400.205	400.215	400.135	400.085	400.015	399.98	399.92	399.855	399.915	399.895	399.76	399.86	399.935	400.03	400.115	400.225
400.065	400.115	400.27	400.295	400.27	400.215	400.16	400.1225	400.05	400.015	399.96	399.92	399.845	399.88	399.87	399.78	399.87	399.935	400.015	400.095	400.215
400.055	400.11	400.26	400.28	400.26	400.19	400.14	400.0925	400.055	399.98	399.96	399.9	399.835	399.83	399.825	399.77	399.895	399.95	400.04	400.085	400.21
400.05	400.1	400.22	400.26	400.23	400.185	400.13	400.09	400.035	399.985	399.9475	399.89	399.8275	399.78	399.76	399.805	399.905	399.95	400.035	400.09	400.2
400.06	400.125	400.21	400.26	400.205	400.165	400.13	400.07	400.01	399.98	399.945	399.89	399.82	399.76	399.74	399.835	399.91	399.97	400.04	400.1	400.215
400.18	400.115	400.215	400.235	400.2	400.165	400.115	400.09	399.935	399.975	399.93	399.89	399.815	399.755	399.745	399.85	399.92	399.97	400.055	400.11	400.21
400.095	400.145	400.195	400.225	400.195	400.155	400.115	400.06	400.01	399.975	399.935	399.89	399.815	399.76	399.77	399.86	399.92	399.98	400.04	400.1	400.235
400.125	400.155	400.205	400.225	400.1975	400.155	400.09	400.07	400.02	399.97	399.94	399.9	399.84	399.77	399.76	399.885	399.95	399.99	400.04	400.11	400.22
400.16	400.18	400.23	400.235	400.1975	400.145	400.095	400.07	400.02	399.96	399.94	399.9	399.845	399.74	399.76	399.875	399.945	399.99	400.06	400.115	400.23
400.19	400.225	400.25	400.24	400.205	400.155	400.115	400.0575	400	399.97	399.94	399.895	399.795	399.75	399.79	399.93	399.96	400.01	400.06	400.13	400.245
400.235	400.26	400.27	400.24	400.195	400.16	400.115	400.07	400.01	399.96	399.93	399.89	399.83	399.735	399.82	399.9	399.97	400.03	400.075	400.155	400.27
400.27	400.3	400.275	400.235	400.1825	400.145	400.11	400.04	400.02	399.98	399.91	399.875	399.76	399.725	399.85	399.91	399.98	400.05	400.1	400.18	400.27
400.315	400.295	400.265	400.23	400.165	400.13	400.09	400.04	399.995	399.94	399.91	399.845	399.745	399.73	399.86	399.94	399.995	400.055	400.15	400.19	400.28
400.31	400.275	400.25	400.22	400.15	400.11	400.06	400.03	399.985	399.945	399.8925	399.84	399.74	399.75	399.895	399.935	400.02	400.07	400.16	400.21	400.295
400.28	400.24	400.21	400.175	400.115	400.085	400.045	400.01	399.985	399.95	399.8925	399.84	399.755	399.76	399.895	399.95	400.025	400.085	400.165	400.215	400.29
400.235	400.18	400.18	400.15	400.09	400.065	400.03	400.015	399.98	399.96	399.905	399.87	399.78	399.755	399.91	399.955	400.025	400.09	400.16	400.22	400.295
400.16	400.14	400.125	400.095	400.05	400.03	400.01	400.01	399.99	399.97	399.915	399.895	399.82	399.765	399.91	399.97	400.03	400.095	400.175	400.215	400.275
400.105	400.08	400.075	400.055	400.01	400.005	399.995	399.9925	399.9975	399.975	399.935	399.925	399.85	399.76	399.93	399.955	400.05	400.085	400.18	400.215	400.28
400.055	400.015	400.015	400	399.97	399.965	399.97	399.975	399.975	399.965	399.93	399.91	399.77	399.75	399.895	399.95	400.04	400.105	400.165	400.22	400.275
399.97	399.975	399.965	399.965	399.925	399.94	399.93	399.935	399.93	399.92	399.93	399.85	399.76	399.75	399.845	399.925	400	400.11	400.16	400.2	400.27
399.945	399.915	399.925	399.905	399.855	399.87	399.89	399.89	399.825	399.77	399.855	399.76	399.88	399.855	399.87	399.875	399.935	400.06	400.135	400.185	400.255
399.9	399.87	399.855	399.845	399.775	399.825	399.77	399.78	399.765	399.82	399.83	399.86	399.92	399.93	399.93	399.96	399.93	400.005	400.1	400.17	400.25
399.81	399.78	399.805	399.78	399.75	399.85	399.74	399.83	399.83	399.865	399.925	399.93	399.98	400.005	400.02	400.02	399.99	399.975	400.075	400.16	400.235
399.705	399.69	399.665	399.695	399.78	399.845	399.85	399.895	399.925	400.02	399.975	400	400.025	400.05	400.07	400.07	400.04	399.99	400.06	400.155	400.22
399.7	399.71	399.73	399.79	399.91	399.895	399.95	399.98	400.04	399.995	400.035	400.06	400.095	400.105	400.13	400.115	400.085	400.01	400.04	400.155	400.215
399.755	399.82	399.875	399.93	399.955	399.96	399.995	400.01	400.03	400.055	400.08	400.105	400.15	400.17	400.17	400.16	400.15	400.05	400.05	400.105	400.19
399.85	399.875	399.9	399.95	399.985	399.99	400.015	400.03	400.035	400.085	400.12	400.13	400.21	400.215	400.215	400.2	400.185	400.15	400.055	400.055	400.12
399.895	399.92	399.98	399.985	400.01	400.005	400.035	400.04	400.0875	400.115	400.14	400.17	400.24	400.25	400.26	400.23	400.215	400.195	400.16	400.09	400.07
399.94	399.95	400.06	400	400.035	400.05	400.07	400.08	400.12	400.135	400.16	400.19	400.235	400.25	400.255	400.25	400.23	400.22	400.21	400.17	400.095
399.975	400.01	400.005	400.03	400.08	400.075	400.095	400.125	400.1325	400.1575	400.2	400.215	400.215	400.23	400.24	400.23	400.24	400.235	400.23	400.215	400.17
399.995	400.02	400.05	400.065	400.105	400.11	400.14	400.15	400.17	400.1975	400.205	400.2375	400.215	400.235	400.21	400.22	400.235	400.245	400.25	400.25	400.245
400.04	400.06	400.085	400.09	400.15	400.15	400.18	400.18	400.205	400.2125	400.225	400.235	400.22	400.215	400.205	400.21	400.23	400.25	400.265	400.275	400.28
400.085	400.11	400.11	400.135	400.18	400.165	400.2	400.21	400.23	400.245	400.25	400.24	400.22	400.215	400.215	400.215	400.24	400.26	400.29	400.28	400.305
400.115	400.14	400.16	400.17	400.21	400.195	400.215	400.225	400.235	400.255	400.26	400.255	400.245	400.24	400.22	400.225	400.245	400.27	400.3	400.305	400.31
400.135	400.2	400.195	400.205	400.23	400.225	400.235	400.24	400.255	400.26	400.275	400.26	400.25	400.25	400.23	400.245	400.26	400.285	400.3	400.29	400.315
400.17	400.185	400.21	400.205	400.235	400.235	400.26	400.26	400.275	400.275	400.28	400.275	400.26	400.26	400.26	400.275	400.29	400.295	400.315	400.29	400.33
400.195	400.195	400.22	400.23	400.25	400.26	400.27	400.285	400.3	400.28	400.285	400.27	400.27	400.27	400.275	400.28	400.31	400.315	400.33	400.33	400.32
400.23	400.245	400.255	400.255	400.265	400.275	400.29	400.295	400.295	400.295	400.285	400.27	400.25	400.235	400.28	400.27	400.285	400.3	400.33	400.34	400.355
400.26	400.27	400.28	400.275	400.24	400.24	400.235	400.235	400.26	400.265	400.265	400.24	400.23	400.225	400.24	400.24	400.255	400.27	400.31	400.335	400.365
400.275	400.295	400.305	400.27	400.215	400.21	400.21	400.21	400.22	400.2225	400.24	400.23	400.215	400.21	400.22	400.225	400.24	400.27	400.29	400.32	400.36
400.3	400.28	400.275	400.23	400.17	400.17	400.16	400.17	400.1775	400.2	400.19	400.2	400.175	400.185	400.21	400.22	400.22	400.26	400.28	400.31	400.335

BVP1 TOPOGRAPHY

distance al	-0.5	-0.25	East base l	0.25	0.5	0.75	1	1.25	1.5	1.75	2	2.25	2.5	2.75	3	3.25	3.5	3.75	4	4.25
0	1336.76	1336.761	1336.761	1336.723	1336.685	1336.675	1336.665	1336.534	1336.403	1336.301	1336.2	1336.101	1336.002	1335.946	1335.89	1335.773	1335.655	1335.638	1335.621	1335.683
0.5	1336.945	1336.885	1336.825	1336.803	1336.78	1336.783	1336.785	1336.643	1336.5	1336.494	1336.488	1336.277	1336.065	1335.988	1335.91	1335.81	1335.71	1335.693	1335.675	1335.735
1	1336.78	1336.803	1336.825	1336.825	1336.825	1336.802	1336.778	1336.649	1336.52	1336.418	1336.315	1336.215	1336.115	1336.063	1336.01	1335.925	1335.84	1335.81	1335.78	1335.795
1.5	1336.825	1336.823	1336.82	1336.833	1336.845	1336.802	1336.758	1336.647	1336.535	1336.44	1336.345	1336.265	1336.185	1336.125	1336.065	1335.97	1335.875	1335.842	1335.808	1335.912
2	1336.855	1336.835	1336.815	1336.858	1336.9	1336.844	1336.788	1336.724	1336.66	1336.595	1336.53	1336.495	1336.46	1336.263	1336.065	1335.968	1335.87	1335.81	1335.75	1335.783
2.5	1336.81	1336.808	1336.805	1336.808	1336.81	1336.793	1336.775	1336.662	1336.548	1336.482	1336.415	1336.3	1336.185	1336.113	1336.04	1335.953	1335.865	1335.772	1335.679	1335.7
3	1336.805	1336.85	1336.895	1336.83	1336.765	1336.737	1336.708	1336.738	1336.768	1336.584	1336.4	1336.333	1336.265	1336.173	1336.08	1335.978	1335.875	1335.775	1335.675	1335.71
3.5	1336.895	1336.847	1336.798	1336.766	1336.733	1336.717	1336.701	1336.631	1336.56	1336.505	1336.45	1336.323	1336.195	1336.143	1336.09	1335.96	1335.83	1335.773	1335.715	1335.758
4	1336.88	1336.833	1336.785	1336.731	1336.678	1336.666	1336.655	1336.593	1336.53	1336.475	1336.42	1336.305	1336.19	1336.12	1336.05	1335.96	1335.87	1335.833	1335.795	1335.86
4.5	1336.845	1336.815	1336.785	1336.72	1336.655	1336.632	1336.608	1336.562	1336.515	1336.47	1336.425	1336.328	1336.23	1336.158	1336.085	1336.053	1336.02	1335.935	1335.85	1335.928
5	1336.84	1336.773	1336.705	1336.703	1336.7	1336.631	1336.562	1336.534	1336.505	1336.453	1336.401	1336.316	1336.23	1336.135	1336.04	1335.968	1335.895	1335.91	1335.925	1336.07
5.5	1336.77	1336.746	1336.721	1336.667	1336.612	1336.576	1336.54	1336.599	1336.658	1336.482	1336.305	1336.2	1336.095	1336.035	1335.975	1335.953	1335.93	1336.005	1336.08	1336.163
6	1336.72	1336.705	1336.69	1336.653	1336.615	1336.56	1336.505	1336.433	1336.36	1336.315	1336.27	1336.173	1336.075	1335.993	1335.91	1335.93	1335.95	1336.053	1336.155	1336.228
6.5	1336.705	1336.666	1336.627	1336.586	1336.545	1336.508	1336.47	1336.43	1336.39	1336.288	1336.185	1336.083	1335.98	1335.91	1335.84	1335.881	1335.922	1336.036	1336.15	1336.22
7	1336.75	1336.675	1336.6	1336.553	1336.505	1336.468	1336.43	1336.318	1336.205	1336.125	1336.045	1335.93	1335.815	1335.803	1335.79	1335.82	1335.85	1335.963	1336.075	1336.255
7.5	1336.67	1336.615	1336.56	1336.488	1336.415	1336.383	1336.35	1336.23	1336.11	1336.01	1335.91	1335.83	1335.75	1335.738	1335.725	1335.735	1335.745	1335.947	1336.148	1336.299
8	1336.63	1336.583	1336.535	1336.473	1336.41	1336.313	1336.215	1336.088	1335.96	1335.905	1335.85	1335.768	1335.685	1335.708	1335.73	1335.793	1335.855	1336.01	1336.165	1336.318
8.5	1336.84	1336.695	1336.55	1336.443	1336.335	1336.198	1336.06	1335.97	1335.88	1335.798	1335.715	1335.645	1335.575	1335.6	1335.625	1335.77	1335.915	1336.058	1336.2	1336.34
9	1336.615	1336.535	1336.455	1336.285	1336.115	1336.02	1335.925	1335.81	1335.695	1335.65	1335.605	1335.54	1335.475	1335.575	1335.675	1335.848	1336.02	1336.163	1336.305	1336.403
9.5	1336.435	1336.393	1336.35	1336.235	1336.12	1335.958	1335.795	1335.738	1335.68	1335.625	1335.57	1335.508	1335.445	1335.628	1335.81	1335.903	1335.995	1336.15	1336.305	1336.448
10	1336.405	1336.323	1336.24	1336.145	1336.05	1335.873	1335.695	1335.643	1335.59	1335.489	1335.388	1335.474	1335.56	1335.668	1335.775	1335.918	1336.06	1336.213	1336.365	1336.488
10.5	1336.315	1336.255	1336.195	1335.975	1335.755	1335.698	1335.64	1335.488	1335.335	1335.355	1335.375	1335.508	1335.64	1335.79	1335.94	1336.063	1336.185	1336.308	1336.43	1336.528
11	1336.115	1336.06	1336.005	1335.88	1335.755	1335.72	1335.685	1335.51	1335.335	1335.385	1335.435	1335.585	1335.735	1335.858	1335.98	1336.098	1336.215	1336.328	1336.44	1336.565
11.5	1336.02	1335.92	1335.82	1335.678	1335.535	1335.58	1335.625	1335.465	1335.305	1335.39	1335.475	1335.675	1335.875	1335.97	1336.065	1336.223	1336.38	1336.458	1336.535	1336.608
12	1335.885	1335.855	1335.825	1335.7	1335.575	1335.46	1335.345	1335.345	1335.345	1335.558	1335.77	1335.863	1335.955	1336.043	1336.13	1336.25	1336.37	1336.503	1336.635	1336.707
12.5	1336.005	1335.865	1335.725	1335.663	1335.6	1335.575	1335.55	1335.465	1335.38	1335.518	1335.655	1335.828	1336	1336.093	1336.185	1336.343	1336.5	1336.588	1336.675	1336.695
13	1336.01	1335.945	1335.88	1335.773	1335.665	1335.565	1335.465	1335.438	1335.41	1335.53	1335.65	1335.855	1336.06	1336.158	1336.255	1336.425	1336.595	1336.638	1336.68	1336.695
13.5	1336.115	1336.07	1336.025	1335.918	1335.81	1335.68	1335.55	1335.463	1335.375	1335.513	1335.65	1335.795	1335.94	1336.073	1336.205	1336.373	1336.54	1336.6	1336.66	1336.67
14	1336.26	1336.168	1336.075	1335.973	1335.87	1335.76	1335.65	1335.51	1335.37	1335.453	1335.535	1335.713	1335.89	1336.04	1336.19	1336.333	1336.475	1336.575	1336.675	1336.69
14.5	1336.31	1336.235	1336.16	1336.06	1335.96	1335.833	1335.705	1335.545	1335.385	1335.5	1335.615	1335.648	1335.68	1335.895	1336.11	1336.35	1336.59	1336.648	1336.705	1336.695
15	1336.425	1336.38	1336.334	1336.247	1336.16	1336	1335.84	1335.59	1335.34	1335.37	1335.4	1335.52	1335.64	1335.818	1335.995	1336.203	1336.41	1336.5	1336.59	1336.653
15.5	1336.53	1336.508	1336.485	1336.29	1336.095	1336.098	1336.1	1335.7	1335.3	1335.323	1335.345	1335.438	1335.53	1335.715	1335.9	1336.115	1336.33	1336.493	1336.655	1336.76
16	1336.575	1336.493	1336.41	1336.365	1336.32	1336.31	1336.3	1335.785	1335.27	1335.355	1335.44	1335.52	1335.6	1335.7	1335.8	1335.98	1336.16	1336.33	1336.5	1336.583
16.5	1336.53	1336.478	1336.425	1336.383	1336.34	1336.16	1335.98	1335.723	1335.465	1335.428	1335.39	1335.495	1335.6	1335.69	1335.78	1335.918	1336.055	1336.278	1336.5	1336.578
17	1336.575	1336.509	1336.442	1336.384	1336.325	1336.255	1336.185	1335.938	1335.69	1335.565	1335.44	1335.513	1335.585	1335.688	1335.79	1335.963	1336.135	1336.298	1336.46	1336.55
17.5	1336.59	1336.515	1336.44	1336.4	1336.36	1336.335	1336.31	1336.045	1335.78	1335.623	1335.465	1335.483	1335.5	1335.605	1335.71	1335.928	1336.145	1336.28	1336.415	1336.528
18	1336.64	1336.588	1336.535	1336.46	1336.385	1336.34	1336.295	1336.303	1336.31	1335.98	1335.65	1335.58	1335.51	1335.565	1335.62	1335.833	1336.045	1336.143	1336.24	1336.423
18.5	1336.65	1336.58	1336.51	1336.445	1336.38	1336.315	1336.25	1336.215	1336.18	1335.995	1335.81	1335.65	1335.49	1335.558	1335.625	1335.768	1335.91	1336.175	1336.44	1336.508
19	1336.69	1336.585	1336.48	1336.463	1336.445	1336.36	1336.275	1336.12	1335.965	1335.865	1335.765	1335.7	1335.635	1335.64	1335.645	1335.715	1335.785	1335.94	1336.095	1336.53
19.5	1336.75	1336.683	1336.615	1336.545	1336.475	1336.513	1336.55	1336.26	1335.97	1335.873	1335.775	1335.763	1335.75	1335.69	1335.63	1335.715	1335.8	1335.905	1336.01	1336.195
20	1336.81	1336.753	1336.695	1336.623	1336.55	1336.525	1336.5	1336.36	1336.22	1336.028	1335.835	1335.748	1335.66	1335.693	1335.725	1335.718	1335.71	1335.835	1335.96	1336.068
20.5	1336.82	1336.783	1336.745	1336.653	1336.56	1336.463	1336.365	1336.243	1336.12	1336.05	1335.98	1335.865	1335.75	1335.743	1335.735	1335.785	1335.835	1335.915	1335.995	1336.05
21	1336.93	1336.858	1336.785	1336.66	1336.535	1336.53	1336.525	1336.38	1336.235	1336.145	1336.055	1335.998	1335.94	1335.843	1335.745	1336.035	1336.325	1336.335	1336.345	1336.288
21.5	1336.9	1336.86	1336.82	1336.675	1336.53	1336.483	1336.435	1336.343	1336.25	1336.213	1336.175	1336.1	1336.025	1335.983	1335.94	1336	1336.06	1336.165	1336.27	1336.32
22	1336.9	1336.853	1336.805	1336.723	1336.64	1336.563	1336.485	1336.38	1336.275	1336.208	1336.14	1336.025	1335.91	1335.948	1335.985	1336.068	1336.15	1336.24	1336.33	1336.448
22.5	1336.89	1336.838	1336.785	1336.658	1336.53	1336.418	1336.305	1336.213	1336.12	1336.085	1336.05	1335.955	1335.86	1335.928	1335.995	1336.098	1336.2	1336.278	1336.355	1336.463
23	1336.81	1336.76	1336.71	1336.57	1336.43	1336.31	1336.19	1336.07	1335.95	1335.883	1335.815	1335.808	1335.8	1335.908	1336.015	1336.08	1336.145	1336.278	1336.41	1336.515

4.5	4.75	5	5.25	5.5	5.75	6	6.25	6.5	6.75	7	7.25	7.5	7.75	8	8.25	8.5	8.75	9	9.25	9.5
1335.745	1335.915	1336.085	1336.195	1336.305	1336.44	1336.575	1336.608	1336.64	1336.643	1336.645	1336.667	1336.688	1337.043	1337.398	1337.344	1337.29	1337.123	1336.955	1336.985	1337.015
1335.795	1335.905	1336.015	1336.165	1336.315	1336.462	1336.608	1336.659	1336.71	1336.68	1336.65	1336.94	1337.23	1337.304	1337.378	1337.293	1337.208	1337.087	1336.965	1337.01	1337.055
1335.81	1335.893	1335.975	1336.163	1336.35	1336.478	1336.605	1336.653	1336.7	1336.739	1336.778	1337.039	1337.3	1337.365	1337.43	1337.305	1337.18	1337.049	1336.918	1336.952	1336.985
1336.015	1336.025	1336.035	1336.163	1336.29	1336.374	1336.457	1336.701	1336.945	1336.824	1336.702	1337.006	1337.31	1337.295	1337.28	1337.128	1336.975	1336.955	1336.935	1336.944	1336.952
1335.815	1335.893	1335.97	1336.053	1336.135	1336.211	1336.287	1336.419	1336.55	1336.596	1336.642	1336.829	1337.015	1336.823	1336.63	1336.743	1336.855	1336.815	1336.775	1336.818	1336.861
1335.72	1335.815	1335.91	1335.93	1335.95	1335.983	1336.015	1336.185	1336.355	1336.403	1336.45	1336.48	1336.51	1336.546	1336.582	1336.571	1336.56	1336.573	1336.585	1336.64	1336.695
1335.745	1335.83	1335.915	1336.018	1336.12	1336.016	1335.912	1335.977	1336.041	1336.101	1336.16	1336.233	1336.305	1336.38	1336.455	1336.403	1336.351	1336.361	1336.37	1336.465	1336.56
1335.8	1335.858	1335.915	1336.07	1336.225	1336.075	1335.925	1335.948	1335.97	1335.958	1335.945	1335.988	1336.03	1336.063	1336.095	1336.13	1336.165	1336.173	1336.18	1336.268	1336.355
1335.925	1335.98	1336.035	1336.103	1336.17	1336.125	1336.08	1335.974	1335.868	1335.832	1335.795	1335.858	1335.92	1335.918	1335.915	1335.88	1335.845	1335.887	1335.928	1335.989	1336.05
1336.005	1336.113	1336.22	1336.228	1336.235	1336.224	1336.212	1336.129	1336.045	1336.057	1336.068	1336.017	1335.965	1335.905	1335.845	1335.905	1335.965	1335.964	1335.962	1336.021	1336.08
1336.215	1336.255	1336.295	1336.34	1336.385	1336.407	1336.429	1336.456	1336.482	1336.326	1336.17	1336.19	1336.21	1336.138	1336.065	1336.155	1336.245	1336.205	1336.165	1336.185	1336.205
1336.245	1336.315	1336.385	1336.45	1336.515	1336.536	1336.557	1336.504	1336.45	1336.425	1336.4	1336.376	1336.352	1336.324	1336.295	1336.34	1336.385	1336.387	1336.388	1336.372	1336.355
1336.3	1336.388	1336.475	1336.528	1336.58	1336.595	1336.61	1336.587	1336.563	1336.563	1336.562	1336.559	1336.555	1336.519	1336.482	1336.519	1336.555	1336.538	1336.52	1336.51	1336.5
1336.29	1336.373	1336.455	1336.513	1336.57	1336.583	1336.595	1336.603	1336.61	1336.633	1336.655	1336.668	1336.681	1336.653	1336.625	1336.633	1336.64	1336.63	1336.62	1336.62	1336.62
1336.435	1336.505	1336.575	1336.59	1336.605	1336.613	1336.62	1336.628	1336.635	1336.668	1336.7	1336.683	1336.666	1336.717	1336.768	1336.749	1336.73	1336.713	1336.695	1336.72	1336.745
1336.45	1336.506	1336.562	1336.584	1336.605	1336.621	1336.637	1336.644	1336.65	1336.678	1336.705	1336.737	1336.768	1336.717	1336.665	1336.7	1336.735	1336.75	1336.765	1336.773	1336.78
1336.47	1336.545	1336.62	1336.635	1336.65	1336.655	1336.66	1336.668	1336.675	1336.707	1336.738	1336.752	1336.765	1336.773	1336.78	1336.75	1336.72	1336.743	1336.765	1336.778	1336.79
1336.48	1336.548	1336.615	1336.625	1336.635	1336.675	1336.715	1336.73	1336.745	1336.748	1336.75	1336.759	1336.768	1336.76	1336.752	1336.716	1336.68	1336.678	1336.675	1336.733	1336.79
1336.5	1336.593	1336.685	1336.703	1336.72	1336.77	1336.82	1336.788	1336.755	1336.783	1336.81	1336.788	1336.765	1336.733	1336.7	1336.675	1336.65	1336.6	1336.55	1336.568	1336.585
1336.59	1336.678	1336.765	1336.763	1336.76	1336.815	1336.87	1336.918	1336.965	1336.905	1336.845	1336.805	1336.765	1336.73	1336.695	1336.608	1336.52	1336.445	1336.37	1336.4	1336.43
1336.61	1336.668	1336.725	1336.745	1336.765	1336.803	1336.84	1336.895	1336.95	1336.913	1336.875	1336.805	1336.735	1336.652	1336.568	1336.529	1336.49	1336.448	1336.405	1336.305	1336.205
1336.625	1336.68	1336.735	1336.768	1336.8	1336.838	1336.875	1336.908	1336.94	1336.885	1336.83	1336.795	1336.76	1336.63	1336.5	1336.448	1336.395	1336.355	1336.315	1336.232	1336.148
1336.69	1336.74	1336.79	1336.808	1336.825	1336.913	1337	1337.033	1337.065	1336.973	1336.88	1336.768	1336.655	1336.588	1336.52	1336.473	1336.425	1336.36	1336.295	1336.235	1336.175
1336.68	1336.753	1336.825	1336.818	1336.81	1336.833	1336.855	1336.905	1336.955	1336.903	1336.85	1336.766	1336.682	1336.604	1336.525	1336.44	1336.355	1336.278	1336.2	1336.148	1336.095
1336.778	1336.779	1336.78	1336.805	1336.83	1336.838	1336.845	1336.903	1336.96	1336.98	1337	1336.815	1336.63	1336.56	1336.49	1336.415	1336.34	1336.265	1336.19	1336.153	1336.115
1336.715	1336.745	1336.775	1336.798	1336.82	1336.85	1336.88	1336.883	1336.885	1337.028	1337.17	1336.92	1336.67	1336.58	1336.49	1336.435	1336.38	1336.32	1336.26	1336.208	1336.155
1336.71	1336.735	1336.76	1336.805	1336.85	1336.885	1336.92	1336.903	1336.885	1336.855	1336.825	1336.778	1336.73	1336.668	1336.605	1336.543	1336.48	1336.425	1336.37	1336.335	1336.3
1336.68	1336.723	1336.765	1336.84	1336.915	1336.908	1336.9	1336.93	1336.96	1336.92	1336.88	1336.818	1336.755	1336.698	1336.64	1336.598	1336.555	1336.518	1336.48	1336.438	1336.395
1336.705	1336.725	1336.745	1336.788	1336.83	1336.87	1336.91	1336.933	1336.955	1336.945	1336.935	1336.898	1336.86	1336.788	1336.715	1336.68	1336.645	1336.62	1336.595	1336.573	1336.55
1336.685	1336.708	1336.73	1336.91	1337.09	1337.028	1336.965	1336.975	1336.985	1336.99	1336.995	1336.975	1336.955	1336.888	1336.82	1336.788	1336.755	1336.745	1336.735	1336.703	1336.67
1336.715	1336.733	1336.75	1336.87	1336.99	1337.075	1337.16	1337.055	1336.95	1336.978	1337.005	1337.015	1337.025	1336.98	1336.935	1336.873	1336.81	1336.833	1336.855	1336.848	1336.84
1336.865	1336.815	1336.765	1336.79	1336.815	1336.998	1337.18	1337.108	1337.035	1337.023	1337.01	1337.005	1337	1337.103	1337.205	1337.245	1337.285	1337.13	1336.975	1336.96	1336.945
1336.665	1336.725	1336.785	1336.805	1336.825	1336.863	1336.9	1336.948	1336.995	1336.983	1336.97	1336.973	1336.975	1336.985	1336.995	1337.188	1337.38	1337.185	1336.99	1336.998	1337.005
1336.655	1336.73	1336.805	1336.813	1336.82	1336.878	1336.935	1336.928	1336.92	1336.935	1336.95	1336.96	1336.97	1336.96	1336.95	1336.97	1336.99	1337.018	1337.045	1337.088	1337.13
1336.64	1336.683	1336.725	1336.778	1336.83	1336.845	1336.86	1336.935	1337.01	1336.988	1336.965	1336.963	1336.96	1337.03	1337.1	1337.05	1337	1336.995	1336.99	1336.985	1336.98
1336.64	1336.69	1336.74	1336.795	1336.85	1336.885	1336.92	1336.915	1336.91	1336.923	1336.935	1336.948	1336.96	1336.955	1336.95	1336.983	1337.015	1337.005	1336.995	1336.988	1336.98
1336.605	1336.685	1336.765	1336.913	1337.06	1337.06	1337.06	1337.063	1337.065	1337.118	1337.17	1337.078	1336.985	1336.985	1336.985	1336.988	1336.99	1337.018	1337.045	1337.025	1337.005
1336.575	1336.713	1336.85	1336.98	1337.11	1337.073	1337.035	1337.07	1337.105	1337.11	1337.115	1337.098	1337.08	1337.065	1337.05	1337.03	1337.01	1337.02	1337.03	1337.015	1337
1336.965	1336.918	1336.87	1336.855	1336.84	1336.803	1336.765	1336.763	1336.76	1336.823	1336.885	1336.903	1336.92	1336.998	1337.075	1337.08	1337.085	1337.113	1337.14	1337.073	1337.005
1336.38	1336.635	1336.89	1336.76	1336.63	1336.655	1336.68	1336.683	1336.685	1336.688	1336.69	1336.713	1336.735	1336.853	1336.97	1336.998	1337.025	1336.975	1336.925	1336.97	1337.015
1336.175	1336.42	1336.665	1336.563	1336.46	1336.475	1336.49	1336.5	1336.51	1336.508	1336.505	1336.51	1336.515	1336.628	1336.74	1336.725	1336.71	1336.698	1336.685	1336.725	1336.765
1336.105	1336.215	1336.325	1336.323	1336.32	1336.558	1336.795	1336.653	1336.51	1336.585	1336.66	1336.638	1336.615	1336.54	1336.465	1336.473	1336.48	1336.438	1336.395	1336.42	1336.445
1336.23	1336.228	1336.225	1336.405	1336.585	1336.693	1336.8	1336.755	1336.71	1336.733	1336.755	1336.758	1336.76	1336.66	1336.56	1336.533	1336.505	1336.53	1336.555	1336.503	1336.45
1336.37	1336.355	1336.34	1336.47	1336.6	1336.673	1336.745	1336.745	1336.745	1336.755	1336.765	1336.783	1336.8	1336.768	1336.735	1336.863	1336.99	1336.855	1336.72	1336.635	1336.55
1336.565	1336.583	1336.6	1336.69	1336.78	1336.805	1336.83	1336.838	1336.845	1336.835	1336.825	1336.87	1336.915	1336.873	1336.83	1336.843	1336.855	1336.85	1336.845	1336.845	1336.845
1336.57	1336.695	1336.82	1336.818	1336.815	1336.818	1336.82	1336.845	1336.87	1336.89	1336.91	1336.918	1336.925	1336.938	1336.95	1336.95	1336.95	1336.93	1336.91	1336.915	1336.92
1336.62	1336.66	1336.7	1336.748	1336.795	1336.843	1336.89	1336.938	1336.985	1336.99	1336.995	1336.983	1336.97	1337.008	1337.045	1337.043	1337.04	1337.023	1337.005	1337.023	1337.04

9.75	10	10.25	10.5	10.75	11	11.25	11.5	11.75	12	12.25	12.5	12.75	13	13.25	13.5	13.75	14	14.25	14.5	14.75
1337.035	1337.055	1337.06	1337.065	1337.065	1337.065	1337.066	1337.067	1337.112	1337.157	1337.173	1337.189	1337.181	1337.172	1337.157	1337.141	1337.001	1336.86	1336.756	1336.652	1336.571
1337.078	1337.1	1337.136	1337.171	1337.125	1337.078	1337.105	1337.131	1337.152	1337.173	1337.172	1337.17	1337.222	1337.274	1337.401	1337.527	1337.295	1337.062	1336.972	1336.882	1336.725
1337.01	1337.035	1337.022	1337.008	1337.02	1337.032	1337.054	1337.075	1337.106	1337.136	1337.136	1337.135	1337.152	1337.169	1337.14	1337.111	1337.128	1337.144	1337.078	1337.012	1336.775
1336.993	1337.033	1337.005	1336.977	1336.983	1336.988	1337.022	1337.055	1337.107	1337.158	1337.167	1337.175	1337.191	1337.206	1337.132	1337.058	1337.127	1337.195	1337.008	1336.82	1336.653
1336.881	1336.9	1336.876	1336.851	1336.845	1336.838	1336.928	1337.018	1337.012	1337.005	1337.08	1337.155	1337.23	1337.305	1337.257	1337.208	1337.123	1337.037	1336.944	1336.85	1336.66
1336.702	1336.708	1336.697	1336.685	1336.684	1336.683	1336.688	1336.692	1336.739	1336.786	1336.894	1337.002	1337.028	1337.053	1337.048	1337.043	1337.047	1337.051	1336.875	1336.698	1336.592
1336.536	1336.512	1336.525	1336.538	1336.552	1336.565	1336.58	1336.595	1336.595	1336.595	1336.66	1336.725	1336.755	1336.785	1336.78	1336.775	1336.868	1336.96	1336.838	1336.715	1336.538
1336.441	1336.527	1336.441	1336.355	1336.363	1336.371	1336.518	1336.665	1336.572	1336.478	1336.517	1336.555	1336.581	1336.606	1336.579	1336.552	1336.557	1336.562	1336.494	1336.425	1336.328
1336.068	1336.086	1336.097	1336.107	1336.131	1336.155	1336.134	1336.112	1336.18	1336.247	1336.314	1336.38	1336.433	1336.485	1336.465	1336.445	1336.458	1336.47	1336.399	1336.327	1336.261
1336.154	1336.228	1336.209	1336.19	1336.198	1336.205	1336.184	1336.163	1336.189	1336.215	1336.185	1336.155	1336.202	1336.248	1336.243	1336.238	1336.272	1336.305	1336.234	1336.162	1336.115
1336.264	1336.322	1336.319	1336.315	1336.32	1336.325	1336.356	1336.387	1336.424	1336.46	1336.495	1336.53	1336.479	1336.428	1336.44	1336.452	1336.24	1336.028	1336.017	1336.005	1336.021
1336.445	1336.535	1336.5	1336.465	1336.488	1336.511	1336.541	1336.57	1336.654	1336.738	1336.714	1336.69	1336.666	1336.642	1336.847	1337.052	1336.655	1336.258	1336.181	1336.103	1336.039
1336.519	1336.538	1336.562	1336.585	1336.615	1336.645	1336.7	1336.755	1336.814	1336.873	1336.859	1336.845	1336.814	1336.782	1336.892	1337.002	1336.694	1336.385	1336.25	1336.115	1336.018
1336.655	1336.69	1336.685	1336.68	1336.763	1336.845	1336.843	1336.84	1336.878	1336.915	1336.928	1336.94	1336.932	1336.923	1336.816	1336.708	1336.604	1336.5	1336.345	1336.19	1336.075
1336.74	1336.735	1336.73	1336.725	1336.75	1336.775	1336.779	1336.782	1336.905	1337.027	1336.964	1336.901	1336.896	1336.891	1336.782	1336.672	1336.574	1336.475	1336.4	1336.325	1336.115
1336.768	1336.755	1336.774	1336.792	1336.814	1336.835	1336.815	1336.795	1336.791	1336.787	1336.888	1336.988	1336.934	1336.879	1336.777	1336.675	1336.6	1336.525	1336.405	1336.285	1336.133
1336.793	1336.795	1336.782	1336.768	1336.762	1336.755	1336.781	1336.806	1336.826	1336.845	1336.884	1336.922	1336.887	1336.852	1336.785	1336.717	1336.661	1336.605	1336.483	1336.36	1336.238
1336.785	1336.78	1336.751	1336.722	1336.734	1336.745	1336.74	1336.735	1336.793	1336.85	1336.848	1336.845	1336.826	1336.807	1336.767	1336.727	1336.689	1336.65	1336.575	1336.5	1336.39
1336.6	1336.615	1336.65	1336.685	1336.657	1336.628	1336.658	1336.688	1336.712	1336.735	1336.758	1336.78	1336.768	1336.756	1336.841	1336.925	1336.835	1336.745	1336.648	1336.55	1336.528
1336.438	1336.445	1336.47	1336.495	1336.525	1336.555	1336.57	1336.585	1336.602	1336.618	1336.653	1336.687	1336.677	1336.667	1336.766	1336.865	1336.913	1336.96	1336.788	1336.615	1336.57
1336.272	1336.338	1336.332	1336.325	1336.334	1336.342	1336.439	1336.535	1336.557	1336.579	1336.586	1336.593	1336.616	1336.639	1336.673	1336.707	1336.686	1336.665	1336.658	1336.65	1336.6
1336.143	1336.138	1336.143	1336.148	1336.197	1336.245	1336.342	1336.438	1336.445	1336.452	1336.486	1336.519	1336.56	1336.6	1336.64	1336.68	1336.674	1336.668	1336.664	1336.66	1336.6
1336.127	1336.078	1336.072	1336.065	1336.067	1336.068	1336.122	1336.175	1336.234	1336.292	1336.359	1336.425	1336.44	1336.455	1336.555	1336.655	1336.67	1336.685	1336.633	1336.58	1336.553
1336.08	1336.065	1336.04	1336.015	1336.024	1336.032	1336.056	1336.08	1336.13	1336.18	1336.271	1336.362	1336.444	1336.525	1336.61	1336.695	1336.708	1336.72	1336.68	1336.64	1336.61
1336.09	1336.065	1336.213	1336.36	1336.345	1336.33	1336.204	1336.077	1336.186	1336.295	1336.375	1336.455	1336.535	1336.615	1336.69	1336.765	1336.79	1336.815	1336.793	1336.77	1336.77
1336.143	1336.13	1336.148	1336.165	1336.205	1336.245	1336.248	1336.25	1336.35	1336.45	1336.473	1336.495	1336.567	1336.638	1336.729	1336.82	1336.853	1336.885	1336.895	1336.905	1336.85
1336.29	1336.28	1336.298	1336.315	1336.342	1336.368	1336.371	1336.373	1336.46	1336.547	1336.621	1336.695	1336.802	1336.909	1336.882	1336.855	1336.875	1336.895	1336.893	1336.89	1336.903
1336.393	1336.39	1336.408	1336.425	1336.482	1336.538	1336.542	1336.545	1336.578	1336.611	1336.646	1336.68	1336.73	1336.779	1336.827	1336.875	1336.91	1336.945	1336.93	1336.915	1336.883
1336.538	1336.525	1336.583	1336.641	1336.643	1336.645	1336.645	1336.645	1336.662	1336.678	1336.703	1336.728	1336.769	1336.81	1336.89	1336.97	1336.91	1336.85	1336.888	1336.925	1336.843
1336.768	1336.865	1336.803	1336.74	1336.735	1336.73	1336.733	1336.735	1336.758	1336.78	1336.795	1336.81	1336.828	1336.845	1336.825	1336.805	1336.82	1336.835	1336.805	1336.775	1336.77
1336.855	1336.87	1336.875	1336.88	1336.874	1336.868	1336.867	1336.865	1336.882	1336.899	1336.947	1336.995	1336.93	1336.865	1336.845	1336.825	1336.833	1336.84	1336.809	1336.778	1336.774
1336.96	1336.975	1336.985	1336.995	1337.01	1337.025	1336.99	1336.955	1336.945	1336.935	1336.945	1336.955	1336.995	1337.035	1336.935	1336.835	1336.82	1336.805	1336.788	1336.77	1336.768
1337.06	1337.115	1337.096	1337.077	1337.104	1337.13	1337.105	1337.08	1337.098	1337.116	1337.053	1336.99	1336.948	1336.905	1336.903	1336.9	1336.86	1336.82	1336.794	1336.768	1336.764
1337.095	1337.06	1337.05	1337.04	1337.029	1337.018	1337.159	1337.3	1337.211	1337.122	1337.076	1337.03	1336.974	1336.918	1336.894	1336.87	1336.838	1336.805	1336.778	1336.75	1336.74
1336.998	1337.015	1337.02	1337.025	1337.073	1337.12	1337.093	1337.065	1337.121	1337.177	1337.194	1337.21	1337.028	1336.845	1336.815	1336.785	1336.793	1336.8	1336.755	1336.71	1336.688
1337	1337.02	1337.095	1337.17	1337.148	1337.125	1337.128	1337.13	1337.028	1336.925	1336.898	1336.87	1336.853	1336.835	1336.818	1336.8	1336.775	1336.75	1336.718	1336.685	1336.675
1337.003	1337	1337.045	1337.09	1337.033	1336.975	1336.988	1337	1336.964	1336.928	1336.894	1336.86	1336.824	1336.788	1336.744	1336.7	1336.71	1336.72	1336.645	1336.57	1336.63
1337.023	1337.045	1337.015	1336.985	1336.965	1336.945	1336.955	1336.965	1336.93	1336.895	1336.81	1336.725	1336.684	1336.642	1336.544	1336.445	1336.513	1336.58	1336.565	1336.55	1336.438
1337.028	1337.05	1337.028	1337.005	1336.973	1336.94	1336.963	1336.985	1336.868	1336.75	1336.643	1336.535	1336.474	1336.412	1336.331	1336.25	1336.275	1336.3	1336.305	1336.31	1336.245
1336.988	1336.96	1336.905	1336.85	1336.833	1336.815	1336.813	1336.81	1336.75	1336.69	1336.514	1336.337	1336.285	1336.232	1336.199	1336.165	1336.188	1336.21	1336.163	1336.115	1336.005
1336.735	1336.705	1336.693	1336.68	1336.7	1336.72	1336.7	1336.68	1336.558	1336.435	1336.351	1336.266	1336.216	1336.165	1336.088	1336.01	1335.985	1335.96	1335.915	1335.87	1335.863
1336.48	1336.515	1336.51	1336.505	1336.498	1336.49	1336.508	1336.525	1336.483	1336.44	1336.208	1335.975	1335.94	1335.905	1335.865	1335.825	1335.798	1335.77	1335.815	1335.86	1335.883
1336.428	1336.405	1336.393	1336.38	1336.373	1336.365	1336.293	1336.22	1336.158	1336.096	1336.036	1335.975	1335.965	1335.955	1335.985	1336.015	1335.993	1335.97	1335.943	1335.915	1335.915
1336.545	1336.54	1336.578	1336.615	1336.658	1336.7	1336.548	1336.395	1336.373	1336.35	1336.363	1336.375	1336.26	1336.145	1336.133	1336.12	1336.108	1336.095	1336.083	1336.07	1336.038
1336.768	1336.69	1336.698	1336.705	1336.695	1336.685	1336.638	1336.59	1336.553	1336.515	1336.505	1336.495	1336.403	1336.31	1336.268	1336.225	1336.203	1336.18	1336.175	1336.17	1336.173
1336.905	1336.89	1336.855	1336.82	1336.815	1336.81	1336.798	1336.785	1336.735	1336.685	1336.583	1336.48	1336.493	1336.505	1336.42	1336.335	1336.315	1336.295	1336.275	1336.255	1336.26
1337.015	1336.99	1336.93	1336.87	1336.855	1336.84	1336.803	1336.765	1336.735	1336.705	1336.675	1336.645	1336.603	1336.56	1336.525	1336.49	1336.458	1336.425	1336.4	1336.375	1336.368

15	15.25	15.5	15.75	16	16.25	16.5	16.75	17	17.25	17.5	17.75	18	18.25	18.5	18.75	19	19.25	19.5	19.75	West base
1336.49	1336.383	1336.275	1336.12	1335.965	1335.969	1335.973	1335.878	1335.782	1335.854	1335.925	1335.948	1335.971	1336.041	1336.111	1336.14	1336.168	1336.169	1336.169	1336.169	1336.168
1336.568	1336.467	1336.365	1336.188	1336.01	1335.936	1335.861	1335.798	1335.735	1335.829	1335.922	1335.929	1335.935	1335.981	1336.027	1336.061	1336.095	1336.075	1336.055	1336.03	1336.005
1336.537	1336.505	1336.472	1336.226	1335.98	1335.94	1335.9	1335.818	1335.735	1335.759	1335.782	1335.854	1335.925	1335.946	1335.966	1335.976	1335.985	1335.98	1335.975	1335.95	1335.925
1336.485	1336.398	1336.31	1336.145	1335.98	1335.883	1335.785	1335.73	1335.675	1335.707	1335.738	1335.802	1335.865	1335.855	1335.845	1335.86	1335.875	1335.854	1335.833	1335.764	1335.695
1336.469	1336.377	1336.285	1336.21	1336.135	1335.948	1335.76	1335.698	1335.635	1335.665	1335.695	1335.8	1335.905	1335.874	1335.842	1335.809	1335.775	1335.698	1335.62	1335.708	1335.795
1336.485	1336.45	1336.415	1336.24	1336.065	1335.952	1335.839	1335.72	1335.6	1335.635	1335.67	1335.769	1335.868	1335.773	1335.678	1335.648	1335.618	1335.653	1335.687	1335.526	1335.365
1336.36	1336.253	1336.145	1336.055	1335.965	1335.868	1335.77	1335.775	1335.78	1335.648	1335.515	1335.61	1335.705	1335.637	1335.569	1335.465	1335.36	1335.37	1335.38	1335.5	1335.62
1336.23	1336.175	1336.12	1336.003	1335.885	1335.805	1335.725	1335.769	1335.812	1335.616	1335.42	1335.548	1335.675	1335.585	1335.495	1335.589	1335.682	1335.736	1335.79	1335.81	1335.83
1336.195	1336.064	1335.932	1335.794	1335.655	1335.633	1335.61	1335.581	1335.552	1335.714	1335.875	1335.884	1335.892	1335.914	1335.935	1335.929	1335.922	1335.891	1335.86	1335.968	1336.075
1336.068	1335.958	1335.848	1335.752	1335.655	1335.65	1335.645	1335.78	1335.915	1335.945	1335.975	1336.038	1336.101	1336.116	1336.13	1336.203	1336.275	1336.187	1336.098	1336.192	1336.285
1336.037	1336.029	1336.02	1335.733	1335.445	1335.555	1335.665	1335.743	1335.82	1335.92	1336.02	1336.213	1336.405	1336.41	1336.415	1336.415	1336.415	1336.393	1336.37	1336.378	1336.385
1335.975	1335.923	1335.87	1335.65	1335.43	1335.68	1335.93	1335.928	1335.925	1336.035	1336.145	1336.288	1336.43	1336.511	1336.592	1336.674	1336.755	1336.685	1336.615	1336.55	1336.485
1335.92	1335.828	1335.735	1335.67	1335.605	1335.69	1335.775	1335.853	1335.93	1336.023	1336.115	1336.31	1336.505	1336.592	1336.678	1336.756	1336.833	1336.801	1336.769	1336.677	1336.585
1335.96	1335.85	1335.74	1335.678	1335.615	1335.705	1335.795	1335.925	1336.055	1336.345	1336.635	1336.689	1336.742	1336.839	1336.935	1336.908	1336.88	1336.866	1336.852	1336.774	1336.695
1335.905	1335.838	1335.77	1335.718	1335.665	1335.778	1335.89	1336.035	1336.18	1336.281	1336.381	1336.49	1336.598	1336.662	1336.725	1336.839	1336.953	1336.938	1336.922	1336.799	1336.675
1335.98	1335.953	1335.925	1335.868	1335.81	1335.88	1335.949	1336.169	1336.389	1336.457	1336.525	1336.615	1336.705	1336.764	1336.822	1336.882	1336.942	1336.911	1336.88	1336.818	1336.755
1336.115	1336.085	1336.055	1335.97	1335.885	1335.915	1335.945	1336.145	1336.345	1336.49	1336.635	1336.678	1336.72	1336.798	1336.875	1336.888	1336.9	1336.868	1336.835	1336.758	1336.68
1336.28	1336.233	1336.185	1336.06	1335.935	1336.05	1336.165	1336.283	1336.4	1336.489	1336.578	1336.642	1336.705	1336.777	1336.848	1336.867	1336.885	1336.843	1336.8	1336.696	1336.592
1336.505	1336.373	1336.24	1336.165	1336.09	1336.083	1336.075	1336.15	1336.225	1336.38	1336.535	1336.593	1336.65	1336.753	1336.855	1336.888	1336.92	1336.849	1336.777	1336.674	1336.57
1336.525	1336.463	1336.4	1336.263	1336.125	1336.113	1336.101	1336.256	1336.41	1336.458	1336.505	1336.563	1336.62	1336.693	1336.765	1336.785	1336.805	1336.775	1336.745	1336.745	1336.745
1336.55	1336.498	1336.445	1336.405	1336.365	1336.32	1336.275	1336.253	1336.23	1336.403	1336.575	1336.57	1336.565	1336.714	1336.862	1336.812	1336.762	1336.774	1336.785	1336.697	1336.608
1336.54	1336.49	1336.44	1336.373	1336.305	1336.272	1336.238	1336.222	1336.205	1336.35	1336.495	1336.489	1336.482	1336.569	1336.655	1336.675	1336.695	1336.69	1336.685	1336.658	1336.63
1336.525	1336.538	1336.55	1336.433	1336.315	1336.29	1336.265	1336.223	1336.18	1336.213	1336.245	1336.325	1336.405	1336.488	1336.57	1336.585	1336.6	1336.628	1336.655	1336.638	1336.62
1336.58	1336.535	1336.49	1336.433	1336.375	1336.358	1336.34	1336.278	1336.215	1336.195	1336.175	1336.203	1336.23	1336.35	1336.47	1336.551	1336.632	1336.589	1336.545	1336.743	1336.94
1336.77	1336.673	1336.575	1336.515	1336.455	1336.418	1336.38	1336.398	1336.415	1336.295	1336.175	1336.125	1336.075	1336.223	1336.37	1336.429	1336.488	1336.489	1336.49	1336.563	1336.635
1336.795	1336.698	1336.6	1336.538	1336.475	1336.408	1336.34	1336.218	1336.095	1336.027	1335.958	1335.884	1335.81	1336	1336.189	1336.301	1336.412	1336.47	1336.528	1336.714	1336.9
1336.915	1336.785	1336.655	1336.575	1336.495	1336.41	1336.325	1336.2	1336.075	1336.015	1335.955	1335.862	1335.769	1335.817	1335.865	1336.098	1336.33	1336.35	1336.37	1336.499	1336.628
1336.85	1336.798	1336.745	1336.695	1336.645	1336.463	1336.28	1336.225	1336.17	1336.095	1336.02	1335.848	1335.675	1335.665	1335.655	1335.825	1335.995	1336.179	1336.363	1336.436	1336.509
1336.76	1336.74	1336.72	1336.71	1336.7	1336.503	1336.305	1336.245	1336.185	1336.155	1336.125	1335.86	1335.595	1335.575	1335.555	1335.655	1335.755	1335.893	1336.03	1336.238	1336.445
1336.765	1336.723	1336.68	1336.655	1336.63	1336.455	1336.28	1336.214	1336.148	1336.037	1335.925	1335.768	1335.61	1335.529	1335.448	1335.467	1335.485	1335.665	1335.845	1336.1	1336.355
1336.77	1336.735	1336.7	1336.613	1336.525	1336.43	1336.335	1336.278	1336.22	1336.113	1336.005	1335.87	1335.735	1335.613	1335.49	1335.466	1335.442	1335.644	1335.845	1336.028	1336.21
1336.765	1336.7	1336.635	1336.618	1336.6	1336.508	1336.415	1336.313	1336.21	1336.133	1336.055	1335.965	1335.875	1335.788	1335.7	1335.534	1335.367	1335.464	1335.56	1335.78	1336
1336.76	1336.7	1336.64	1336.59	1336.54	1336.553	1336.565	1336.423	1336.28	1336.2	1336.12	1336.195	1336.27	1335.905	1335.54	1335.492	1335.443	1335.407	1335.37	1335.523	1335.675
1336.73	1336.705	1336.68	1336.63	1336.58	1336.533	1336.485	1336.424	1336.362	1336.296	1336.23	1336.208	1336.185	1335.925	1335.665	1335.623	1335.58	1335.528	1335.475	1335.488	1335.5
1336.665	1336.645	1336.625	1336.595	1336.565	1336.525	1336.485	1336.45	1336.415	1336.325	1336.235	1336.178	1336.12	1335.94	1335.76	1335.703	1335.645	1335.598	1335.55	1335.54	1335.53
1336.665	1336.625	1336.585	1336.575	1336.565	1336.515	1336.465	1336.385	1336.305	1336.25	1336.195	1336.155	1336.115	1336.058	1336	1335.858	1335.715	1335.665	1335.615	1335.653	1335.69
1336.69	1336.64	1336.59	1336.475	1336.36	1336.278	1336.195	1336.083	1335.97	1336.038	1336.105	1336.08	1336.055	1335.977	1335.899	1335.845	1335.79	1335.825	1335.86	1335.873	1335.885
1336.325	1336.325	1336.325	1336.23	1336.135	1336.08	1336.025	1335.955	1335.885	1335.895	1335.905	1335.883	1335.86	1335.856	1335.852	1335.874	1335.895	1335.9	1335.905	1336.005	1336.105
1336.18	1336.14	1336.1	1336.013	1335.925	1335.89	1335.855	1335.85	1335.845	1335.845	1335.845	1335.885	1335.925	1335.88	1335.835	1335.883	1335.93	1335.998	1336.065	1336.083	1336.1
1335.895	1335.865	1335.835	1335.828	1335.82	1335.828	1335.835	1335.885	1335.935	1335.945	1335.955	1335.993	1336.03	1336.005	1335.98	1336.021	1336.062	1336.071	1336.08	1336.078	1336.075
1335.855	1335.888	1335.92	1335.86	1335.8	1335.838	1335.875	1335.885	1335.895	1335.965	1336.035	1336.225	1336.415	1336.3	1336.185	1336.155	1336.125	1336.093	1336.06	1336.014	1335.968
1335.905	1335.883	1335.86	1335.828	1335.795	1335.848	1335.9	1335.89	1335.88	1335.99	1336.1	1336.093	1336.085	1336.093	1336.1	1336.105	1336.11	1336.06	1336.01	1335.953	1335.895
1335.915	1335.943	1335.97	1335.923	1335.875	1335.865	1335.855	1335.85	1335.845	1335.898	1335.95	1335.988	1336.025	1336.043	1336.06	1336.055	1336.05	1336.075	1336.1	1335.985	1335.87
1336.005	1335.988	1335.97	1335.94	1335.91	1335.9	1335.89	1335.885	1335.88	1335.88	1335.88	1335.913	1335.945	1335.98	1336.015	1336.038	1336.06	1336.035	1336.01	1335.945	1335.88
1336.175	1336.118	1336.06	1336.035	1336.01	1336.01	1336.01	1335.993	1335.975	1335.958	1335.94	1335.96	1335.98	1335.96	1335.94	1336.025	1336.11	1336.123	1336.135	1336.013	1335.89
1336.265	1336.22	1336.175	1336.138	1336.1	1336.098	1336.095	1336.068	1336.04	1336.02	1336	1336.04	1336.08	1336.165	1336.25	1336.23	1336.21	1336.17	1336.13	1335.998	1335.865
1336.36	1336.32	1336.28	1336.263	1336.245	1336.228	1336.21	1336.23	1336.25	1336.245	1336.24	1336.213	1336.185	1336.183	1336.18	1336.18	1336.18	1336.12	1336.06	1335.963	1335.865

BVP2 TOPOGRAPHY DATA

distance al	0	0.25	0.5	0.75	1	1.25	1.5	1.75	2	2.25	2.5	2.75	3	3.25	3.5	3.75	4	4.25	4.5	4.75
0	1327.355	1327.205	1327.055	1327.045	1327.035	1327.006	1326.977	1327.029	1327.08	1327.133	1327.185	1327.295	1327.405	1327.456	1327.507	1327.58	1327.652	1327.711	1327.769	1327.812
0.5	1327.34	1327.337	1327.333	1327.174	1327.015	1326.998	1326.98	1327.048	1327.115	1327.175	1327.235	1327.242	1327.248	1327.332	1327.415	1327.524	1327.632	1327.619	1327.605	1327.648
1	1327.48	1327.345	1327.21	1327.128	1327.046	1327.008	1326.97	1327.05	1327.13	1327.21	1327.29	1327.328	1327.365	1327.365	1327.364	1327.29	1327.215	1327.348	1327.48	1327.491
1.5	1327.485	1327.37	1327.255	1327.195	1327.135	1327.143	1327.15	1327.189	1327.228	1327.289	1327.35	1327.39	1327.43	1327.458	1327.485	1327.488	1327.49	1327.51	1327.53	1327.55
2	1327.525	1327.388	1327.25	1327.219	1327.188	1327.234	1327.28	1327.342	1327.403	1327.434	1327.464	1327.477	1327.49	1327.529	1327.568	1327.564	1327.56	1327.561	1327.561	1327.561
2.5	1327.548	1327.454	1327.36	1327.33	1327.3	1327.333	1327.365	1327.483	1327.6	1327.678	1327.755	1327.755	1327.755	1327.721	1327.687	1327.719	1327.75	1327.75	1327.75	1327.708
3	1327.565	1327.515	1327.465	1327.445	1327.424	1327.472	1327.52	1327.658	1327.795	1327.831	1327.866	1327.901	1327.935	1327.96	1327.985	1327.95	1327.915	1327.895	1327.875	1327.874
3.5	1327.65	1327.605	1327.56	1327.54	1327.52	1327.602	1327.684	1327.76	1327.835	1327.907	1327.978	1328.01	1328.042	1328.075	1328.108	1328.105	1328.102	1328.075	1328.047	1328.058
4	1327.78	1327.727	1327.673	1327.657	1327.64	1327.695	1327.75	1327.809	1327.868	1327.939	1328.01	1328.045	1328.08	1328.109	1328.138	1328.167	1328.195	1328.208	1328.22	1328.215
4.5	1327.855	1327.772	1327.688	1327.672	1327.655	1327.72	1327.785	1327.865	1327.944	1328	1328.055	1328.1	1328.145	1328.162	1328.178	1328.227	1328.275	1328.374	1328.472	1328.476
5	1328	1327.915	1327.83	1327.733	1327.635	1327.638	1327.64	1327.75	1327.86	1327.93	1328	1328.07	1328.14	1328.191	1328.242	1328.285	1328.328	1328.384	1328.44	1328.5
5.5	1328.138	1327.989	1327.84	1327.685	1327.53	1327.515	1327.5	1327.583	1327.665	1327.743	1327.82	1327.921	1328.022	1328.121	1328.22	1328.288	1328.355	1328.439	1328.522	1328.577
6	1328.048	1327.894	1327.74	1327.7	1327.66	1327.533	1327.405	1327.408	1327.41	1327.525	1327.64	1327.848	1328.055	1328.078	1328.1	1328.183	1328.265	1328.398	1328.53	1328.607
6.5	1327.86	1327.829	1327.798	1327.689	1327.58	1327.455	1327.33	1327.34	1327.35	1327.508	1327.665	1327.8	1327.935	1328.045	1328.155	1328.23	1328.305	1328.393	1328.48	1328.553
7	1327.74	1327.703	1327.665	1327.6	1327.535	1327.448	1327.36	1327.34	1327.32	1327.503	1327.685	1327.77	1327.855	1327.908	1327.96	1328.094	1328.228	1328.284	1328.34	1328.418
7.5	1327.643	1327.594	1327.545	1327.53	1327.515	1327.403	1327.29	1327.35	1327.41	1327.557	1327.703	1327.744	1327.785	1327.855	1327.925	1328.003	1328.08	1328.193	1328.305	1328.354
8	1327.595	1327.588	1327.58	1327.578	1327.575	1327.447	1327.318	1327.352	1327.385	1327.525	1327.665	1327.763	1327.86	1327.818	1327.775	1327.888	1328	1328.07	1328.14	1328.209
8.5	1327.77	1327.695	1327.62	1327.593	1327.565	1327.5	1327.435	1327.498	1327.56	1327.641	1327.722	1327.739	1327.755	1327.763	1327.77	1327.795	1327.82	1327.928	1328.035	1328.133
9	1327.905	1327.857	1327.808	1327.729	1327.65	1327.555	1327.46	1327.449	1327.438	1327.453	1327.468	1327.516	1327.563	1327.611	1327.658	1327.723	1327.787	1327.846	1327.905	1327.989
9.5	1328.028	1327.946	1327.863	1327.814	1327.765	1327.689	1327.613	1327.547	1327.48	1327.443	1327.405	1327.496	1327.587	1327.63	1327.673	1327.697	1327.72	1327.78	1327.84	1327.885
10	1328.225	1328.115	1328.005	1327.938	1327.87	1327.77	1327.67	1327.635	1327.6	1327.563	1327.525	1327.537	1327.548	1327.613	1327.678	1327.695	1327.712	1327.76	1327.808	1327.847
10.5	1328.24	1328.184	1328.128	1328.034	1327.94	1327.853	1327.765	1327.718	1327.67	1327.629	1327.587	1327.626	1327.665	1327.655	1327.645	1327.683	1327.72	1327.748	1327.775	1327.806
11	1328.21	1328.213	1328.215	1328.068	1327.92	1327.86	1327.8	1327.753	1327.705	1327.69	1327.675	1327.669	1327.663	1327.707	1327.75	1327.77	1327.79	1327.81	1327.83	1327.795
11.5	1328.268	1328.264	1328.26	1328.173	1328.085	1328.15	1328.215	1327.97	1327.725	1327.755	1327.785	1327.757	1327.728	1327.807	1327.885	1327.902	1327.918	1327.949	1327.98	1328.006
12	1328.3	1328.223	1328.145	1328.142	1328.138	1328.062	1327.985	1327.935	1327.885	1327.903	1327.92	1327.865	1327.81	1327.868	1327.925	1327.965	1328.005	1328.067	1328.128	1328.102

5	5.25	5.5	5.75	6	6.25	6.5	6.75	7	7.25	7.5	7.75	8	8.25	8.5	8.75	9	9.25	9.5	9.75	10
1327.855	1327.841	1327.827	1327.811	1327.795	1327.802	1327.808	1327.799	1327.79	1327.754	1327.717	1327.61	1327.502	1327.471	1327.44	1327.439	1327.438	1327.443	1327.448	1327.437	1327.426
1327.69	1327.673	1327.655	1327.689	1327.722	1327.786	1327.85	1327.843	1327.835	1327.701	1327.567	1327.551	1327.535	1327.47	1327.405	1327.435	1327.464	1327.456	1327.448	1327.47	1327.492
1327.502	1327.531	1327.56	1327.575	1327.59	1327.649	1327.707	1327.777	1327.847	1327.686	1327.525	1327.527	1327.529	1327.525	1327.52	1327.548	1327.575	1327.625	1327.675	1327.7	1327.725
1327.57	1327.545	1327.52	1327.55	1327.58	1327.584	1327.588	1327.625	1327.662	1327.654	1327.645	1327.716	1327.787	1327.729	1327.67	1327.698	1327.725	1327.793	1327.86	1327.873	1327.885
1327.56	1327.587	1327.613	1327.734	1327.855	1327.773	1327.69	1327.695	1327.7	1327.777	1327.853	1327.852	1327.85	1327.848	1327.845	1327.905	1327.965	1328.013	1328.06	1328.071	1328.082
1327.665	1327.7	1327.735	1327.75	1327.765	1327.766	1327.767	1327.831	1327.895	1327.964	1328.032	1328.056	1328.08	1328.083	1328.086	1328.126	1328.166	1328.293	1328.42	1328.333	1328.245
1327.872	1327.939	1328.005	1328.061	1328.117	1328.016	1327.915	1328.02	1328.125	1328.154	1328.182	1328.222	1328.262	1328.252	1328.242	1328.257	1328.272	1328.331	1328.39	1328.393	1328.396
1328.068	1328.092	1328.115	1328.169	1328.222	1328.234	1328.245	1328.307	1328.368	1328.387	1328.406	1328.411	1328.416	1328.393	1328.37	1328.38	1328.39	1328.403	1328.416	1328.396	1328.375
1328.209	1328.304	1328.398	1328.386	1328.373	1328.399	1328.425	1328.454	1328.482	1328.475	1328.468	1328.452	1328.435	1328.429	1328.422	1328.407	1328.392	1328.376	1328.36	1328.283	1328.205
1328.48	1328.533	1328.585	1328.575	1328.565	1328.547	1328.528	1328.509	1328.49	1328.424	1328.358	1328.359	1328.36	1328.409	1328.458	1328.394	1328.329	1328.316	1328.303	1328.243	1328.183
1328.56	1328.625	1328.69	1328.713	1328.735	1328.674	1328.613	1328.548	1328.482	1328.379	1328.275	1328.243	1328.21	1328.213	1328.215	1328.219	1328.223	1328.183	1328.142	1328.147	1328.151
1328.632	1328.703	1328.774	1328.747	1328.72	1328.69	1328.66	1328.555	1328.45	1328.325	1328.2	1328.156	1328.112	1328.098	1328.084	1328.073	1328.062	1328.041	1328.02	1328.001	1327.982
1328.683	1328.697	1328.71	1328.693	1328.675	1328.592	1328.508	1328.524	1328.54	1328.423	1328.306	1328.194	1328.082	1328.061	1328.04	1328.025	1328.01	1328	1327.99	1327.98	1327.97
1328.625	1328.64	1328.655	1328.65	1328.645	1328.659	1328.672	1328.554	1328.436	1328.352	1328.268	1328.184	1328.1	1328.073	1328.045	1328.03	1328.015	1328.005	1327.995	1327.989	1327.982
1328.495	1328.566	1328.637	1328.644	1328.65	1328.628	1328.605	1328.53	1328.455	1328.414	1328.372	1328.316	1328.26	1328.181	1328.102	1328.056	1328.01	1328.043	1328.075	1328.098	1328.121
1328.403	1328.521	1328.638	1328.629	1328.62	1328.6	1328.58	1328.583	1328.586	1328.551	1328.515	1328.469	1328.422	1328.364	1328.305	1328.264	1328.222	1328.241	1328.259	1328.295	1328.33
1328.277	1328.406	1328.535	1328.579	1328.622	1328.618	1328.614	1328.633	1328.652	1328.667	1328.682	1328.641	1328.6	1328.536	1328.472	1328.446	1328.42	1328.416	1328.411	1328.416	1328.42
1328.23	1328.273	1328.315	1328.41	1328.505	1328.568	1328.63	1328.647	1328.663	1328.615	1328.566	1328.572	1328.577	1328.555	1328.533	1328.514	1328.495	1328.458	1328.42	1328.433	1328.446
1328.073	1328.064	1328.055	1328.25	1328.445	1328.368	1328.29	1328.415	1328.539	1328.547	1328.555	1328.47	1328.385	1328.391	1328.396	1328.41	1328.423	1328.382	1328.34	1328.372	1328.404
1327.93	1328.008	1328.085	1328.14	1328.195	1328.161	1328.126	1328.136	1328.145	1328.259	1328.372	1328.299	1328.225	1328.214	1328.202	1328.201	1328.2	1328.198	1328.195	1328.23	1328.265
1327.885	1327.935	1327.985	1328.014	1328.043	1328.062	1328.08	1328.094	1328.107	1328.081	1328.055	1328.038	1328.02	1328.038	1328.055	1328.078	1328.1	1328.095	1328.09	1328.078	1328.065
1327.837	1327.876	1327.915	1327.953	1327.99	1328.021	1328.052	1328.061	1328.069	1328.037	1328.005	1327.964	1327.922	1328.044	1328.165	1328.118	1328.07	1328.073	1328.075	1328.082	1328.088
1327.759	1327.804	1327.848	1327.884	1327.919	1327.957	1327.995	1328.008	1328.021	1327.97	1327.918	1327.967	1328.015	1328.048	1328.08	1328.081	1328.082	1328.084	1328.086	1328.055	1328.023
1328.031	1327.936	1327.84	1327.853	1327.865	1327.898	1327.93	1327.948	1327.965	1327.938	1327.91	1327.966	1328.022	1328.036	1328.05	1328.05	1328.05	1328.059	1328.067	1328.054	1328.04
1328.075	1328.048	1328.02	1327.922	1327.823	1327.854	1327.885	1327.899	1327.912	1327.934	1327.955	1328	1328.045	1328.048	1328.05	1328.036	1328.022	1328.044	1328.065	1328.073	1328.08

10.25	10.5	10.75	11	11.25	11.5	11.75	12	12.25	12.5	12.75	13	13.25	13.5	13.75	14	14.25	14.5	14.75	15	15.25
1327.416	1327.406	1327.466	1327.525	1327.477	1327.428	1327.449	1327.47	1327.512	1327.554	1327.615	1327.675	1327.76	1327.844	1327.89	1327.935	1327.931	1327.926	1327.971	1328.015	1328.08
1327.484	1327.475	1327.522	1327.568	1327.543	1327.518	1327.403	1327.287	1327.39	1327.492	1327.539	1327.585	1327.637	1327.688	1327.718	1327.748	1327.808	1327.868	1327.909	1327.95	1328.02
1327.674	1327.622	1327.649	1327.675	1327.665	1327.655	1327.602	1327.548	1327.503	1327.457	1327.445	1327.432	1327.455	1327.478	1327.514	1327.55	1327.666	1327.782	1327.856	1327.93	1328.013
1327.839	1327.793	1327.884	1327.975	1327.89	1327.805	1327.744	1327.682	1327.6	1327.518	1327.479	1327.44	1327.349	1327.258	1327.315	1327.371	1327.516	1327.66	1327.722	1327.783	1327.84
1328.015	1327.948	1327.988	1328.027	1328.034	1328.04	1327.993	1327.945	1327.778	1327.61	1327.568	1327.525	1327.444	1327.362	1327.338	1327.313	1327.423	1327.532	1327.614	1327.695	1327.728
1328.181	1328.116	1328.144	1328.172	1328.175	1328.178	1328.148	1328.118	1327.959	1327.8	1327.718	1327.635	1327.481	1327.327	1327.289	1327.25	1327.297	1327.343	1327.463	1327.582	1327.625
1328.328	1328.26	1328.279	1328.298	1328.204	1328.11	1328.051	1327.992	1327.926	1327.86	1327.715	1327.57	1327.48	1327.39	1327.302	1327.214	1327.242	1327.27	1327.365	1327.46	1327.566
1328.391	1328.406	1328.312	1328.218	1328.144	1328.07	1328.009	1327.948	1327.868	1327.788	1327.714	1327.64	1327.567	1327.493	1327.392	1327.29	1327.27	1327.25	1327.315	1327.38	1327.45
1328.226	1328.246	1328.216	1328.185	1328.124	1328.063	1328.009	1327.955	1327.899	1327.842	1327.789	1327.735	1327.68	1327.625	1327.527	1327.428	1327.393	1327.357	1327.344	1327.33	1327.425
1328.168	1328.153	1328.178	1328.203	1328.157	1328.11	1328.05	1327.99	1327.95	1327.91	1327.865	1327.82	1327.818	1327.815	1327.793	1327.77	1327.648	1327.525	1327.544	1327.563	1327.501
1328.138	1328.125	1328.167	1328.208	1328.172	1328.135	1328.105	1328.074	1328.037	1328	1327.96	1327.92	1327.87	1327.82	1327.778	1327.735	1327.733	1327.73	1327.685	1327.64	1327.674
1327.992	1328.002	1328.079	1328.155	1328.208	1328.26	1328.25	1328.24	1328.16	1328.08	1328.093	1328.105	1328.038	1327.97	1327.935	1327.9	1327.891	1327.882	1327.831	1327.78	1327.7
1328.06	1328.15	1328.187	1328.224	1328.247	1328.269	1328.249	1328.228	1328.204	1328.18	1328.169	1328.157	1328.136	1328.115	1328.073	1328.03	1328.039	1328.048	1328.008	1327.968	1327.834
1328.044	1328.105	1328.208	1328.31	1328.329	1328.348	1328.317	1328.285	1328.27	1328.255	1328.263	1328.27	1328.235	1328.2	1328.195	1328.19	1328.208	1328.225	1328.223	1328.22	1328.136
1328.16	1328.198	1328.257	1328.315	1328.35	1328.385	1328.378	1328.37	1328.353	1328.335	1328.342	1328.348	1328.332	1328.315	1328.372	1328.428	1328.38	1328.332	1328.339	1328.345	1328.277
1328.35	1328.37	1328.406	1328.442	1328.391	1328.34	1328.351	1328.362	1328.344	1328.325	1328.325	1328.325	1328.325	1328.325	1328.375	1328.425	1328.438	1328.45	1328.46	1328.47	1328.37
1328.414	1328.407	1328.431	1328.455	1328.446	1328.437	1328.413	1328.388	1328.373	1328.358	1328.364	1328.37	1328.36	1328.35	1328.398	1328.445	1328.47	1328.494	1328.474	1328.453	1328.357
1328.44	1328.433	1328.437	1328.44	1328.433	1328.425	1328.411	1328.397	1328.383	1328.368	1328.377	1328.385	1328.448	1328.51	1328.47	1328.43	1328.406	1328.382	1328.389	1328.395	1328.313
1328.481	1328.558	1328.493	1328.427	1328.398	1328.368	1328.362	1328.355	1328.338	1328.32	1328.325	1328.33	1328.386	1328.442	1328.431	1328.42	1328.41	1328.4	1328.408	1328.415	1328.371
1328.293	1328.32	1328.325	1328.33	1328.245	1328.159	1328.143	1328.127	1328.136	1328.145	1328.163	1328.18	1328.233	1328.285	1328.273	1328.26	1328.308	1328.355	1328.368	1328.38	1328.363
1328.083	1328.1	1328.083	1328.065	1328.006	1327.946	1327.967	1327.988	1327.99	1327.992	1328.009	1328.025	1328.037	1328.048	1328.103	1328.158	1328.249	1328.34	1328.325	1328.31	1328.325
1327.995	1327.902	1327.924	1327.945	1327.925	1327.905	1327.934	1327.962	1327.976	1327.99	1328.038	1328.085	1328.063	1328.04	1328.096	1328.152	1328.219	1328.286	1328.308	1328.33	1328.328
1328.017	1328.01	1328.034	1328.057	1328.004	1327.95	1327.959	1327.967	1328.027	1328.086	1328.057	1328.028	1328.059	1328.09	1328.148	1328.205	1328.3	1328.395	1328.403	1328.41	1328.383
1328.112	1328.184	1328.147	1328.11	1328.208	1328.305	1328.183	1328.06	1328.099	1328.138	1328.17	1328.202	1328.234	1328.265	1328.296	1328.326	1328.355	1328.384	1328.428	1328.472	1328.431
1328.104	1328.127	1328.153	1328.178	1328.217	1328.255	1328.218	1328.18	1328.188	1328.195	1328.28	1328.365	1328.364	1328.363	1328.434	1328.504	1328.5	1328.495	1328.47	1328.444	1328.462

15.5	15.75	16	16.25	16.5	16.75	17	17.25	17.5	17.75	18
1328.145	1328.202	1328.258	1328.298	1328.337	1328.359	1328.38	1328.39	1328.399	1328.419	1328.439
1328.09	1328.146	1328.201	1328.258	1328.314	1328.326	1328.338	1328.441	1328.543	1328.495	1328.447
1328.095	1328.113	1328.13	1328.276	1328.422	1328.394	1328.365	1328.398	1328.43	1328.413	1328.395
1327.897	1327.978	1328.058	1328.157	1328.255	1328.255	1328.255	1328.273	1328.29	1328.309	1328.327
1327.76	1327.821	1327.882	1327.936	1327.99	1328.055	1328.119	1328.166	1328.212	1328.264	1328.315
1327.667	1327.693	1327.718	1327.771	1327.824	1327.876	1327.928	1328.033	1328.137	1328.197	1328.257
1327.672	1327.664	1327.655	1327.692	1327.728	1327.792	1327.855	1327.953	1328.05	1328.118	1328.185
1327.52	1327.525	1327.53	1327.58	1327.63	1327.69	1327.75	1327.856	1327.962	1328.027	1328.092
1327.52	1327.54	1327.56	1327.563	1327.565	1327.613	1327.66	1327.782	1327.903	1327.972	1328.04
1327.438	1327.488	1327.537	1327.549	1327.56	1327.595	1327.63	1327.704	1327.778	1327.93	1328.082
1327.707	1327.701	1327.695	1327.607	1327.518	1327.562	1327.605	1327.64	1327.675	1327.794	1327.913
1327.619	1327.655	1327.69	1327.57	1327.45	1327.455	1327.46	1327.555	1327.65	1327.746	1327.842
1327.7	1327.669	1327.638	1327.693	1327.748	1327.632	1327.515	1327.548	1327.58	1327.718	1327.855
1328.052	1327.951	1327.85	1327.745	1327.64	1327.605	1327.57	1327.669	1327.768	1327.862	1327.955
1328.208	1328.098	1327.987	1327.829	1327.67	1327.624	1327.577	1327.631	1327.685	1327.813	1327.94
1328.27	1328.057	1327.844	1327.791	1327.737	1327.671	1327.605	1327.665	1327.725	1327.823	1327.92
1328.26	1328.14	1328.02	1327.924	1327.828	1327.792	1327.755	1327.733	1327.71	1327.819	1327.927
1328.23	1328.18	1328.13	1328.036	1327.942	1327.891	1327.84	1327.836	1327.832	1327.864	1327.895
1328.327	1328.235	1328.142	1328.095	1328.047	1328.021	1327.995	1328.009	1328.022	1328.086	1328.15
1328.345	1328.293	1328.24	1328.23	1328.22	1328.165	1328.11	1328.11	1328.109	1328.191	1328.273
1328.34	1328.323	1328.305	1328.295	1328.285	1328.268	1328.25	1328.404	1328.557	1328.473	1328.388
1328.325	1328.315	1328.305	1328.308	1328.31	1328.317	1328.324	1328.297	1328.27	1328.268	1328.265
1328.355	1328.355	1328.355	1328.333	1328.31	1328.308	1328.305	1328.275	1328.245	1328.263	1328.28
1328.39	1328.43	1328.47	1328.413	1328.355	1328.316	1328.277	1328.261	1328.245	1328.215	1328.185
1328.48	1328.459	1328.438	1328.399	1328.36	1328.345	1328.33	1328.325	1328.32	1328.288	1328.255

Appendix III:

GPR processing Batch files

Batch files processing:

MS DOS (Microsoft Disk Operating system) batch files run in command prompt and used in conjunction with pulseEKKO GPR processing software can be used to process multiple lines with one set of commands. The use of batch files in command prompt allows a 3D data set to be processed to the same specifications and at the same time, saving time and ensuring consistency within the processed results. As the GPR data sets for this thesis involved multiple 3d cube surveys as well as different geophysical methods Batch files were used as a far more efficient use of the time available. Batch files are easier to check for mistakes or omissions within the commands as they can be reviewed and edited as a single complete text file.

Batch files were used to migrate the data sets and add topography, using “migrate”; “topo_add”, and “toposhift” functions of pulseEKKO 4.2 software. To track changes each batch file also contained a renaming command and files were assigned a “T” or “M” referring to “topographically corrected” or, “topographically corrected and migrated” respectively. (refer appendix III for complete batch file scripts used for processing of data presented in this thesis)

Renaming:

ren original file name .* replacement file name .*

Resampling:

\ekko42\analysis\resample file name sample rate .

New window:

\ekko42\analysis\new_wind file name new window length .

Migration:

\ekko42\analysis\migrate file name .

Topoadd:

\ekko42\tools\topo_add file name .

Toposhift:

\ekko42\tools\toposhft file name velocity .

Batch file processing requires the creation of a batch file containing a series of MS DOS commands using a program like WordPad or notepad and saving the file with a “.BAT” file extension. Using the MS DOS commands stated above, a command line must be written for each file and action that is to be completed. For the migration

batch file to work there must also be a migration parameter file containing values for the average velocity, taper X, taper Z, skip X, anti alias and the gain factor to be used in the migration. Table 3 shows an example of parameter values for batch file processing of VVP2 data.

Table 3 Batch file migration parameters.

Parameter	Value
Skip X (traces)	30
Taper X direction (traces)	15
Taper Z direction (Points)	20
Anti-alias filter	0
Anti-alias factor	1
Gain factor	2.00
Average velocity (m/ns)	0.13

Running batch files must be done using the command prompt in windows operating systems or if possible rebooting in DOS (Windows 98 or earlier operating systems are capable of doing this but Windows 2000 or later are not). Batch files must be run from the C:\ drive and from the same folder as the data you wish to process. For the purposes of processing the multiple GPR data sets from the Dry Valleys folders containing copies of data and batch files for each polygon, frequency and time lapse run were created directly on the C:\ drive and run from there using the following commands:

P> C: (to enter C drive)

C>dir (to display the files and directories found in C:\ drive)

C> cd __folder name containing batch file to be run e.g. bp1A_mig__ (to change directory to the folder containing the data to be worked on.)

C> dir (to display the files within the directory this should contain all of your data files and the batch file)

C> __batch file name e.g. migrate.bat__ (pressing enter will run the batch file)

Each command line written in the batch file will then be executed, one after the other in the order written.

In this way migration and topographic correction is completed for the data sets making them ready for concatenation into three dimensional cubes.

In addition to processing the data using batch file scripts the individual profile lines were also drawn using batch file commands:

\ekko42\base\draw file name velocity .

This command produced .PCX files of the files which could then be imported and formatted in graphics programs.

Copies of the batch files used can be seen in full on the data disk of Appendix VII.

Appendix IV:

GPR data

Appendix V

Resistivity data

The inversion equation used in Res2D:

$$(J^T J + uF)d = J^T g$$

Where $F = f_x f_x^T + f_z f_z^T$

f_x = horizontal flatness filter, f_z = vertical flatness filter, J matrix of partial derivatives, u = dampening factor, d = model perturbation vector, g = discrepancy vector

The inversion settings applied to the data sets:

Inversion settings
Initial damping factor (0.01 to 1.00)
0.1600
Minimum damping factor (0.001 to 0.75)
0.0150
Line search option (0=Never, 1=Sometimes, 2=Always)
2
Convergence limit for relative change in RMS error in percent (0.1 to 20)
5.0000
Minimum change in RMS error for line search in percent (0.5 to 100)
0.5000
Number of iterations (1 to 30)
10
Vertical to horizontal flatness filter ratio (0.25 to 4.0)
1.0000
Model for increase in thickness of layers (0=default 10, 1=default 25, 2=user defined)
2
Number of nodes between adjacent electrodes (2 or 4)
2
Flatness filter type, Include smoothing of model resistivity (0=model changes only,1=directly on model)
0
Reduce number of topographical datum points? (0=No,1=Yes. Recommend leave at 0)
0
Carry out topography modelling? (0=No,1=Yes)
1
Type of topography trend removal (0=Average,1=Least-squares,2=End to end)
0

Type of Jacobian matrix calculation (0=Quasi-Newton, 1=Gauss-Newton, 2=Mixed)

1

Increase of damping factor with depth (1.0 to 2.0)

1.0500

Type of topographical modeling (0=None, 1=No longer supported so do not use, 2=uniform distorted FEM, 3=underwater, 4=damped FEM, 5=FEM with inverse Swartz-Christoffel)

4

Robust data constrain? (0=No, 1=Yes)

1

Cutoff factor for data constrain (0.0001 to 0.1))

0.0500

Robust model constrain? (0=No, 1=Yes)

1

Cutoff factor for model constrain (0.0001 to 1.0)

0.0050

Allow number of model parameters to exceed datum points? (0=No, 1=Yes)

1

Use extended model? (0=No, 1=Yes)

0

Reduce effect of side blocks? (0=No, 1=Slight, 2=Severe, 3=Very Severe)

2

Type of mesh (0=Normal,1=Fine,2=Finest)

0

Optimise damping factor? (0=No, 1=Yes)

1

Time-lapse inversion constrain (0=None,1=Least-squares,2=Smooth,3=Robust)

0

Type of time-lapse inversion method (0=Simultaneous,1=Sequential)

0

Thickness of first layer (0.25 to 1.0)

0.5000

Factor to increase thickness layer with depth (1.0 to 1.25)

1.1000

USE FINITE ELEMENT METHOD (YES=1,NO=0)

1

WIDTH OF BLOCKS (1=NORMAL WIDTH, 2=DOUBLE, 3=TRIPLE, 4=QUADRAPLE, 5=QUINTIPLE)

1

MAKE SURE BLOCKS HAVE THE SAME WIDTH (YES=1,NO=0)

1

RMS CONVERGENCE LIMIT (IN PERCENT)
3.000
USE LOGARITHM OF APPARENT RESISTIVITY (0=USE LOG OF APPARENT RESISTIVITY,
1=USE RESISTANCE VALUES, 2=USE APPARENT RESISTIVITY)
0
TYPE OF IP INVERSION METHOD (0=CONCURRENT,1=SEQUENTIAL)
0
PROCEED AUTOMATICALLY FOR SEQUENTIAL METHOD (1=YES,0=NO)
0
IP DAMPING FACTOR (0.01 to 1.0)
0.100
USE AUTOMATIC IP DAMPING FACTOR (YES=1,NO=0)
0
CUTOFF FACTOR FOR BOREHOLE DATA (0.0005 to 0.02)
0.00300
TYPE OF CROSS-BOREHOLE MODEL (0=normal,1=halfsize)
0
LIMIT RESISTIVITY VALUES(0=No,1=Yes)
0
Upper limit factor (10-50)
50.000
Lower limit factor (0.02 to 0.1)
0.020
Type of reference resistivity (0=average,1=first iteration)
0
Model refinement (1.0=Normal,0.5=Half-width cells)
0.50
Combined Combined Marquardt and Occam inversion (0=Not used,1=used)
0
Type of optimisation method (0=Gauss-Newton,2=Incomplete GN)
2
Convergence limit for Incomplete Gauss-Newton method (0.005 to 0.05)
0.005
Use data compression with Incomplete Gauss-Newton (0=No,1=Yes)
0
Use reference model in inversion (0=No,1=Yes)
0
Damping factor for reference model (0.0 to 0.3)
0.05000
Use fast method to calculate Jacobian matrix. (0=No,1=Yes)

1

Use higher damping for first layer? (0=No,1=Yes)

0

Extra damping factor for first layer (1.0 to 100.0)

2.50000

Type of finite-element method (0=Triangular,1=Trapezoidal elements)

1

Factor to increase model depth range (1.0 to 5.0)

1.000

Reduce model variations near borehole (0=No, 1=Yes)

0

Factor to control the degree variations near the boreholes are reduced (2 to 100)

5.0

Factor to control variation of borehole damping factor with distance (0.5 to 5.0)

1.0

Floating electrodes survey inversion method (0=use fixed water layer, 1=Incorporate water layer into the model)

0

Resistivity variation within water layer (0=allow resistivity to vary freely,1=minimise variation)

1

```
Initial damping factor is 0.1600.
Minimum damping factor is 0.0150.
Line search is always used.
Convergence limit is 3.0000.
Minimum change in RMS error is 0.5000.
Number of iterations is 10.
Vertical to horizontal flatness filter ratio is 1.0000.
User defined increase in layer thickness.
Number of nodes between adjacent electrodes is 2.
Smoothness constrain is only used on changes in model resistivity values.
Number of topographical datum points is not reduced.
Topographical modeling is to be carried out.
Average topographical trend to be removed.
Jacobian matrix is recalculated after each iteration.
Increase of damping factor with depth is 1.0500.
Finite element method is used for topographic modeling.
Robust data inversion constrain is used with cutoff factor 0.0500.
Robust model inversion constrain is used with cutoff factor 0.0050.
Extended model is not used.
Effect of side blocks is severely reduced.
Normal mesh is used.
Damping factor is optimised at each iteration.
No inter-model constrain is used in time-lapse inversion.
Simultaneous time-lapse inversion is used.
Thickness of first layer is 0.5000.
Factor to increase thickness layer with depth is 1.1000.
Finite element method is used
Width of blocks used is 1 times the unit electrode spacing
All models blocks must have the same width
RMS convergence limit is 3.0 percent
Logarithm of apparent resistivity values are used for the inversion
Resistivity/IP data are inverted sequentially
Do not proceed automatically in sequential IP inversion
IP damping factor is 0.1000
Automatic IP damping factor is not used
Cutoff factor for borehole data is 0.00300
Range of resistivity values are limited.
Upper resistivity cutoff limit is 50.00000
Lower resistivity cutoff limit is 0.02000
Average resistivity used.
```

Summary of inversion parameters:

The following plots are the images made from inverted data sets:

The inversion process: measured apparent resistivity through modelled apparent resistivity from the modelled resistivity that was the result of the inversion process. The measured apparent resistivity should be similar to the modelled apparent resistivity. This gives an impression on how much the modelled resistivity values fit the real world measured apparent resistsivities.

Model sensitivity shows where the greatest resolution of features occurs. This should be near to the surface as that is where the greatest resolution occurs due to the close electrode spacing.

Model uncertainty plots the percentage uncertainty that occurs within the model and is determined by the percentage change of the modelled resistivity from the measured resistivity. These values are the closer to zero the better.

Maximum and minimum resistivity models are the range of solutions produced by the inversion process. For models that were stable under inversion the range of resistivity values seen in the maximum and minimum models should be near identical. Models with differences between the maximum and minimum models represent lower reliability.

Topographic data models show the data with the distorted finite topographic grid applied.

VVP1: Northern most West to East resistivity line (line 2) with 32 electrodes at 1 m spacing:

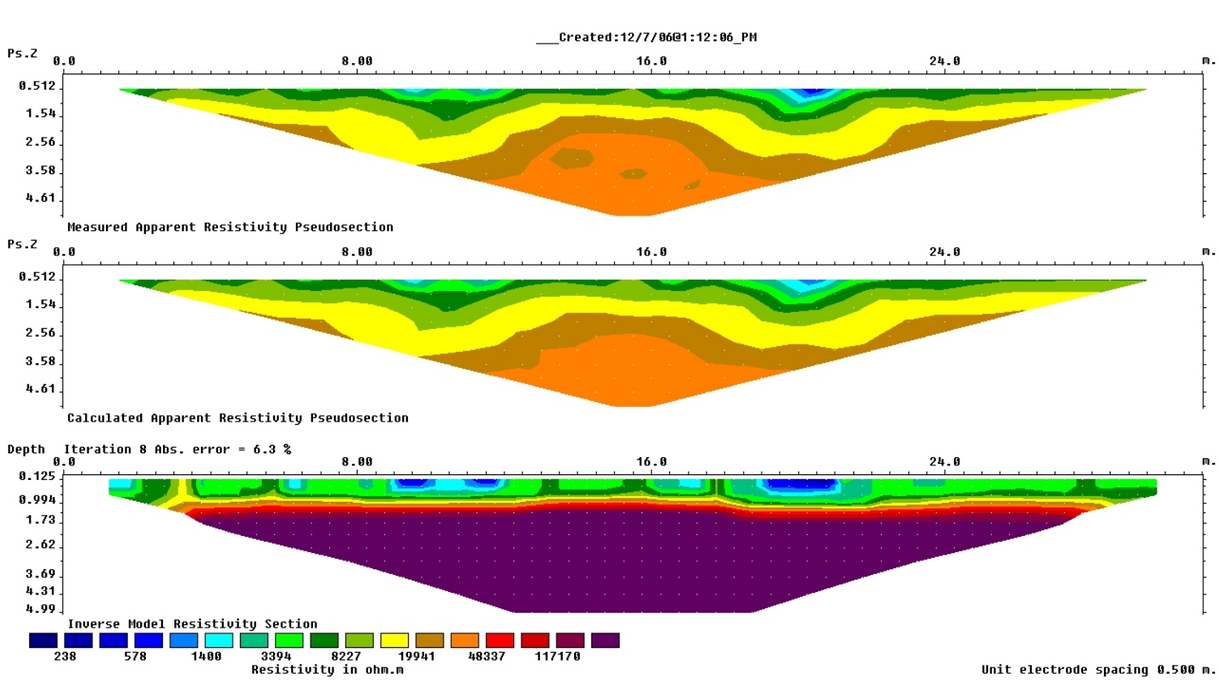

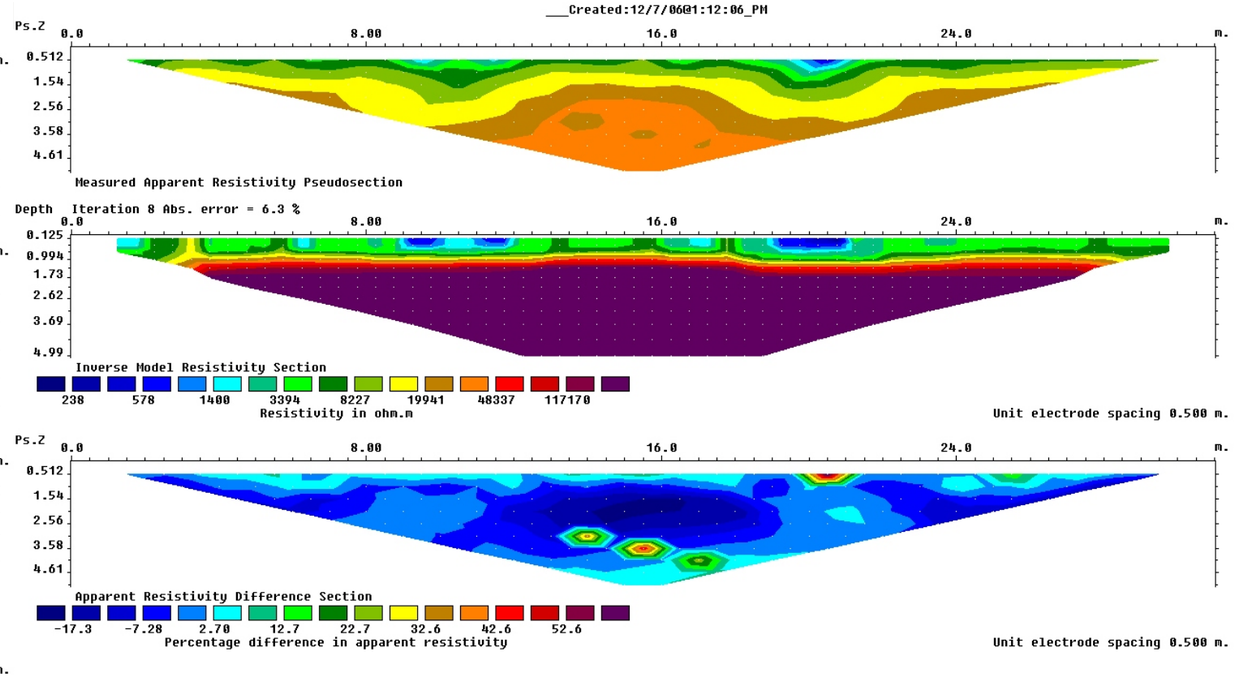

This data did not contain topographic corrections

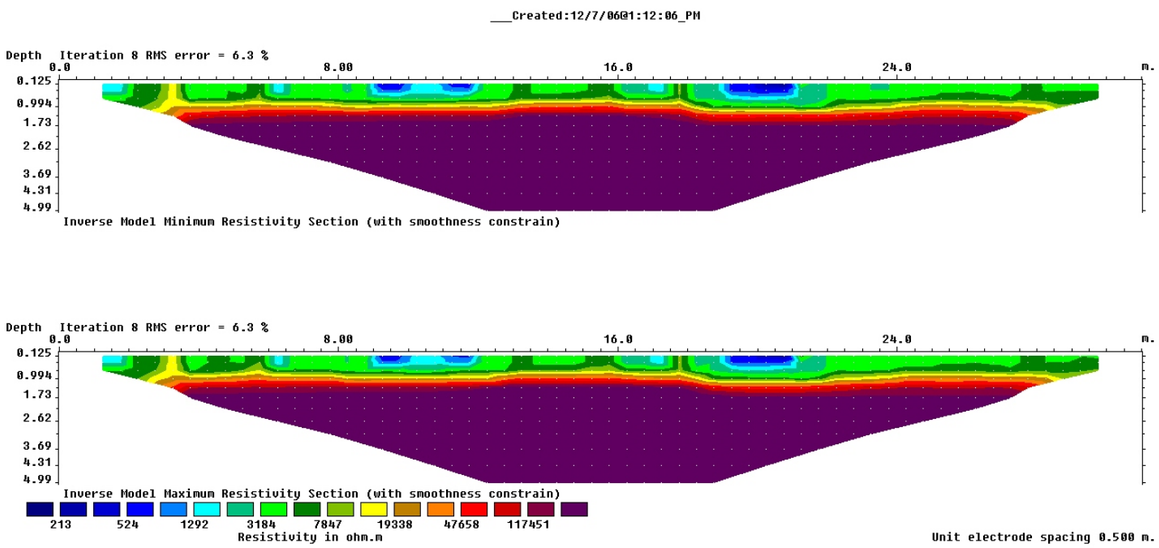

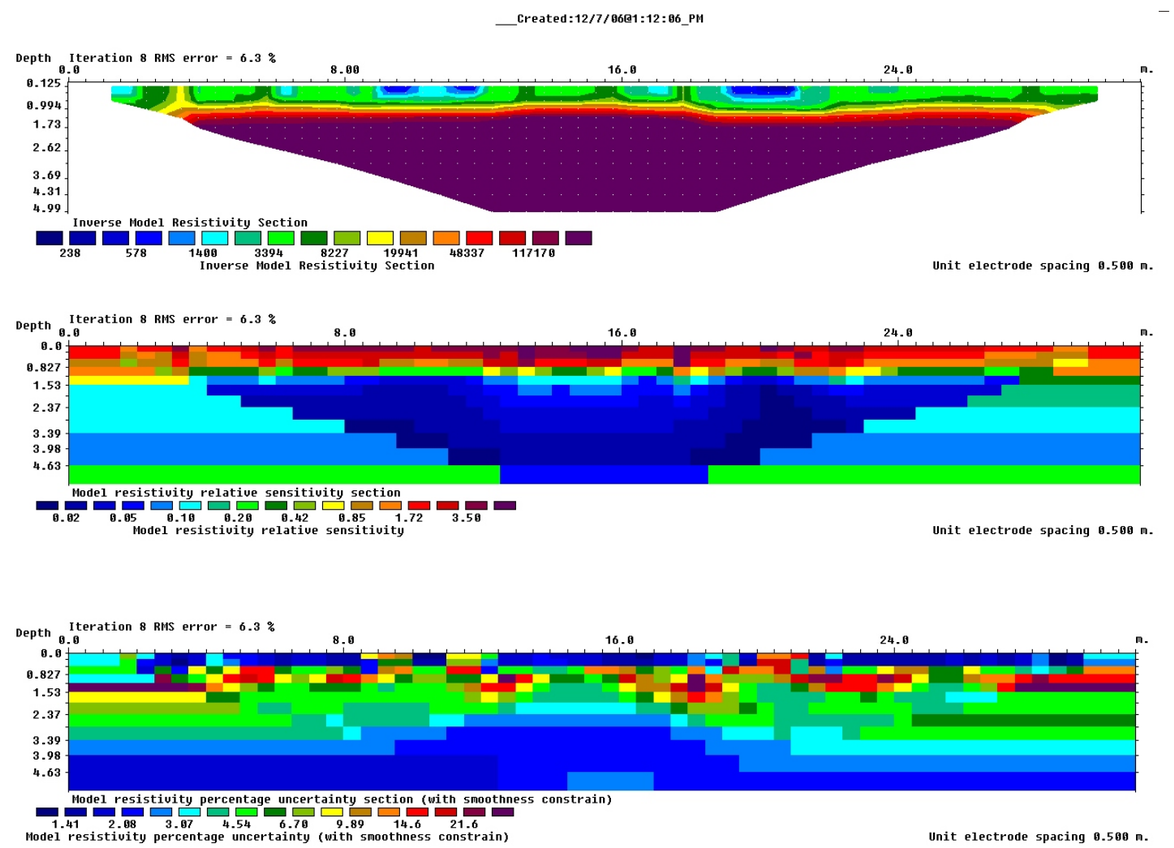

VVP1: Sothern most West to East resistivity line (line 1) with 32 electrodes at 1 m spacing:

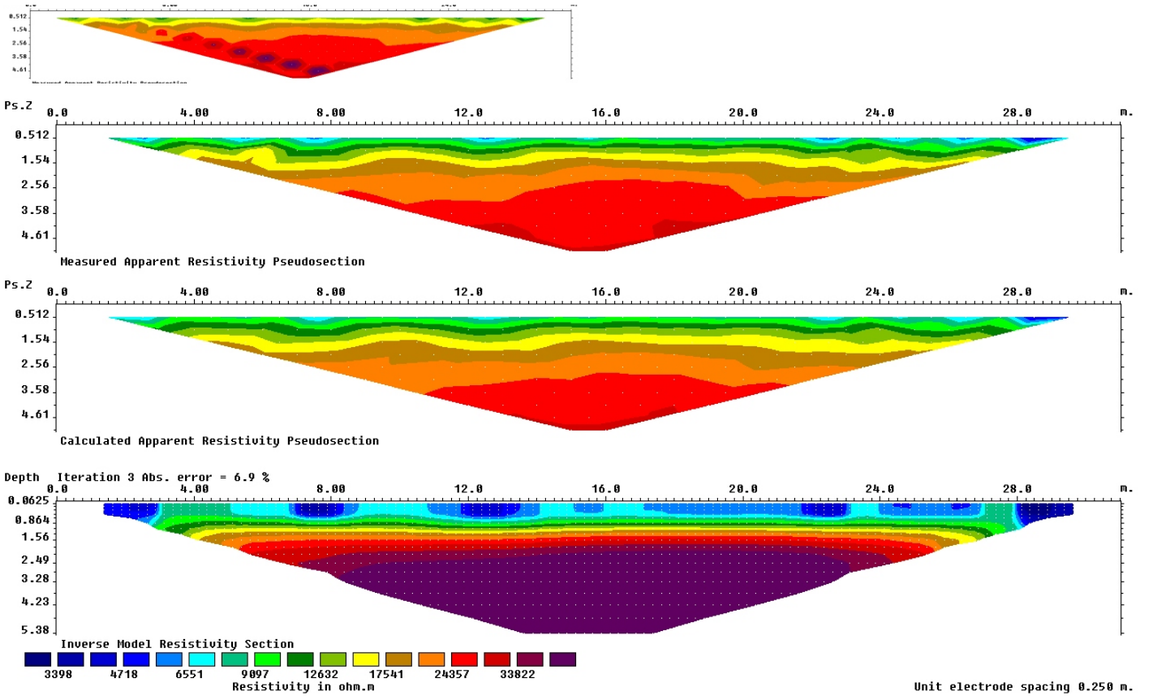

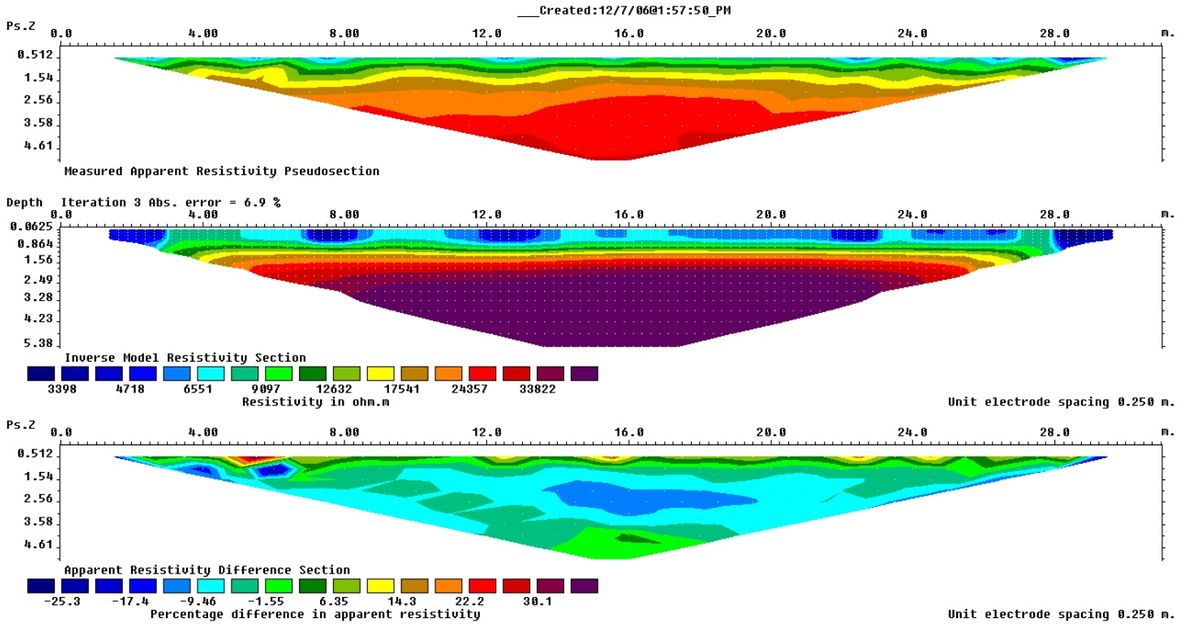

This data did not contain topographic corrections

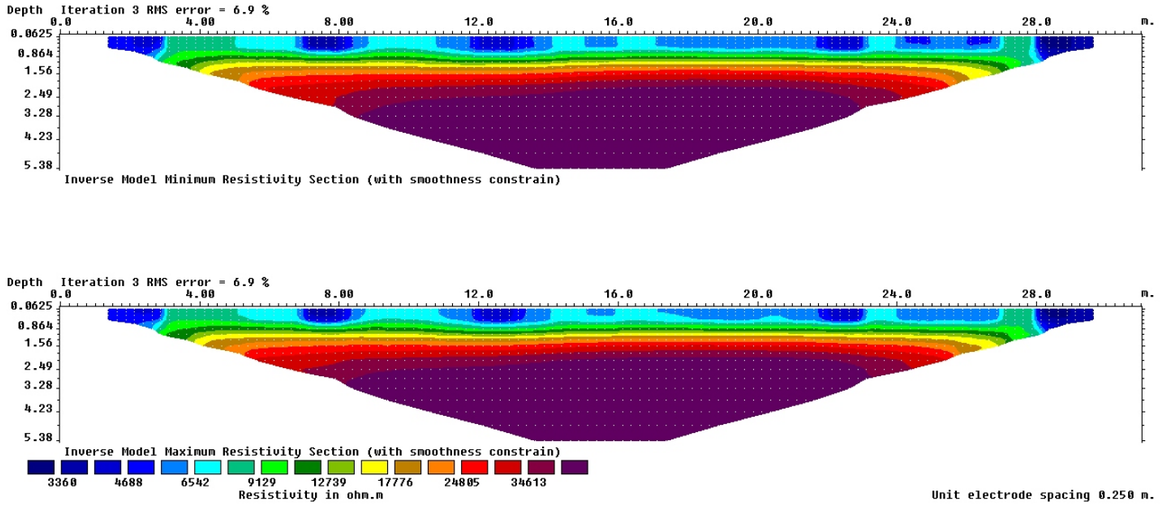

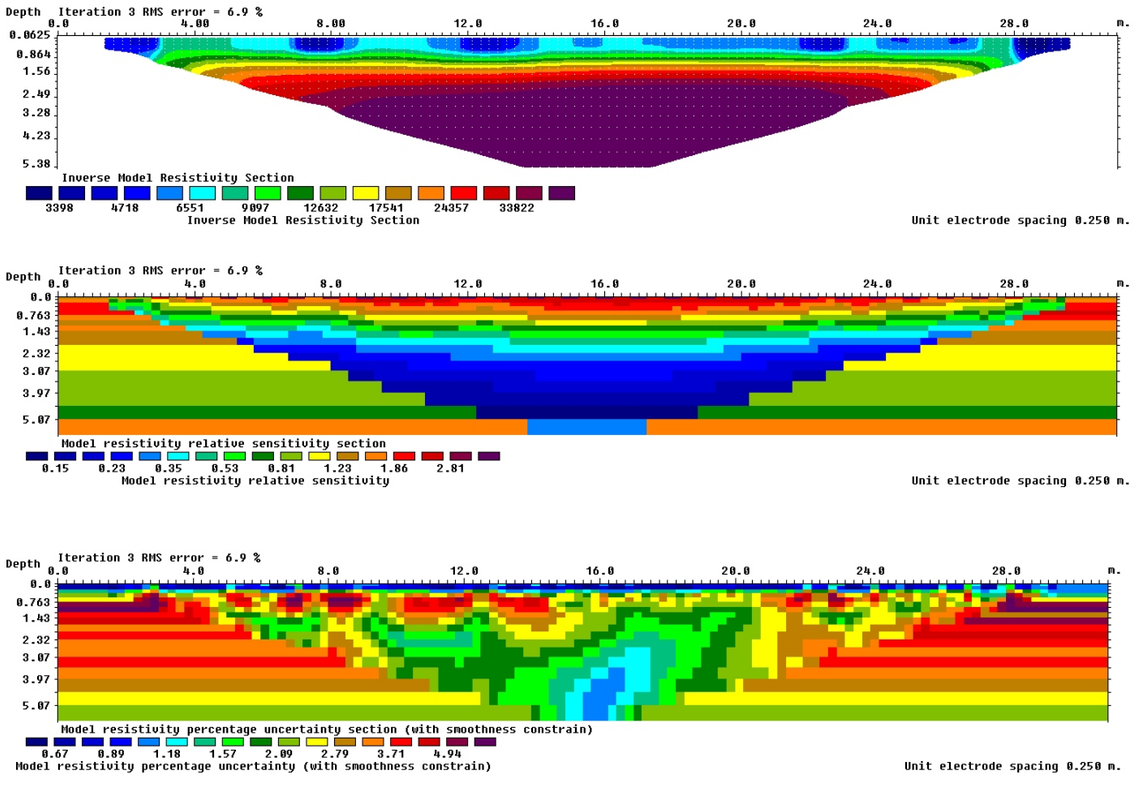

VVP1: Eastern most South to North resistivity line (line 2) with 32 electrodes at 1 m spacing:

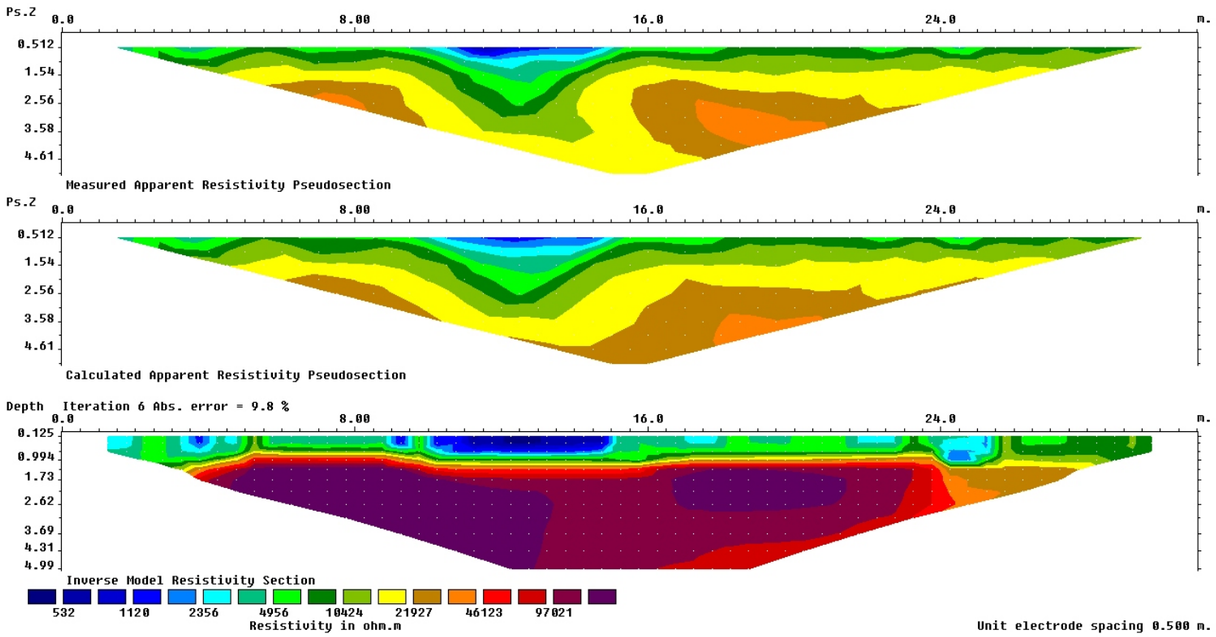

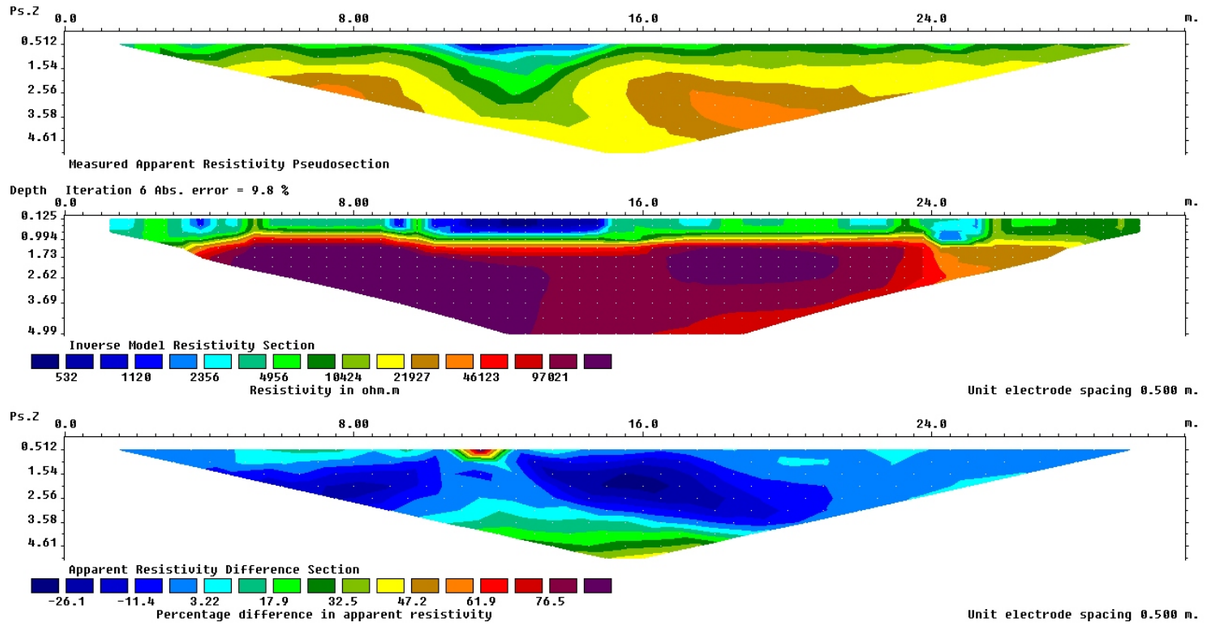

This data did not contain topographic corrections

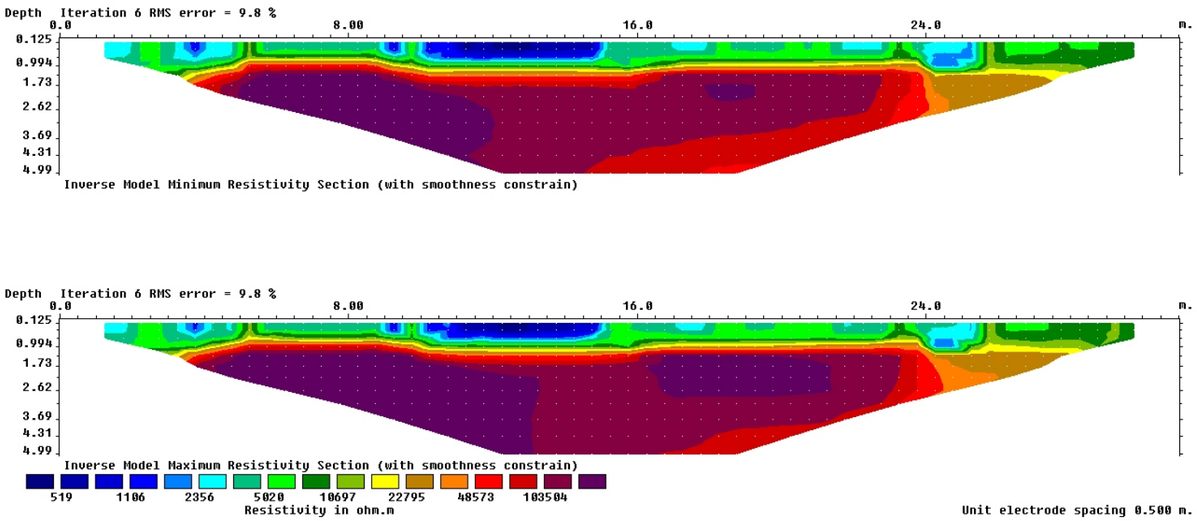

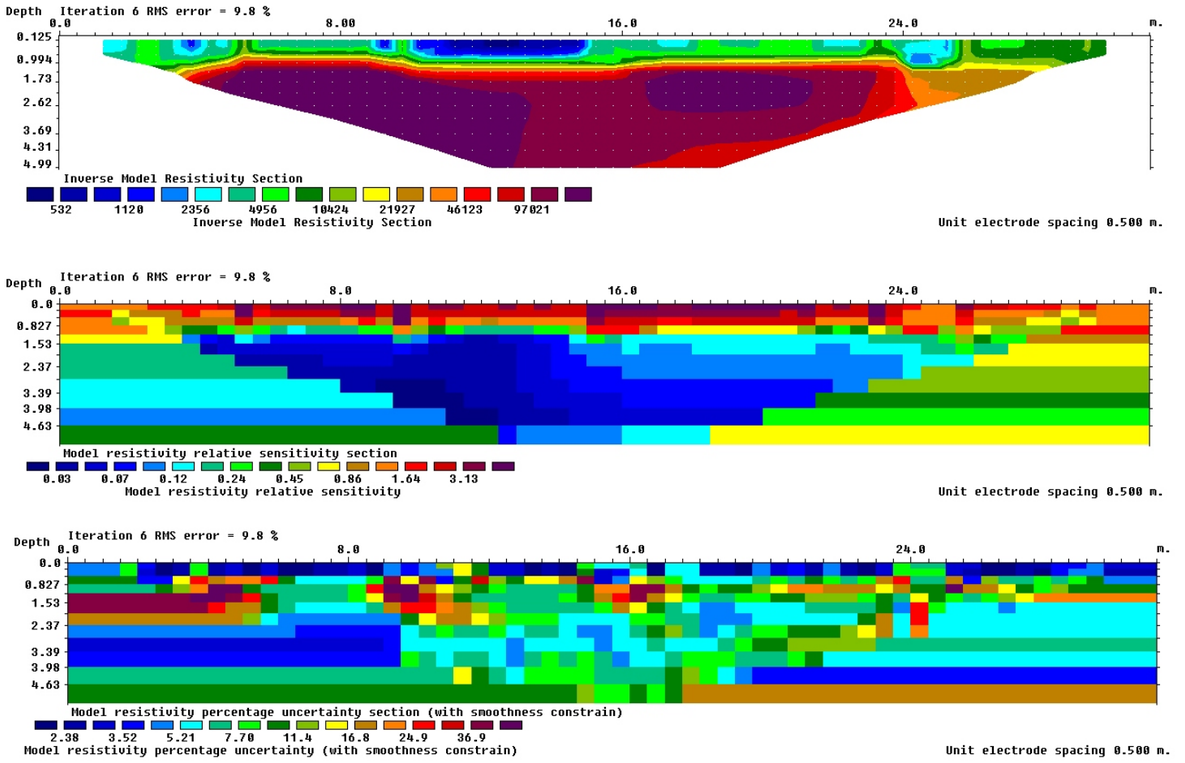

VVP1: Western most South to North resistivity line (line 1) with 32 electrodes at 1 m spacing:

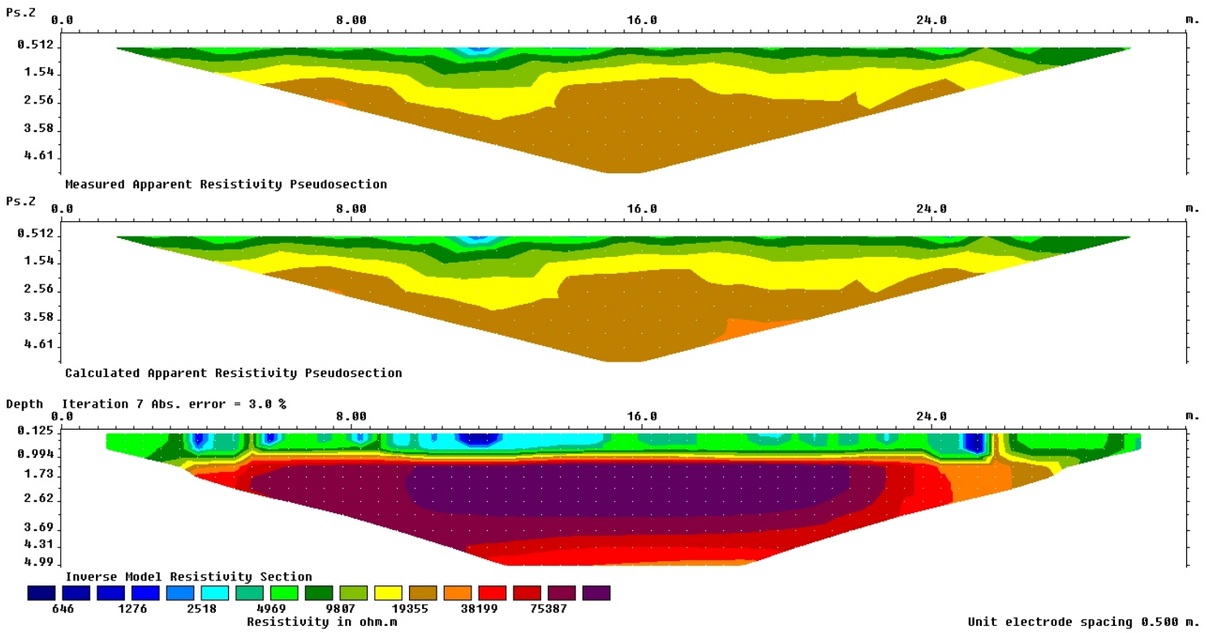

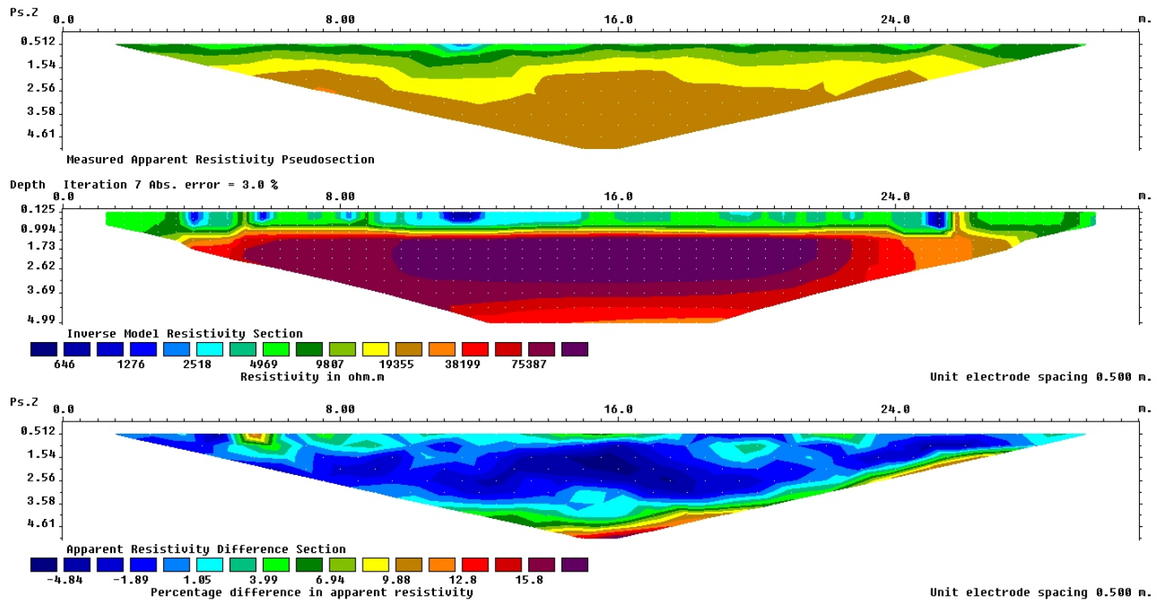

This data did not contain topographic corrections

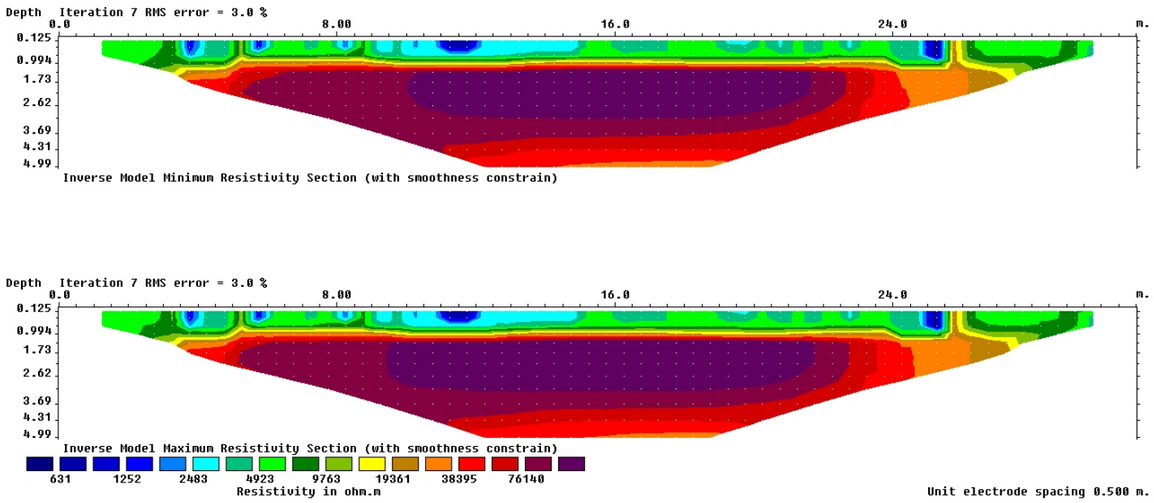

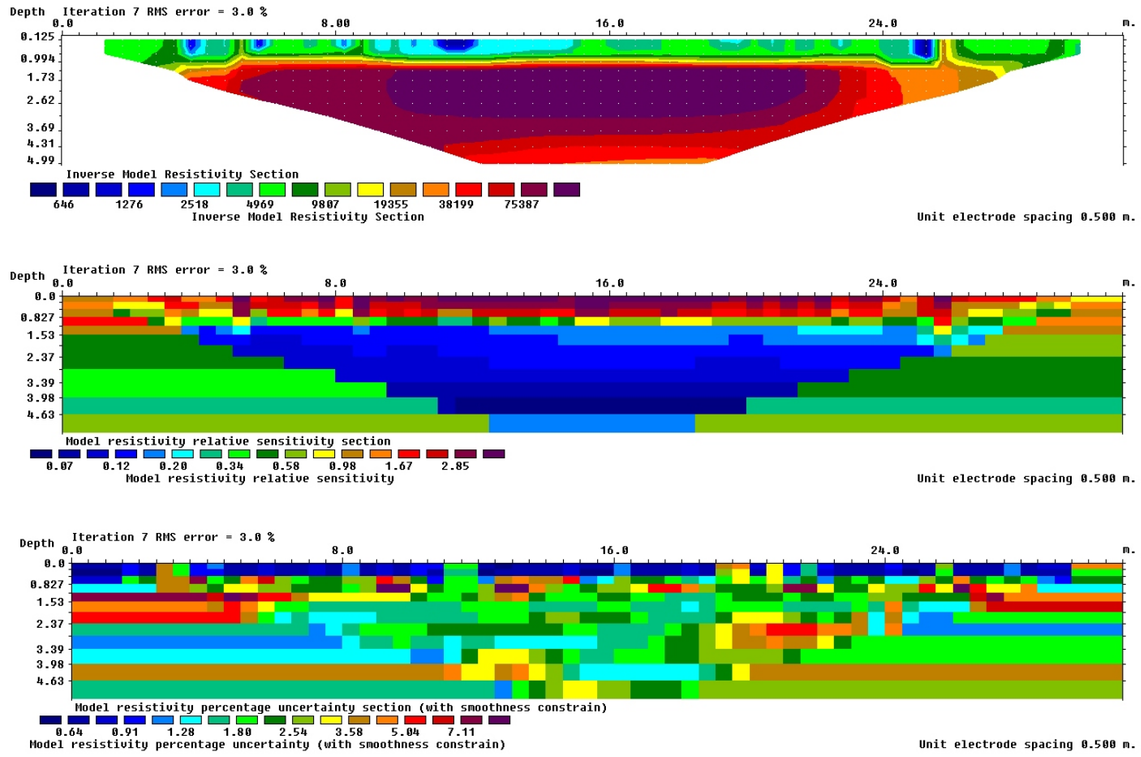

VVP2 South to North resistivity line with 32 electrodes at 1 m spacing (edited data):

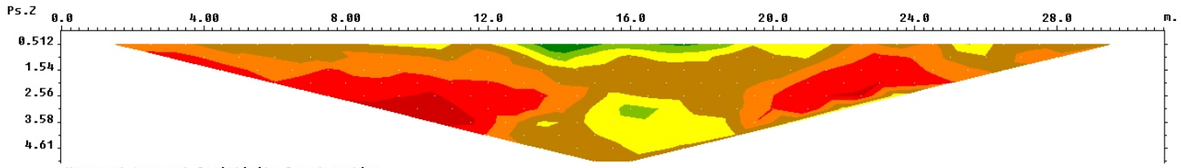

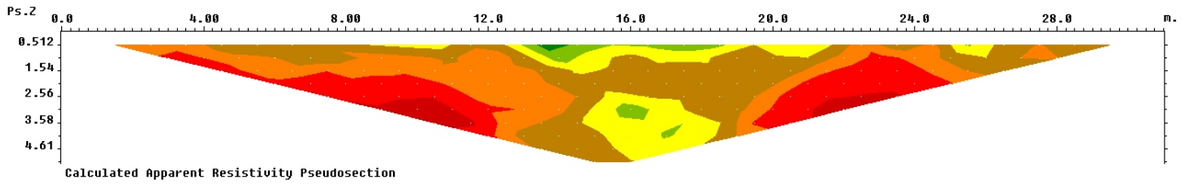

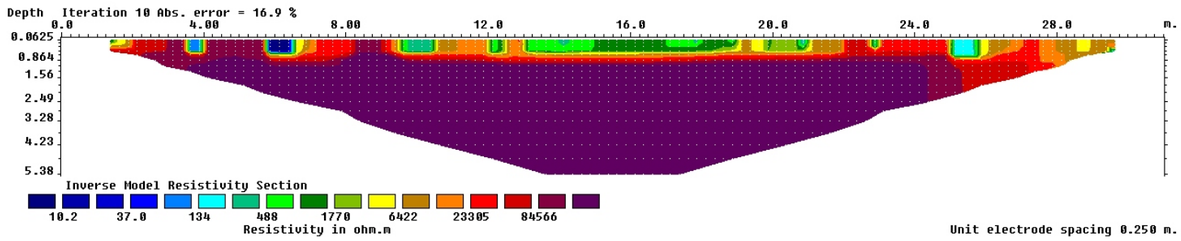

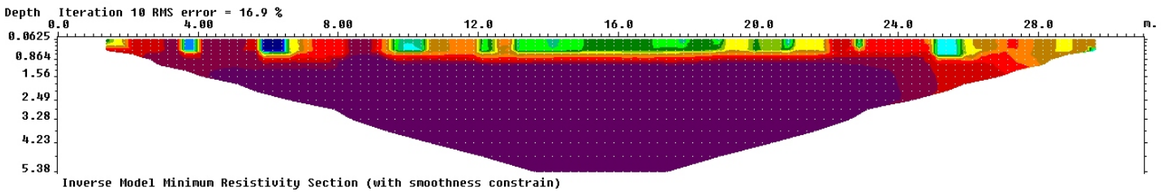

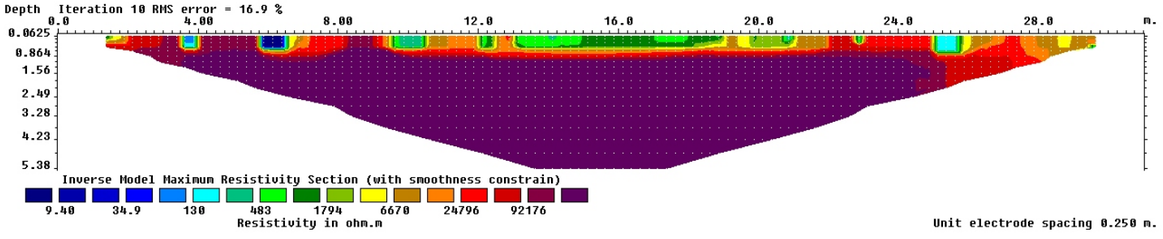

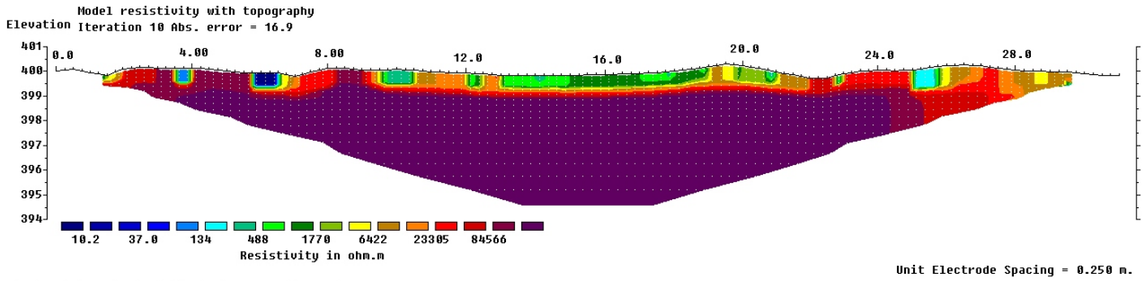

Horizontal scale is 9.67 pixels per unit spacing
Vertical exaggeration in model section display = 0.71
First electrode is located at 0.0 m.
Last electrode is located at 31.0 m.

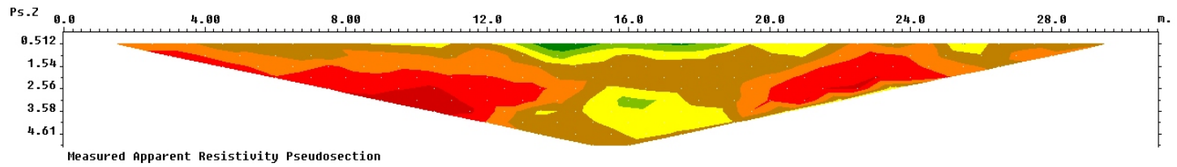

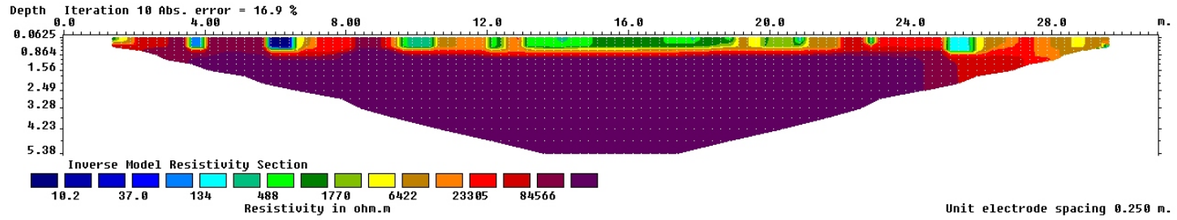

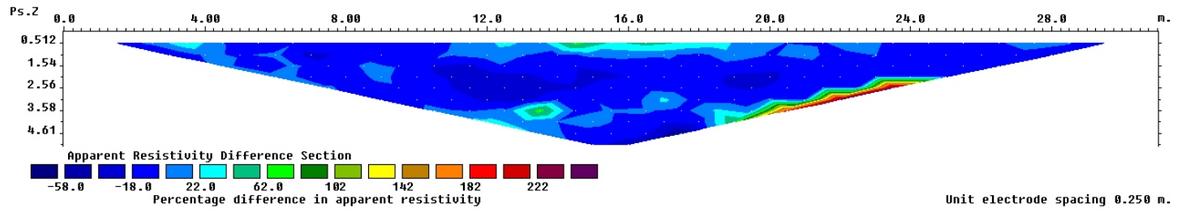

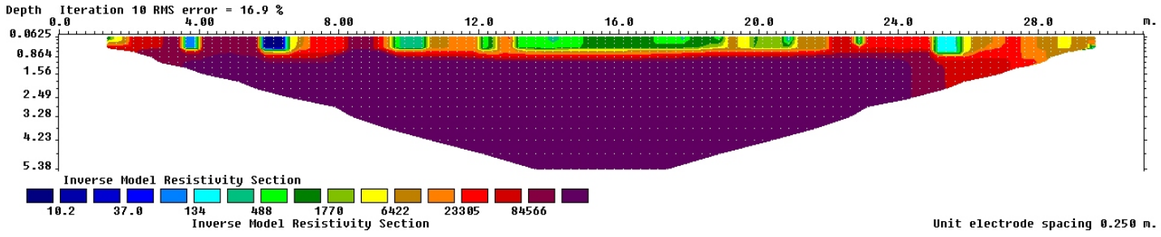

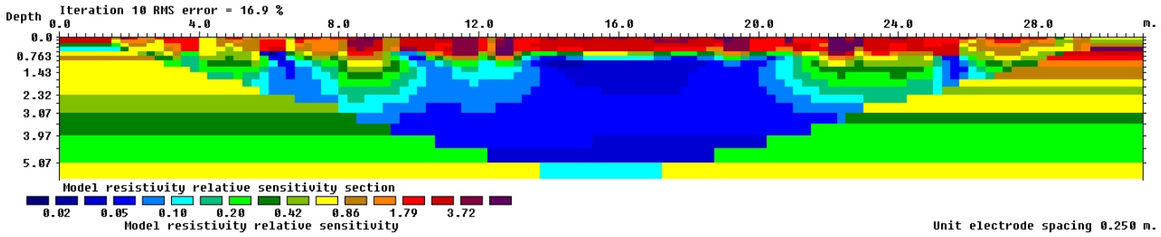

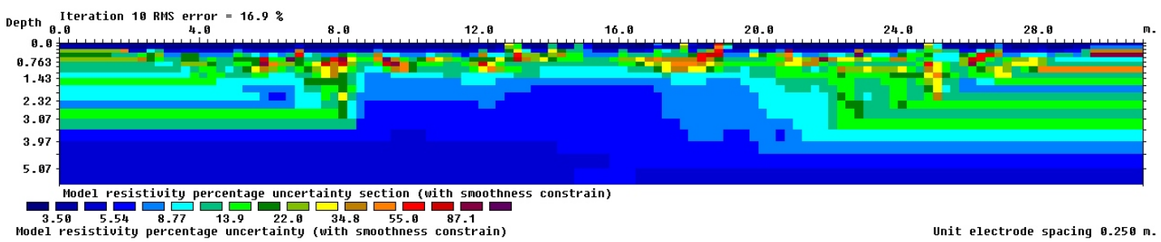

VVP2 West to East resistivity line 1 with 32 electrodes at 0.5 m spacing (Southern) :

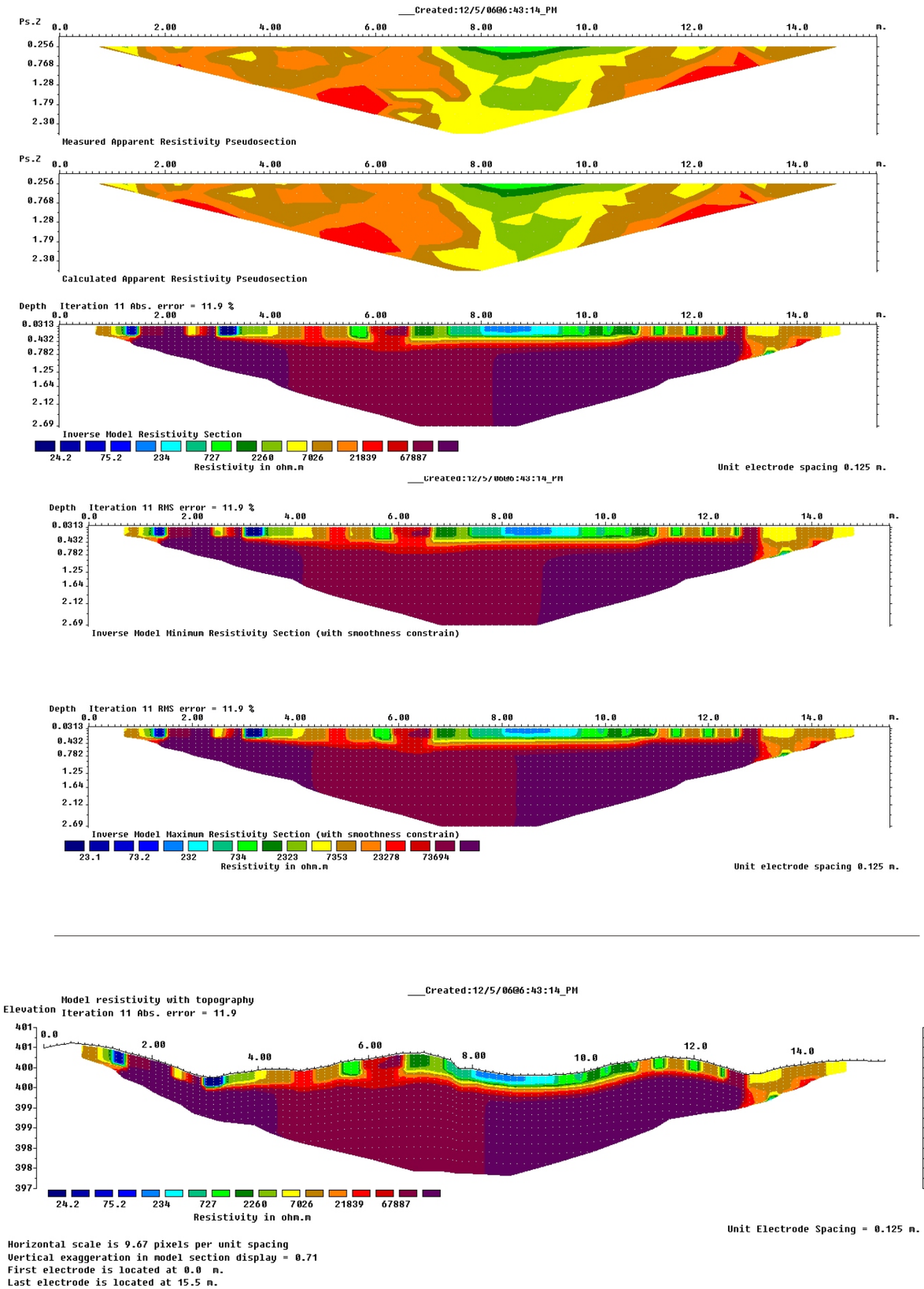

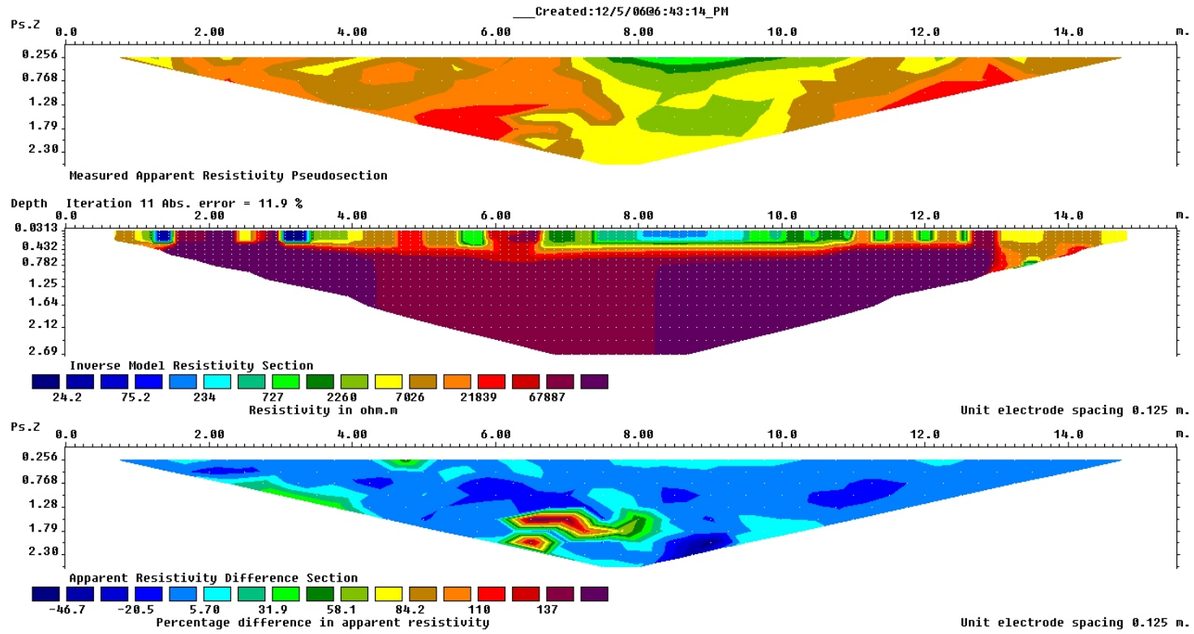

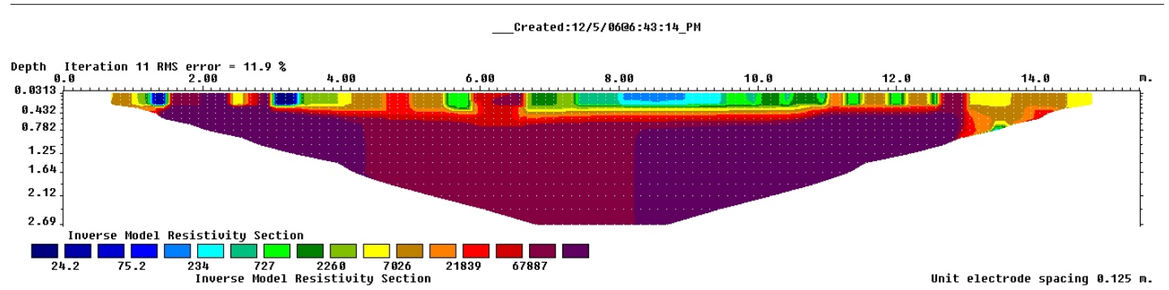

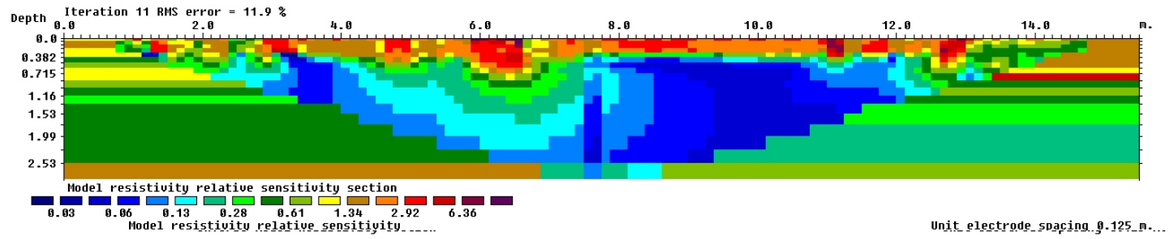

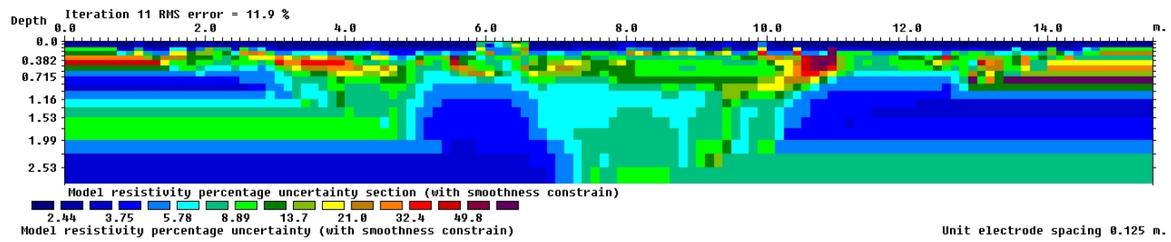

VVP2 West to East resistivity line 2 with 32 electrodes at 0.5 m spacing (Northern) :

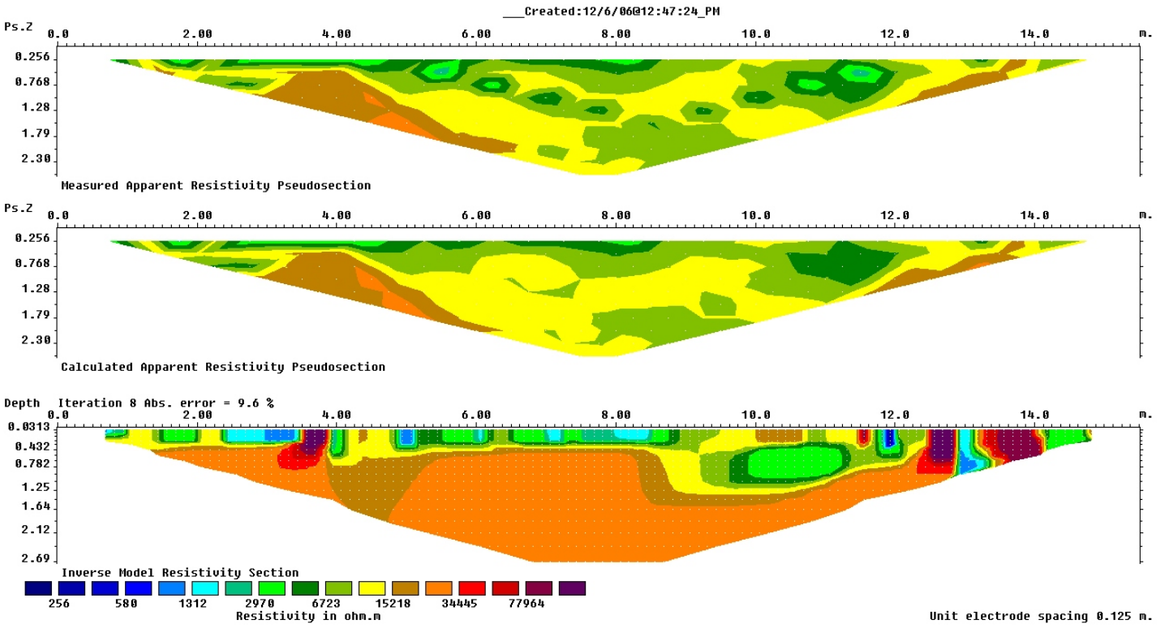

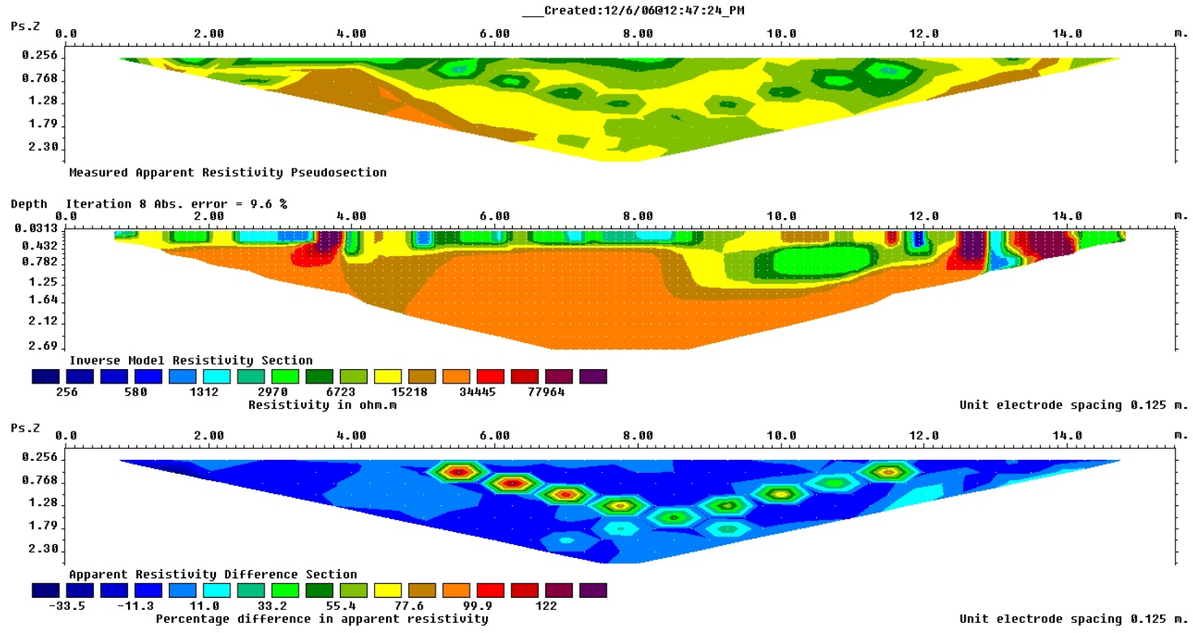

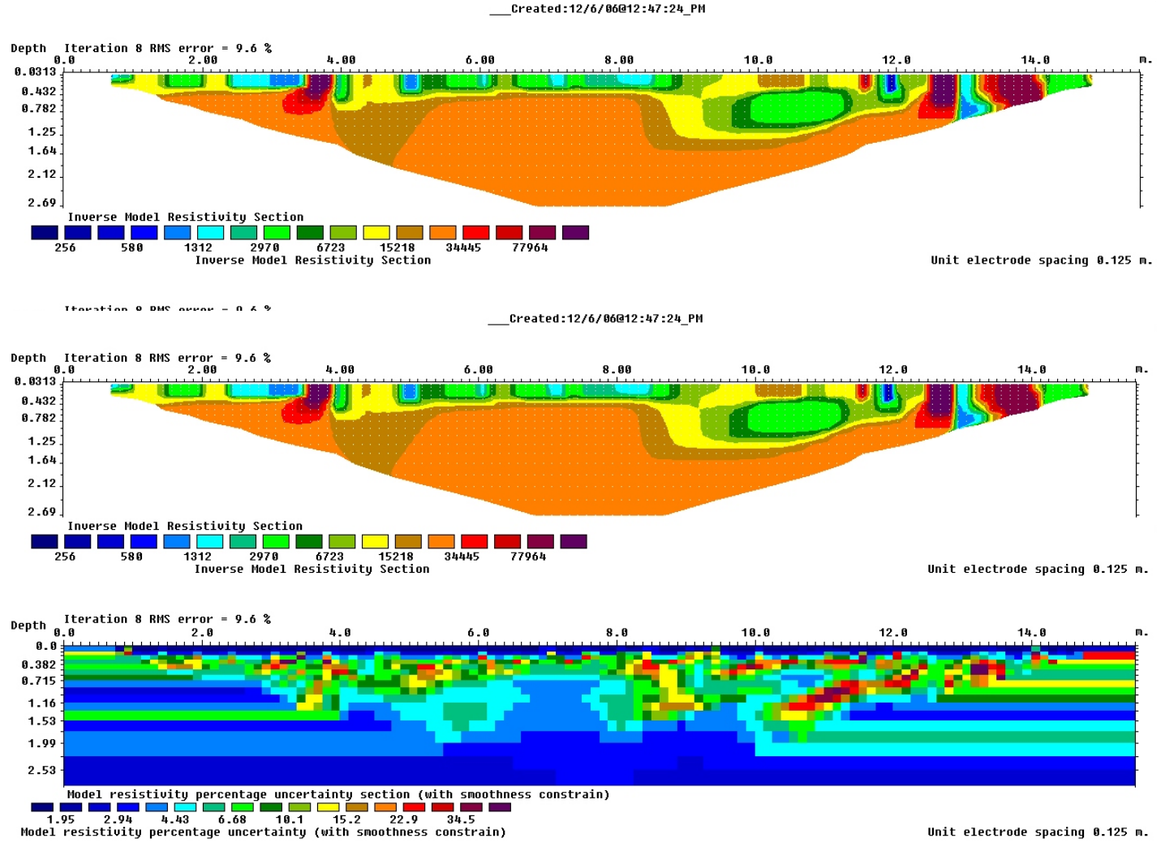

BVP1 South to North resistivity line with 64 electrodes at 0.5 m spacing.

Inversion:

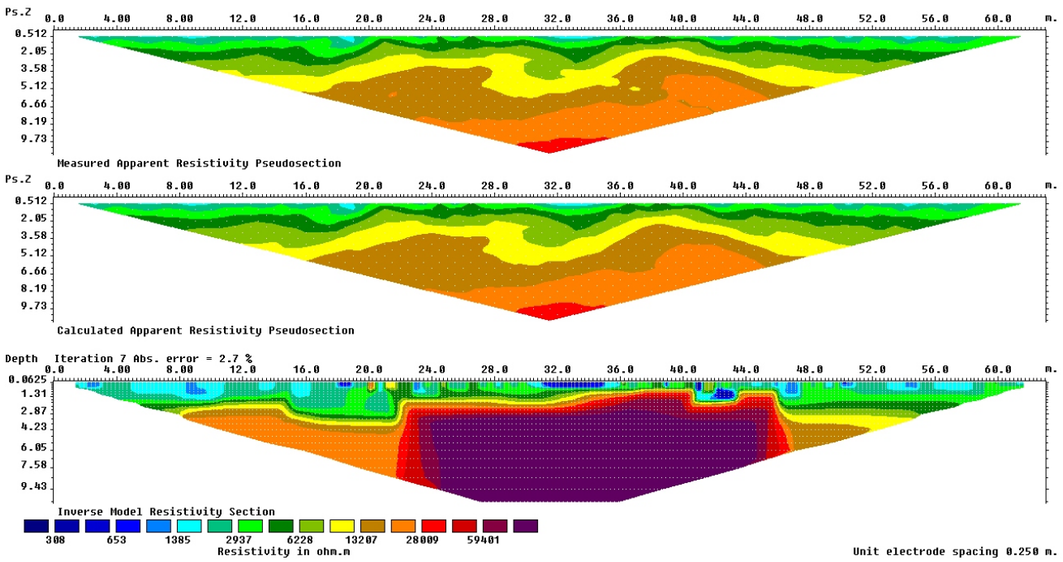

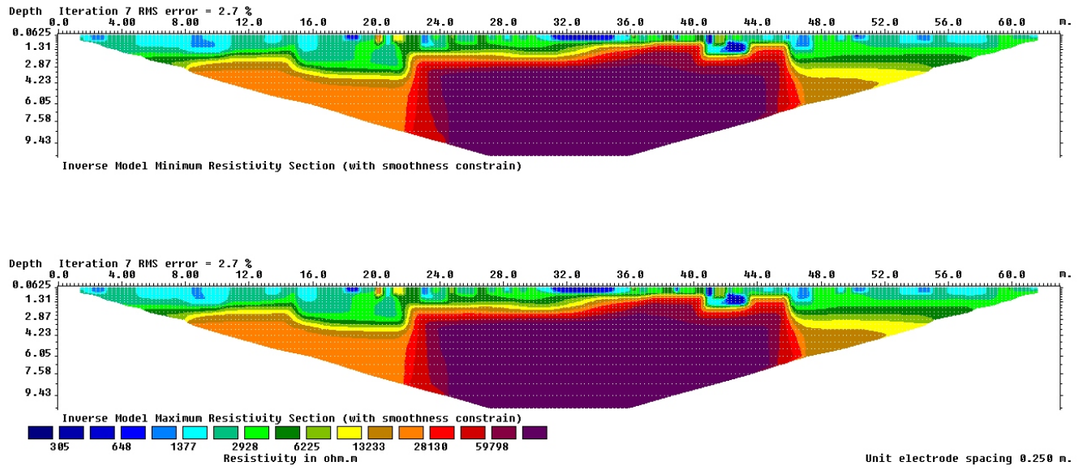

Topography:

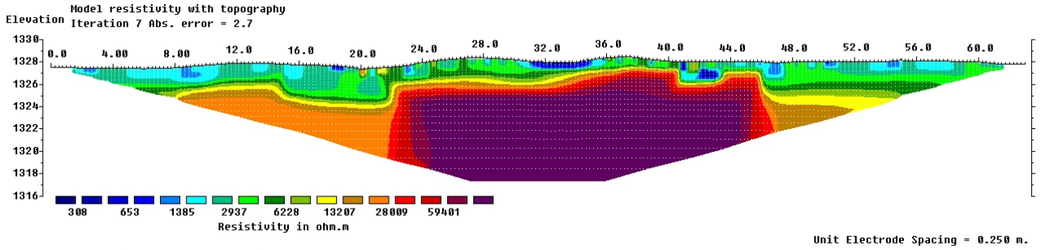

Horizontal scale is 4.76 pixels per unit spacing
Vertical exaggeration in model section display = 0.72
First electrode is located at 0.0 m.
Last electrode is located at 63.0 m.

Apparent resistivity psuedosections:

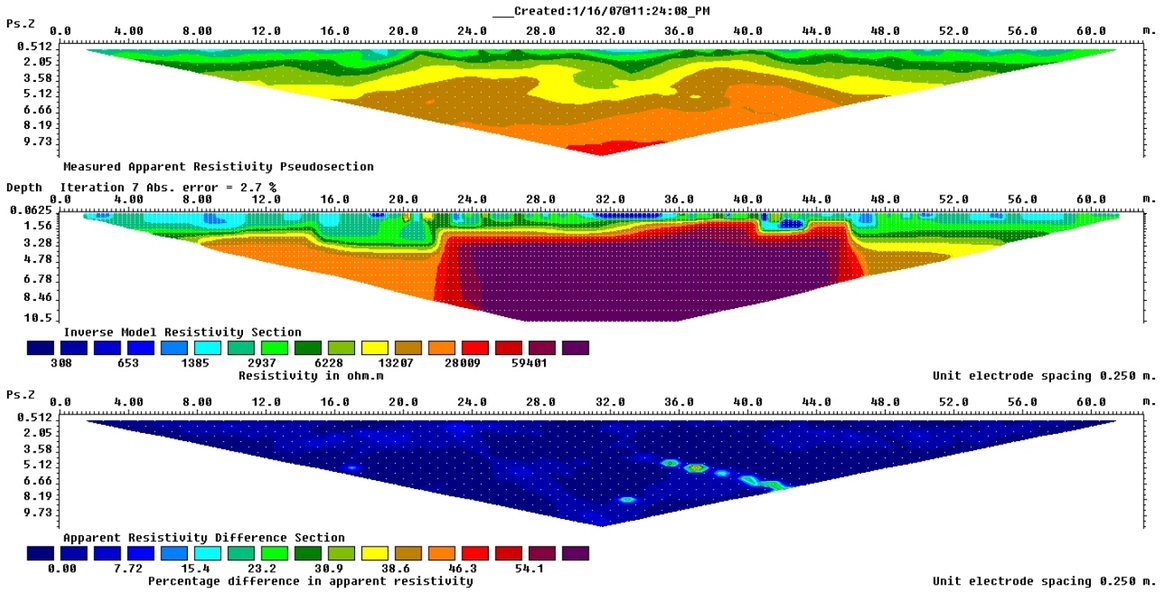

Block analysis:

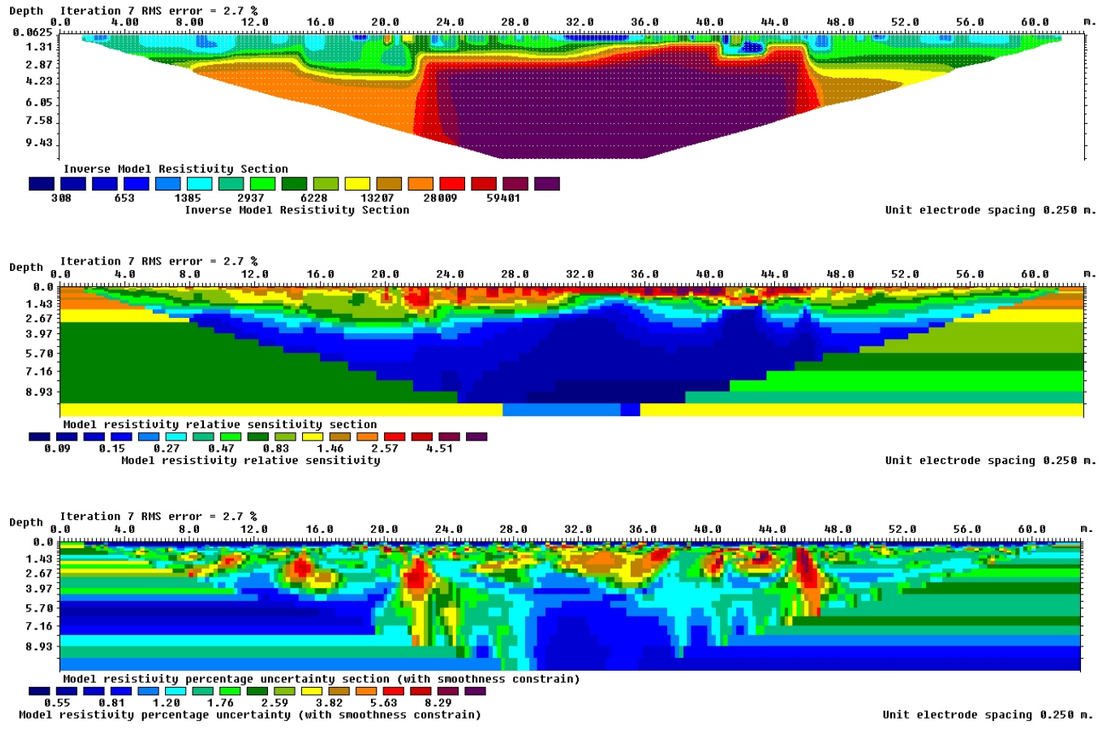

BVP1 South to North resistivity line with 32 electrodes at 1 m spacing.

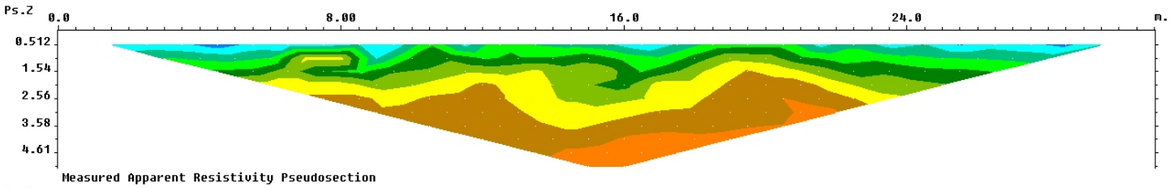

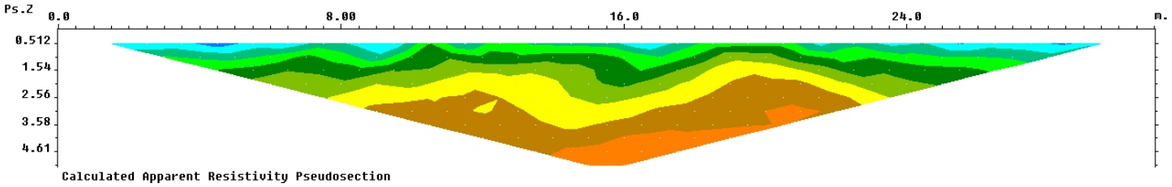

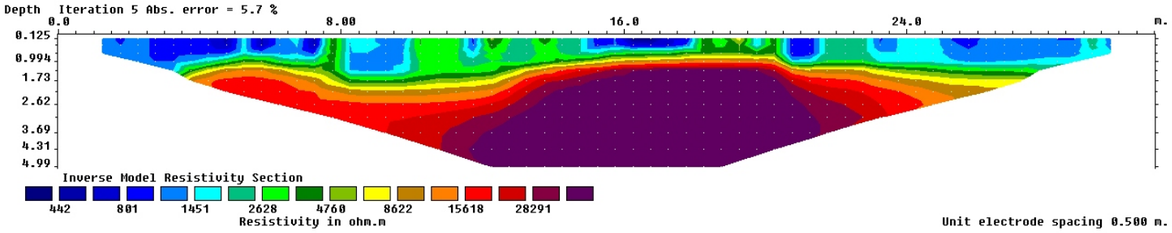

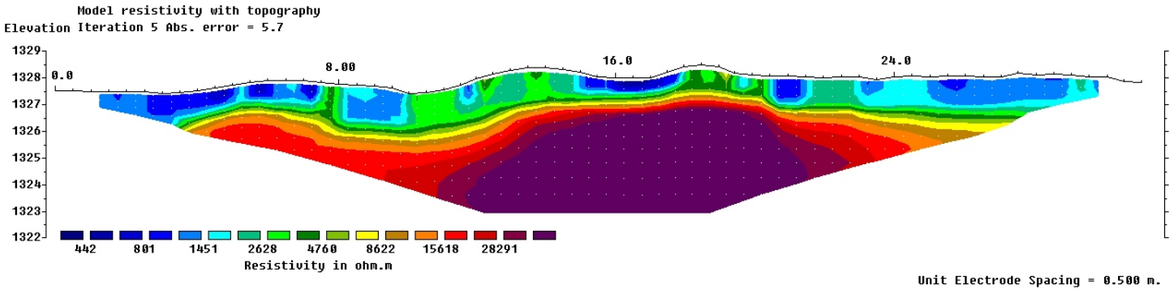

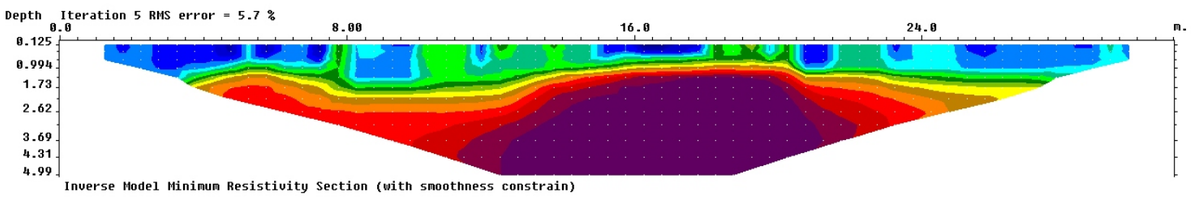

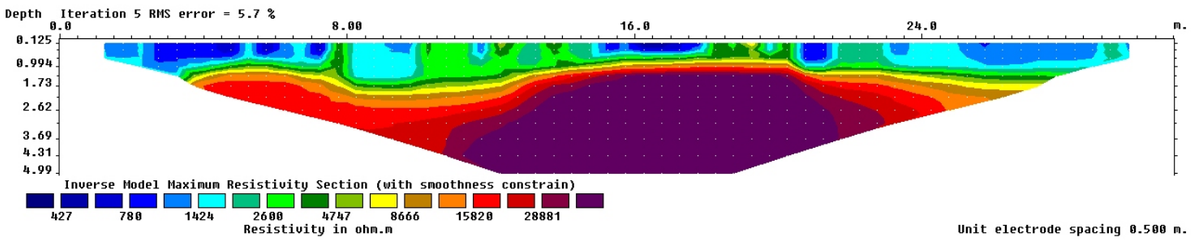

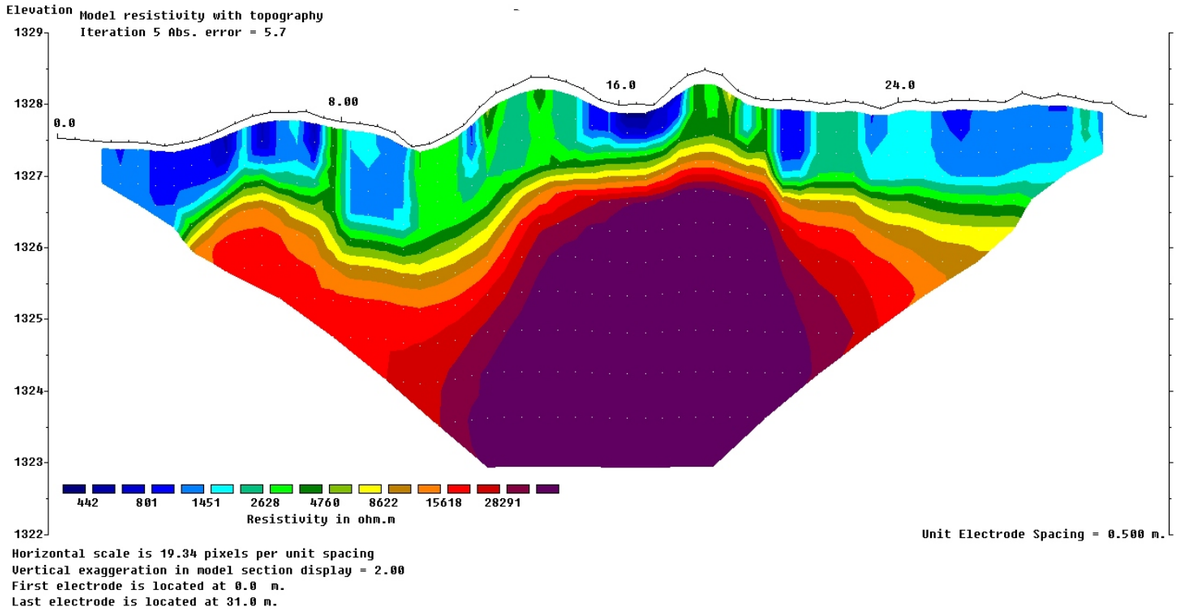

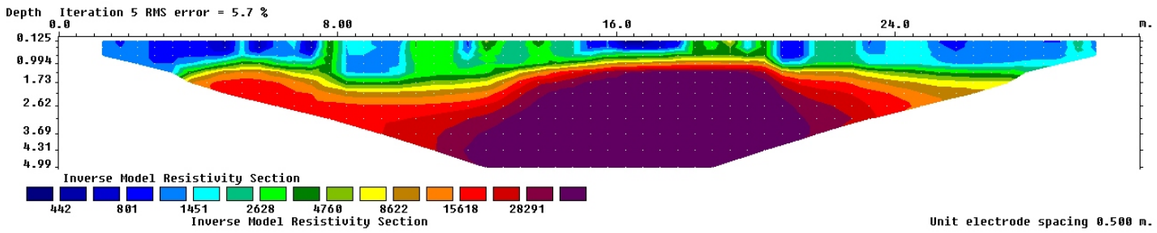

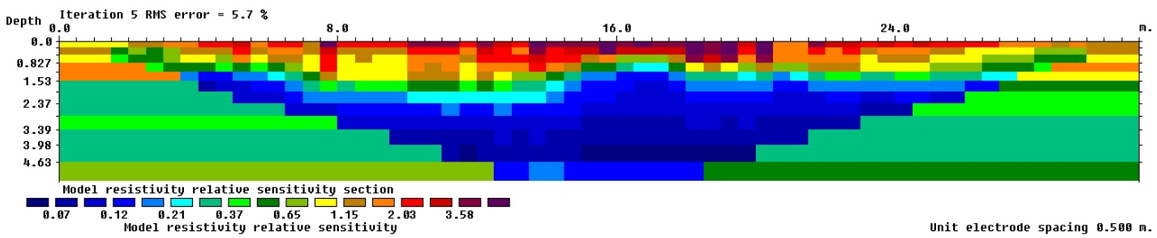

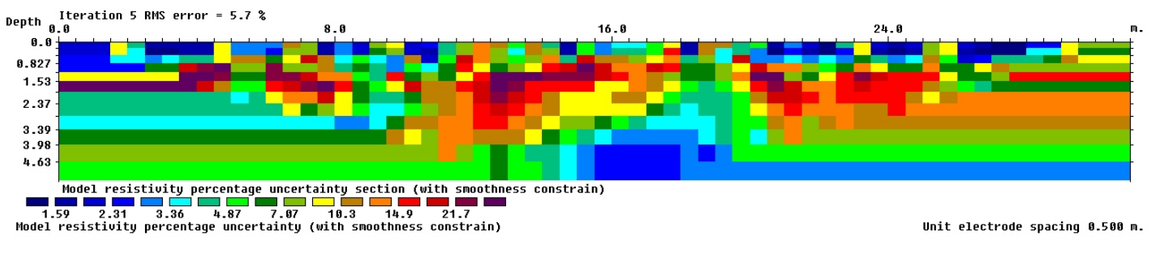

BVP1 West to East resistivity line with 64 electrodes at 0.5 m spacing.

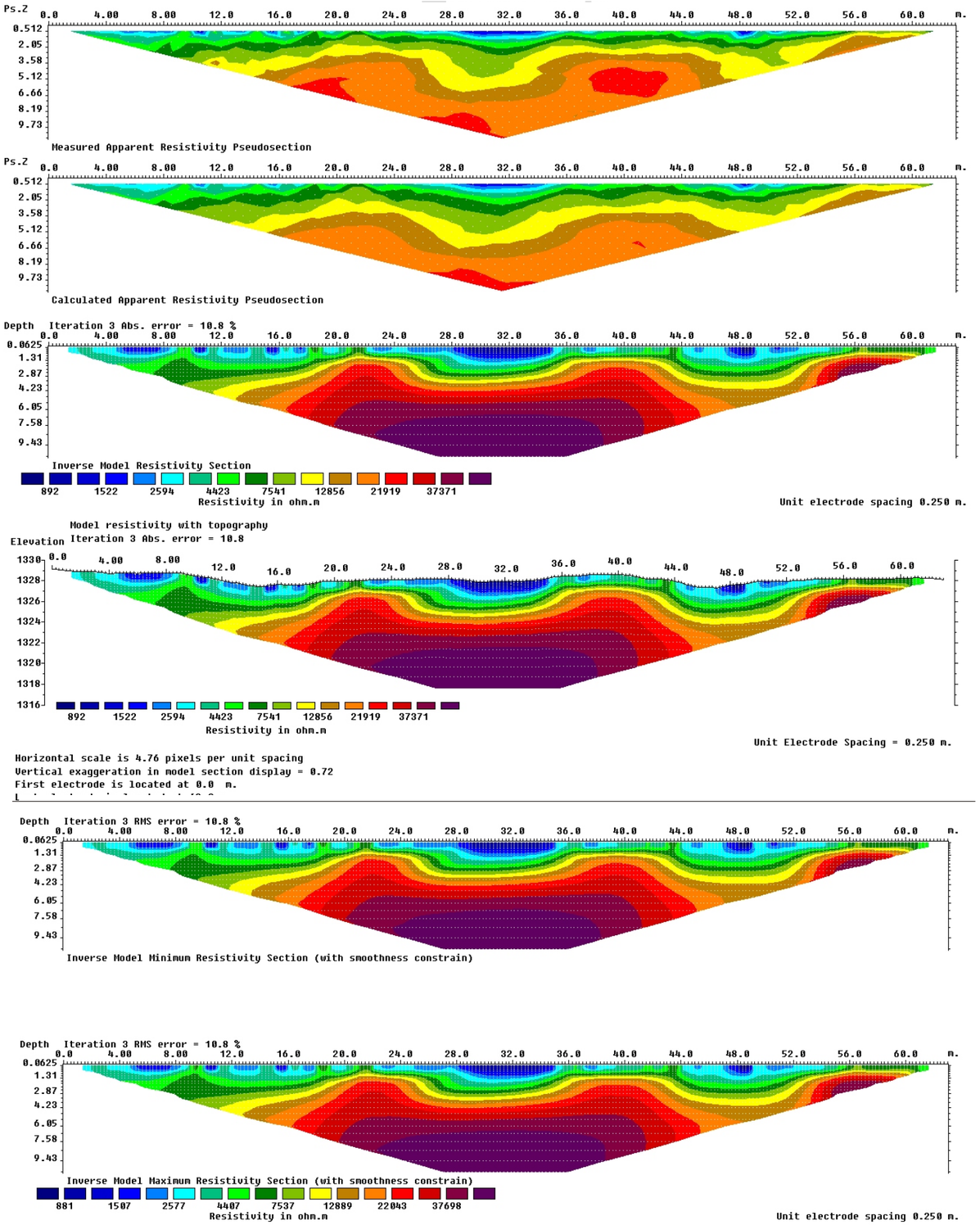

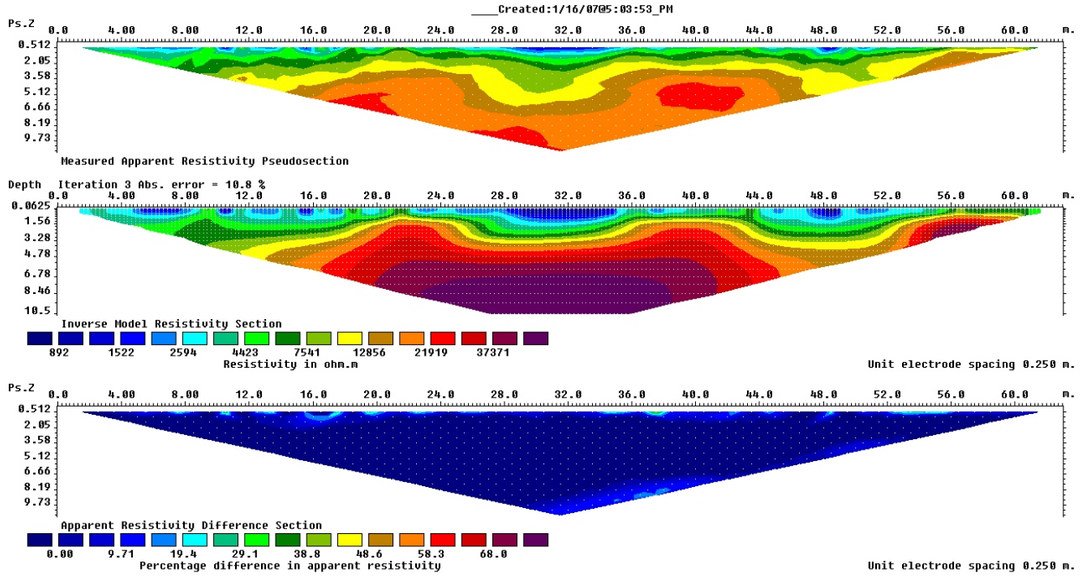

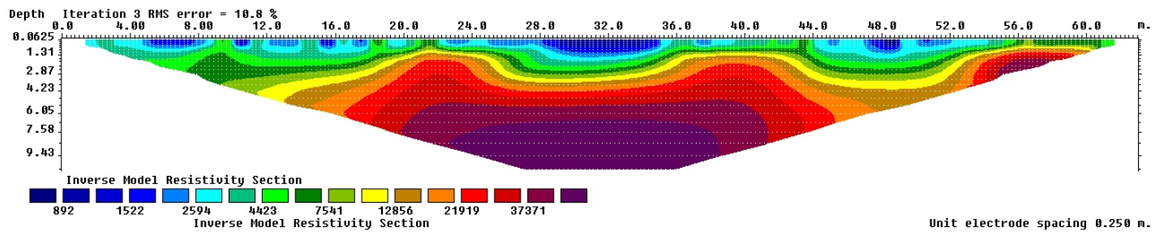

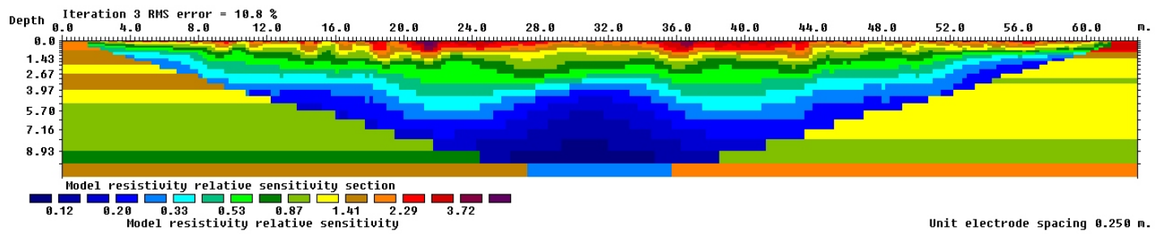

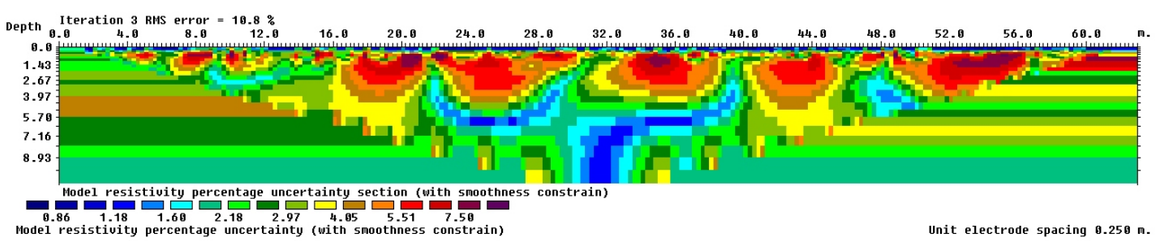

BVP1 West to East resistivity line with 32 electrodes at 1 m spacing.

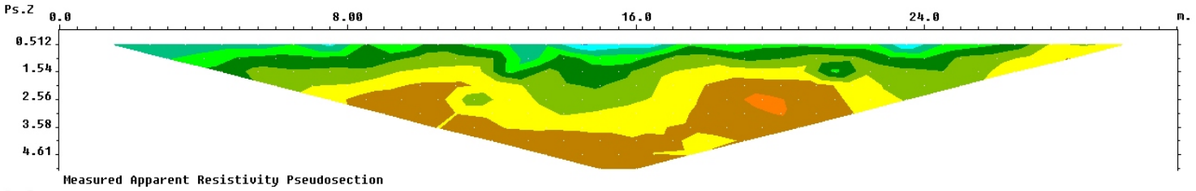

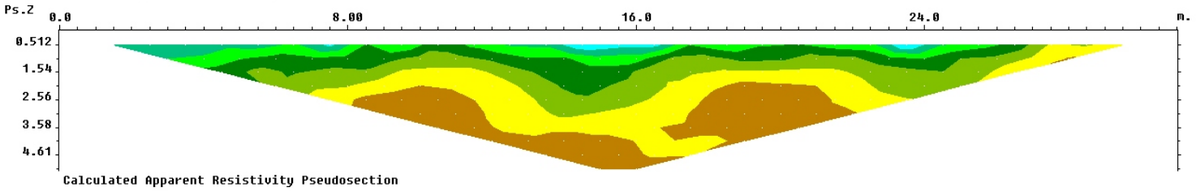

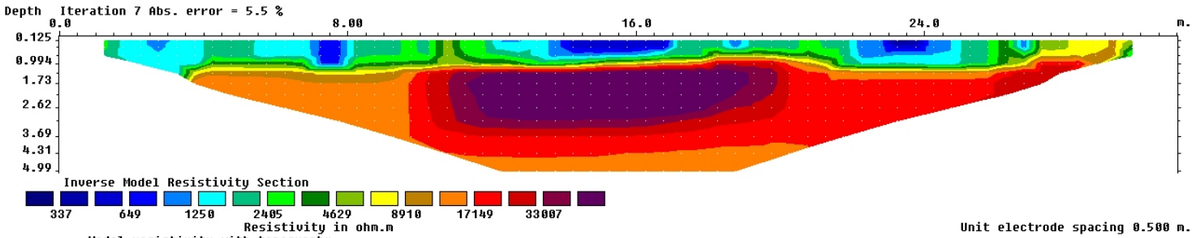

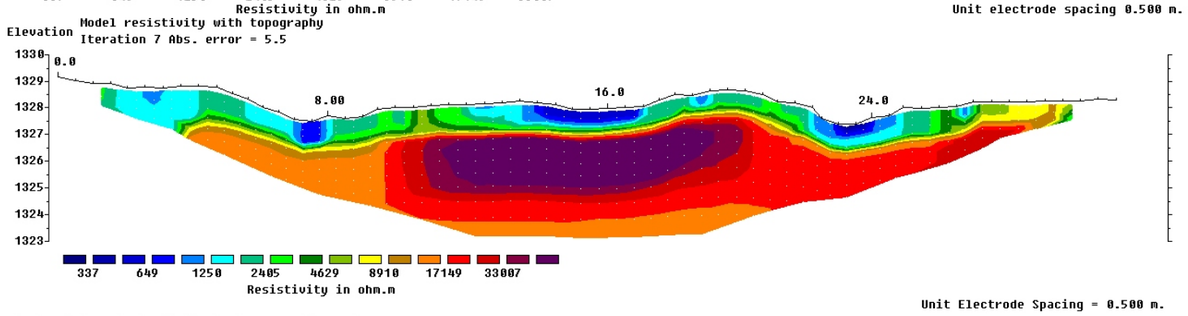

Horizontal scale is 19.34 pixels per unit spacing
Vertical exaggeration in model section display = 0.75
First electrode is located at 0.0 m.
Last electrode is located at 31.0 m.

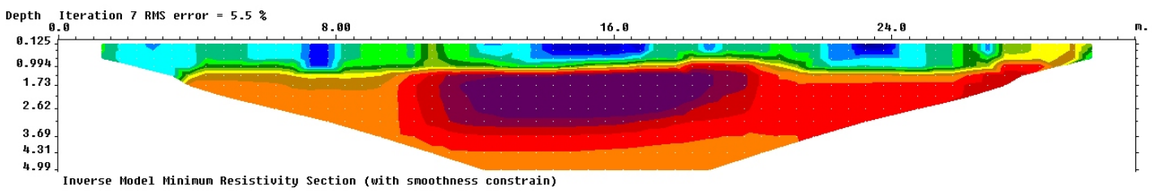

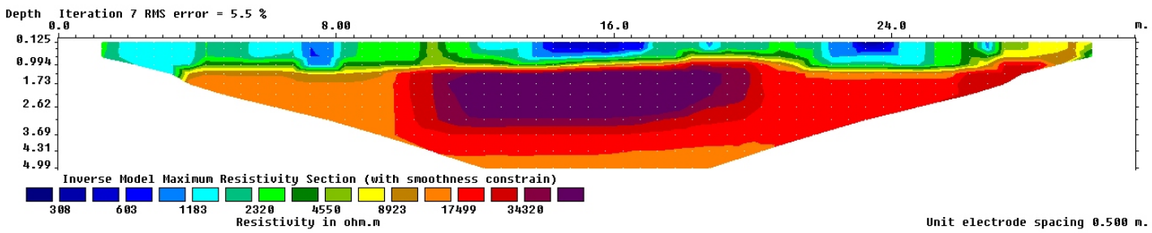

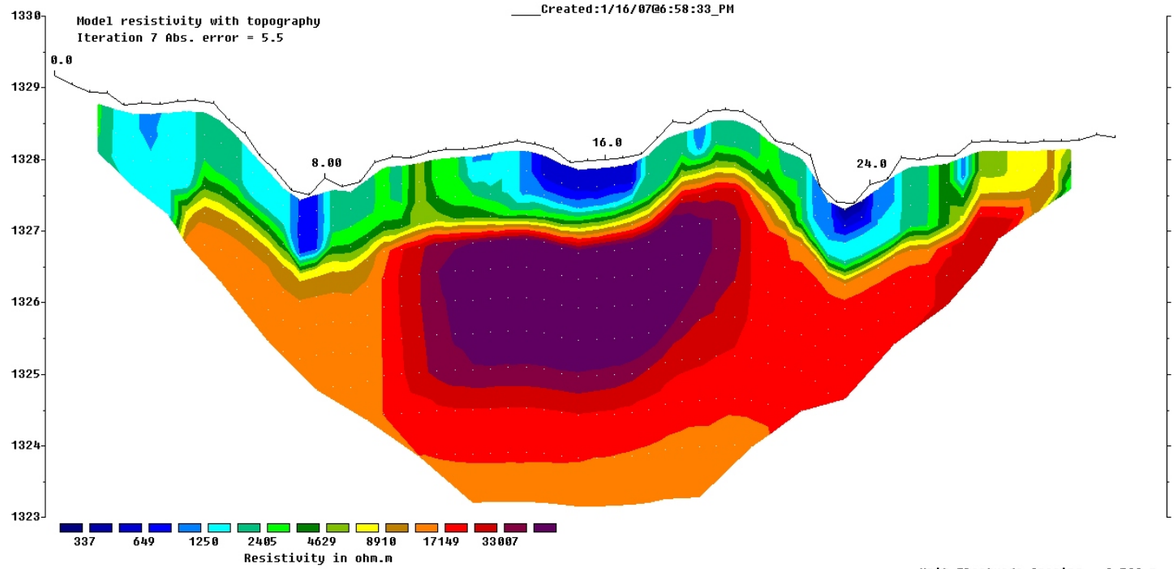

Horizontal scale is 19.34 pixels per unit spacing
Vertical exaggeration in model section display = 2.00
First electrode is located at 0.0 m.
Last electrode is located at 31.0 m.

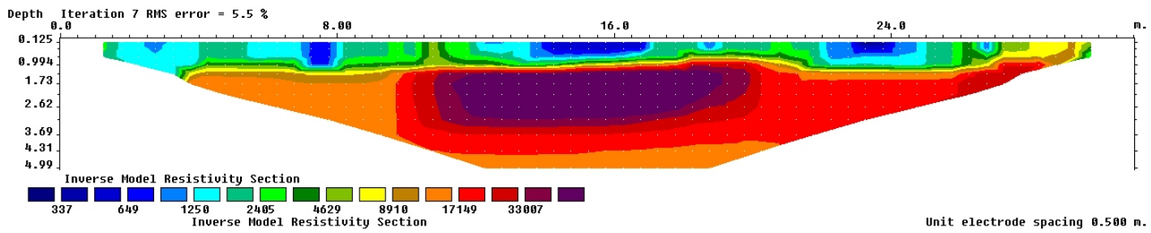

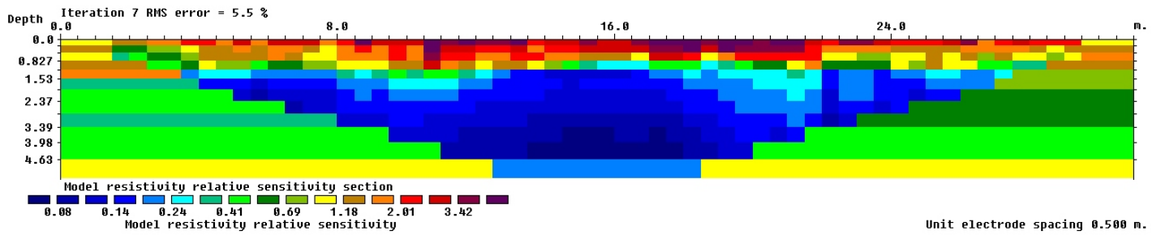

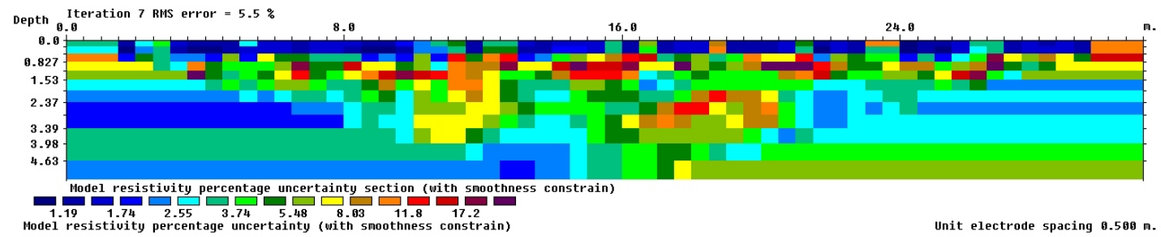

BVP2 South to North resistivity line with 64 electrodes at 0.5m spacing:

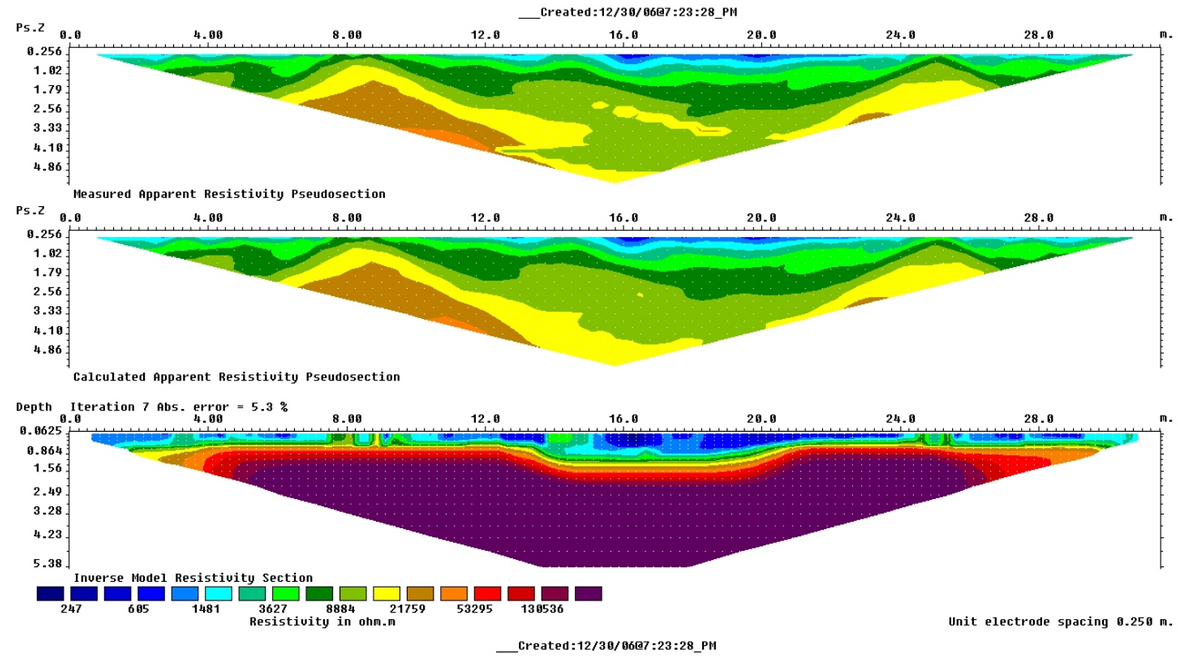

Horizontal scale is 9.52 pixels per unit spacing
Vertical exaggeration in model section display = 0.72
First electrode is located at 0.0 m.
Last electrode is located at 31.5 m.

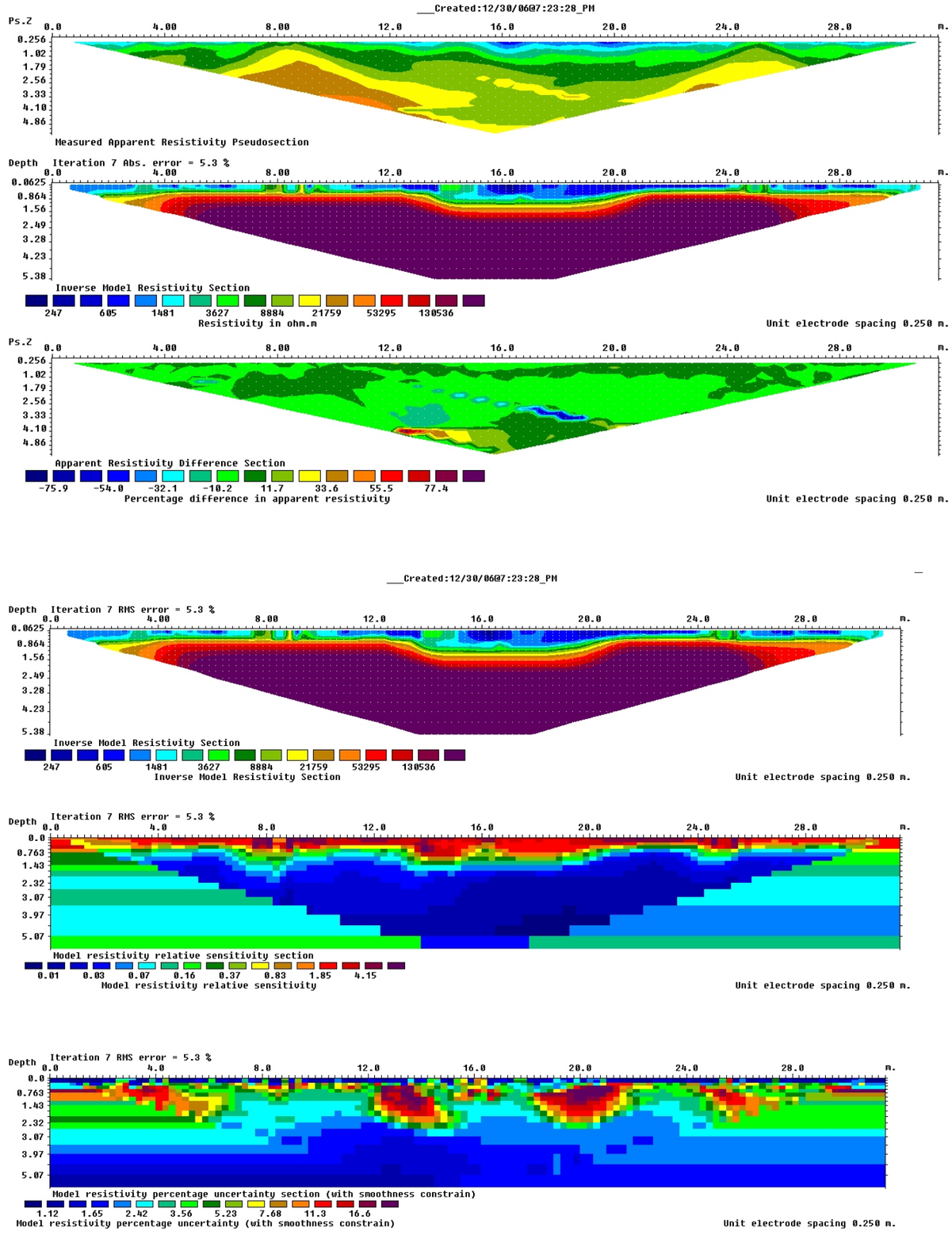

BVP2 South to North resistivity line with 32 electrodes at 1 m spacing:

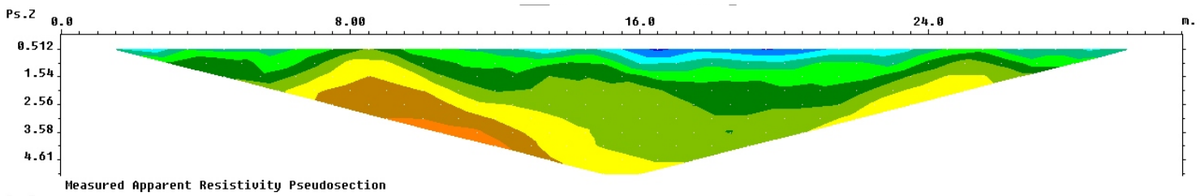

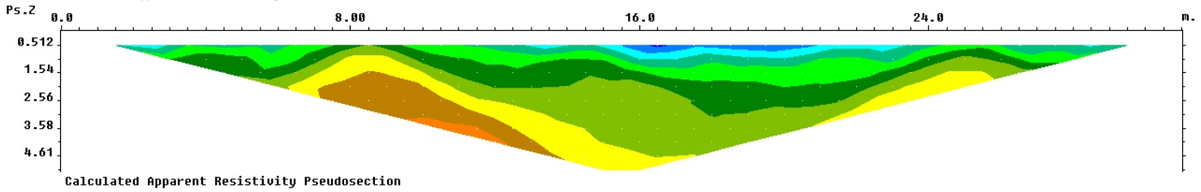

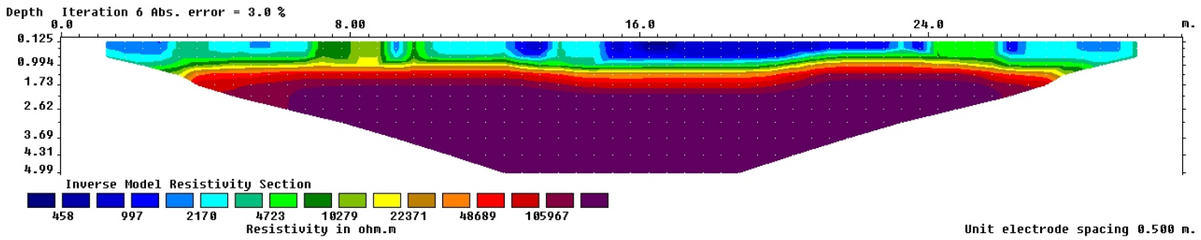

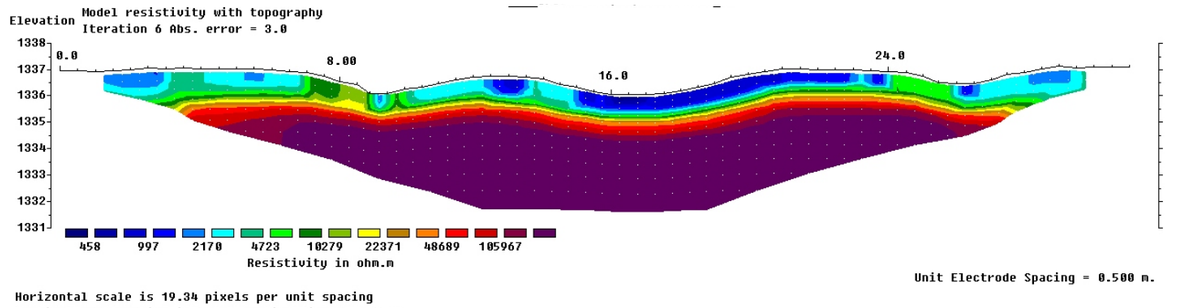

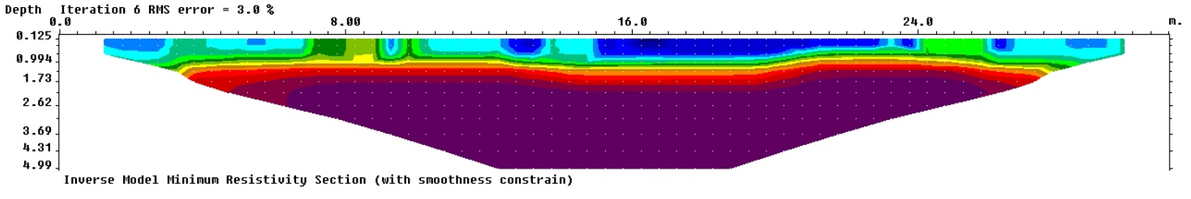

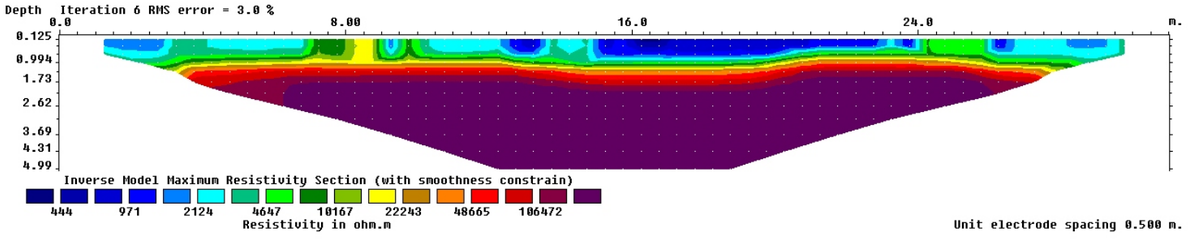

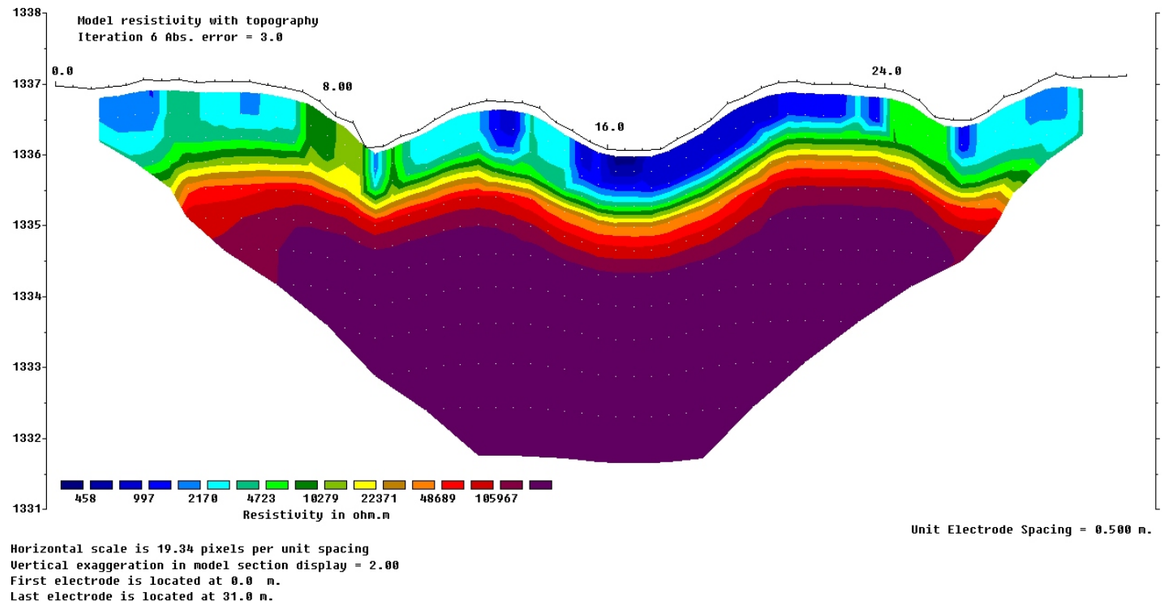

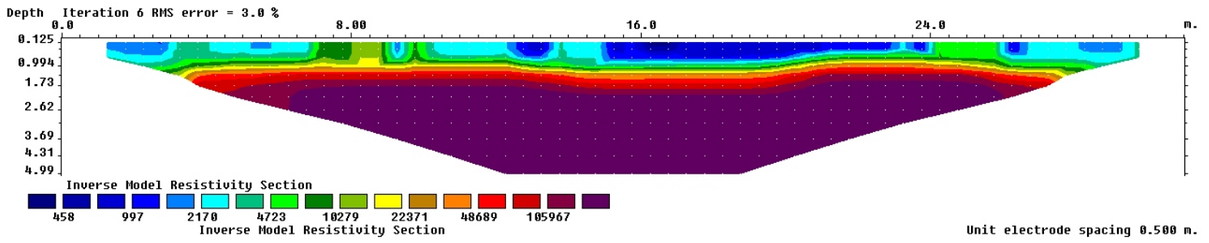

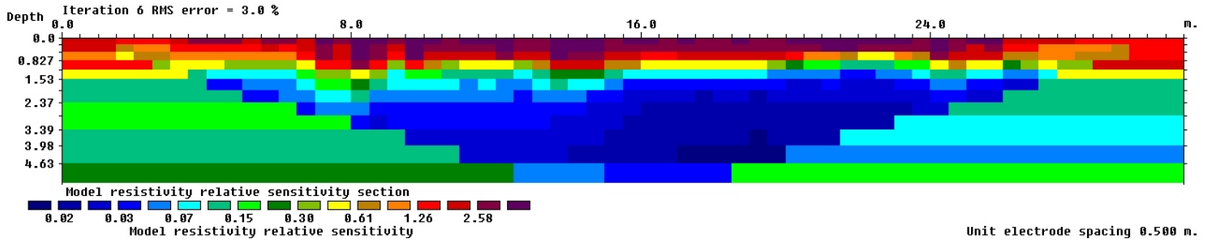

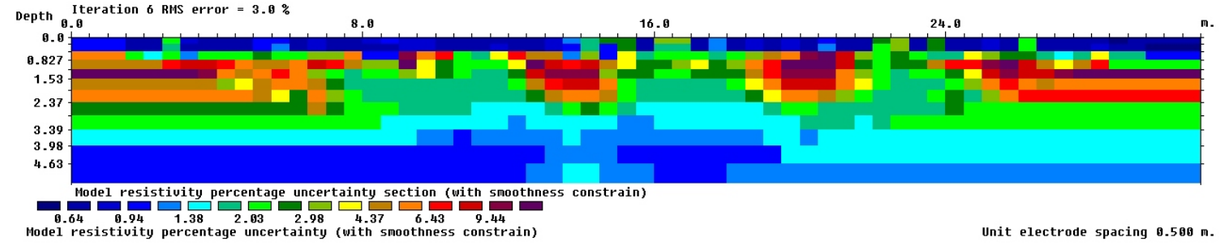

BVP2 West to East resistivity line with 64 electrodes at 0.5m spacing:

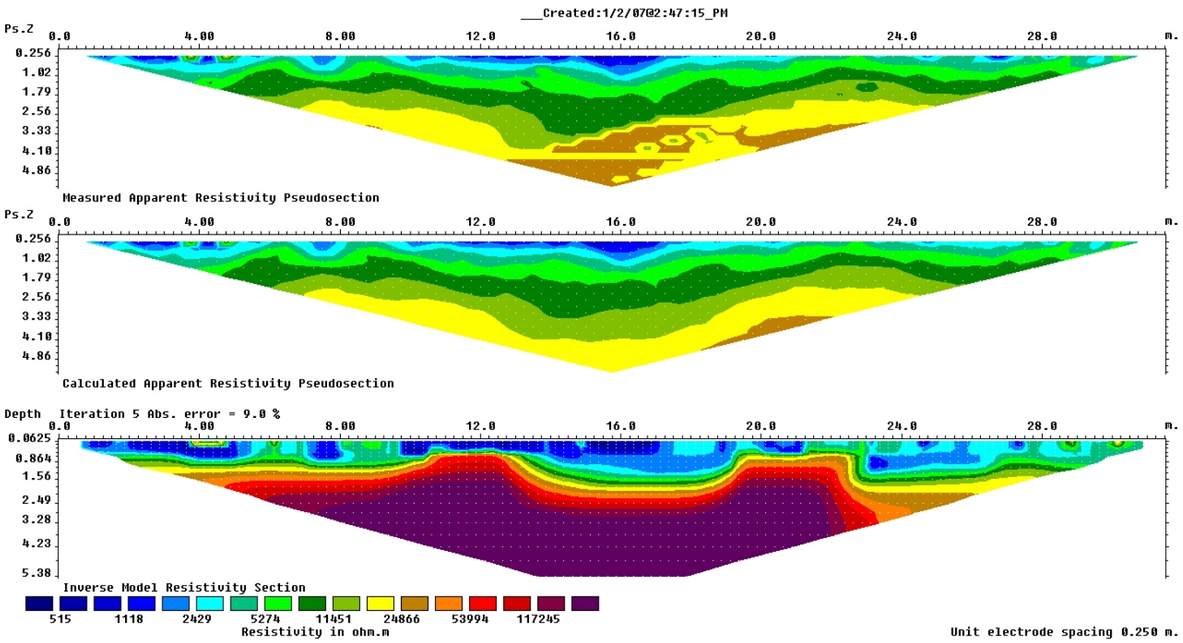

Horizontal scale is 9.52 pixels per unit spacing
Vertical exaggeration in model section display = 0.72
First electrode is located at 0.0 m.
Last electrode is located at 31.5 m.

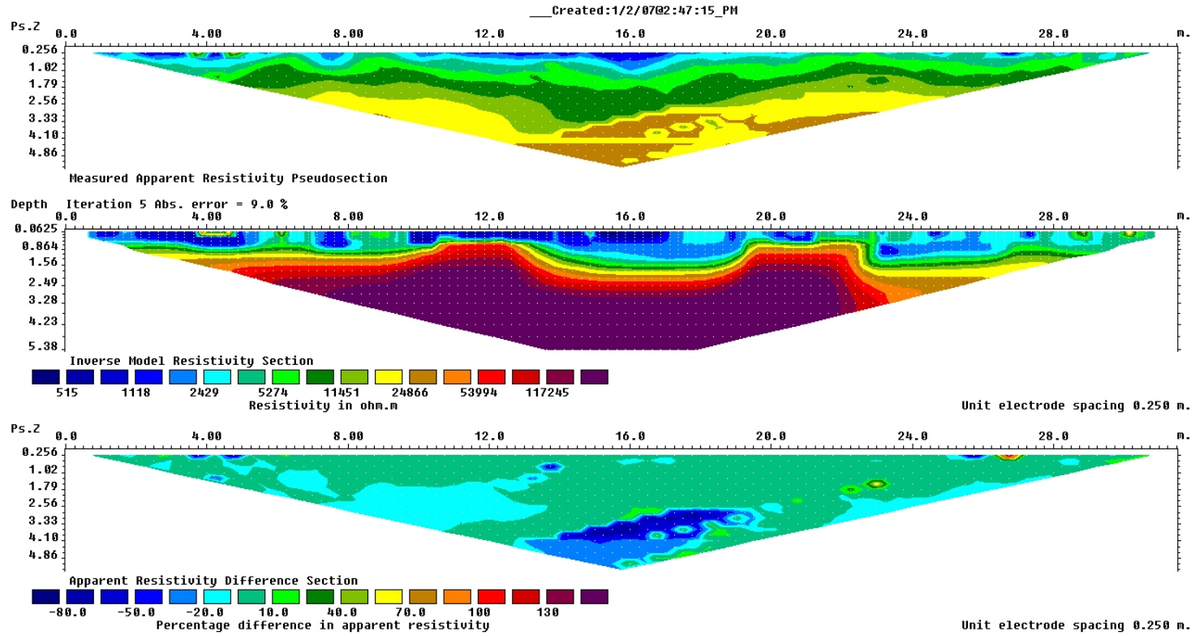

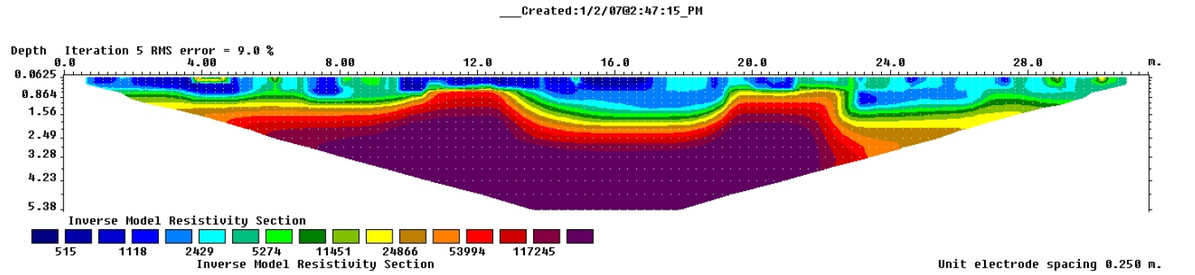

BVP2 West to East resistivity line with 32 electrodes at 0.5m spacing:

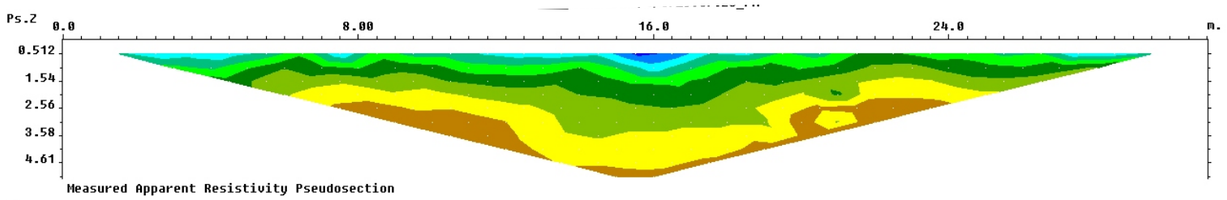

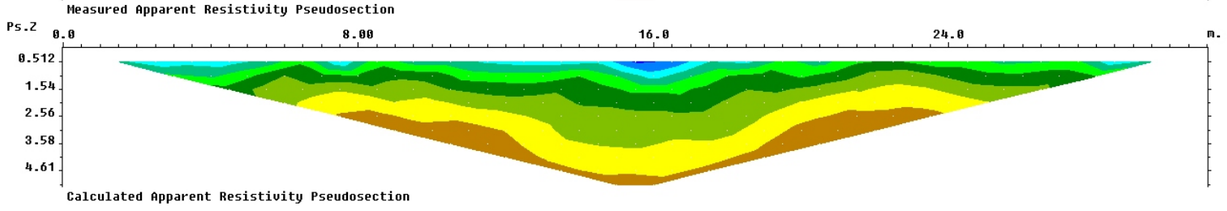

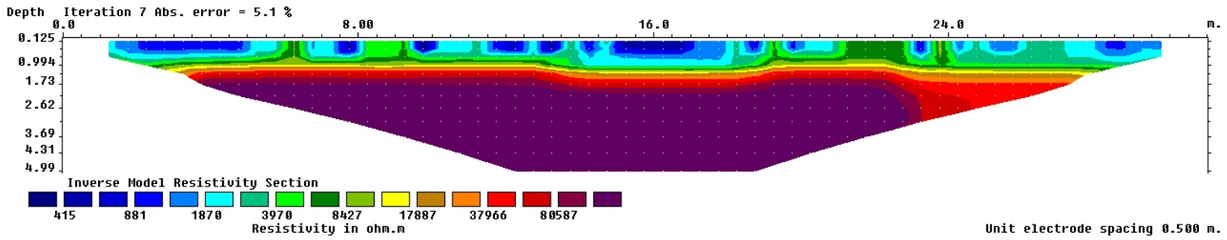

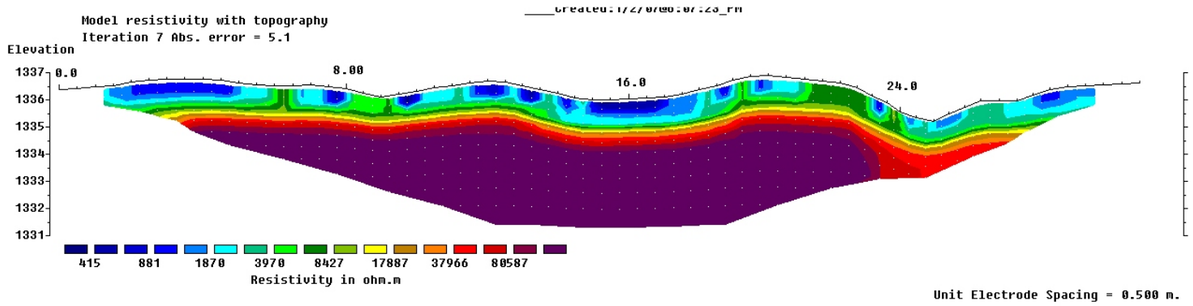

Horizontal scale is 19.34 pixels per unit spacing
Vertical exaggeration in model section display = 0.75
First electrode is located at 0.0 m.
Last electrode is located at 31.0 m.

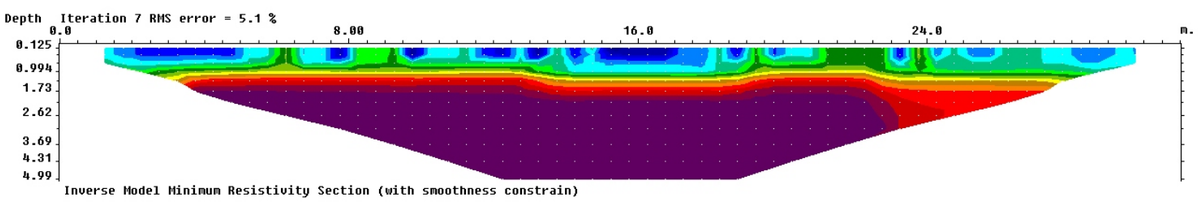

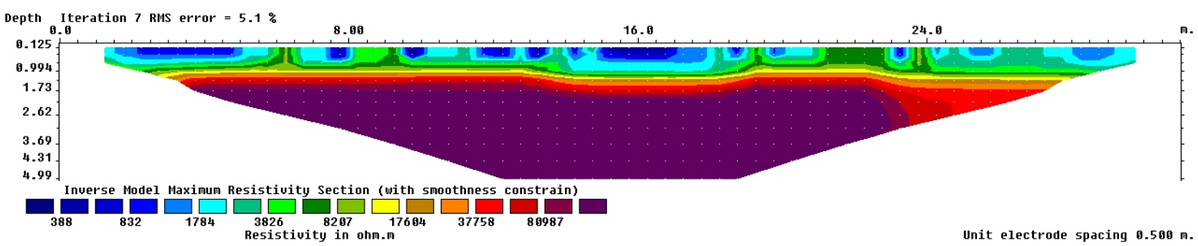

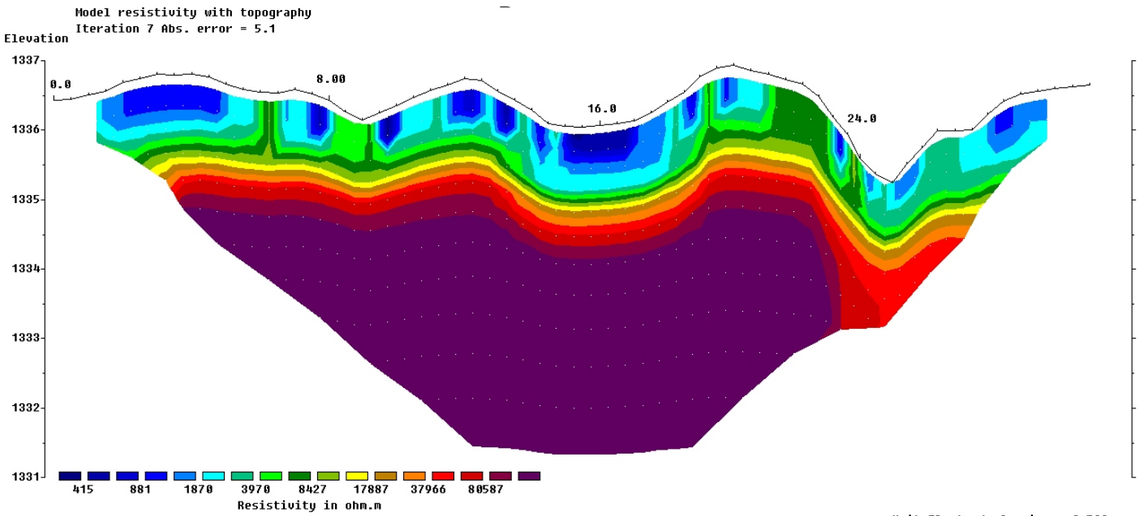

Horizontal scale is 19.34 pixels per unit spacing
Vertical exaggeration in model section display = 2.00
First electrode is located at 0.0 m.
Last electrode is located at 31.0 m.

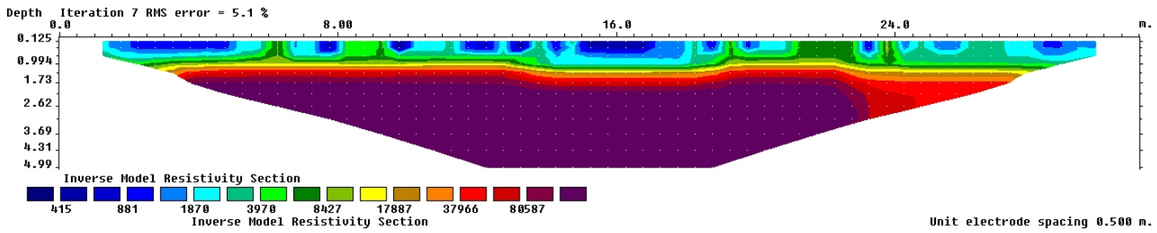

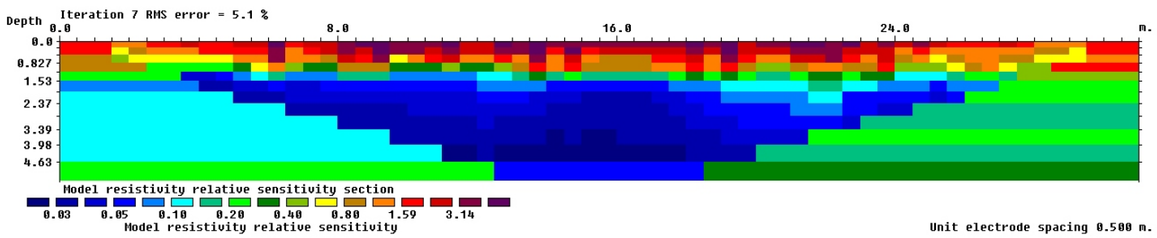

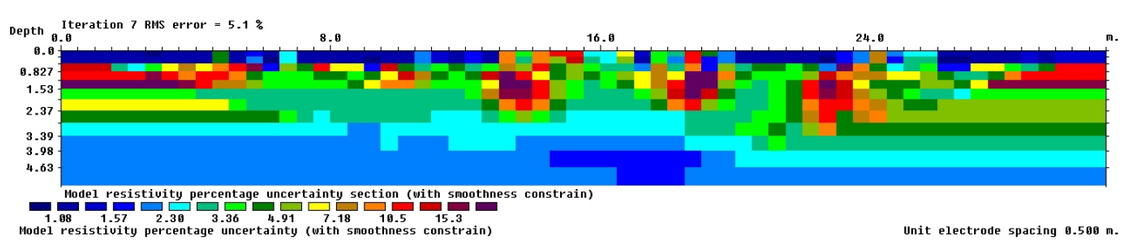

Appendix VI

Electromagnetism data

The digital spreadsheets used for calculation of the electromagnetism data displayed in this thesis can be found in the preceding data disk.

The following pages are a summary of the electromagnetic plots and the transformations required to make the plots displayed in Chapter 5 Results and Discussion.

VVP1 electromagnetism results (Quadrature):

Raw parallel:

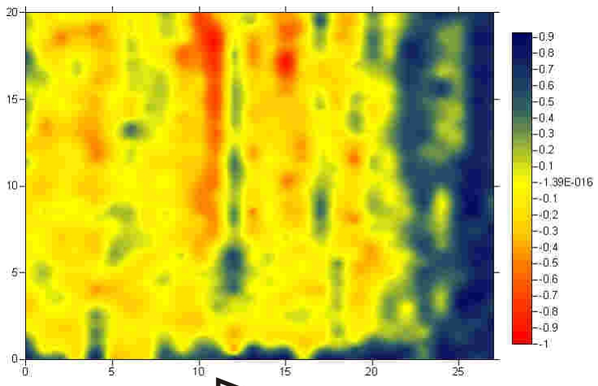

Raw perpendicular

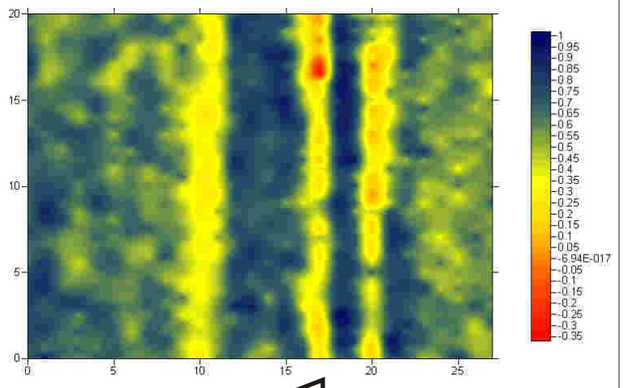

Line median subtracted from raw Parallel:

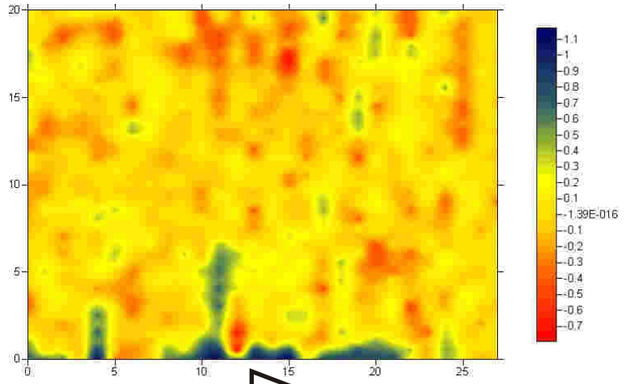

Line median subtracted from raw Perpendicular

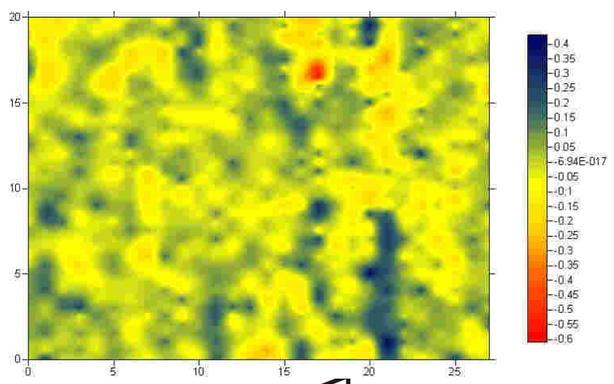

Average of Raw parallel and perpendicular:

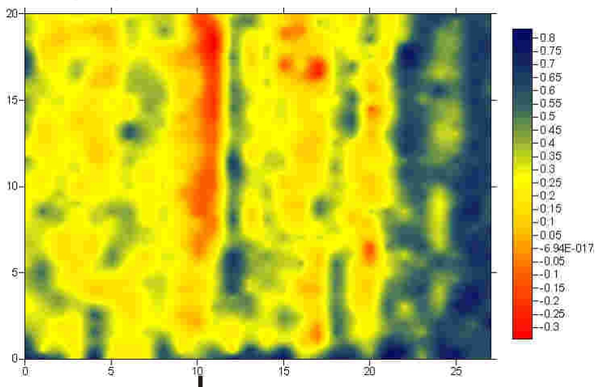

Difference of Raw parallel and perpendicular

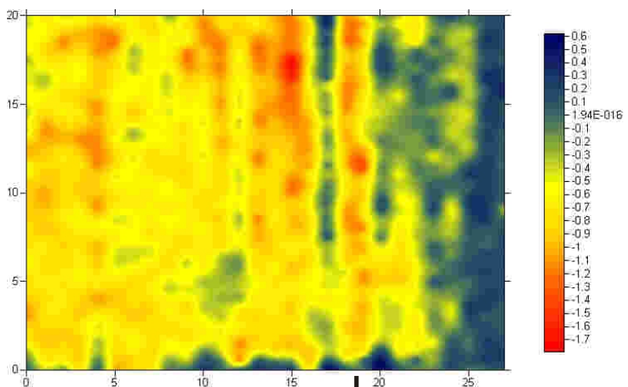

Average of line median subtracted parallel and perpendicular

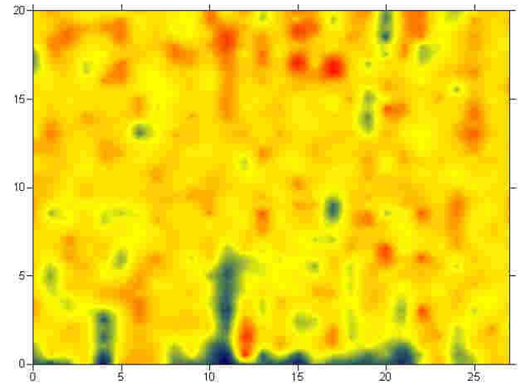

Difference of line median subtracted parallel and perpendicular:

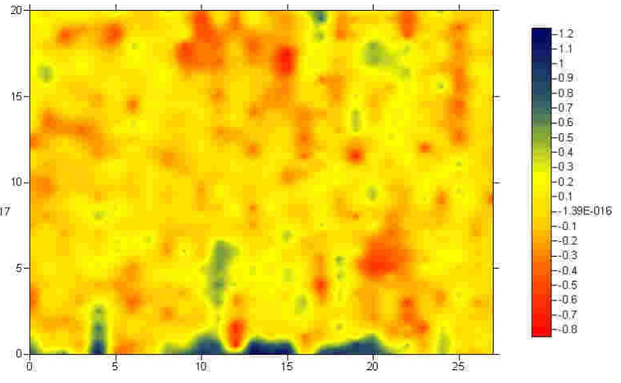

Line median subtracted from average.

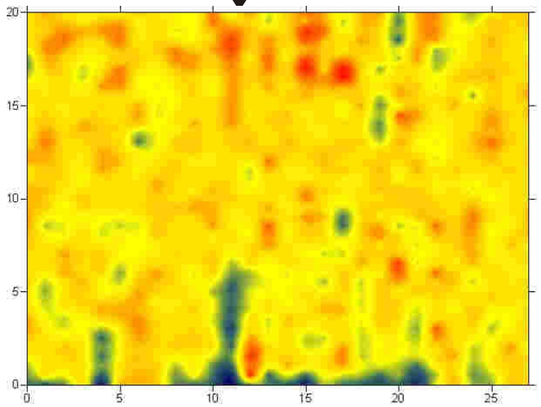

Line median subtracted from difference

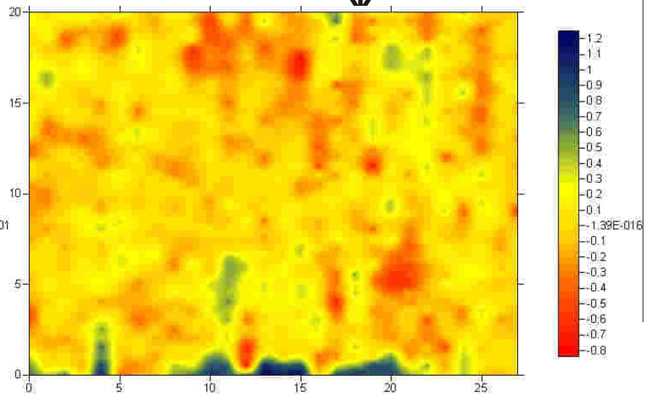

VVP1 electromagnetism results (Real):

Raw parallel:

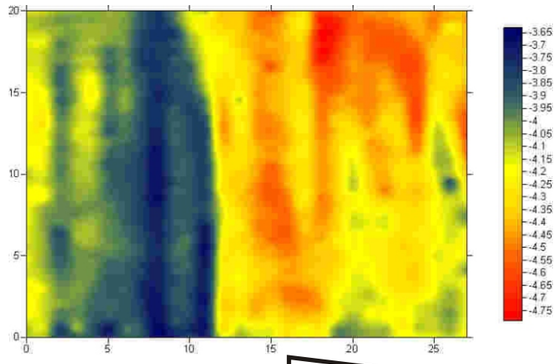

Raw perpendicular

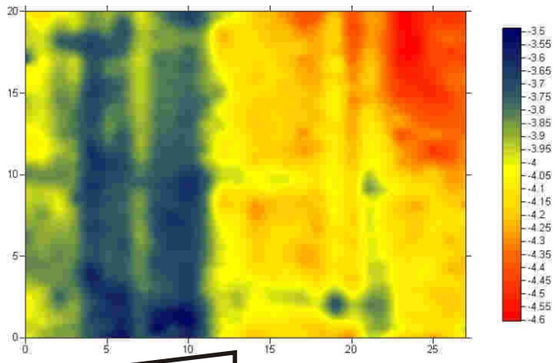

Average of raw parallel and perpendicular:

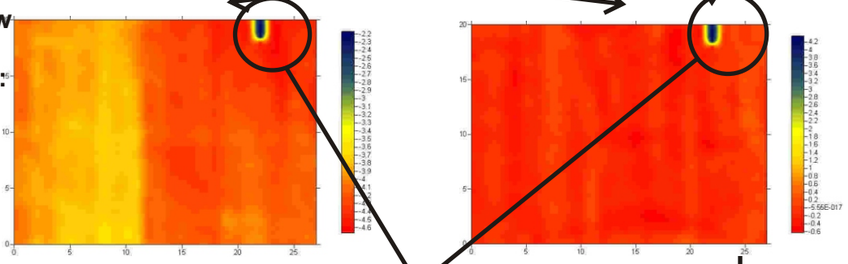

Difference of raw parallel and perpendicular

Edited average of raw parallel and perpendicular

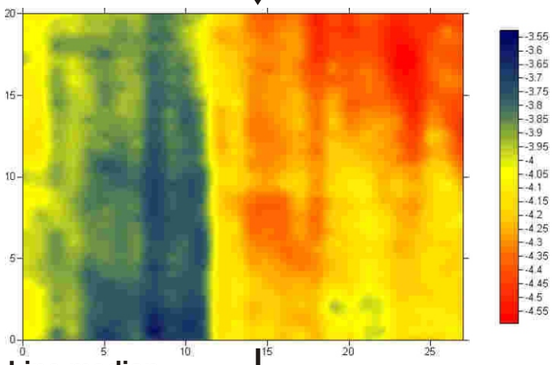

Anomalous results edited out

Edited difference of raw parallel and perpendicular

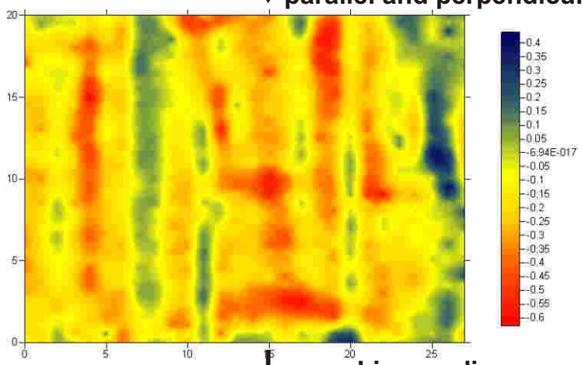

Line median subtracted from edited average.

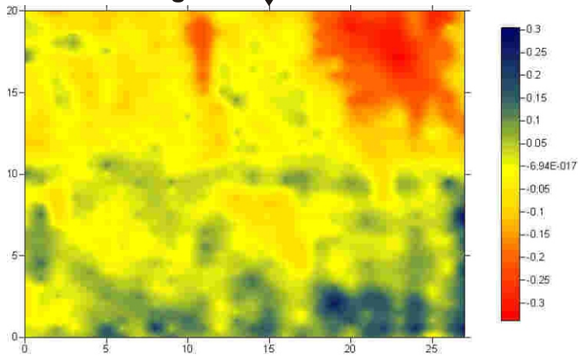

Line median subtracted from edited difference

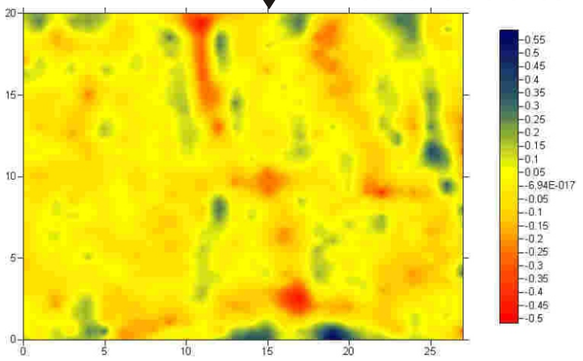

Line median subtracted from raw Parallel:

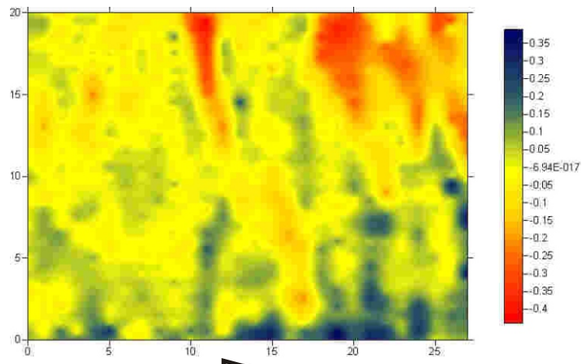

Line median subtracted from raw Perpendicular

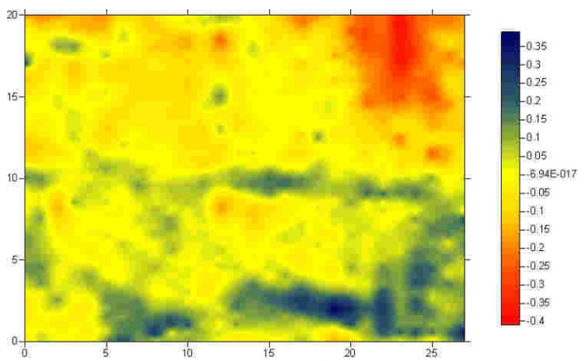

Average of line median subtracted parallel and perpendicular

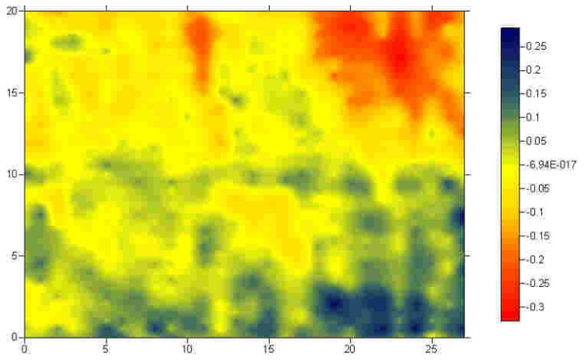

Difference of line median subtracted parallel and perpendicular:

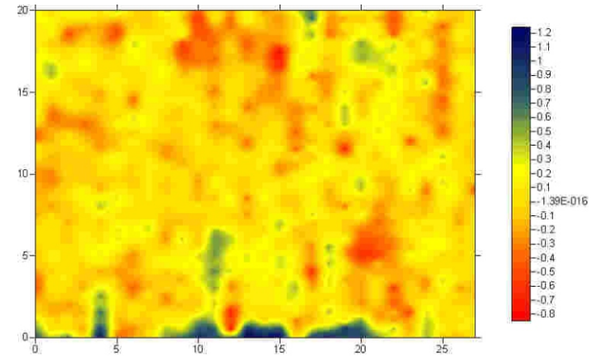

Average of line median subtracted from edited raw.

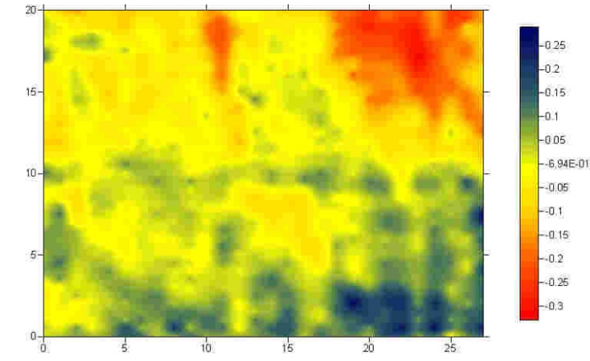

Average of line median subtracted from edited difference

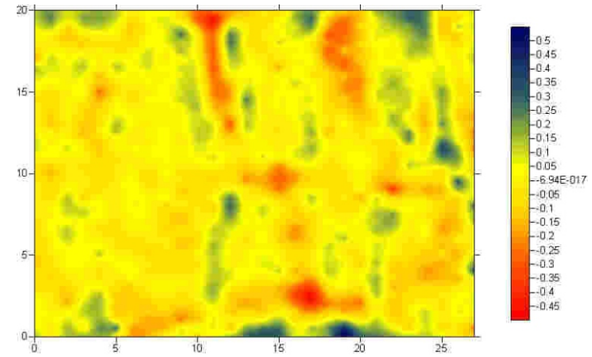

VVP2 electromagnetism results (Quadrature):

Raw parallel:

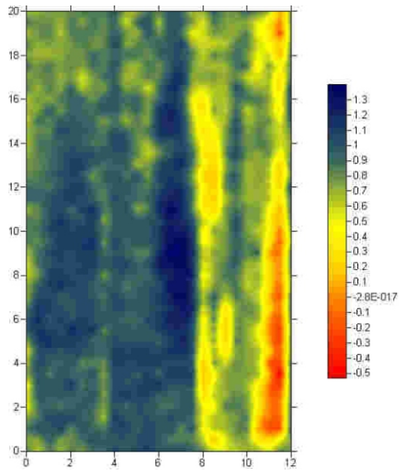

Raw perpendicular

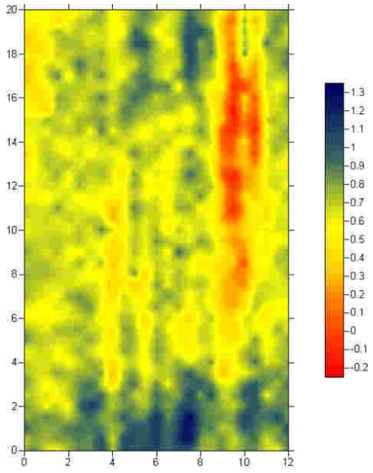

Average of Raw parallel and perpendicular:

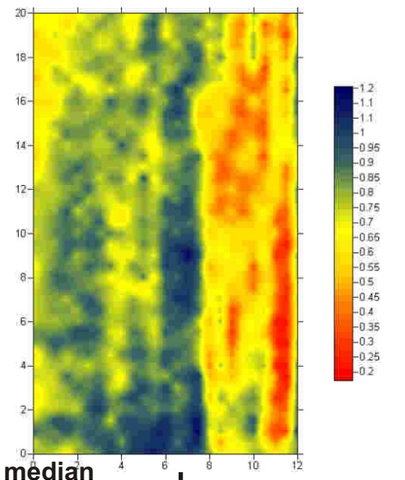

Difference of Raw parallel and perpendicular

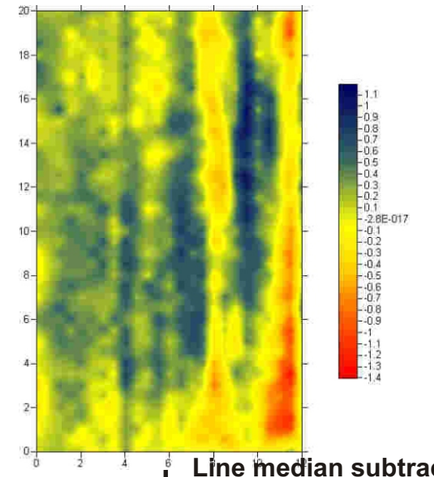

Line median subtracted from average.

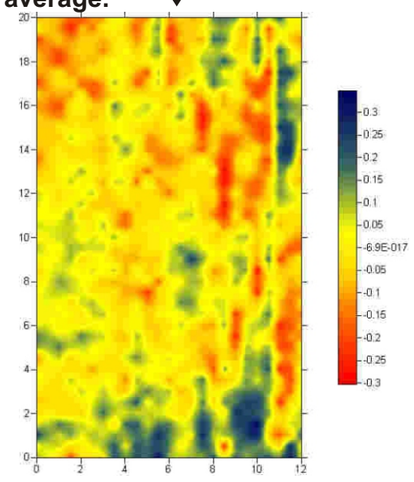

Line median subtracted from difference

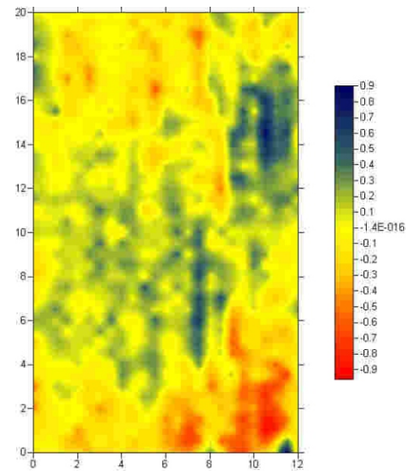

Line median subtracted from raw Parallel:

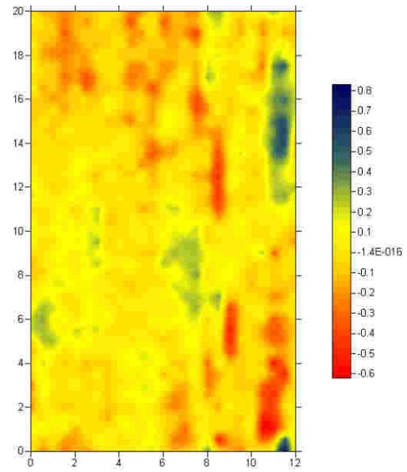

Line median subtracted from raw Perpendicular

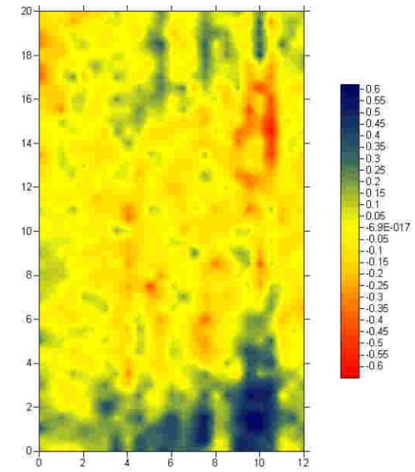

Average of line median subtracted parallel and perpendicular

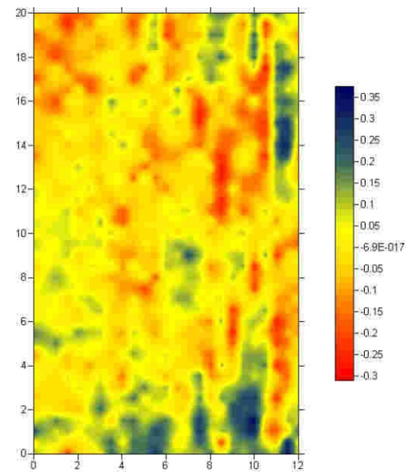

Difference of line median subtracted parallel and perpendicular:

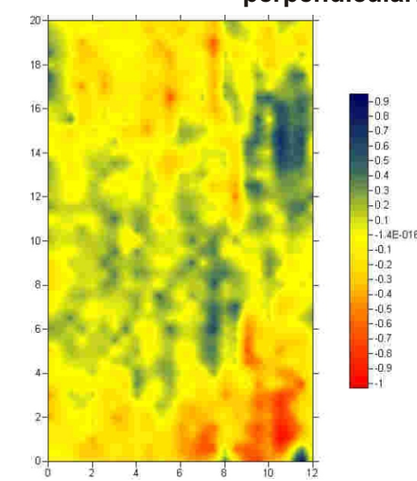

VVP2 electromagnetism results (Real):

Raw parallel:

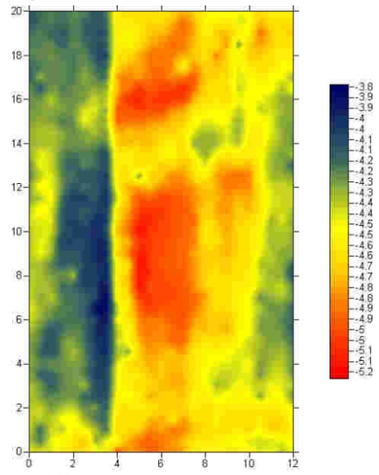

Raw perpendicular

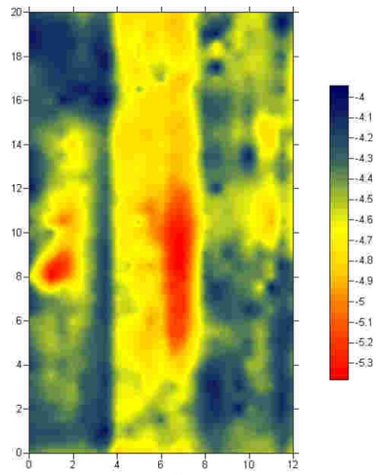

Average of Raw parallel and perpendicular:

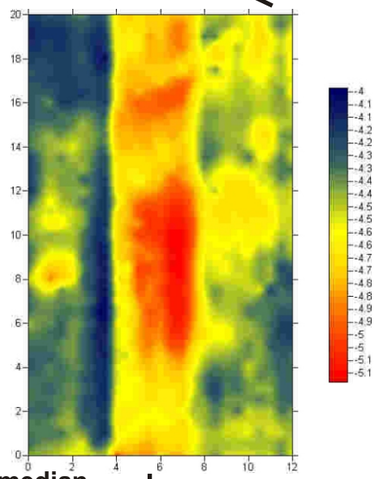

Difference of Raw parallel and perpendicular

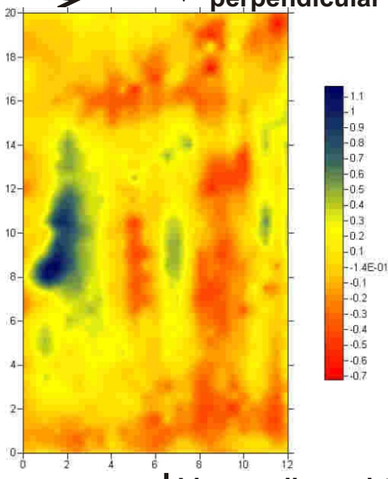

Line median subtracted from average.

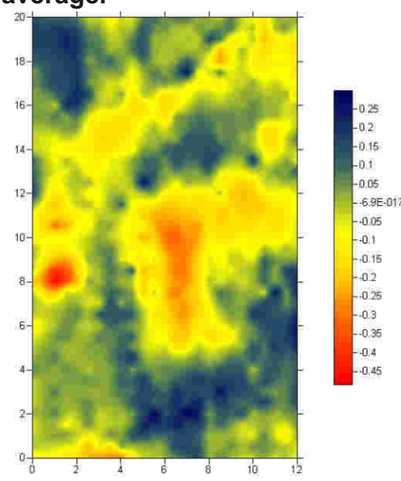

Line median subtracted from difference

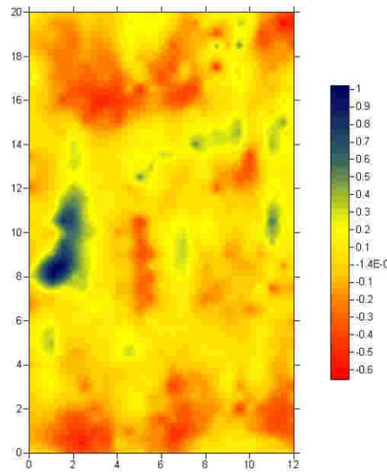

Line median subtracted from raw Parallel:

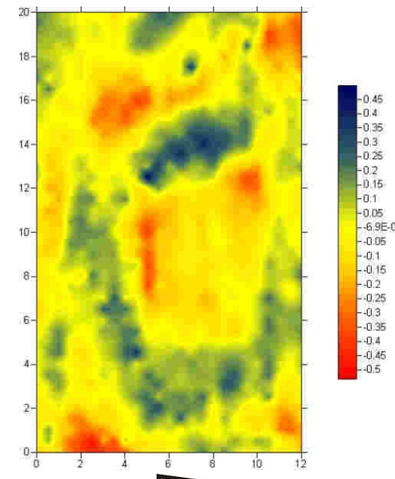

Line median subtracted from raw Perpendicular

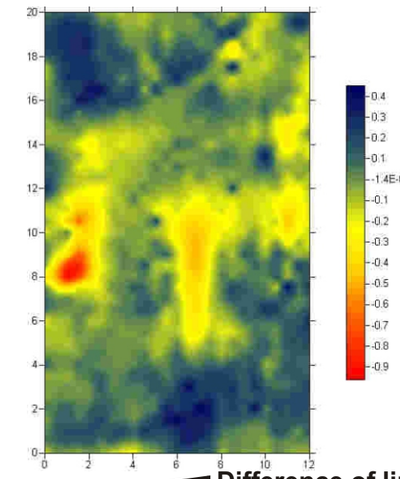

Average of line median subtracted parallel and perpendicular

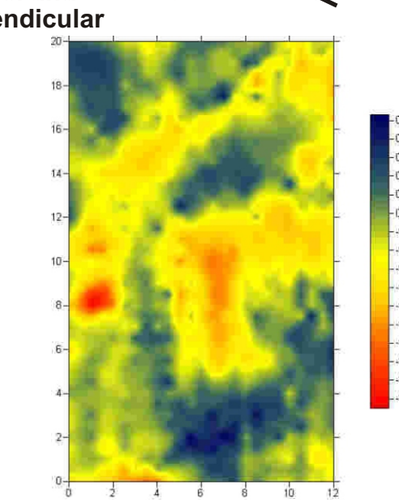

Difference of line median subtracted parallel and perpendicular:

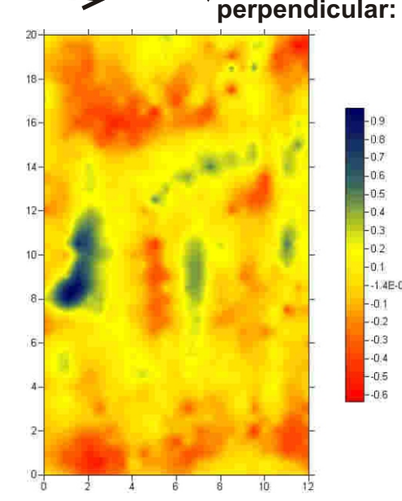

BVP1 electromagnetism results (Quadrature):

Raw parallel:

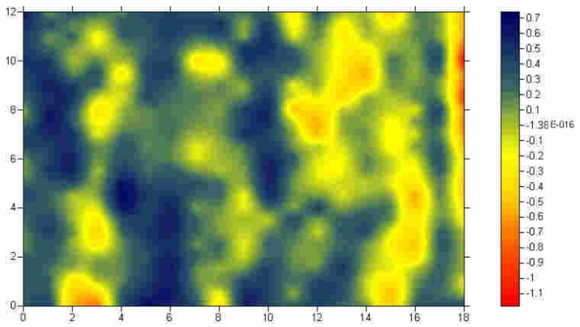

Raw perpendicular

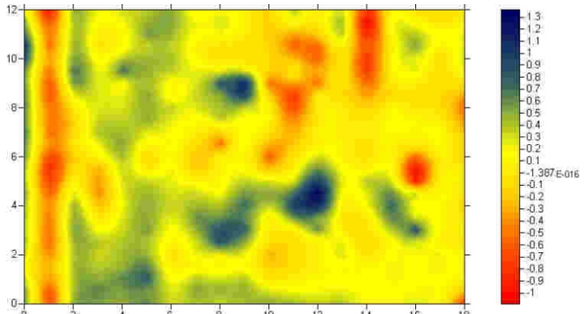

Average of Raw parallel and perpendicular:

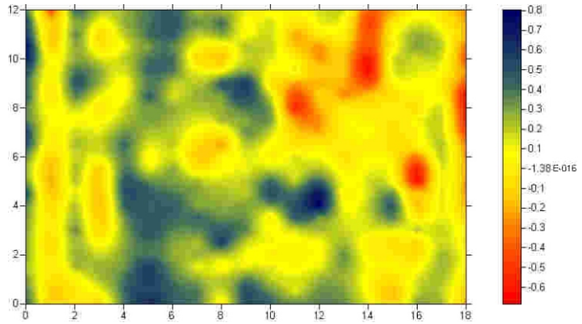

Difference of Raw parallel and perpendicular

Line median subtracted from average.

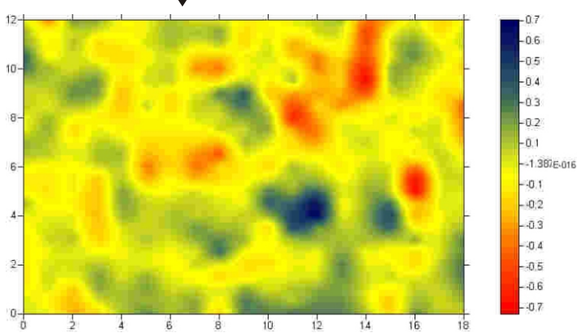

Line median subtracted from difference

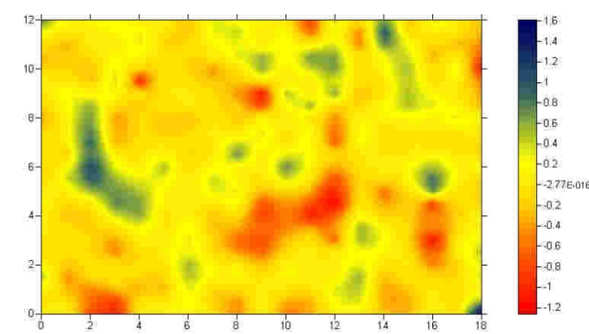

Line median subtracted from raw Parallel:

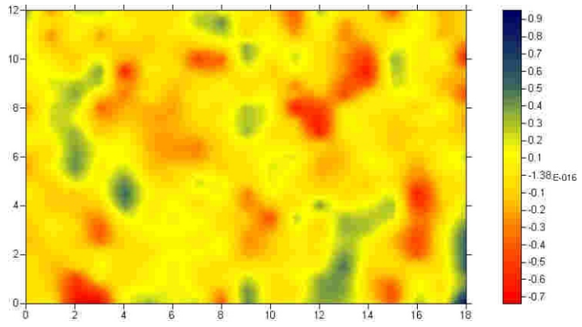

Line median subtracted from raw Perpendicular

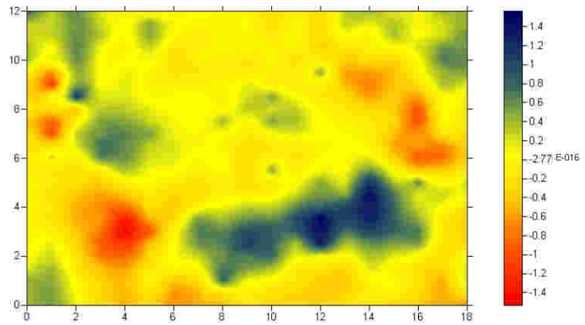

Average of line median subtracted parallel and perpendicular

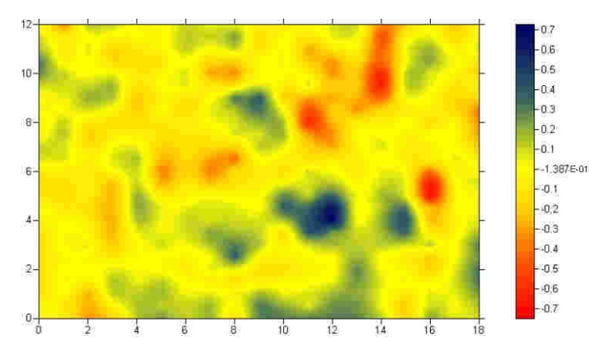

Difference of line median subtracted parallel and perpendicular:

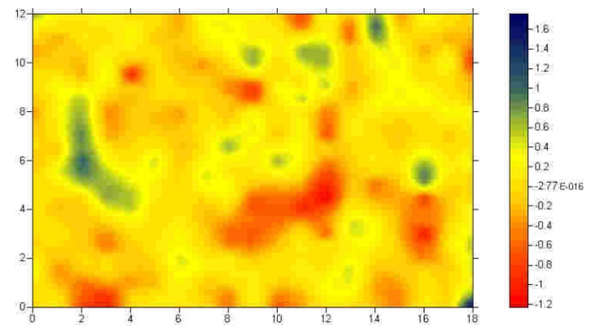

BVP1 electromagnetism results (Real):

Raw parallel:

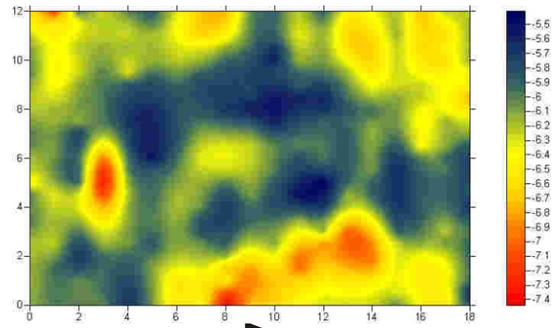

Raw perpendicular

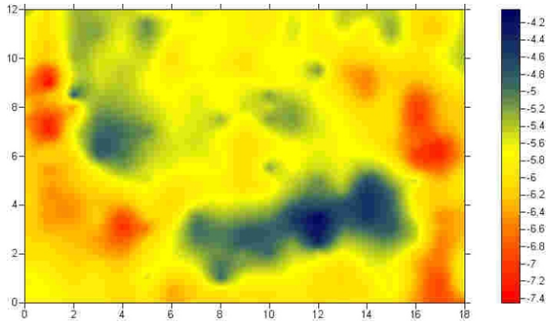

Average of Raw parallel and perpendicular:

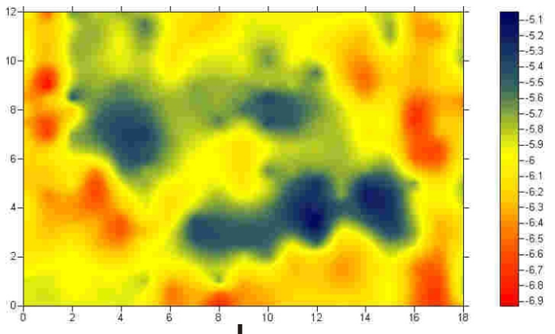

Difference of Raw parallel and perpendicular

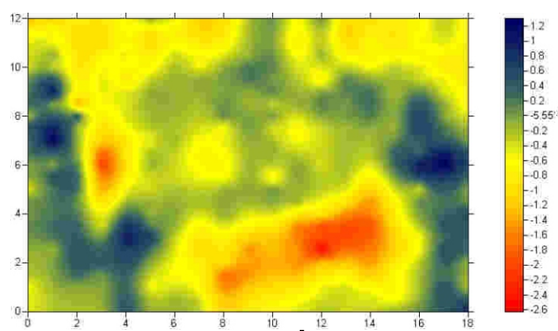

Line median subtracted from average.

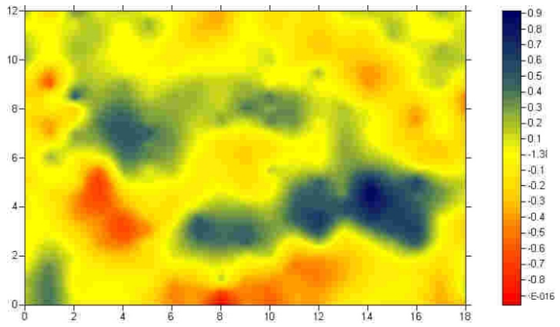

Line median subtracted from difference

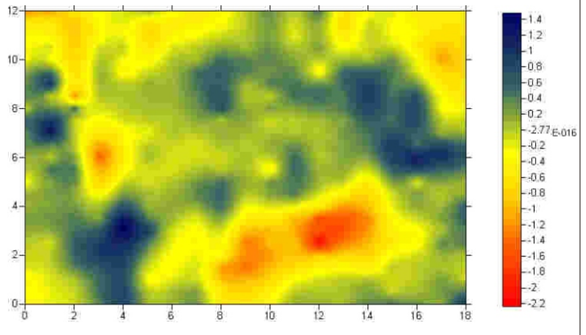

Line median subtracted from raw Parallel:

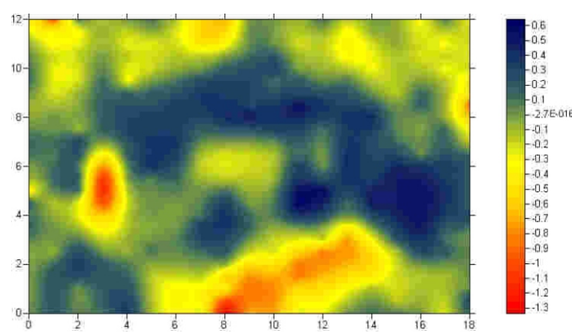

Line median subtracted from raw Perpendicular

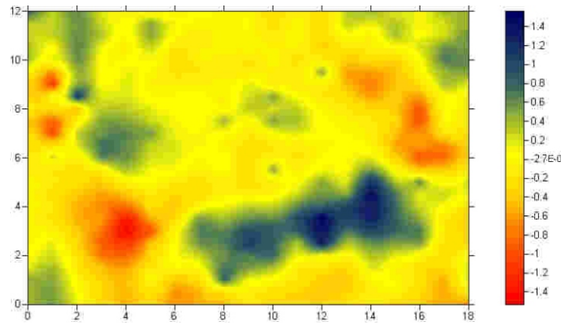

Average of line median subtracted parallel and perpendicular

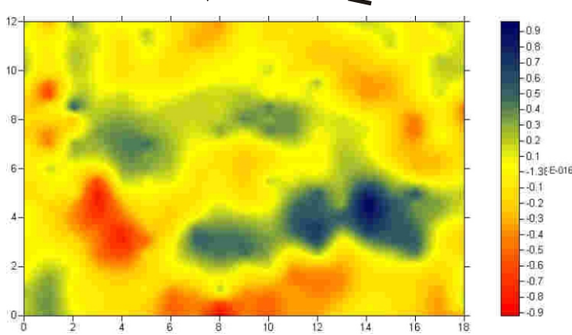

Difference of line median subtracted parallel and perpendicular:

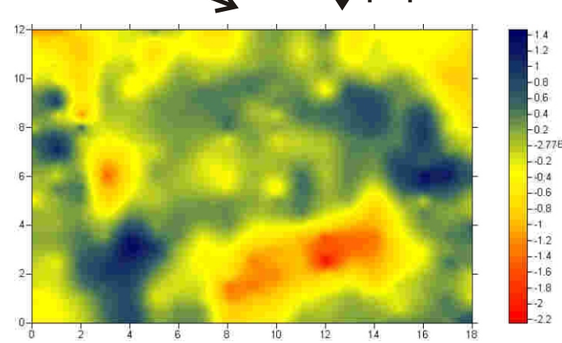

BVP2 electromagnetism results (Quadrature):

Raw parallel:

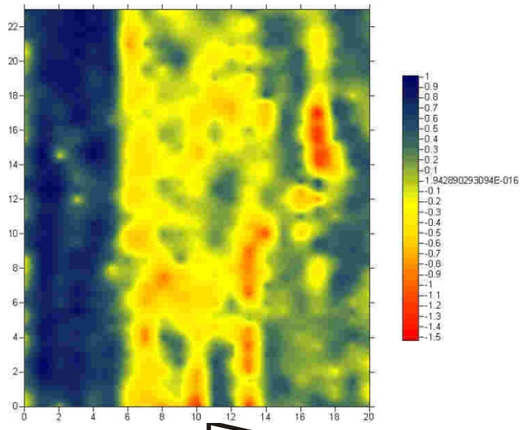

Raw perpendicular

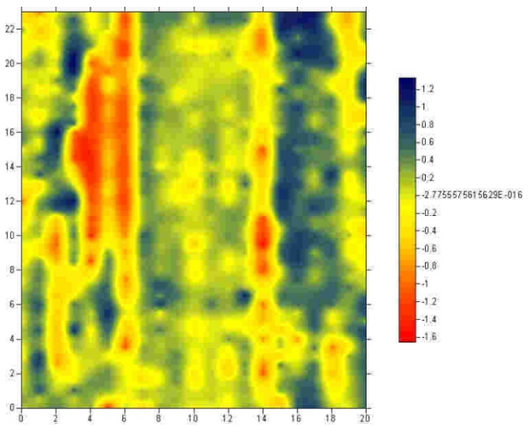

Average of Raw parallel and perpendicular:

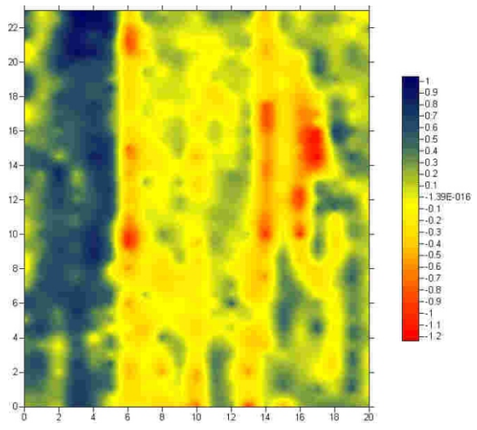

Difference of Raw parallel and perpendicular

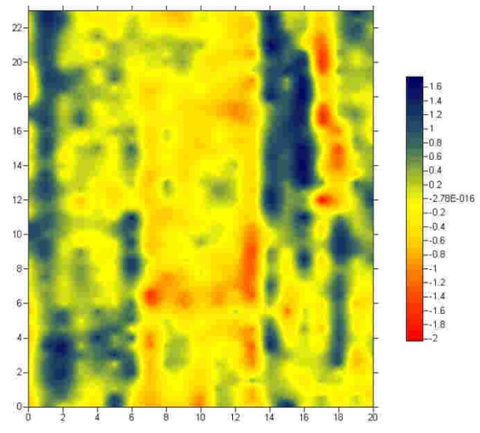

Line median subtracted from average.

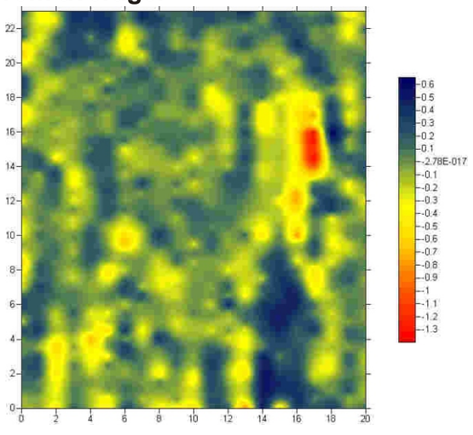

Line median subtracted from difference

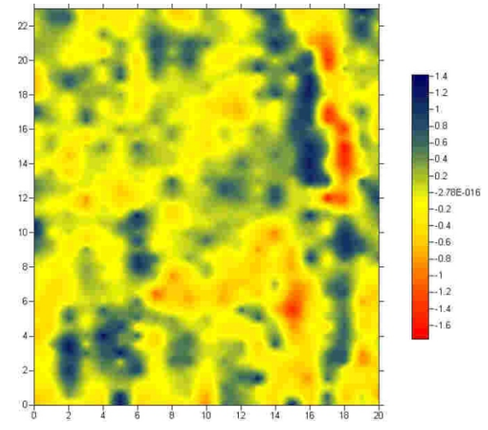

Line median subtracted from raw Parallel:

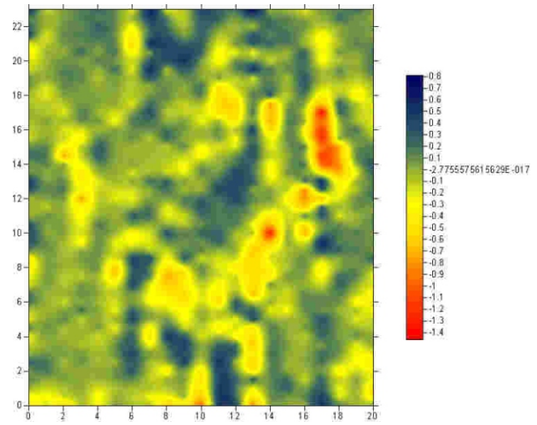

Line median subtracted from raw Perpendicular

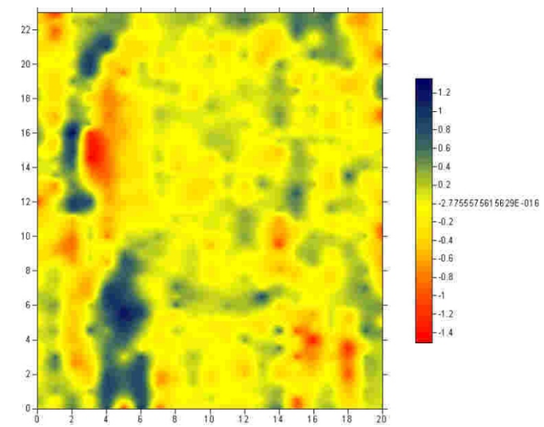

Average of line median subtracted parallel and perpendicular

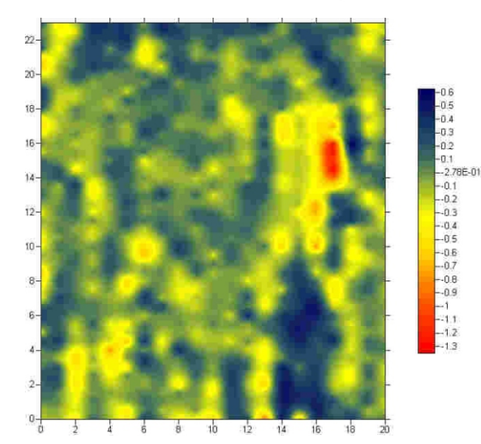

Difference of line median subtracted parallel and perpendicular:

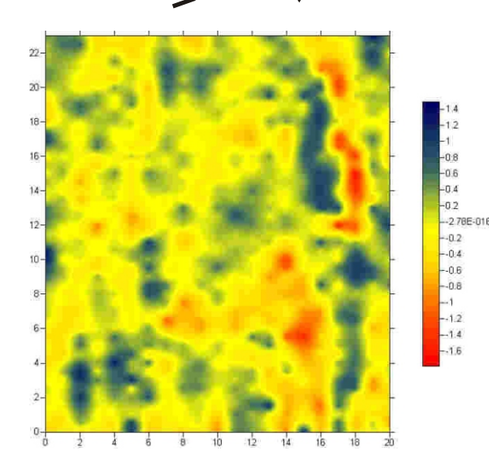

BVP2 electromagnetism results (Real):

Raw parallel:

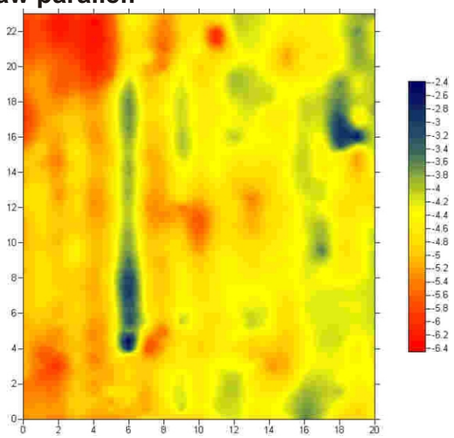

Raw perpendicular

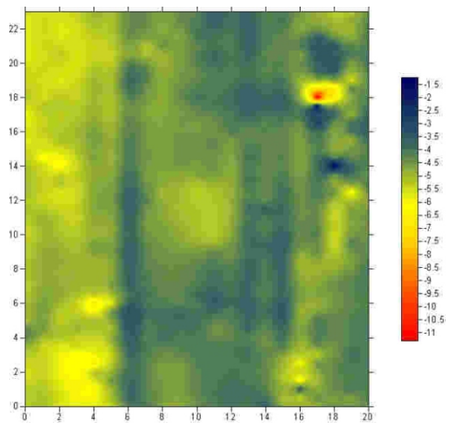

Raw Average:

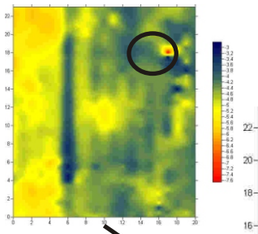

Edited Raw average

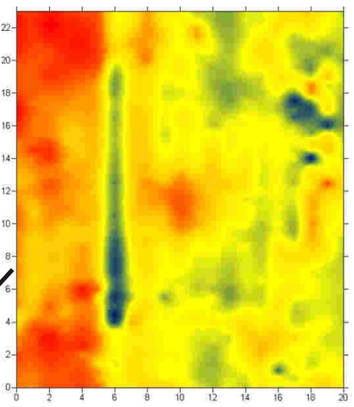

Raw Difference

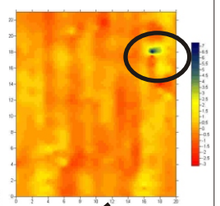

Edited Raw difference

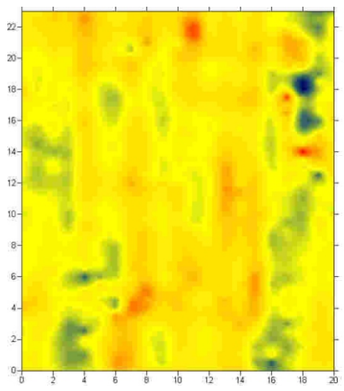

Edited with line median subtracted after averaging

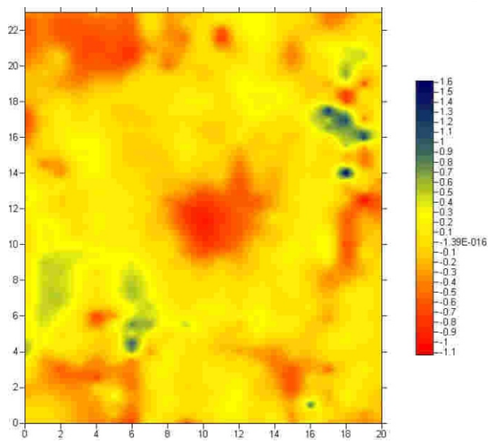

Edited with line median subtracted after difference taken

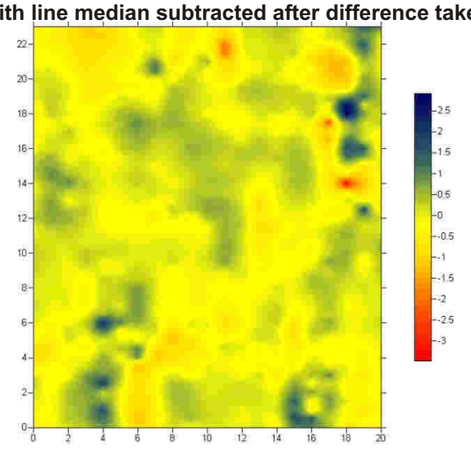

Line median subtracted parallel:

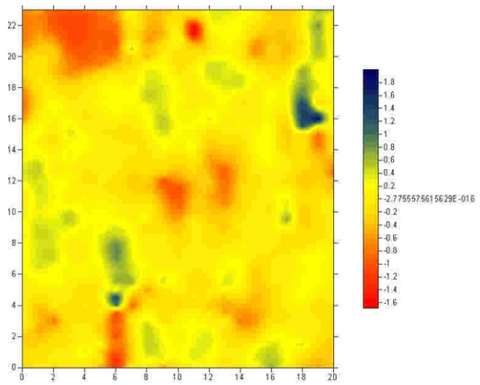

Line median subtracted perpendicular

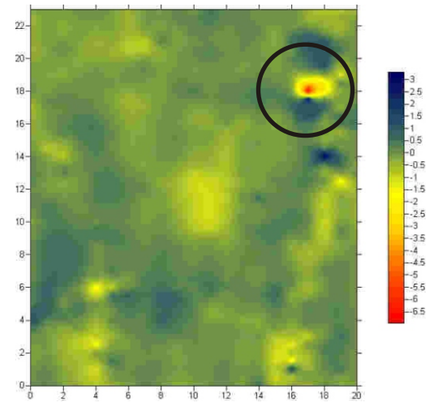

Line median subtracted before average:

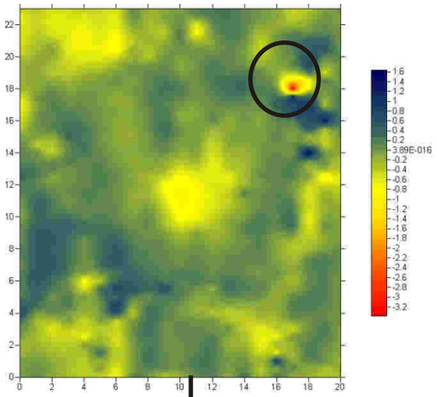

Line median subtracted before difference taken